



NATIONAL AND KAPODISTRIAN UNIVERSITY OF ATHENS

FACULTY OF SCIENCES

DEPARTMENT OF CHEMISTRY

Ph.D. THESIS

**Photocatalytic degradation of cyanotoxins and water taste
and odor compounds using TiO₂ based nanocatalysts and
polyoxometalates**

THEODORA FOTIOU

ATHENS

May 2014

Ph.D. THESIS

Photocatalytic degradation of cyanotoxins and water taste and odor compounds using
TiO₂ based nanocatalysts and polyoxometalates

THEODORA FOTIOU

R.N.: 263/01020

SUPERVISOR:

Prof. Athanasios Valavanidis, Dpt of Chemistry, University of Athens

SUPERVISORY COMMITTEE:

Prof. Athanasios Valavanidis, Dpt of Chemistry, University of Athens

Prof. Manos Dassenakis, Dpt of Chemistry, University of Athens

Dr. Anastasia Hiskia, Researcher Rank A, NCSR "Demokritos"

EXAMINATION COMMITTEE

Prof. Athanasios Valavanidis, Dpt of Chemistry, University of Athens

Prof. Manos Dassenakis, Dpt of Chemistry, University of Athens

Dr. Anastasia Hiskia, Researcher Rank A, NCSR "Demokritos"

Prof. Michael Scoullas, Dpt of Chemistry, University of Athens

Assoc. Prof. Nikolaos S. Thomaidis, *Dpt of Chemistry, University of Athens*

Prof. Dionisios Dionysiou, Dpt DBCEE, *University of Cincinnati*

Dr Jussi Meriluoto, Dpt of Biosciences, *Abo Akademi University*

DATE OF EXAMINATION 06/05/2014

ABSTRACT

Titanium dioxide (TiO₂) photocatalysis has been considered a promising advanced oxidation process, which in combination with solar energy could effectively address the ever increasing concerns for pollution abatement and water purification. Although it appears to degrade a great variety of compounds in water, it generally requires UV irradiation for activation of the catalyst. Consequently, research on the development of new TiO₂ based catalysts has been receiving increased attention. TiO₂ photocatalysis can be effective for water purification from new classes of emerging pollutants such as cyanobacterial toxins (cyanotoxins) and metabolites, which can be produced by several genera of cyanobacteria. Cyanotoxins are considered an important risk for water quality since they are harmful to human and animal health. In this study, the photocatalytic degradation of cyanotoxins (microcystin-LR, MC-LR and Cylindrospermopsin, CYN) and water taste and odor compounds (Geosmin, GSM and 2-methylisoborneol, MIB) was studied. TiO₂ based photocatalysts (Degussa P25, Kronos vlp-7000, Ref-TiO₂, N-TiO₂, NF-TiO₂, GOTiO₂ and ECT-1023t) were tested for their photocatalytic ability towards degradation and mineralization of target analytes in water using UV-A, solar and visible light. In order to evaluate the photocatalytic performance of the materials, several parameters such as light intensity, presence of oxygen, catalyst loading, initial concentration of substrate, adsorption, pH, irradiation wavelength, mineralization, intermediate products and toxicity, were investigated. Identification of the intermediate and final products was carried out and a complete degradation pathway is proposed where hydroxyl radicals ([•]OH) play a key role. Assessment of the residual toxicity in the case of MCLR using TiO₂ photocatalysis, complete detoxification of the solutions can be achieved. In addition, photocatalytic degradation of GSM and MIB using a polyoxometalate photocatalyst, H₄SiW₁₂O₄₀ was studied and compared with TiO₂. Elucidation of the mechanism using [•]OH radical scavengers showed that process takes place via [•]OH radicals for both catalysts. Overall results of this study show that TiO₂ based photocatalysis can be very effective in removing cyanobacterial toxins and taste and odor compounds from water and its applications can be extended to the visible-solar region of the spectrum by development of novel modified photocatalytic materials.

SUBJECT AREA: Photocatalysis

KEYWORDS: Titanium Dioxide, Polyoxometalates, Cyanotoxins, Water Taste & Odor Compounds, Degradation & Mechanism Elucidation

ΠΕΡΙΛΗΨΗ

Η φωτοκατάλυση με χρήση διοξειδίου του τιτανίου (TiO_2) είναι μία προηγμένη τεχνολογία οξειδωσης, η οποία σε συνδυασμό με την ηλιακή ενέργεια μπορεί να εφαρμοστεί αποτελεσματικά για τον καθαρισμό του νερού από μεγάλο φάσμα τοξικών ενώσεων. Η απαίτηση όμως υπεριώδους ακτινοβολίας για να ξεπεραστεί το ενεργειακό χάσμα του TiO_2 , αποτελεί το λόγο της έντονης ερευνητικής δραστηριότητας γύρω από την ανάπτυξη νέων βελτιωμένων καταλυτών. Η παρουσία κυανοβακτηρίων στα νερά αποτελεί σημαντικό πρόβλημα, δεδομένου ότι διάφορα γένη μπορούν να παράγουν τοξίνες (κυανοτοξίνες) με σημαντικές επιπτώσεις στην ανθρώπινη υγεία. Επιπλέον, είναι πιθανόν να παραχθούν ενώσεις που προσδίδουν γεύση και οσμή στο νερό με αποτέλεσμα την υποβάθμιση της ποιότητάς του. Στη παρούσα εργασία μελετήθηκε η φωτοκαταλυτική αποικοδόμηση κυανοτοξινών (microcystin-LR, MC-LR και Cylindrospermopsin, CYN) και ουσιών που προσδίδουν οσμή στα νερά (Geosmin, GSM and 2-methylisoborneol, MIB). Έγινε χρήση φωτοκαταλυτών με βάση το TiO_2 (Degussa P25, Kronos vlp-7000, Ref- TiO_2 , N- TiO_2 , NF- TiO_2 , GO- TiO_2 and ECT-1023t) για την πλήρη αποικοδόμηση των ενώσεων αυτών σε υδατικά διαλύματα με χρήση υπεριώδους, ηλιακής και ορατής ακτινοβολίας. Για την αξιολόγηση της δραστηριότητας των φωτοκαταλυτών, εξετάστηκε η επίδραση διαφόρων παραμέτρων όπως η παρουσία οξυγόνου, το είδος και η ένταση ακτινοβολίας, η συγκέντρωση των καταλυτών και των υποστρωμάτων, το pH, η προσρόφηση στον φωτοκαταλύτη, καθώς και ο σχηματισμός ενδιάμεσων προϊόντων και η τοξικότητα. Με βάση τον προσδιορισμό των ενδιάμεσων και τελικών προϊόντων προτείνεται μηχανισμός αποικοδόμησης, στον οποίο σημαντικό ρόλο έχουν οι ρίζες υδροξυλίου ($\cdot\text{OH}$). Επιπλέον μελετήθηκε η φωτοκαταλυτική αποικοδόμηση των ενώσεων GSM και MIB παρουσία της πολυοξομεταλλικής ένωσης $\text{H}_4\text{SiW}_{12}\text{O}_{40}$. Συγκριτική μελέτη με τη χρήση δεσμευτών $\cdot\text{OH}$ κατέληξε σε μηχανισμό αντίστοιχο με εκείνο παρουσία TiO_2 . Τα συνολικά αποτελέσματα της εργασίας αυτής δείχνουν ότι η φωτοκατάλυση με TiO_2 είναι πολύ αποτελεσματική στην απομάκρυνση κυανοτοξινών και ουσιών που προσδίδουν δυσάρεστη γεύση και οσμή στο νερό. Οι εφαρμογές της τεχνολογίας αυτής μπορούν να επεκταθούν και στην ορατή-ηλιακή περιοχή του φάσματος με ανάπτυξη νέων τροποποιημένων φωτοκαταλυτικών υλικών.

ΘΕΜΑΤΙΚΗ ΠΕΡΙΟΧΗ: Φωτοκατάλυση

ΛΕΞΕΙΣ ΚΛΕΙΔΙΑ: Διοξείδιο του τιτανίου, Πολυοξομεταλλικές ενώσεις, Κυανοτοξίνες, Οσμές, Μηχανισμός Φωτοκαταλυτικής Αποικοδόμησης

Dedicated to my Father

ACKNOWLEDGEMENTS

Primarily, I would like to express my appreciation to my supervisor at National Center for Scientific Research “Demokritos” where the experimental work was done, Dr. Anastasia Hiskia for her guidance, support, generosity all these years and for her motivation to excel to my doctoral studies. I am grateful to my supervisor at University of Athens, Prof. Athanasios Valavanidis, for giving me this opportunity to start my doctoral studies and explore the potential of my research abilities. I also would like to thank Prof. Manos Dassenakis, member of my Ph.D. committee, for his constant support. Sincere thanks are extended to all members of the thesis committee Prof. Dionisios Dionysiou, Dr Jussi Meriluoto, Prof. Michael Scoullou and Assoc. Prof. Nikolaos S. Thomaidis, for willingly accepting to be part of the committee as well as for their constructive criticism and advice.

I am also grateful to NCSR “Demokritos” Institute of Advanced Materials, Physicochemical Processes, Nanotechnology and Microsystems for the Ph.D. fellowship, making this thesis possible.

This work was funded by the European Commission (Clean Water – Grant Agreement number 227017). Clean Water was a Collaborative Project co-funded by the Research DG of the European Commission within the joint RTD activities of the Environment and NMP Thematic Priorities. Also, this work was co-funded by the European Social Fund and Greek national funds through operational program “Education and Lifelong Learning” in the frame of (a) the Action ARISTEIA: “CYANOWATER - Cyanotoxins in Fresh Waters, Advances in Analysis, Occurrence and Treatment” and (b) the National Strategic Reference Framework (NSRF) - Research Funding Program: THALIS, investing in knowledge society through the European Social Fund. In addition, I would like to acknowledge the European Cooperation in Science and Technology, COST Actions ES 1105 "CYANOCOST- Cyanobacterial blooms and toxins in water resources: Occurrence, impacts and management" and CM1203 "PoCheMoN – Polyoxometalate Chemistry for Molecular Nanoscience" for adding value to this study through networking and knowledge sharing with European experts and researchers in the field.

Special thanks to Dr. Theodoros Triantis, for being there to every step off the way, encouraging, supporting and even comforting me when needed, he is one of a kind.

Also Dr. Triantafyllos Kaloudis, for his constant support, willingness to help in any way he could, amazing ideas and of course for imparting his enthusiasm. I could not be more thankful to Dr. Elias Papaconstantinou for advice and sharing his knowledge. I would also like to express my deepest gratitude to Sevasti and Giannis for their collaboration and all the group members for the companionship and friendship all this years. Also, Katrin this journey would not have been the same without our lunches discussing the horoscope and the highlights of the day.

Last but not least, I would like to thank my family. I am grateful for all the support and love. Mum thank you for being strong when I was not, Lola and Takis for their constant faith in my abilities, my sisters Skevi, Anna, Katerina and cousins Catherine, Andreas, and brothers in law Giannos, Panayiotis, for filling my place when I couldn't and of course my amazing nephew Lambros and beautiful niece Despo for brightening our lives.

Table of Contents

Chapter 1	25
Introduction	25
1.1. OBJECTIVES AND CHALLENGES OF THE STUDY	26
1.1.1. OBJECTIVE I DEGRADATION AND MINERALIZATION OF CYANOBACTERIAL TOXINS AND WATER TASTE AND ODOR COMPOUNDS UNDER UV-A, SOLAR AND VISIBLE LIGHT	26
1.1.2. Objective II Determination of mechanistic pathways followed during UV-A, solar and visible light degradation of MC-LR in water	27
1.1.3. Objective III Determination of mechanistic pathways followed during UV-A, solar and visible light degradation of CYN in water	27
1.1.4. Objective IV. Determination of mechanistic pathways followed during UV-A and solar light degradation of GSM and MIB in water	28
1.1.5. Objective V. Evaluation of the photocatalytic activity of TiO ₂ based catalysts....	29
CHAPTER 2	31
Cyanotoxins: New generation of water contaminants	31
2.1. INTRODUCTION	31
2.2. CYANOBACTERIA AND CYANOTOXINS	31
2.2.1. Cyclic Peptides - Microcystins and Nodularins.....	32
2.2.2. Alkaloids - Cylindrospermopsin.....	37
2.2.3. Lipopolysaccharides	41
2.3. TASTE AND ODOR COMPOUNDS – GEOSMIN, 2-METHYLISOBORNOEL.....	42
2.4. SUMMARY	44
CHAPTER 3	45
Destruction of cyanobacterial metabolites by conventional and advanced oxidation processes	45
3.1. INTRODUCTION	45
3.2. CONVENTIONAL OXIDATION METHODS.....	45

3.2.1. Chlorination.....	46
3.2.2. Ozonation	47
3.2.3. Oxidation with Permanganate	49
3.3. PHOTOLYSIS AND ADVANCED OXIDATION PROCESSES.....	50
3.3.1. Photolysis	50
3.3.2. UV/H ₂ O ₂ process	51
3.3.3. Ultrasonic degradation	52
3.3.4. TiO ₂ photocatalysis	53
3.3.5. Polyoxometalates photocatalysis	54
3.4. SUMMARY	55

Chapter 4 57

Photocatalysis with Titanium Dioxide and Polyoxometalates..... 57

4.1 INTRODUCTION	57
4.2 TITANIUM DIOXIDE TiO ₂	57
4.2.1. TiO ₂ photocatalysis, new TiO ₂ based photocatalysts	58
4.3. POLYOXOMETALATES	61
4.3.1. Polyoxometalates and their Photocatalytic Cycle.....	61
4.3.1. Comparison with Metal Oxide Particles.....	64

CHAPTER 5..... 67

Materials – Instrumentation – Methods – Experimental 67

5.1. MATERIALS.....	67
5.1.1. TiO ₂ based nanocatalysts	67
5.1.2. Cyanotoxins, Taste and Odor Standards, Chemicals	69
5.2. INSTRUMENTATION.....	69
5.2.1. Analytical Instruments.....	69
5.2.3. Photolysis Systems	70
5.3. METHODS.....	71
5.3.1. HPLC-UV for MC-LR determination	71
5.3.2. HPLC-UV for CYN determination	72
5.3.3. SPME-GC/MS for GSM and MIB determination.....	72

5.3.4. LC-MS/MS for MC-LR Intermediates products.....	73
5.3.5. LC-MS/MS for CYN Intermediates products	73
5.3.6. LLE-GC-MS for GSM and MIB Intermediates products.....	74
5.3.7. Toxicity Measurements	74
5.4. EXPERIMENTAL	78
5.4.1. Degradation Experiments.....	78
5.4.2. Mineralization Experiments	79
5.4.3. Intermediates Elucidation Experiments	79

CHAPTER 6..... 81

Photocatalytic degradation and Mineralization of MC-LR, CYN, GSM and MIB in water under UV-A, Solar and visible light..... 81

6.1. INTRODUCTION	81
6.2. PHOTOCATALYTIC DEGRADATION AND MINERALIZATION OF MC-LR UNDER UV-A AND SOLAR LIGHT	81
6.2.1. Photocatalytic Degrad. and Mineralization of MC-LR under UV-A irradiation	81
6.2.2. Photocatalytic Degradation and Mineralization of MC-LR under solar light.....	86
6.3. PHOTOCATALYTIC DEGRADATION AND MINERALIZATION OF CYN UNDER UV-A AND SOLAR LIGHT	87
6.3.1. Photocatalytic Degradation of CYN under UV-A and solar light.....	88
6.3.2. Photocatalytic mineralization of CYN under UV-A light.....	89
6.4. PHOTOCATALYTIC DEGRADATION AND MINERALIZATION OF GSM AND MIB UNDER UV-A AND SOLAR LIGHT	91
6.4.1. Photocatalytic Degradation of GSM and MIB under UV-A and solar light.....	92
6.4.2. Photocatalytic Mineralization of MIB and GSM under UV-A and solar light irradiation	94
6.5. APPLICATION IN REAL WATER SAMPLES	95
6.6. PHOTOCATALYTIC DEGRAD. OF MC-LR, CYN, GSM AND MIB UNDER VISIBLE LIGHT	97
6.7. CONCLUSIONS	99

CHAPTER 7	101
Degradation Pathway of MC-LR	101
7.1. INTRODUCTION	101
7.2. INTERMEDIATE PRODUCTS OF MC-LR UNDER UV-A AND SOLAR LIGHT USING TiO ₂	102
7.3. TOXICITY MEASUREMENTS	112
7.4. CONCLUSIONS	116
CHAPTER 8	117
Degradation Pathway of CYN	117
8.1. INTRODUCTION	117
8.2. INTERMEDIATE PRODUCTS OF CYN UNDER UV-A AND SOLAR LIGHT USING TiO ₂	117
8.3. TOXICITY EXPERIMENTS CONCERNING CYN	122
8.4. CONCLUSIONS	124
CHAPTER 9	125
Degradation Pathways of GSM and MIB	125
9.1. INTRODUCTION	125
9.2. PHOTOCATALYTIC DEGRADATION OF GSM AND MIB IN THE PRESENCE OF TiO ₂ AND POM, USE OF •OH SCAVENGERS.....	126
9.2.1. Photocatalytic Degradation of GSM and MIB in the presence of TiO ₂ and POM	126
9.2.2. Photocatalytic Degradation of GSM and MIB in the presence of in the presence of •OH radicals scavengers	127
9.3. PHOTOCATALYTIC MINERALIZATION OF GSM AND MIB WITH OF TiO ₂ AND POM	130
9.4. INTERMEDIATE PRODUCTS OF GSM USING TiO ₂ AND POM UNDER UV-A LIGHT	131
9.5. INTERMEDIATE PRODUCTS OF MIB USING TiO ₂ AND POM UNDER UV-A LIGHT	138
9.6. TOXICITY EXPERIMENTS CONCERNING MIB AND GSM	142
9.7. PHOTOCATALYTIC DEGRADATION MECHANISMS OF GSM/MIB IN THE PRESENCE OF SiW ₁₂ O ₄₀ ⁴⁻ AND TiO ₂ : A COMPARISON STUDY.....	143
9.8. CONCLUSIONS	144

CHAPTER 10.....	145
Photocatalytic degrad. of MC-LR, CYN, GSM and MIB in water using TiO₂ under visible light. Unveiling new degradation Pathways	145
10.1. INTRODUCTION	145
10.2. PHOTOCATALYTIC DEGRAD. OF MC-LR, CYN, GSM AND MIB UNDER VISIBLE LIGHT	145
10.3. INTERMEDIATE PRODUCTS OF MC-LR UNDER VISIBLE LIGHT USING TiO ₂	146
10.3.1. Toxicity assessment.....	147
10.4. INTERMEDIATE PRODUCTS OF CYN UNDER VISIBLE LIGHT USING TiO ₂	148
10.5. CONCLUSIONS.....	148
 Chapter 11	 149
Parameters influencing TiO₂ photocatalysis towards degradation of MC-LR, CYN, GSM and MIB in water.....	149
11.1. INTRODUCTION	149
11.2. LIGHT INTENSITY	149
11.3. PRESENCE OF OXYGEN.....	151
11.4. CATALYST LOADING.....	152
11.5. INITIAL CONCENTRATION OF SUBSTRATE.....	153
11.6. ADSORPTION ON CATALYSTS SURFACE.....	155
11.7. INITIAL SOLUTION PH.....	157
11.8. IRRADIATION WAVELENGTH.....	159
11.9. CONCLUSIONS.....	162
 Chapter 12 163	
Recommendations	163
12.1. RECOMMENDATIONS	163
 ABBREVIATIONS	 166
Appendix I	167
References	171

List of Figures

Figure 2.1. Structures of common cyanotoxins produced by cyanobacteria	35
Figure 2.2. Global distribution of algal blooms known to contain CYN or a CYN-analog....	40
Figure 2.3. Structures of (a) geosmin and (b) 2-methylisoborneol.....	43
Figure 6.1. Photocatalytic degradation of MC-LR under UV-A irradiation in the presence of different TiO ₂ based nanostructured materials.....	82
Figure 6.2. Carbon mineralization and time evolution of nitrate, nitrite, ammonium ions and total nitrogen during MC-LR degradation under UV-A irradiation in the presence of Degussa P25 TiO ₂ [20].....	83
Figure 6.3. Mineralization of MC-LR using N-TiO ₂ under UV-A light [20].....	84
Figure 6.4. Mineralization of MC-LR using NF-TiO ₂ under UV-A light.	85
Figure 6.5. Photocatalytic degradation of MC-LR under Solar light irradiation (AM 1.5G), in the presence of TiO ₂ based materials. Experimental conditions: MC-LR C ₀ =10 ppm, catalyst concentration 200 ppm, 25 °C, oxygenated and non buffered solutions.....	86
Figure 6.6. Mineralization of MC-LR using N-TiO ₂ under solar light [20].	87
Figure 6.7. Degradation of CYN (10 mg L ⁻¹) in the absence and presence of photocatalyst (Degussa P25 or Kronos vlp-700, 200 mg L ⁻¹) under UV-A light [277]...	88
Figure 6.8. Photocatalytic degradation of CYN (10 mg L ⁻¹) using TiO ₂ photocatalysts (200 mg L ⁻¹) under solar light (AM 1.5 G) [277].....	89
Figure 6.9. Carbon mineralization and time evolution of total nitrogen (NO ₂ ⁻ , NO ₃ ⁻ and NH ₄ ⁺ ions) and total sulphur (SO ₄ ²⁻ ion) during CYN degradation under UV-A irradiation in the presence of P25 TiO ₂ [277].	90
Figure 6.10. Photocatalytic degradation of 1 mgL ⁻¹ GSM under UV-A (λ _{max} =365 nm) in the presence of different TiO ₂ based nanostructured materials.	92
Figure 6.11. Photocatalytic degradation of 1 mgL ⁻¹ MIB under UV-A (λ _{max} =365 nm) in the presence of different TiO ₂ based nanostructured materials.	92
Figure 6.12. Photocatalytic degradation of 1 mgL ⁻¹ GSM under solar light (AM 1.5 G) in the presence of different TiO ₂ based nanostructured materials.	93

Figure 6.13. Photocatalytic degradation of 1 mgL ⁻¹ MIB under solar light (AM 1.5 G) in the presence of different TiO ₂ based nanostructured materials.	93
Figure 6.14. Photocatalytic Mineralization of GSM and MIB under UV-A (λ_{\max} = 365 nm) irradiation using Degussa P25 TiO ₂ catalyst.	94
Figure 6.15. Photocatalytic Mineralization of GSM and MIB under solar light (AM 1.5 G) irradiation using GO- TiO ₂ catalyst.	95
Figure 6.16. Photocatalytic degradation of MC-LR (10 mg L ⁻¹) under solar light irradiation, using GO-TiO ₂ photocatalyst (200 mg L ⁻¹) in real water samples [270].	97
Figure 6.17. Photocatalytic degradation of MIB and GSM (1 mg L ⁻¹) under solar light irradiation, using GO-TiO ₂ photocatalyst (200 mg L ⁻¹) in real water samples [270].	97
Figure 6.18. Photocatalytic degradation of MC-LR (10 mg L ⁻¹) under visible light illumination in the presence of TiO ₂ nanomaterials (200 mg L ⁻¹).	98
Figure 6.19. Photocatalytic degradation of CYN (10 mg L ⁻¹) using TiO ₂ photocatalysts (200 mg L ⁻¹) under solar light (AM 1.5 G) [277].	99
Figure 7.1. Chromatograms resulted from MC-LR photocatalytic degradation using (a) Degussa P25 under UV-A irradiation and (b) GO-TiO ₂ under solar light irradiation [270].	104
Figure 7.2. LC-MS chromatograms of MC-LR photocatalytic degradation in the presence of Degussa P25 after irradiation with UV-A for 5 min [270].	105
Figure 7.3. Residual toxicity measured during the photocatalytic degradation of MC-LR (10 mg L ⁻¹) under UV-A (λ_{\max} =365 nm) irradiation in the presence of Degussa P25 and GO-TiO ₂ (200 mg L ⁻¹) [270].	112
Figure 7.4. Residual toxicity measured during the photocatalytic degradation of MC-LR (10 mg L ⁻¹) solar light (AM 1.5 G) irradiation in the presence of Degussa P25 and GO-TiO ₂ (200 mg L ⁻¹) [270].	113
Figure 7.5. Enzyme activity (Toxicity) and mineralization extent (TOC) during MC-LR photocatalytic degradation using Degussa P25 TiO ₂ , under UV-A.	114
Figure 7.6. Enzyme activity (Toxicity) and mineralization extent (TOC) during MC-LR photocatalytic degradation using N-TiO ₂ , under UV-A.	114
Figure 7.7. Enzyme activity (Toxicity) and mineralization extent (TOC) during MC-LR photocatalytic degradation using NF-TiO ₂ , under UV-A.	114

Figure 7.8. Enzyme activity (Toxicity) and mineralization extent (TOC) during MC-LR photocatalytic degradation using N-TiO ₂ , solar light.....	114
Figure 7.9. PPIA measurements and evolution of products <i>m/z</i> 1009.5, 1027.5 and 1045.5 during photocatalytic degradation of MC-LR (10 mg L ⁻¹) using Degussa P25 TiO ₂ (200 mg L ⁻¹) under UV-A irradiation [284].....	115
Figure 7.10. Evolution of products <i>m/z</i> 781.5 and 1015.5 during photocatalytic degradation of MC-LR (10 mg L ⁻¹) using Degussa P25 TiO ₂ (200 mg L ⁻¹) under UV-A or GO-TiO ₂ (200 mg L ⁻¹) under solar light irradiation [284].....	116
Figure 8.1. Relative abundance chromatograms for products <i>m/z</i> (a) 432 and (b) 287 of CYN photocatalytic degradation in the presence of Degussa P25 after 3 min of irradiation under UV-A light [277].	118
Figure 8.2. Relative abundance chromatograms for products <i>m/z</i> (a) 227, (b) 320, (c) 338, (d) 350, (e) 375, (f) 434 and (g) 448 of CYN photocatalytic degradation in the presence of Degussa P25 after 3 min of irradiation under UV-A light [277].	119
Figure 9.1. Photocatalytic degradation of GSM (1 mg L ⁻¹) under UV-A (λ_{\max} = 365 nm) irradiation with (a) SiW ₁₂ O ₄₀ ⁴⁻ (7x10 ⁻⁴ M, 200 mg L ⁻¹) and (b) TiO ₂ (200 mg L ⁻¹) in the presence and absence of scavengers. Conditions (♦) Photolysis, (●) No scavenger, (▼) KBr and (■) TBA [245].	128
Figure 9.2. Photocatalytic degradation of MIB (1 mg L ⁻¹) under UV-A (λ_{\max} = 365 nm) irradiation with (a) SiW ₁₂ O ₄₀ ⁴⁻ (7x10 ⁻⁴ M, 200 mg L ⁻¹) and (b) TiO ₂ (200 mg L ⁻¹) in the presence and absence of scavengers. Conditions (♦) Photolysis, (●) No scavenger, (▼) KBr and (■) TBA [245].	129
Figure 10.1. Photocatalytic degradation of target analytes using Kronos TiO ₂ under visible light.	146
Figure 10.2. Evolution of products during the photocatalytic degradation of MC-LR under visible light.	147
Figure 10.3. Evolution of products during the photocatalytic degradation of CYN under visible light.	148
Figure 11.1. Photocatalytic degradation of MC-LR (10 mg L ⁻¹) using of Degussa P25 TiO ₂ (200 mg L ⁻¹) under light sources with different intensity (150 W Xe lamp and Black light) [284].	150

Figure 11.2. Photocatalytic degradation of MC-LR (10 mg L ⁻¹) under UV-A ($\lambda \geq 320$ nm) irradiation in the presence of Degussa P25 TiO ₂ (1000 mg L ⁻¹) with different oxygen concentrations in the solution (deaerated, air saturated and oxygen saturated) [284].	151
Figure 11.3. Dependence of initial rate of MC-LR degradation towards TiO ₂ loading. UV-A irradiation ($\lambda_{\max}=365$ nm) in the presence of Degussa P25 TiO ₂ ; MC-LR 10 mg L ⁻¹ [284].	152
Figure 11.4.	153
Figure 11.5. Variation of the initial rate of the GSM and MIB degradation as a function of increased initial concentration; Inesert: Photocatalytic degradation of (a) GSM and (b) MIB (2×10^{-3} , 0.2 and 1 mg L ⁻¹) under UV-A ($\lambda_{\max} = 365$ nm) irradiation in the presence of Degussa P25 TiO ₂ (200 mg L ⁻¹) [284].	154
Figure 11.6. Adsorption% of MC-LR on Degussa P25 TiO ₂ , Kronos TiO ₂ , Ref-TiO ₂ , N-TiO ₂ , NF-TiO ₂ , ECT-10213t and GO-TiO ₂ ; 10 mgL ⁻¹ initial concentration of MC-LR and 200 mgL ⁻¹ of catalyst loading at pH 5.7 [284].	155
Figure 11.7. Adsorption% of (a) GSM and (b) MIB on Degussa P25 TiO ₂ , Kronos TiO ₂ , Ref-TiO ₂ , N-TiO ₂ , NF-TiO ₂ , ECT-10213t and GO-TiO ₂ ; 10 mgL ⁻¹ initial concentration of MC-LR and 200 mgL ⁻¹ of catalyst loading at pH 5.7 [284].	156
Figure 11.8. Adsorption in dark of CYN (10 mg L ⁻¹) under UV-A using Degussa P25 and Kronos vlp-700 photocatalysts (200 mg L ⁻¹) [284].	157
Figure 11.9. Photocatalytic degradation of MC-LR (10 mg L ⁻¹) under UV-A irradiation ($\lambda_{\max}=365$ nm) in the presence of Degussa P25 TiO ₂ (200 mg L ⁻¹) at pH 3, 5.7 and 7 [284].	158
Figure 11.10. Initial rates of photocatalytic degradation of GSM and MIB (1 mg L ⁻¹) under UV-A irradiation ($\lambda_{\max} = 365$ nm) in the presence of Degussa P25 TiO ₂ (200 mg L ⁻¹) at pH 3, 5.7 and 7 [284].	159
Figure 11.11. Photocatalytic degradation of MC-LR (10 mg L ⁻¹) under using a cut-off filter at (a) 420 nm and at (b) 435 nm in the presence of TiO ₂ nanomaterials (200 mg L ⁻¹). (c) The transmittance spectrum of the 420 nm and 435 nm cut-off filters [284].	161

LIST OF SCHEMES

Scheme 7.1. Objective of Chapter 7	101
Scheme 8.1. Observed intermediate products and proposed degradation pathway for CYN under UV-A or solar light irradiation using TiO ₂	120
Scheme 9.1. Objective of Chapter 9	126
Scheme 9.2. Intermediates formed during photocatalytic degradation of GSM by SiW ₁₂ O ₄₀ ⁴⁻ or TiO ₂	136
Scheme 9.3. Intermediates formed during photolysis and photocatalytic degradation of MIB by SiW ₁₂ O ₄₀ ⁴⁻ or TiO ₂	141

LIST OF TABLES

Table 2.1. Cyanobacteria known to produce the major classes of cyanotoxins.....	36
Table 5.1. Gradient elution program applied with Agilent Eclipse XDB C-18 column.	72
Table 5.2. GC conditions for GSM and MIB quantification	72
Table 5.3. The MS conditions are as in the following table:.....	73
Table 6.1. Physicochemical parameters of surface water samples (before spiking).....	96
Table 7.1. Products observed from MC-LR degradation using Degussa P25/UV-A and GO-TiO ₂ /solar light irradiation	106
Table 7.2. Proposed structure and molecular formula of the new intermediates observed from MC-LR degradation using Degussa P25/UV-A and GO-TiO ₂ /solar light irradiation	108
Table 8.1. CYN standard solutions (0.0065 - 20 ppm).....	122
Table 8.2. CYN degradation under UV-A using Degussa P25.....	123
Table 8.3. CYN degradation under solar	123
Table 8.4. CYN degradation under solar light.....	123
Table 9.1. Observed rate constants from the initial rates of photodegradation of GSM in the presence of POM or TiO ₂ and scavengers, calculated from Figure 9.1	129
Table 9.2. Observed rate constants from the initial rates of photodegradation of MIB in the presence of POM or TiO ₂ and scavengers, calculated from Figure 9.2	130
Table 9.3. Intermediates identified during the photocatalytic degradation of GSM with their retention time (t_R) and their spectral characteristics (M^+ , m/z), in Scheme 9.2...	135
Table 9.4. Intermediates identified during photolysis and the photocatalytic degradation of MIB with their spectral characteristics (M^+ , m/z), in Scheme 9.3	140
Table 9.5. Odors standard solutions (0.125 - 1 ppm).	142
Table 9.6. Odors degradation under UV-A using Degussa P25	143
Table 9.7. Odors degradation under UV-A using SiW ₁₂ O ₄₀ ⁴⁻	143

Chapter 1

Introduction

Cyanobacteria (blue-green algae) are considered an important water quality problem, since several genera can produce toxins, called cyanotoxins that are harmful to human health. Continuous occurrence of associated human and animal toxicoses confirms the health significance of these products, which include genotoxic-, tumour-promoting-, hepato- and neurotoxic agents [1, 2]. Because of cyanotoxins increasing appearance in water resources and their high lethality, cyanotoxins are considered of a new class of emerging contaminants.

Microcystins (MCs, MC-LR) are within the family of cyanotoxins and present high hepatotoxicity. During the last years there is a growing concern regarding the health effects of MCs, because they act as tumor promoters, through the inhibition of protein phosphatases 1 and 2A, which play a key role in cell regulation [3]. In response to this concern, WHO has recommended for provisional adoption the value of 1 µg/L as a Guideline Value for MC-LR concentration in drinking water [4]. Humans are exposed to toxigenic cyanobacteria via drinking water and accidental ingestion while engaging in recreational activities.

Cylindrospermopsin (CYN) an alkaloid-type cyanotoxin has been shown to be cytotoxic, dermatotoxic, genotoxic, hepatotoxic and may be carcinogenic. It was first isolated in a tropical cyanobacteria, *Cylindrospermopsis raciborskii*. The toxin is now approaching an almost cosmopolitan distribution pattern with CYN producers being recorded from habitats including lakes, reservoirs, rivers, ponds and dams [5].

In addition, potential production of taste and odor compounds from cyanobacteria can cause many water quality concerns. The most usually occurring taste and odor compounds produced by cyanobacterial blooms as secondary metabolites, are geosmin (GSM) and 2-methylisoborneol (MIB) [6]. They are often found in surface waters, such as lakes, rivers and eutrophic drinking water reservoirs [7]. GSM has a distinct earthy-muddy flavor and aroma, and is responsible for the earthy taste of and is often responsible for the musty taste and odor to drinking water and to malodorous off-flavor in fish and aquaculture products. Human nose can detect the odor of GSM and MIB and

their threshold odor concentration in water has been reported to be 9 and 4 pg mL^{-1} respectively [8, 9].

Communities whose water supply depends on surface water periodically experience episodes of unpleasant water. Upon cellular death of these cyanobacteria, GSM/MIB are released into the local water supply, impacting greatly on the aesthetic quality and general consumer acceptability of drinking water [10]. For these reasons, the removal of these compounds from water is very important for its use and consumption.

1.1. Objectives and Challenges of the Study

This dissertation aimed in the photocatalytic degradation and mineralization of cyanobacteria metabolites such as cyanotoxins (MC-LR and CYN) and taste and odor compounds (GSM and MIB). TiO_2 photocatalysts (Degussa P25, Kronos vlp-7000, Ref-TiO₂, N-TiO₂, NF-TiO₂, GO-TiO₂ and ECT-1023t) were tested for their photocatalytic ability towards degradation and mineralization of the analytes from aqueous solutions using UV-A, solar and visible light. Parameters like light intensity, presence of oxygen, catalyst loading, initial concentration of substrate, adsorption, pH, different irradiation wavelength, were investigated for their influence in the process. Also, mineralization and the identification of intermediate products and their toxicity under different experimental conditions was studied. Emphasis was given to the mechanistic understanding of the process by identification of intermediate and final products formed during photocatalysis process and a complete degradation pathway is proposed for MC-LR, CYN, GSM and MIB. Assessment of the residual toxicity during the course of treatment showed that detoxification of the solutions was achieved.

1.1.1. Objective I Degradation and mineralization of cyanobacterial toxins and water taste and odor compounds under UV-A, solar and visible light

A variety of traditional water treatment methods were used for the removal of MC-LR, CYN, GSM and MIB but with limited success. Consequently, research on new methods for water purification is developing in different ways, including advanced oxidation processes (AOPs) which have been receiving increased attention for the detoxification of the aquatic environment. Among those, TiO_2 photocatalysis demonstrated [11-18, 20]

that can be effectively applied for the degradation of cyanotoxins and taste and odor compounds in aqueous solution [15, 20-24], while studies concerning the mineralization of cyanobacterial metabolites are limited.

This dissertation aimed in the study of the photocatalytic degradation and mineralization of cyanobacterial metabolites (MC-LR, CYN, GSM and MIB) using TiO₂ based nanomaterials under UV-A, solar and visible light irradiation. Within the study of the mineralization of each compound, final products will be determined using TOC and inorganic ions (NO₂⁻, NO₃⁻, SO₄²⁻ and NH₄⁺) measurements.

1.1.2. Objective II Determination of mechanistic pathways followed during UV-A, solar and visible light degradation of MC-LR in water

Even though employing TiO₂ photocatalysis has been proved to be very useful and successive for the degradation of organic pollutants in aquatic environment, the elucidation of degradation pathway and the determination of intermediate products, is also necessary for the verification of detoxification. So far, a number of studies have examined degradation pathways of MC-LR when conventional oxidants or AOPs are applied, including ozonation [25, 26], chlorination [27], ultra-sonication [28], photolysis [29], TiO₂/UV-A [18, 19, 30, 31] and N-TiO₂/UV-A [18]. Aim of this study was also to study the reaction mechanism for the photocatalytic degradation of MC-LR, through identification of intermediate products formed during the process under UV-A and solar light and compare. Assessment of the residual toxicity was also carried out using the protein phosphatase inhibition assay (PPIA), enabling the evaluation of the detoxification activity of the nanostructured TiO₂ photocatalysts under different experimental conditions.

1.1.3. Objective III Determination of mechanistic pathways followed during UV-A, solar and visible light degradation of CYN in water

So far, studies have demonstrated that TiO₂ photocatalysis can effectively destroy CYN in aqueous solution [21, 22]. However, the assessment of CYN disappearance is not sufficient to ensure the absence of residual products since the photocatalytic treatment is a complex procedure leading to the formation of degradation products, which in some

cases may be more toxic and stable than the parent compound. To the best of my knowledge so far, no other study dealt with identification of intermediate products of CYN formed during the photocatalytic process using TiO₂. Based on the identified intermediates, a degradation pathway can be proposed.

1.1.4. Objective IV. Determination of mechanistic pathways followed during UV-A and solar light degradation of GSM and MIB in water

Polyoxometalates (POM) have previously been used for degradation of several organic pollutants in water [32-36]. In almost all cases final degradation products were CO₂, H₂O and inorganic anions. POM are acid condensation products, mainly of molybdenum and tungsten [37-39], that upon excitation with near visible and UV light become powerful oxidizing reagents capable of destroying a great variety of organic compounds in aqueous solutions through a hole-electron ($h^+ + e^-$) mechanism [40-42]. Hydroxyl radicals ($\cdot\text{OH}$) generated by reaction of POM with H₂O seem to play a key role in the process [42]. Oxygen oxidizes (regenerates) the catalyst and through reductive activation may or may not participate further in the process, depending on the substrate [43]. Due to their photocatalytic performance, POM can be recognized as an AOP [33-35]. POM are almost as effective as the widely published TiO₂ [42], presenting similar behaviour with the semi-conducting oxide [42]. $\cdot\text{OH}$ radicals have been used to explain similarities of the two photocatalysts although in some cases the nature of substrate and the mode of investigation seem to play an important role in the process [44].

Objective of this work was to study and compare the photocatalytic degradation and mineralization of GSM and MIB in water using a representative POM (SiW₁₂O₄₀⁴⁻) and TiO₂. The comparative study of processes included also the identification of intermediate products formed as well as the effect of hydroxyl radical scavengers. To the best of my knowledge (a) the photocatalytic degradation of both GSM and MIB with POM and (b) the mineralization and the complete degradation pathways in the presence of POM or TiO₂ is reported here for the first time.

1.1.5. Objective V. Evaluation of the photocatalytic activity of TiO₂ based catalysts

Heterogeneous TiO₂ photocatalysis has been considered as a very promising AOP, which in combination with solar energy could effectively address the ever increasing concerns for pollution abatement and water purification. Although it appears to degrade a great variety of compounds, it requires UV irradiation to overcome its wide band gap-energy. Consequently, research on the development of new TiO₂ based catalysts has been receiving increased attention. Evaluation of the photocatalytic activity of TiO₂ based photocatalysts is highly depended on a number of parameters that govern the kinetics of photodegradation and mineralization. Parameters that were taken under consideration in this study for the photocatalytic degradation of cyanobacterial toxin MC-LR, CYN and water taste and odor compounds GSM and MIB, might be the light intensity, dissolved oxygen concentration, catalyst loading, initial concentration of the substrate, adsorption, pH, light wavelength and even mineralization, intermediate products and toxicity. All those parameters are able to affect in a different way the photocatalytic activity of a catalyst, and the evaluation should be performed under investigation of those.

CHAPTER 2

Cyanotoxins: New generation of water contaminants

2.1. Introduction

Cyanobacteria belong to a group of prokaryotic organisms identified by a variety of names, including cyanobacteria, blue-greens, blue-green algae, myxophyceans, cyanophytes, cyanophyceans, and cyanoprokaryotes. These primitive and highly adaptable organisms are most often referred to as either blue-green algae or cyanobacteria [45].

They produce a wide range of biologically active compounds in marine, transient, freshwater and terrestrial ecosystems, with some of them showing very high toxicity (mg kg^{-1} body weight) in mammalian systems. Continuous occurrence of associated human and animal toxicoses confirms the health significance of these products, which include genotoxic-, tumour-promoting-, hepato- and neurotoxic agents [1].

Cyanobacteria secondary metabolites play a key role in their interactions with the environment. Although the functions of some of these secondary metabolites are still unknown, cyanobacteria have undergone to develop strategies beneficial for their survival and/or dominance in an environment. Some of these secondary metabolites include taste and odor compounds, terpenoids, anti-microbials, metal chelators, lactones, protease inhibitors, indole alkaloids, and most importantly potent toxins frequently called cyanobacterial toxins or cyanotoxins known to affect a wide range of living organisms [2].

2.2. Cyanobacteria and Cyanotoxins

Cyanotoxins are formed at all stages of cyanobacteria growth and are generally found in the cell (intracellular toxin) from where they are released into the surrounding medium via secretory pathways, senescence or cell lysis (extracellular toxin). Cyanotoxins are classified into three main groups based on their chemical structure, i.e. cyclic peptides, alkaloids, and lipopolysaccharides [46].

2.2.1. Cyclic Peptides - Microcystins and Nodularins

These cyclic peptides comprise two groups of molecules, the cyclic heptapeptide microcystins and the cyclic pentapeptide nodularins.

Microcystins (MCs) are produced by various cyanobacteria genera such as *Microcystis*, *Anabaena*, *Plankothrix* and *Nostoc* [47]. They have the general structure cyclo(-d-Ala-L-X-D-erythro- β -ethylAsp(iso-linkage)-l -Y-Adda-D-Glu(iso-linkage)- N -methyldehydro-Ala) where Adda is the novel β -amino acid, 3-amino-9-methoxy-2,6,8- trimethyl-10-phenyldeca-4 (E), 6(E)-dienoic acid and X and Y are sites of amino acid substitutions at positions 2 and 4 of the peptide ring. For example, microcystin-LR possesses L-leucine and L-arginine at the variable amino acid positions and this is the basis for the nomenclature of microcystin variants [48], as shown in Figure 2.1.a. The Adda is the amino acid common to all cyclic cyanobacterial toxins.

To date, more than 90 variants of MCs have been isolated. The most common variant is **Microcystin-LR (MC-LR)**. Other common MCs variants include YR, RR, and LW. MCs are inhibitors of serine/threonine phosphatases 1 (PP1), PP2A, PP3 and PP4 leading to excessive phosphorylation of proteins in the cells [49]. Protein phosphatases play a central role in the control of many cellular processes, including the control of the cell cycle, metabolic regulation, and growth factor signaling pathways, protein synthesis, transcriptional regulation and neurotransmission in animals and plants. MCs are potent tumor promoters and cause an acute and chronic hazard to wildlife, domestic animals and humans. Some symptoms include vomiting, diarrhea, anorexia, cold extremities, general malaise, and pallor of the mucous membranes. The major concern, however, is the long-term chronic human health hazard. Continuous sublethal or low-level exposures to MCs can potentially lead to the development of gastrointestinal and liver disorders [50-52].

Microcystin production appears to be widespread, throughout cyanobacterial taxa, with examples from fresh, transient and marine waters, and terrestrial environments. Microcystin-producers in the latter include free-living [53] and symbiotic cyanobacteria (Table 2.1.) [1].

Nodularins (NODs) are another group of potent inhibitor of eukaryotic protein phosphatases. NODs are cyclic pentapeptides closely related to the MC toxins, which are two amino acids smaller than microcystins, have the general structure cyclo(-D-erythro- b –methylAsp (iso-linkage) –L –Y -Adda -DGlu (iso - linkage) -2- methylamino - 2 (Z)- dehydrobutyric acid). The nodularins generally show less structural variability than the microcystins and L-Arg is often the amino acid at position Y in nodularin-R [54]. There are about 10 variants of NODs of which NOD-R (Figure 2.1.b) with the variable L-amino acid to be arginine, is the most commonly found in blooms. They primarily are regarded as potent hepatotoxins since their main target organ is the liver and enters the hepatocyte via the bile-acid transport system and NOD was first isolated from cyanobacterium, *Nodularia spumigena*, in brackish water in New Zealand [48]. Nodularin production, by contrast to MCs, currently appears to be restricted to *Nodularia spumigena*, with the possibility of a similar pentapeptide in the marine sponge *Theonella*, originating from a cyanobacterial symbiont (Table 2.1.).

The drinking water industry is constantly challenged with surface water contaminants that must be removed to protect human health. Toxic cyanobacterial blooms are an emerging issue worldwide due to increased source water nutrient pollution caused by eutrophication. Stable nature and persistence of peptide cyanotoxins pose a challenge to public health authorities and water treatment plant operators. The cyclic structure and presence of novel amino acids render the MCs resistant to heat, hydrolysis, and oxidation and they can persist for months or even years in cooler, dark bodies of water [55].

Human and animal exposure to these toxins occurs most frequently through ingestion of water, through drinking or during recreational activities in which water is swallowed. Microcystin initially binds rapidly to PP1 and PP2A followed by a slower covalent interaction (within hours). Inactivation of PP1/PP2A involves the interaction of the nucleophilic phosphatase residue and the Mdha in the toxin which precedes covalent complex formation. The covalent adduct is formed between the cysteine residues of PP1 and PP2A and the bound toxin [56, 57].

Varying levels of toxicity have been reported for each microcystin isoform. For example, the LD50 of the most common isoform, MC-LR, is 50 µg per kilogram of body weight in mice [58], while the MC-RR requires a significantly higher dose of 600 µg to produce the same lethal effect [59]. Microcystins can accumulate in multiple organs and tissues

in mammals and fish: heart, liver, gonad, lung, brain and kidney with consequent physiological, tissue and cell damage [60, 61]. In mammals, microcystins and nodularins in acute doses can cause death by hypovolaemic shock. Several studies showed that chronic exposure to microcystin can indeed promote skin and liver tumors in rats and mice [62]. Epidemiological data suggest that hepatocellular carcinoma may also be observed in humans [63]. The consumption of water containing toxic blooms with NOD has led to the death of domestic and native animals by massive liver haemorrhage [48]. In sub-acute doses, nodularin, like microcystin, is thought to act as a liver tumor initiator and promoter [64].

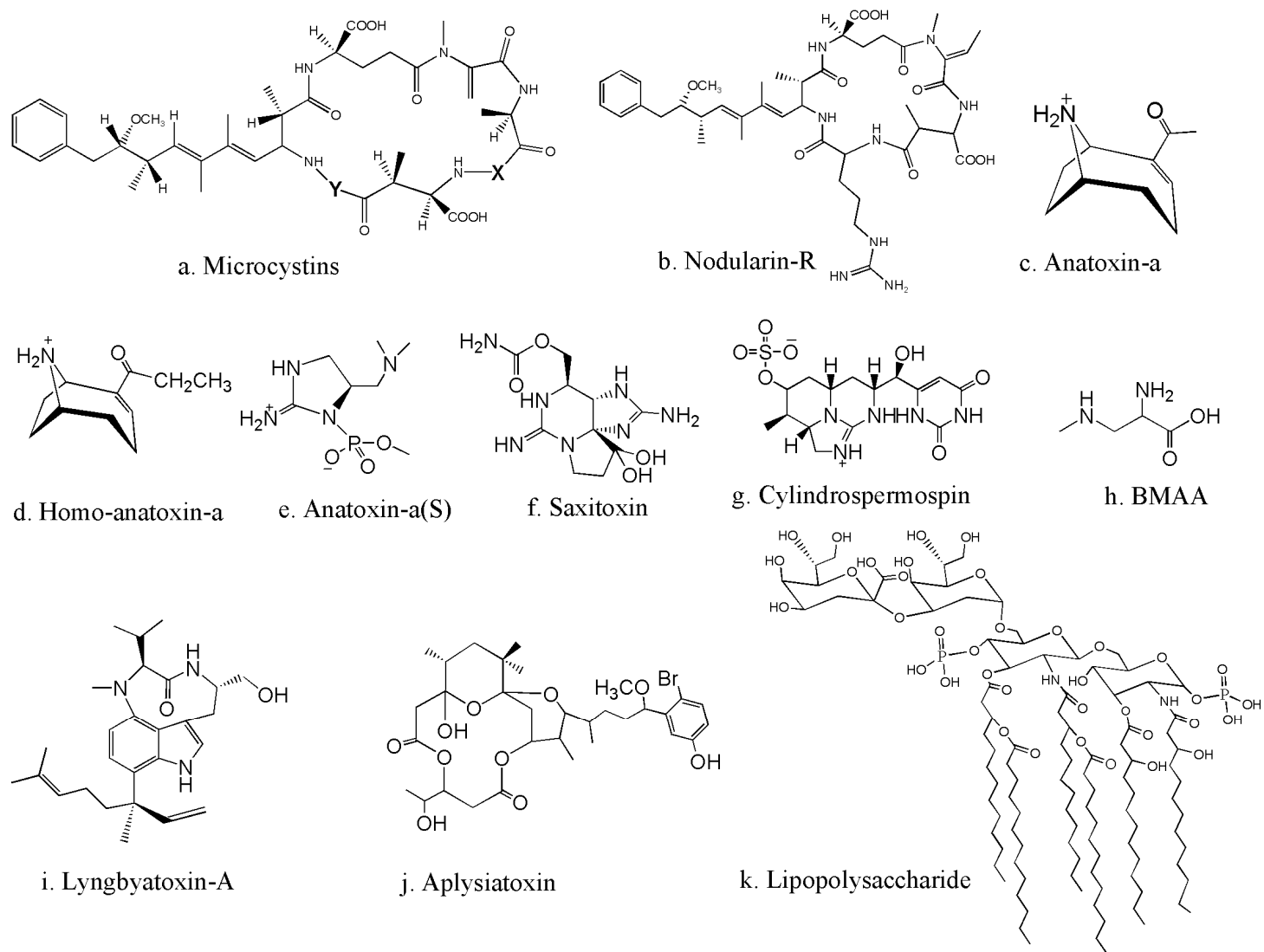


Figure 2.1. Structures of common cyanotoxins produced by cyanobacteria [2].

Table 2.1. Cyanobacteria known to produce the major classes of cyanotoxins (Adapted from Sivonen and Jones 1999 [65]; Dow and Swoboda 2000 [66]; Codd *et al.* 2005 [67]) [1]

Toxin	Published producers
Microcystins	<p>Chroococcales: <i>Microcystis</i> spp., <i>M. aeruginosa</i>, <i>M. viridis</i></p> <p>Oscillatoriales: <i>Oscillatoria</i> (<i>Planktothrix</i>) <i>agardhii</i>, <i>Plectonema boryanum</i>, <i>Phormidium corium</i>, ^a<i>Phormidium splendidum</i>, ^b<i>Arthrospira fusiformis</i> ^c</p> <p>Nostocales: <i>Anabaenasp.</i>, <i>Anabaena flos-aquae</i>, <i>A. subcylindrica</i>, ^a<i>A. variabilis</i>, ^a<i>Nostocsp.</i>, <i>Nostoc spongiaeforme</i>, ^a<i>Anabaenopsissp.</i>, <i>Gloeotrichia echinulata</i>, ^d<i>Rivularia biasoletiana</i>, <i>R. haematites</i>, ^b<i>Tolypothrix distorta</i>^b</p> <p>Stigonematales: <i>Hapalosiphon</i> sp.</p>
Nodularins	Nostocales: <i>Nodularia spumigena</i>
Anatoxin-a and homoanatoxin-a	<p>Oscillatoriales: <i>Arthrospira fusiformis</i>, <i>Phormidium formosum</i>, ^e<i>Phormidium</i> sp., <i>Oscillatoria</i> sp.</p> <p>Nostocales: <i>Anabaena</i> spp., <i>Aphanizomenon</i> sp., <i>Anabaena flos-aquae</i>, <i>Anabaena planktonica</i>, <i>Cylindrospermum</i> sp., <i>Raphidiopsis mediterranea</i></p>
Anatoxin-a(S)	Nostocales: <i>Anabaena flos-aquae</i> , <i>Anabaena lemmermannii</i>
Saxitoxins	<p>Oscillatoriales: <i>Lyngbya wollei</i>, <i>Planktothrix</i> sp.</p> <p>Nostocales: <i>Aphanizomenon flos-aquae</i>, <i>Anabaena circinalis</i>, <i>Cylindrospermopsis raciborskii</i></p>
Cylindrospermopsins	<p>Nostocales: <i>Cylindrospermopsis raciborskii</i>, <i>Aphanizomenon ovalisporum</i>, <i>Anabaena</i> sp., <i>Anabaena lapponica</i>, ^{f,g}<i>Raphidiopsis curvata</i></p> <p>Stigonematales: <i>Umezakia natans</i></p>

^a Mohamed *et al.* (2006), ^b Aboal *et al.* (2005), ^c Ballot *et al.* (2004), ^d Carey *et al.* (2007), ^e Skulberg *et al.* (1992), ^f Spoof *et al.* (2006), ^g Kokociński *et al.* (2009)

2.2.2. Alkaloids - Cylindrospermopsin

Alkaloids are compounds produced by cyanobacteria that contain mostly basic nitrogen atoms and generally exhibit bioactivities and pharmacologic effects in humans, animals, and plants. Alkaloid neurotoxins are mostly produced by species and strains of *Anabaena*, *Aphanizomenon*, *Planktothrix* (*Oscillatoria*), *Cylindrospermopsis*, *Microcystis* and *Trichodesmium* [68].

Anatoxins [anatoxin-a, homoanatoxin-a and anatoxin-a(S)] which are commonly known as fast death factor, are neurotoxic alkaloids that can also cause gastrointestinal irritation and “swimmer’s itch”. They were also implicated in fatal and nonfatal poisonings in humans, dogs, livestock, fish and waterfowl that ingested water containing cyanobacterial blooms producing the toxin. Anatoxin-a (ana-a) (Figure 2.1.c) is a bicyclic amine neurotoxin which is an analogue of acetylcholine was the first toxin to be structurally characterised from a cyanobacterium [69, 70], this neurotoxin acts rapidly in mammalian and avian systems, with a toxic dose being able to kill mice in under 20 min. Anatoxin-a has been identified in planktonic species/strains of *Anabaena*, *Arthrospira*, *Aphanizomenon*, *Planktothrix* and *Raphidiopsis*, and in mats of benthic *Oscillatoria* (*Phormidium*). Ana-a binds to and stimulates the nicotinic acetylcholine receptor 3.6 times greater than acetylcholine. When anatoxin-a binds to acetylcholine receptors, it is not degraded by cholinesterase or any other cellular enzymes resulting in muscle cells continuous stimulation that causes muscular twitching, fatigue, and paralysis. Severe over-stimulation of the respiratory muscle may result in respiratory arrest and rapid death [71] with such paralysis been observed for example in birds, where contraction of muscles at the base of the neck results in opisthotonus: the forced positioning of the bird’s neck and head along its back. Homoanatoxin-a (Figure 2.1.d) is a methylated variant of anatoxin-a, and is of similar toxicity to anatoxin-a [72]. Anatoxins share toxicological properties and are analogs of cocaine. The phosphorylated cyclic *N*-hydroxyguanine anatoxin-a(S) [ana-a(S)] (Figure 2e) Ana-a(S) is a potent acetylcholinesterase inhibitor and 10 times more toxic than ana-a [73]. Like synthetic organophosphorus pesticides, anatoxin-a(S) causes hypersalivation (hence the suffix “S”) and lachrymation in mammals. Anatoxin-a(S) production has so far only been found in strains of *Anabaena flos-aquae* and *Anabaena lemmermannii* [74-76] and has been found to be responsible for wildlife poisonings.

The most significant harmful algal bloom toxins are commonly known as paralytic shellfish poisons (PSPs, “red tides” toxins) [77], with this name applied since human illness and deaths have been caused by the consumption of shell fish contaminated after filter-feeding on marine dinoflagellates. PSPs are neurotoxins produced by microscopic algae, such as dinoflagellates, diatoms, and cyanobacteria. PSPs comprise of over 21 analogues have been identified in strains and environmental samples of the fresh and transient water genera *Anabaena*, *Aphanizomenon*, *Planktothrix*, *Cylindrospermopsis* and *Lyngbya*, with varying toxicity and are classified into saxitoxins, neosaxitoxins, gonyautoxins, decarbamoyl gonyautoxins and decarbamoyl saxitoxins, depending upon the functional groups in their molecule. Saxitoxin (STX) (Figure 2f) is the most toxic cyanobacterial toxin ($LD_{50} = 5 \mu\text{g}/\text{kg}$) and is 1000 times more toxic than the nerve gas sarin and a single dose of 200 μg is fatal to human. Produced by at least eight species of marine dinoflagellates, evidence for saxitoxin production by marine macroalgae also exists and it is possible that saxitoxins are produced by marine bacteria, including free-living species and bacterial symbionts associated with dinoflagellates [78].

Saxitoxins block voltage-gated sodium channels in excitable membranes by reversible binding to specific regions of the saxiphilin protein [78-80], inhibiting the generation of functional action potential in nerves and muscle fibres and can rapidly (minutes) lead to paralysis and death by respiratory arrest. Are classified as Scheduled Chemical Weapons [81, 82].

Cylindrospermopsin (CYN) (Figure 2.1.g) is a tricyclic guanidine alkaloid and has been shown to be cytotoxic, dermatotoxic, genotoxic, hepatotoxic *in vivo*, developmentally toxic, and may be carcinogenic. The toxin molecule is a sulfated guanidinium zwitterion and is stable in varying heat, light and pH conditions [83]. It is also highly water-soluble, and has a relatively low molecular weight of 415 Daltons [84]. At present, three structural variants of cylindrospermopsin have been identified: cylindrospermopsin, 7-epicylindrospermopsin and deoxycylindrospermopsin and it is unclear if 7-epi-CYN and 7-deoxy-CYN are precursors, CYN variants, or degradation products [85]. It was first isolated in a tropical cyanobacteria, *Cylindrospermopsis raciborskii* which is present in rivers, lakes, and water supply reservoirs [86]. This organism is believed to be responsible for a major human poisoning in the “Palm Island mystery disease”, a serious incident of human poisoning from cyanobacterial toxins in Australia, in 1979 [87]. Cylindrospermopsin and 7-epi-CYN showed similar toxicity in

mouse bioassay [88]. The 7-deoxy-CYN (no hydroxyl group in C-7) is generally nontoxic in mouse bioassay by intraperitoneal injection exhibiting about 1/10th the toxicity to that of CYN [89], however, it was shown to be cytotoxic and a potent inhibitor of protein synthesis and cell proliferation *in vitro* similar to CYN [90, 91]. Toxicity assessment of breakdown products of cylindrospermopsin has indicated that the uracil moiety of the molecule is necessary for toxicity [92]. The pathology of mice administered with cylindrospermopsin indicated that this cyanotoxin causes multiple organ and tissue damage [93]. CYN has been shown to inhibit glutathione and cytochrome P450; and induces breaks and adducts formation of DNA. CYNs are produced by species such as *Anabaena bergii*, *Aphanizomenon flos-aquae*, *Anabaena planctonica*, *Anabaena lapponica*, *Aphanizomenon ovalisporum*, *Aphanizomenon gracile*, *Rhaphidiopsis mediterranea*, *Rhaphidiopsis curvata*, *Umezakia natans* and *Lyngbia wollei* [94]. Distribution of *C. raciborskii* was reviewed by Padisák [95], who catalogued blooms occurring in tropical and subtropical nations as well as those expanding into temperate climates. The toxin is thus now reported from Asia, Africa, North and South America, central, southern and northern Europe, and Australia/New Zealand—every continent except the Antarctic (Figure 2.2.). The toxin is now approaching an almost cosmopolitan distribution pattern and CYN producers are recorded from habitats including lakes, reservoirs, rivers, ponds and dams [5]. According to Kling [96], improvements in water quality monitoring is a key contributor to the number of new locations from which *C. raciborskii* has been recorded. However, it is also likely that the organism is expanding into suitable habitats made newly available by a combination of climate change, increased eutrophication and the species' own adaptability [96]. Padisák [95] noted that the ability of *C. raciborskii* to travel long river courses, to survive swampy or slightly saline conditions, and to produce resistant akinetes has contributed to expansion of this species on a global scale. Global climate change has also been examined as a trigger for the increasingly widespread distribution, frequency and duration of *C. raciborskii* blooms, especially into the sub-tropical and temperate regions [97-99].

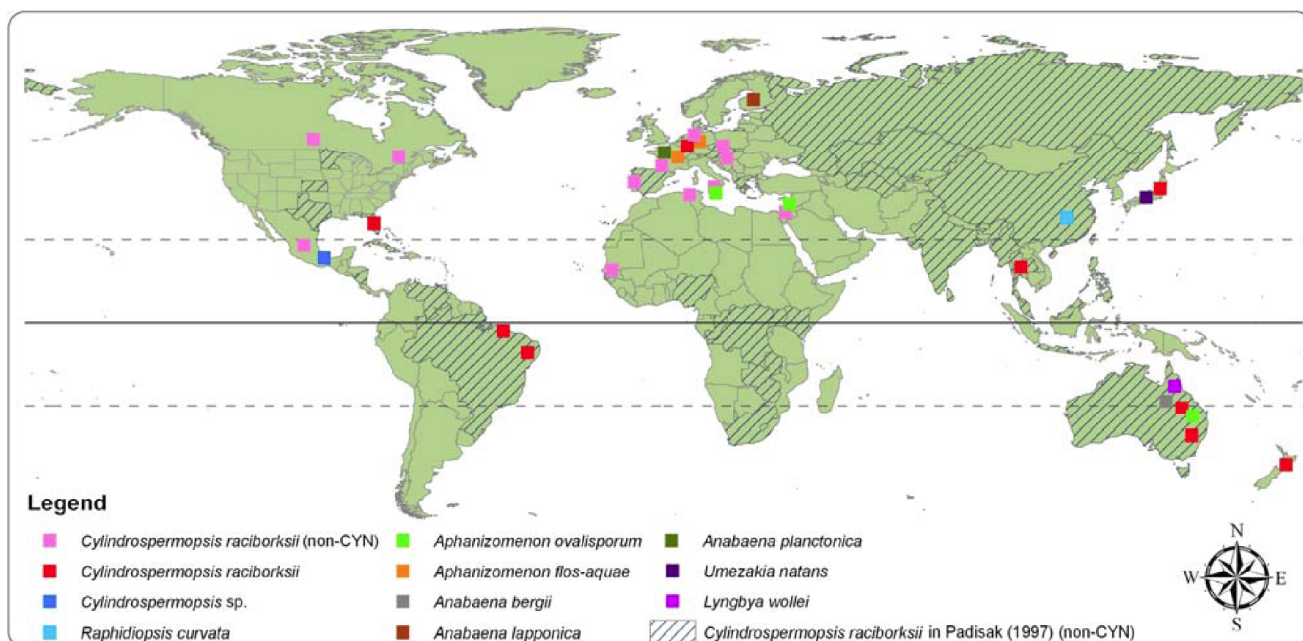


Figure 2.2. Global distribution of algal blooms known to contain CYN or a CYN-analog.

Note: 'non-toxic' denotes a bloom from which toxicity was not confirmed or not studied; Figures are not exhaustive as some records from central and eastern United States not shown [5].

The excitotoxic non-protein amino acid β - *N*-methylamino-L-alanine (BMAA) (Figure 2.1.h) was originally discovered in marine cyanobacteria and extracted and characterized from cycad seeds [100] originating from the symbiotic *Nostoc* growing in the cycad's coralloid roots [101]. Bell [102] first associated BMAA with Amyotrophic Lateral Sclerosis/Parkinson Dementia Complex (ALS-PDC), a motor-neuron disease. Is an amino acid and has now been detected in majority of field and laboratory isolates of free and symbiotic freshwater cyanobacteria. Controversy still exists on the nature of BMAA neurotoxicity due to the inability to reproduce human ALS-PDC pathology in animal models [103].

Lyngbyatoxins is a group of cyclic peptide indole alkaloid toxins first isolated in *Lyngbya majuscula* collected from Hawaiian Islands [104]. It is known to cause "swimmer's itch" and a potent protein kinase (PK) C activation. Malfunction of PKC can lead to tumor development and diabetic complications. The biological function of lyngbyatoxins in cyanobacteria is still unclear but studies suggested they are defensive secretion to protect cyanobacteria from predation [105]. In Figure 2.1.i the chemical structure of lyngbyatoxin-a is presented.

Aplysiatoxins (brominated and debrominated poly-acetates) are structurally different from lyngbyatoxin-a and can cause “swimmer’s itch” [106]. The acute contact dermatitis involves severe cutaneous inflammation with blistering, erythema and desquamation. Aplysiatoxins are also protein kinase C activators [107]. Aplysiatoxin is produced by strains of *Lyngbya majuscula* and the similarly toxic debromoaplysiatoxin is produced by *Schizothrix calcicola* and *Oscillatoria nigroviridis*. Both cyanotoxin classes are protein kinase C activators, and thereby tumour-promoters [108, 109]. It is not clear whether aplysiatoxin and debromoaplysiatoxin are exclusively cyanobacterial products. In animal intoxications by extracts of the red alga *Gracilaria coronopifolia*, the toxins may originate from the growth of cyanobacterial endophytes or from the rhodophyte [110].

2.2.3. Lipopolysaccharides

A characteristic of the cyanobacteria, as with other Gram negative bacteria, is the presence of the lipopolysaccharide toxins (LPS) (Figure 2.1.k) in the outer membrane of the cell envelope [111] which are the least studied and frequently assumed to have similar activities of heterotrophic bacterial LPS [112]. LPS from cyanobacteria have different chemical and biological characteristics compared to the heterotrophic bacteria [113]. The structure of LPS consists of a core oligosaccharide, an O-polysaccharide (outermost) component and an innermost lipid A region, and are structural components of the outer membrane of Gram-negative heterotrophic bacteria (including cyanobacteria) [114].

The lipid A moiety of LPS (highly hydrophobic) is primarily responsible for LPS toxicity, including in humans: hypertension, inflammatory responses and gastrointestinal upset and LPS had been implicated for skin irritations in swimmers and for gastrointestinal illness in people who ingested water from a reservoir contaminated with cyanobacteria. Since cyanobacterial LPS are less toxic than salmonella LPS, health concerns about them have received little interest [113]. If untreated in susceptible humans, exposure to LPS from some of the *Enterobacteriaceae*, including *Salmonella* spp., may result in death. A high variation occurs in lipid A composition between cyanobacterial species and strains of the same species and between enteric bacteria and cyanobacteria [111, 115, 116]. Few *in vivo* toxicity determinations with purified cyanobacterial LPS

conducted have been conducted and indicated low toxicity identified by multiple physicochemical methods [117, 118]

2.3. Taste and Odor Compounds – Geosmin, 2-methylisoborneol

Cyanobacteria cause many water quality concerns, including potential production of toxins and taste and odor compounds. The most usually occurring taste and odor compounds produced by cyanobacterial blooms as secondary metabolites, are geosmin (GSM) and 2-methylisoborneol (MIB) [6]. They are often found in surface waters, such as lakes, rivers and eutrophic drinking water reservoirs, [7] indoor air, [119] fish tissues [120, 121] and foods. [122-124] Both GSM and MIB (Figure 2.3.) are neutral bicyclic alcohols with moderate solubility, volatility and hydrophobicity, that exist as (+) and (-) enantiomers, with the naturally produced (-) enantiomers being far more potent taste & odor contributors than the (+) molecules. GSM (4S,4aS,8aR-4,8a-Dimethyl-1,2,3,4,5,6,7,8-octahydronaphthalen-4a-ol) whose name in Greek means “earth odor”, is a bicyclic tertiary alcohol (Figure 2.3.a) produced by certain species of *Oscillatoria*, [125, 126] *Anabaena* [127] and actinomycetes. [128] GSM has a distinct earthy-muddy flavor and aroma, and is responsible for the earthy taste of beets and contributes strongly to “petrichor”, the scent of rain falling on dry earth. MIB (1,6,7,7-Tetramethylbicyclo[2.2.1]heptan-6-ol) is a terpenoid (Figure 2.3.b) also produced by the cyanobacterial species of *Oscillatoria* [125, 126] and *Phormidium* [129]. Although MIB is often responsible for the musty taste and odor to drinking water and to malodorous off-flavor in fish and aquaculture products [130], it is the source of pleasing aromas of Brie and Camembert cheeses. Human nose can detect the odor of GSM and MIB and their threshold odor concentration in water has been reported to be 9 and 4 pg mL^{-1} respectively [8, 9], while the lowest concentration at which an odor can be sensed is about 1 ng/L [131].

Communities whose water supply depends on surface water periodically experience episodes of unpleasant water. Upon cellular death of these bacteria, GSM/MIB are released into the local water supply, impacting greatly on the aesthetic quality and general consumer acceptability of drinking water [10]. For these reasons, the removal of these compounds from water is very important for its use and consumption.

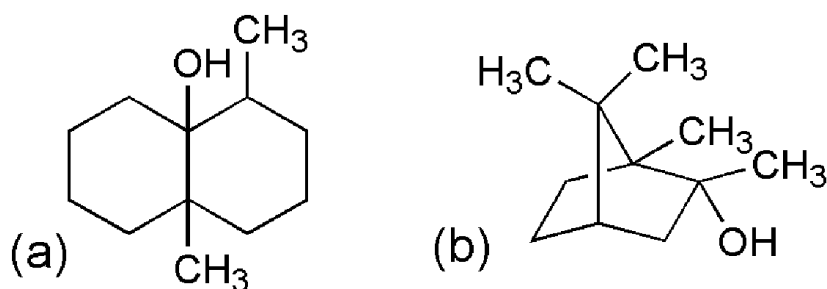


Figure 2.3. Structures of (a) geosmin and (b) 2-methylisoborneol

The biochemical and genetic mechanisms responsible for the production of GSM are not yet fully understood. However, a recent discovery of the geosmin synthase gene in cyanobacteria, that catalyzes the conversion of farnesyl diphosphate to GSM has provided the fundamental knowledge on investigating how growth conditions affect the expression of the gene and the production of GSM [132]. Accordingly, MIB is synthesized by the cyclization of the methylated isoprenoid substrate, 2-methylgeranyl diphosphate, a reaction catalyzed by 2-methylisoborneol synthase [133].

GSM and MIB production by cyanobacteria during their growth depends on environmental factors and these compounds are released in water mainly after the death and biodegradation of the cells. It is essential to recognize that GSM and MIB occur in surface waters as cellular (cell-bound) and dissolved fractions and that the differentiation between these two fractions is key to the effective management of water quality control and treatment [130]. They have been reported several incidents of heavy GSM/MIB contamination of surface and drinking waters [130] with concentrations reaching 4.000 ng/L GSM (Carcoar Dam, Australia) and 3600 ng/L MIB (Sakagawa River, Japan).

The presence of GSM and MIB in water was shown by numerous studies that they are not associated with serious health effects, being mainly an aesthetic concern [134] and as a result, these compounds are not regulated. However, Graham *et al.* [135] in a recent study showed that toxins and taste-and-odor compounds are frequently co-occurring (in 91% of blooms), indicating odor may serve as a warning that cyanotoxins likely are present. However, odor alone does not provide sufficient warning to ensure human-health protection due to the fact that toxins seemed to occur more frequently than taste-and-odor compounds.

2.4. Summary

Cyanobacteria (blue-green algae) are a group of prokaryotic organisms that occur worldwide in fresh, brackish and saline waters. Under favourable conditions, cyanobacteria can multiply rapidly to form blooms and mats [136]. A lot of cyanobacteria species and strains are toxigenic, i.e. able to produce a diverse range of potent cyanotoxins [137, 138]. Toxic cyanobacteria blooms can be especially detrimental to human and animal health, to aquatic habitats and to economy [139-141]. During the last years there is a growing concern regarding the health effects of MCs, because they act as tumor promoters, through the inhibition of protein phosphatases 1 and 2A, which play a key role in cell regulation [3]. In response to this concern, WHO has recommended for provisional adoption the value of 1 µg/L as a Guideline Value for MC-LR concentration in drinking water [4]. Humans are exposed to toxigenic cyanobacteria via drinking water and accidental ingestion while engaging in recreational activities. In addition to ingestion, exposure can also occur through skin contact with contaminated water or by inhalation when toxins become aerosolized and via food. Cyanobacterial metabolites have also been detected in food supplements, shellfish, fish and may be present in edible plants [142] exacerbating concern on exposure to these metabolites.

A variety of traditional water treatment methods, including coagulation/sedimentation [143], activated carbon adsorption [144] and membrane separation [145], have been attempted for the removal of cyanotoxins and taste and odor compounds, but with limited success. Previous studies have demonstrated that TiO₂ photocatalysis [11-18] can effectively destroy cyanotoxins in aqueous solution and emphasis was given to the mechanistic understanding of the process by identification of the intermediates formed during photocatalysis [19].

The assessment of pollutant disappearance is not sufficient to ensure the absence of residual products since the photocatalytic treatment is a complex procedure leading to the formation of degradation products, which in some cases may be more toxic and stable than the parent compound. Therefore careful analytical and/or toxicological monitoring using various techniques is important in order to control all transformation steps, but also the final degradation products.

CHAPTER 3

Destruction of cyanobacterial metabolites by conventional and advanced oxidation processes

3.1. Introduction

Human exposure to cyanobacterial metabolites is most common through the ingestion of drinking water, contaminated by cyanobacteria. Cyanotoxins (MC-LR, CYN) are released into the water after death and lysis of the cyanobacteria cells and they can enter water treatment plants, while their removal is necessary. For the removal of the toxins, physical and/or chemical oxidation methods are commonly used. Although, some physical methods, for example, activated carbon filtration [146] [147], membrane filtration [148, 149] [150], flotation [151] or coagulation [152] showed in some cases high removal efficiencies but under extended treatment times and it is notable that these methods are not destructive [153]. On the other hand, the use of conventional oxidation processes such as chlorination, ozonation and permanganate oxidation have been studied for the destruction of cyanobacterial toxins. Advanced oxidation processes (AOPs), have been also proposed as alternatives to chemical oxidation.

3.2. Conventional Oxidation methods

The oxidation of microcystins by common chemical oxidants used in conventional water treatment such as chlorine, chlorine dioxide, ozone, and permanganate has been extensively reported [154]. With respect to oxidation rate, the following general trend is typically observed for microcystins: ozone > permanganate > chlorine >>> chlorine-based oxidants. However, differences have been observed depending both on the type of toxin that is oxidized and the water quality parameters.

A variety of oxidants have also been studied in degrading CYN, among them free chlorine [155], chlorine dioxide [156], chloramine [157], permanganate [158] and ozone [159], with the majority of those techniques being effective.

When GSM and MIB are released during cyanobacterial bloom events, removal processes are required. Studies have shown that employment of standard water treatments such as coagulation, sedimentation or filtration, for GSM/MIB removal appeared to be ineffective, especially at very low concentrations of the compounds [160]. These compounds are resistant in common oxidants such as Cl_2 , ClO_2 and KMnO_4 [161, 162]. Even though aeration is considered to be effective for volatile compounds removal, due to low Henry's Law constant of GSM/MIB, their removal using air stripping presented to also be ineffective [163].

3.2.1. Chlorination

Chlorine is the most common reagent used in water treatment as both oxidant and disinfectant. It is effective, easy to use and affordable in both centralized and point-of-use treatments. Chlorine can be applied for water treatment in different forms such as Cl_2 , sodium hypochlorite (NaClO), chlorine dioxide (ClO_2) and chloramines (NH_2Cl , NHCl_2).

A number of studies used free chlorine for microcystins oxidation and indicated that the process was effective [164-176]. Chlorine-based weaker oxidants such as chlorine dioxide and chloramines have been used as alternative to chlorine, but were found to be ineffective for microcystins destruction [171, 174, 177]. Ho *et al.* studied the differences in the chlorine reactivity of four MC analogues; the oxidation of the microcystins was related to the chlorine exposure with the ease of oxidation following the trend: MC-YR > MC-RR > MC-LR > MC-LA [175]. Tsuji *et al.* [178] examined the effect of sodium hypochlorite on MC-LR and -RR and were the first to report by-products of MC-LR during chlorination.

Chlorine efficiency depends on experimental parameters, including the nature of the chlorine compounds used. In a study on MC-LR in 30 min treatments at 1 mg L^{-1} dose of the oxidant, toxin concentration decreased by more than 95% with aqueous chlorine and calcium hypochlorite, and only by $\sim 40\%$ with sodium hypochlorite [179]. The observed difference is due to the effect of pH (sodium hypochlorite solutions are highly alkaline).

The type of MCs analogues present in a water source and the characteristics of the water have to be evaluated [175], due to the different reactivities of MC variants with chlorine based on the interactions of natural organic matter (NOM) with a microcystin or the formation of highly reactive quaternary chloramines may also play a role in [174, 179, 180]. However, it is considered that, overall, MCs are efficiently degraded when treated with > 0.5 mg/L residual chlorine, pH <8 and with > 30 min contact time [174, 179].

Also, a major parameter influencing MCs oxidation efficiency is chlorine dose. Merel *et al.* [170] showed that one mole of MC-LR reacts with 12 moles of chlorine within 30 min of reaction. Chlorine dose must be sufficient to react with both MCs and NOM present in water, which competes with toxins and can potentially reduce chlorination efficiency [165].

Studies on the chlorination of CYN have been conducted much more often than other treatment methods [94]. More than half of 20 $\mu\text{g L}^{-1}$ CYN was degraded with a chlorine exposure of 1.7 mg min L^{-1} at pH = 8. At 4 mg min L^{-1} of chlorine exposure complete inactivation of *C. raciborskii* could be achieved, with no accumulation of CYN in the reaction solution. The chlorination efficiency is highly dependent on the water quality such as the pH and the presence of NOM. Speciation of chlorine and CYN is influenced by the solution pH and the maximum oxidation rate of CYN by chlorine was observed in ultrapure water at neutral pH [157]. Merel *et al.* [181] and Banker *et al.* [92] have studied oxidation of CYN by chlorination, identification of the chlorination by-products.

3.2.2. Ozonation

Ozonation process is one of the most affordable treatment technologies that can be used for cyanotoxins removal from drinking water. Ozone is a strong oxidizing agent that proceeds through direct molecular reaction pathway and/or indirect radical formation [182]. A number of studies have been performed dealing with the ozonation of cyanotoxins and they mainly focused on the investigation of doses required for toxins destruction [25, 143, 159, 171, 183-188], the effect of water quality parameters [159, 171, 184-187] and the mechanistic aspects of ozone's reactivity with the cyanotoxins [159]. With the majority of those focused on MC-LR degradation [143, 159, 171, 183-

187], results indicated that ozonation as a treatment process for cyanotoxins is highly efficient.

In a study by Rositano *et al.*, 1998 [183], with laboratory scale ozonation experiments on pure toxin solutions, at pH=7.0, it took only 15 s and an ozone dose of 0.22 mg L⁻¹ to completely remove 1.0 mg L⁻¹ MC-LR. They also investigated the effect of pH for the removal of MC-LR in algal extracts and it was found that at alkaline pH the efficiency of ozone was significantly reduced, attributed to the lower oxidation potential of ozone at alkaline pH and the accelerated decomposition of O₃ to HO• in the presence of OH⁻. The non-selective oxidizing nature of the HO• in contrast to the selective reactivity of ozone (selective to organic molecules that have nucleophilic moieties) [189] result in the advantage of ozone for treatment of waters with high levels of dissolved organic content (DOC) [159]. Shawwa *et al.* [187] investigated the effect of pH during ozonation reported that the pseudo-first order rate constant (k') of MC-LR increases by a factor of 20 between pH values from 2 to 7. In a later study [171], it was reported that ozone was more efficient in degrading MC-LR and CYN than chlorine, chlorine dioxide and permanganate.

Onstad *et al.* [159] conducted detailed studies on the kinetics of several cyanotoxins, including CYN with ozone, showing that the reaction of ozone with CYN is pH dependent between pH 4-10. The ozonation of CYN in natural waters is proportional to the rate constants for the reactions of CYN with ozone, while ozone primarily attacks the uracil ring responsible for the toxic.

Ozone being one of the strongest oxidants is capable for degrading taste and odor compounds. Ozonation process efficiency mainly depends on solution pH, ozone dose and water quality. In several studies ozone process was applied for GSM/MIB removal in combination with other methods, such as UV irradiation or H₂O₂. According to that, Duguet *et al.* [190] observed that GSM and MIB removal by ozonation was influenced by solution pH and with an addition of hydrogen peroxide, degradation was 10 fold faster than that obtained with ozone alone. Confirming water media influence Terashima, [191] Jung *et al.* [192] and also Glaze *et al.*, [162] presented different results of the destruction of GSM and MIB, attributed to the nature of the water studied in each case, resulting to different ozone dose and reaction time demand. For that reason, Ho *et al.* [193] studied the effect of NOM fractionations presence on removal efficiencies of gsm/mib, suggesting that NOM with higher MW fractions (higher specific UV

absorbance (SUVA) characteristics) had lower contact times, thus faster reaction with ozone, resulting in higher removal efficiencies. In contrary with that, Liang *et al.* [194] found that no significant effect on the ozonation of gsm/mib was resulted in the presence of background organics, but confirmed the significance of pH as a factor as it is directly related to the concentration of hydroxyl radicals. Collivingarelli *et al.*, [195] using ozone for removal of GSM/MIB, found the compounds to be resistance to ozone showing low removal rates, with better results followed by UV employment.

3.2.3. Oxidation with Permanganate

In the 1960s, application of potassium permanganate began in the water industry having many potential uses as an oxidant, destroying micro-organisms and organic pollutants [196]. Permanganate in general attacks functional bonds with multiple bonds and may oxidize organic compounds via several reaction pathways, primarily electron exchange, hydrogen atom abstraction, hydride ion abstraction or oxygen donation.

In an early study Rositano *et al.* [197] and in few more recent studies [171, 198-200], it was reported that oxidation of MC-LR with permanganate appeared to be an effective process for its removal in water samples. The removal of microcystins by permanganate was also tested in natural water [199]. A fast consumption of permanganate occurred, followed by the removal of MCs. Under the experimental conditions used (1.1 mg L⁻¹ permanganate at pH 7) about 1 h was enough for the complete removal of MCs. The degradation of MC-RR and MC-YR was slightly faster than MC-LR.

Rodriguez *et al.* (2007)[157] reported that 1.5 mg L⁻¹ dose of permanganate could only remove 10% of CYN and an estimated half life of 4 days. Oxidation of CYN by permanganate concentrations used in water treatment is insufficient to remove CYN. In another study the degradation of CYN and the inactivation of *C. raciborskii* were both investigated [155] by permanganate along with other oxidants and again, it was found that very little or no degradation of CYN could be achieved by a permanganate dose of 360 mg min L⁻¹. However, partial inactivation of *C. raciborskii* with an initial concentration of 2 x10⁵ cell mL⁻¹ could be achieved at around 65% for 240 mg min L⁻¹ permanganate.

GSM/MIB removal appeared to be ineffective in common oxidants including KMnO_4 [161, 162]. KMnO_4 has been found to have low removal efficiencies for GSM and MIB even at higher dosages [161, 162].

3.3. Photolysis and Advanced Oxidation processes

Alternative to conventional oxidative methods, advanced oxidation processes (AOPs) appeared to establish their effectiveness to completely remove compounds from water and in the case of cyanobacterial metabolites. AOPs are environment friendly and they mainly involve UV light in the presence of hydrogen peroxide or ozone, UV-near visible light in the presence of TiO_2 , sonolysis, radiolysis, polyoxometalate photocatalysis etc. These methods can achieve degradation and even mineralization of pollutants, and they are based mainly on the formation of the highly oxidizing HO^\bullet . Hydroxyl radicals are effective in destroying pollutants, reacting rapidly and non selectively with nearly all electron rich organic compounds.

3.3.1. Photolysis

Direct irradiation of a pollutant can lead to its degradation. When a molecule absorbs light, leading to its promotion from the fundamental state to an excited state, which can undergo to homolysis, heterolysis or photoionization, among other processes. When light is absorbed directly by a pollutant its bonds can be broken photolytically. In the presence of water or oxygen, highly reactive species like HO^\bullet and O_2^\bullet radicals can be generated, capable to oxidize a great variety of pollutants.

For a pollutant to be degraded only in the presence of UV light, the pollutant must absorb light at a wavelength emitted by the light source. Many organic pollutants absorb light at lower wavelengths and for that reason solar light is not capable to degrade them, due to only a small part of $\sim 3.5 - 8\%$ of the solar spectrum corresponds to UV light [201]. MCs are known to have no absorption under natural sunlight irradiation, having a UV-vis absorption at $\lambda = 238 \text{ nm}$. Thus direct photolysis does not contribute to their elimination in natural waters. MC-LR degradation was studied under natural sunlight in distilled water, and irradiation alone had little effect on MCs with 86% of the toxin being

present after photolysis for 26 days [29]. Addition of naturally photosynthetic pigments greatly enhanced the destruction process with the degradation rate depending on the pigment concentration [202] [29]. When UV-C light at 254 nm was applied, MCs were decomposed by while decomposition depended on the intensity of the light [203].

Photodegradation of CYN is highly dependent on UV-A light, and is generally limited under natural conditions [204]. Kutschera *et al.* [205] investigated GSM/MIB removal using VUV and found that was more effective compared to UV.

3.3.2. UV/H₂O₂ process

UV/H₂O₂ has been widely studied and used in the degradation of organic pollutants in water [206-210]. It is known that H₂O₂ upon illumination undergoes homolytic splitting into HO• radicals, which can cause degradation and mineralization of a great variety of pollutants [211, 212]. This process is influenced by many factors such as pH, concentration of H₂O₂, wavelength and intensity of irradiation, as well as initial concentration of the substrate [213]. UV/H₂O₂ has been applied for the degradation of MCs in water because of its advantages, such as, relatively low operational cost, no sludge production, and ease of operation [214-217].

Li *et al.* [216] using UV/H₂O₂ process reported the degradation of MC-LR in water. The degradation rate of MC-LR increased with an increase in H₂O₂ concentration without inhibiting effects at a high UV light intensity (153 μW cm⁻²) or at a high H₂O₂ dose (3 mM). It was also reported that at low concentrations of MC-LR, high degradation rate was observed. Degradation of MC-LR was also investigated in the presence of various anions including Cl⁻, NO₃⁻, CO₃²⁻, and SO₄²⁻. Destruction of MC-LR was significantly reduced in the presence of CO₃²⁻ and NO₃⁻, because NO₃⁻ could reduce UV light intensity as an inner filter [218] and CO₃²⁻ could act as a scavenger of hydroxyl radicals [219]. Cronish *et al.* [214] investigated the role of hydrogen peroxide in the enhancement of the photocatalytic oxidation of MC-LR using TiO₂. Higher initial rates of the MC-LR photocatalytic destruction were observed when H₂O₂ was present which is was attributed to the increase of the oxidising power of the system due to additional oxidizing hydroxyl radicals generated during the process.

Combination of methods hydrogen peroxide with ultraviolet irradiation (H_2O_2/UV) was applied in several studies for GSM and MIB, presenting successful removal of the compounds to a level below their odor threshold. Rosenfeld *et al.* [220] applied direct photolysis with UVC and addition of hydrogen peroxide improved their removal efficiencies more than 70%. The same conclusions on improving gsm/mib removal had Romain [221] and Royce and Stefan [222], in similar studies. Peter and Gunten [223] using UV/ H_2O_2 on water from two different lakes in Switzerland, they determined second order reaction rates for oxidation with hydroxyl radicals generated from UV/ H_2O_2 . In agreement to this study, Park *et al.* [224] using H_2O_2 , indicated hydroxyl radicals as the main mechanism in mib/gsm destruction.

3.3.3. Ultrasonic degradation

Ultrasonic irradiation unlike other AOPs, does not require addition of chemicals. Ultrasonic-induced degradation of organic compounds is a complex process that can involve hydroxyl radicals, supercritical water oxidation, and pyrolysis. Ultrasonic irradiation is based on the phenomenon of acoustic cavitation, which involves the formation and subsequent collapse of gas bubbles (cavitation) from acoustical wave induced compression/rarefaction leading to extreme conditions (5000 K, 1000 atm), under which the pyrolysis of water produces H^\bullet and OH^\bullet . [225]. Generated radicals can either react with each other or diffuse into the bulk liquid to serve as oxidants.

Studies dealt with the destruction of cyanotoxins by ultrasonic irradiation, including a series of papers on the destruction of MCs [28, 226, 227]. The results demonstrated that ultrasonic irradiation can lead to rapid degradation of MCs. Degradation of MC-LR in cyanobacterial extracts was effective under a variety of conditions, with OH^\bullet oxidation being responsible for a major fraction of the observed degradation [226]. Song and O'Shea [227] used ultrasonic irradiation and a complete degradation of GSM and MIB was achieved in a matter of minutes; due to degradation of the compounds caused by pyrolysis resulted from the heat generated when water is subjected to ultrasonic irradiation.

3.3.4. TiO₂ photocatalysis

TiO₂ photocatalysis is among the most efficient emerging processes for the treatment of cyanotoxin contaminated water [154, 228-230]. This “green” emerging process is known to efficiently perform water purification, disinfection and detoxification without necessitating the use or resulting in the production of hazardous compounds [231-233]. Previous studies have demonstrated that TiO₂ photocatalysis can effectively degrade both cyanotoxins as well as taste and odor compounds in aqueous solutions [12, 13, 17, 18, 20, 23, 234-236].

Removal of MC-LR, -YR and -YA was evaluated using a laboratory-scale photocatalytic reactor with TiO₂ in suspension under UV-C light irradiation (λ_{\max} at 254 nm) [237]. Addition of TiO₂ to the UV-illuminated process led to an enhancement in the removal of all MCs and when natural lake water samples were spiked with MCs subjected to photocatalytic treatment, degradation for MCs was achieved but slower degradation rates were obtained in natural water. Shepard *et al.* also immobilized TiO₂ onto a fiberglass sheet and modified the design of a laboratory-scale reactor for the removal of MC-LR, -YR and -RR with UV-C light [238]. Lawton *et al.* [239] studied the processes that affect surface interactions of four MCs, MC-LR, -RR, -LW, and -LF, with TiO₂ in water.

Dark adsorption and rate of toxin destruction were found to be influenced by the solution pH, and for MC-LR, about 50% of the toxin was adsorbed on the surface of TiO₂ at pH 4.0 [239]. In alkaline solutions, all MCs, except MC-RR, exhibited very low adsorption capacity on TiO₂. Higher degradation rates were obtained at high extent of adsorption, which suggests that the photocatalytic oxidation takes place at the surface of the catalyst. MC-LR is structured by a D-methylaspartic acid and a D-glutamic acid, having free carboxylic groups. The pKa for both aminoacids is around 3.0. MC-LR, also contains an L-arginine unit having a basic amino group with pKa=12.48. With increasing pH (3 < pH < 12), MC-LR loses two protons from the carboxylic groups, making the overall charge -1. At extremely basic pH (>12), MC-LR loses the proton from the protonated basic group and the overall charge is -2 [240]. The pH of zero point charge (pH_{zpc}) of TiO₂ is 6.25 [231]; below this pH the surface is positively charged. When pH < pH_{zpc} the surface charge of the catalysts becomes positively charged and presents electrostatic attractions towards negatively charged species [241].

To the best of my knowledge a few studies have used TiO₂ photocatalysis for CYN degradation [21, 22, 242]. Employment of TiO₂ photocatalysis appeared to be an effective process for CYN elimination in aqueous solutions [21, 22, 242]. Senogles *et al.* [21] examined the photocatalytic degradation of CYN with different TiO₂ nanoparticles (Evonik P25 and UV-100) under UV irradiation. When using Evonik P25 nanoparticles, the degradation rates were independent of temperature but dependent on pH. Higher pH values resulted in higher degradation rates although no significant adsorption (under dark conditions) onto the TiO₂ surface was observed. CYN can be adsorbed on TiO₂ surface via electrostatic interactions between the positively charged surface of catalysts and the negatively charged group (SO₄²⁻) of CYN. In another study [242], where polymorphic TiO₂ was used, the CYN's negative group also reach the positively charged photocatalyst's surface at pH lower than its p*H*_{zpc}. On the contrary, no significant adsorption was observed reported with NF-TiO₂ photocatalytic films at pH 3, since CYN at this pH is positively charged as is the photocatalyst's surface [22].

Lawton *et al.* [239] reported rapid degradation of both GSM and MIB with more than 99% removal within 60 minutes of illumination in the presence of suspended TiO₂. Bellu *et al.* [23], using a pellet form of TiO₂ completely removed GSM within 25 minutes of treatment. In a later study using the same material in a heavy water solvent, an isotopic effect was observed upon GSM destruction. The results of the study showed the dependence on the photocatalyst material used and also suggested that the photocatalytic degradation took place on the catalysts surface with [•]OH radicals generation being the rate determining step [243]. In another study, TiO₂ entrapped into EFAL (extra-framework-aluminium)-removed Y-zeolites was applied for MIB degradation presenting enhanced photocatalytic activity. This was due to modification of the surface states of TiO₂ that leads to enhancement of the photocatalyst adsorption capability [244]. A preliminary study was also performed by Pemu *et al.* [24] using TiO₂ photocatalysis of GSM in which few intermediate products were identified.

3.3.5. Polyoxometalates photocatalysis

Polyoxometalates (POM) are acid condensation products, mainly of molybdenum and tungsten [37-39], that upon excitation with near visible and UV light become powerful

oxidizing reagents capable of destroying a great variety of organic compounds in aqueous solutions [40, 41]. $\cdot\text{OH}$ radicals generated by reaction of POM with H_2O seem to play a key role in the process [42]. Oxygen oxidizes (regenerates) the catalyst and through reductive activation may or may not participate further in the process, depending on the substrate [43]. Due to their photocatalytic performance, POM can be recognized as an advanced oxidation process. POM are at least as effective as the widely published TiO_2 , presenting similar behavior with the semi-conducting oxide [42].

Photocatalytic degradation of GSM and MIB under UV and near visible light in the presence of POM photocatalyst, $\text{SiW}_{12}\text{O}_{40}^{4-}$, in aqueous solution has been studied and compared with the photodegradation by TiO_2 suspensions for the first time, in this study and results are presented in Chapters 5 and 8 [245].

3.4. Summary

All conventional oxidation processes (chlorination, ozonation and oxidation with permanganate) were able to degrade at some grade cyanotoxins MC-LR and CYN, but were found to be ineffective in degrading GSM or MIB in water. Alternative to conventional oxidative methods, AOPs are generally more effective on degradation of pollutants and are based mainly on the formation of the highly oxidizing $\text{HO}\cdot$ radicals. Among those, TiO_2 photocatalysis demonstrated [11-18, 20] that it can effectively degrade cyanotoxins and taste and odor compounds in aqueous solution [15, 20-24].

Chapter 4

Photocatalysis with Titanium Dioxide and Polyoxometalates

4.1 Introduction

Water detoxification has become an environmental issue of ever increasing importance. Traditional water treatment methods have been attempted for the removal of cyanobacterial metabolites, but with limited success. In addition to conventional technologies used for purification of water, another type of treatment process, commonly referred as advanced oxidation processes (AOPs) is emerging. AOPs are increasingly being considered as alternatives to conventional technologies because they destroy hazardous organic compounds rather than transferring them to another phase. AOPs are generally characterized by their ability to generate strong oxidizing species, some examples being UV light in the presence of hydrogen peroxide or ozone, and UV–A light in the presence of semiconducting photocatalysts [211, 231, 246]. TiO₂ photocatalysis being widely used as an AOP, although it appears to degrade a great variety of compounds, it requires UV irradiation to overcome its wide band gap-energy. Consequently, research on the development of new TiO₂ based catalysts has been receiving increased attention.

4.2 Titanium Dioxide TiO₂

Titanium dioxide occurs in three different forms, anatase, rutile and brookite, with rutile being the most stable form [247]. Is typically an n-type semiconductor due to oxygen deficiency [248]. TiO₂ is the most widely investigated photocatalyst due to its high photoactivity, low cost, low toxicity and chemical/thermal stability [231].

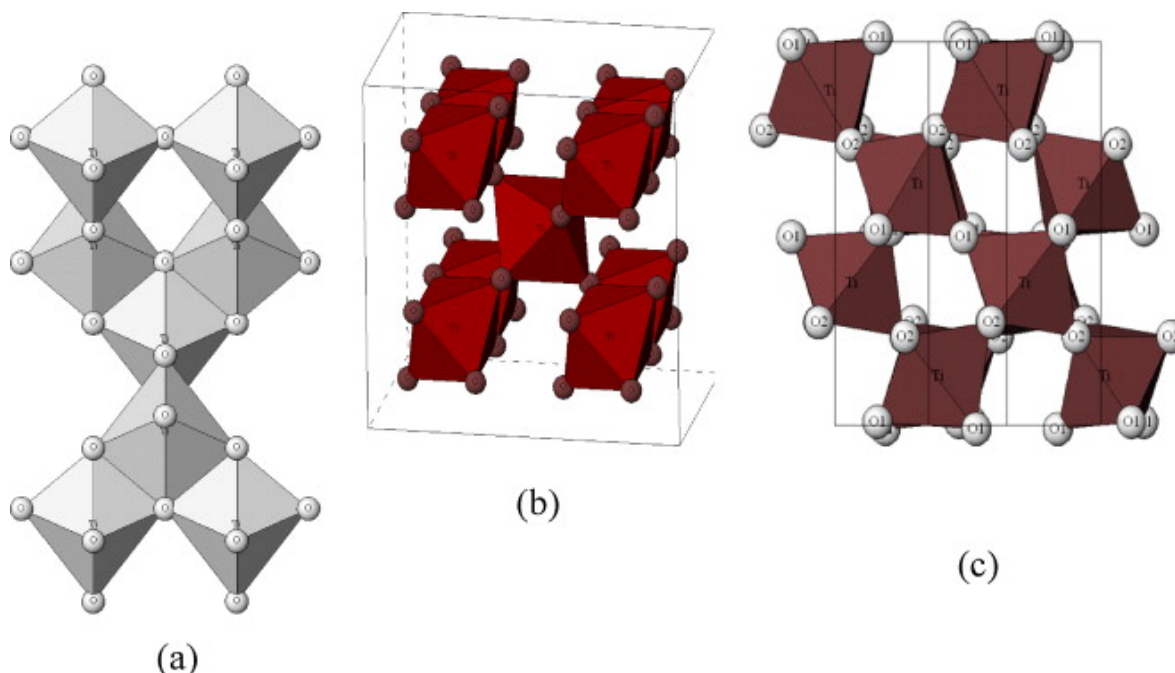
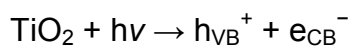


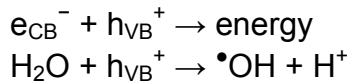
Figure 4.1. Crystalline structures of titanium dioxide (a) anatase, (b) rutile, (c) brookite [249].

4.2.1. TiO_2 photocatalysis, new TiO_2 based photocatalysts

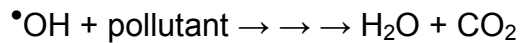
TiO_2 photocatalysis which have been widely studied during the last decades is mainly based on the generation of electron/hole pairs and highly oxidizing $\cdot\text{OH}$ radicals leading to oxidation and mineralization of organic pollutants. This 'green' process is based on the generation of highly reactive oxygen species (e.g., $\text{HO}\cdot$, $\text{O}_2\cdot^-$) through the photoexcitation of the catalyst by absorbing radiation with energy equal to or greater than its band gap. The adsorption of a photon excites an electron to the conduction band (e_{cb}^-) generating a positive hole in the valence band (h_{vb}^+).



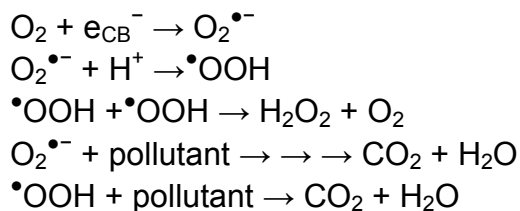
Charge carriers can be trapped as Ti^{3+} and O^- defect sites in the TiO_2 lattice, or the excited electron and hole can recombine and release the energy gained from the excitation of the electron as heat (energy) [250]. The charge carriers can migrate to the catalyst surface and initiate redox reactions with the adsorbed organic compounds. The positive holes react with the moisture present on the surface and produce a hydroxyl radicals which are extremely powerful oxidants.



Hydroxyl radicals can subsequently oxidize organic species with mineralization producing mineral salts, CO₂ and H₂O [251].



A reductive path can also take place, with electron in the conduction band can be rapidly trapped by the adsorbed on the titania molecular oxygen, which is reduced to form superoxide radical anion (O₂^{•-}). O₂^{•-} can further react with H⁺ to generate hydroperoxyl radical ([•]OOH) and further electrochemical reduction yields H₂O₂ [252].



These reactive oxygen species may also contribute to the oxidative pathways such as the degradation of the organic compound [251].

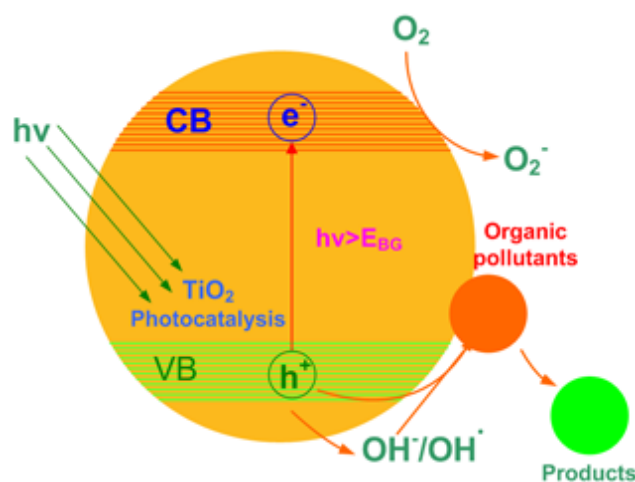


Figure 4.2. Schematic of TiO₂ photocatalytic mechanism [154].

However, TiO₂-based photocatalytic processes require UV radiation ($\lambda < 400$ nm) to account for the wide band gap energy (~ 3.2 eV for anatase phase) that is needed for photocatalytic activation.

Doping of TiO₂ is a technique used to reduce its band gap energy requirements. As an example, non-metal doping with nitrogen (N), fluorine (F) or carbon (C) has been shown to yield improved materials with good photocatalytic performance in the visible light [253-257].

In nitrogen and fluorine doping, energy states are formed inside the titania band gap accounting for the red shift of the energy gap and the induced visible light photocatalytic activity [258]. Similarly, C-doping e.g. Kronos TiO₂, involves substitution of oxygen by carbon atoms producing new energy states deep in the TiO₂ band gap, which are responsible for the visible light absorption [256, 257].

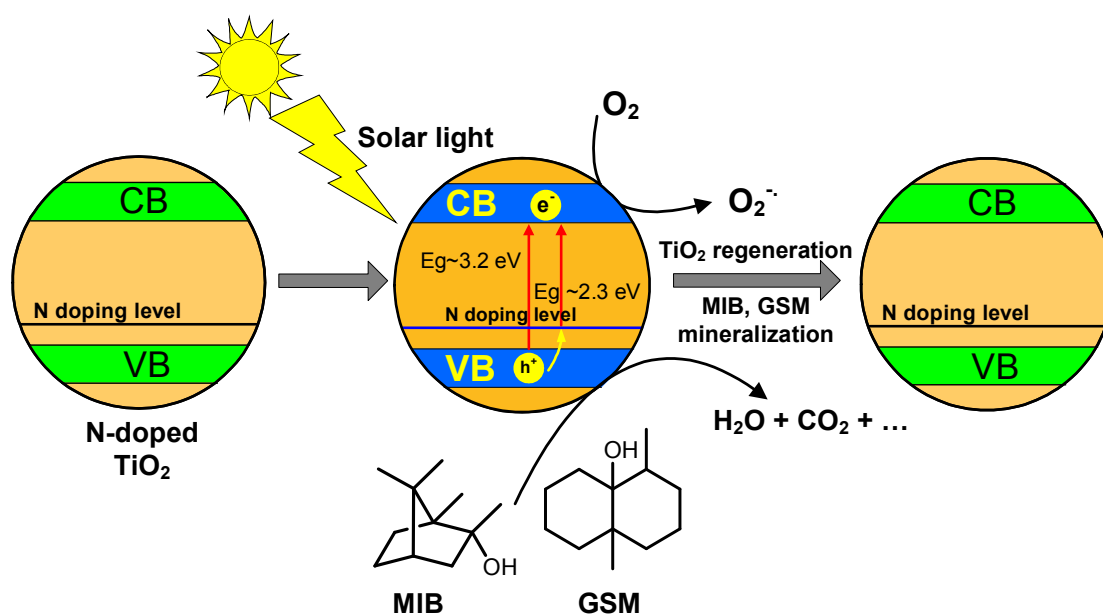


Figure 4.3. Photocatalytic cycle for the destruction of GSM and MIB using nitrogen doped titania (N-TiO₂) nanocatalyst.

Other materials, such as the graphene oxide (GO)-TiO₂ composite photocatalysts exhibit systematically enhanced photocatalytic activity that is mainly related to the scavenging and subsequent transport of photogenerated electrons by GO after excitation in the conduction band of TiO₂ by UV illumination, promoting thus charge separation as well as the enhanced capacity of the composites for the physical and chemical adsorption of pollutant molecules [259]. Another photocatalyst used was ECT-1023t, which was prepared by a sol-gel method in which aggregates have been selected before thermal treatment. The high photoactivity of this new catalyst has been attributed to the different distribution of surface defects and its increased capacity to yield H₂O₂ [268].

During the last decade, there is a remarkable number of industrial applications based on photocatalytic materials for air cleaning, i.e. self-cleaning glazing and concretes, photocatalytic cements and paints and indoor air purification systems. Although photocatalytic applications for water purification are fewer there is an increasing interest on using photocatalysis for water treatment. Recently, it has been demonstrated that TiO₂ based photocatalysis (Degusa P25, N-TiO₂, NF-TiO₂, Kronos and GO-TO₂) can effectively degrade cyanobacterial toxins as well as water taste and odor compounds in aqueous solutions [12, 13, 17, 18, 20, 23, 234-236]. Cyanotoxins and taste and odor compounds can potentially be released in water during incidents of harmful algal bloom causing many water-quality concerns [6, 125, 260].

4.3. Polyoxometalates

Polyoxometalates (POM) have previously been used for degradation of several organic pollutants in water [32-36]. In almost all cases final degradation products were CO₂, H₂O and inorganic anions. POM are acid condensation products, mainly of molybdenum and tungsten [37-39], that upon excitation with near visible and UV light become powerful oxidizing reagents capable of destroying a great variety of organic compounds in aqueous solutions through a hole-electron ($h^+ + e^-$) mechanism [40-42]. Hydroxyl radicals ($\cdot OH$) generated by reaction of POM with H₂O seem to play a key role in the process [42]. Oxygen oxidizes (regenerates) the catalyst and through reductive activation may or may not participate further in the process, depending on the substrate [43]. Due to their photocatalytic performance, POM can be recognized as an AOP [33-35]. They have also been recognized as building blocks for efficient photocatalysts by hybridizing with photofunctional semiconductor nanostructures [261]. POM are almost as effective as the widely published TiO₂ [42], presenting similar behaviour with the semi-contacting oxide [42].

4.3.1. Polyoxometalates and their Photocatalytic Cycle

One of the characteristic properties of POM is that they keep their structure intact, upon undergoing stepwise multielectron redox reactions. POM can also serve as oxygen reals, replenishing the consumed oxygen with atmospheric oxygen.

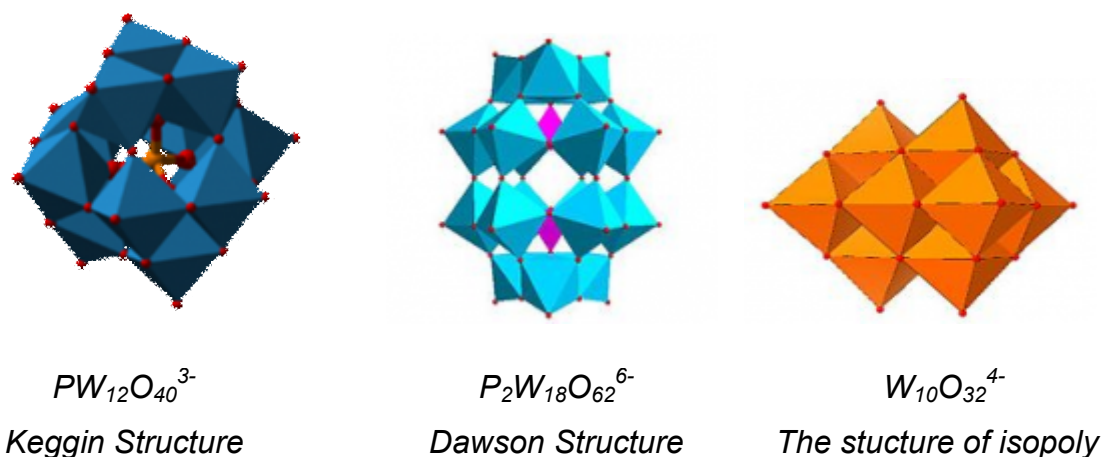


Figure 4.4. The structures of several categories of POM. $PW_{12}O_{40}^{3-}$, Keggin structure; $P_2W_{18}O_{62}^{6-}$, Dawson-Wells structure. The structure of isopoly $W_{10}O_{32}^{4-}$ [262].

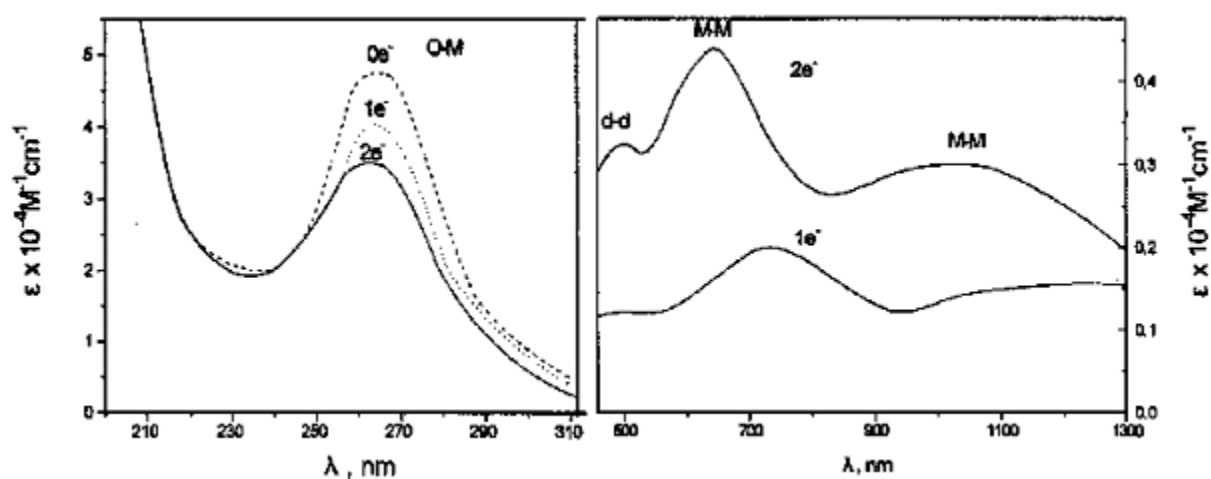


Figure 4.5. Oxidized and reduced (by one and two electrons) spectra of $PW_{12}O_{40}^{3-}$, showing the O → M CT band, d-d transitions and the intervalence electron transfer band (M-M CT) [262].

Illumination of POM in the oxygen to metal charge-transfer (O → MCT) band i.e. below 400 nm enhances their oxidizing ability, making them powerful oxidizing reagents able to oxidize a great variety of organic substances through a hole-electron mechanism similar to semiconductor photocatalysis [42].

Most of the proposed mechanisms concerning photocatalytic degradation of organic substances (S) in the presence of POM, are supposed to proceed through the reaction

of excited POM (POM*) with water producing highly oxidizing $\cdot\text{OH}$ radicals. In the presence of oxygen, the overall reaction that takes place in the photocatalytic cycle is:



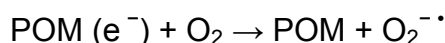
Excited POM has been reported to react with the substrate via direct reaction



And via indirect reaction through $\cdot\text{OH}$ radicals [263]



Several oxidants, including oxygen, are effective in oxidation of reduced POM, regenerating the catalyst [43].



This superoxide radical anion can further participate in oxidative processes.

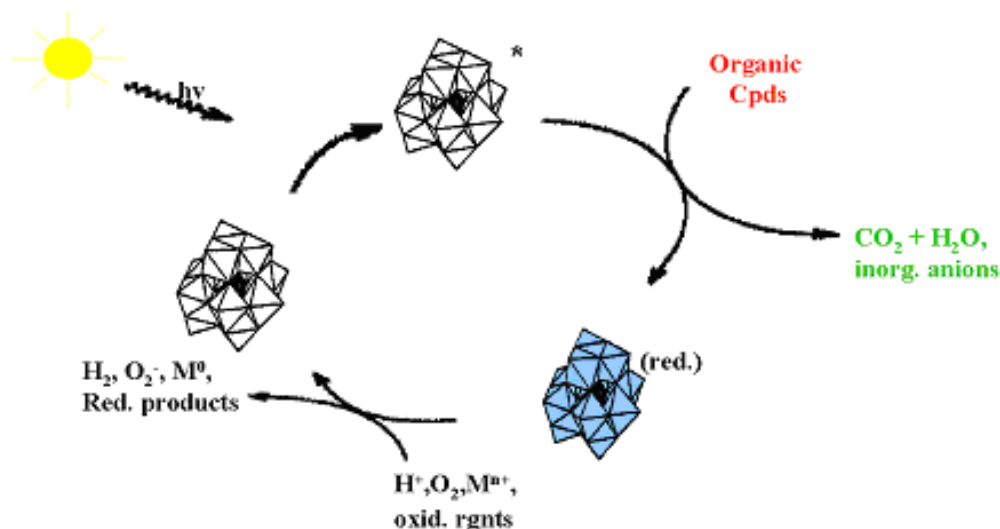


Figure 4.6. Schematic diagram of the photocatalytic cycle with the Keggin structure [42].

To summarise, upon photocatalysis of an aqueous solution in the presence of POM both oxidative and reductive species are formed. The excited POM, the $\cdot\text{OH}$ radicals and the superoxide radical anions are the oxidative species, whereas the reductive species are the reduced POM, $\text{POM} (e^-)$ and the superoxide radical anions [32]. It

should be noticed that POM, for example $\text{SiW}_{12}\text{O}_{40}^{4-}$, at the beginning of the photoredox process, participate exclusively as oxidants, since tungsten exist at its highest oxidation state (W^{6+}).

4.3.1. Comparison with Metal Oxide Particles

As mentioned earlier POMs photochemistry resembles very much the chemistry of metal oxide particles. POM are well-defined anions that when are dissolved in water form homogeneous solutions, whereas, metal oxide particles (i.e., TiO_2), that is SC, disperse in water forming heterogeneous solutions. Despite that difference, these two photocatalysts present a lot of similarities [42].

POMs can be reduced by various means, chemical, electrochemical, photolytic, etc. producing blue species. There is a stepwise addition of several electrons for POM, whereas, accumulation of electrons takes place also in SC depending on the strength of the reducing reagent. Both photocatalysts absorb at the near-Vis and UV area. For POM this absorption corresponds to $\text{O} \rightarrow \text{M}$ CT band, whereas, for SC (i.e., TiO_2) corresponds to band gap, e.g. that is promotion of an electron from the valence band (VB) to conduction band (CB) resulting in electron hole (h^+) separation. The common photocatalytic cycle of both systems is shown in Figure 4.7. [264]. It has been accounted for the overall similar picture presented by these two categories of catalysts. Several research groups have undertaken the task to elucidate the main oxidant in the primary photochemical reaction, i.e., whether it is exercised via OH radicals or holes or both. A common oxidant, i.e., OH radicals will explain the similar behavior, whereas, the opposite will produce diversified results.

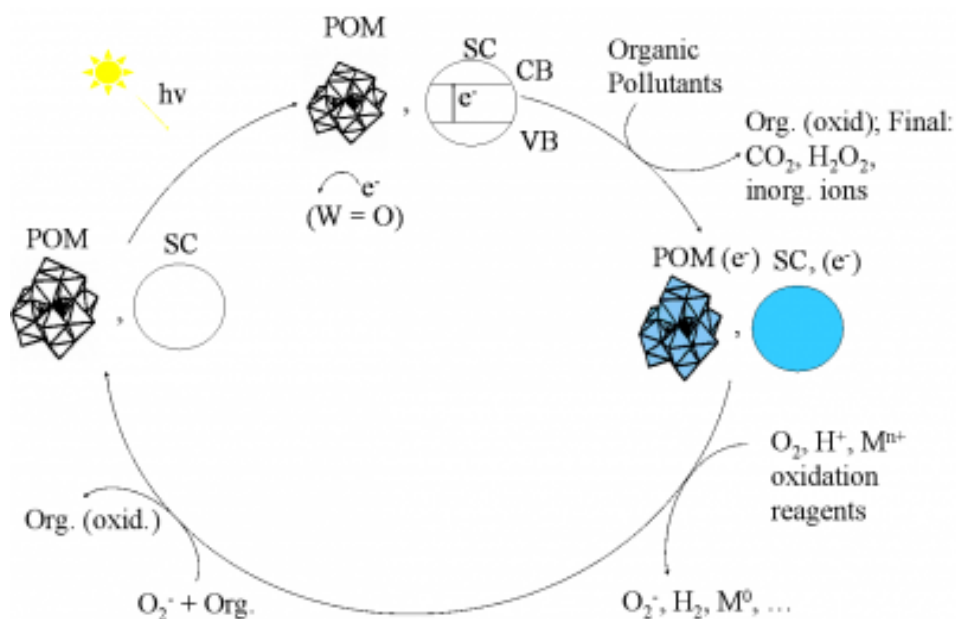


Figure 4.7. Schematic diagram showing the parallel photocatalytic action of POM and semiconducting particles [42].

Several examples, from both photocatalysts, have been reported to demonstrate that their performance is similar in terms of the overall mechanism of photodecomposition of organic compounds, the intermediate species involved and the final photodegradation products (i.e., CO_2 , H_2O and inorganic anions) [42]. However, parallel experiments under similar conditions, using various substrates (atrazine, fenitrothion, 4-chlorophenol and 2,4-dichlorophenoxyacetic acid) and $\cdot\text{OH}$ radical scavengers, have shown that the photooxidizing mode of POM and TiO_2 , i.e., $\cdot\text{OH}$ radicals and/or holes (h^+), depends on the nature of substrate and the mode of investigation [44, 265]. Atrazine showed that both POM and TiO_2 mainly operate through $\cdot\text{OH}$ radicals and with a lower extent with h^+ , whereas fenitrothion suggested the almost exclusive operation of both photocatalysts via $\cdot\text{OH}$ radicals. On the other hand, differences between the two photocatalysts have been proposed with 4-chlorophenol and 2,4-dichlorophenoxyacetic acid, with POM operating via $\cdot\text{OH}$ radicals and TiO_2 mainly via h^+ . Overall, the action of $\cdot\text{OH}$ radicals relative to h^+ appears to be more pronounced with POM than TiO_2 [54]. An example against the above mechanism for POM has been reported for the degradation of dichlorobenzene in the presence of $\cdot\text{OH}$ radical scavengers suggesting that POM act via h^+ rather than $\cdot\text{OH}$ mediated oxidations [266]. As a conclusion, whether an $\cdot\text{OH}$ or h^+ mediated mechanism is followed depends on various parameters (e.g., the kind of substrates, the substrate-photocatalyst interaction) and should be considered on a case by case basis [265].

CHAPTER 5

Materials – Instrumentation – Methods – Experimental

5.1. Materials

5.1.1. TiO₂ based nanocatalysts

Commercial available materials such as Degussa P25 TiO₂ obtained by Degussa AG-Germany and Kronos vlp-7000, by Kronos Titan GmbH-Germany were used as reference materials for comparison reasons. TiO₂ based nanocatalysts were synthesized by other collaborating groups according to the procedures described [258] [136] [267] [268] and given for the evaluation of their photocatalytic activity. N-doped TiO₂ powders (N-TiO₂) were synthesized as the hydrolysis condensation product of tetrabutyl titanate reaction with urea. The reference TiO₂ (Ref-TiO₂) nanopowders was prepared without adding urea. NF-doped TiO₂ nanoparticles were prepared by a novel synthesis route employing a simple sol-gel method containing a nonionic fluorosurfactant, fluorine dopant and ethylenediamine. Graphene Oxide-TiO₂ composites were synthesized by using the liquid phase deposition method (LPD) at room temperature. ECT-1023t was synthesized by a sol-gel method, dispersed mechanically and followed by annealing at 1023 °C.

N-TiO₂

For the preparation of the nitrogen-doped photocatalyst, tetrabutyl orthotitanate (15 ml, 97%) was added dropwise into 100 ml of H₂O, acidified with nitric acid (3.0 ml). After vigorous stirring for 4 hours, *n*-propanol (30 ml) was added and the translucent colloidal solution became completely transparent. Then, urea (25% w/v) was added, followed by a first annealing step at 100 °C, in order to dry, and further calcination for 2 hours at 450 °C [258].

NF-TiO₂

The pore directing agent and fluorine source employed in the modified sol-gel solution was a nonionic fluorosurfactant (Zonyl FS-300 (FS), ~50% solids in H₂O, R_fCH₂CH₂O-

$(\text{CH}_2\text{CH}_2\text{O})_x\text{H}$; $R_f = \text{F}(\text{CF}_2\text{CF}_2)_y$ where $x = 14$ and $y = 3$). The fluorosurfactant was dissolved in isopropanol (i-PrOH) and then a specific amount of acetic acid was added to maintain a low pH and for esterification reaction with isopropanol to produce water molecules *in situ*. Before adding the titania precursor, anhydrous ethylenediamine (EDA) was introduced in the solution as nitrogen source. Then, titanium (IV) isopropoxide (TTIP, 97%) was added dropwise under vigorous stirring and more acetic acid was added for peptidization. The final solution obtained was transparent, homogeneous and stable after stirring overnight at room temperature [136].

GO-TiO₂

GOT composite was synthesized by using the liquid phase deposition method (LPD) at room temperature. Graphene oxide dispersion (0.5 g L^{-1}) was diluted with distilled water (250 mL), ammonium hexafluorotitanate (IV), $(\text{NH}_4)_2\text{TiF}_6$ (0.1 mol L^{-1}), and boric acid, H_3BO_3 (0.3 mol L^{-1}), were added to the dispersion heated in an oil bath ($60 \text{ }^\circ\text{C}$ for 2 h) under vigorous stirring with the aim to obtain a homogeneous suspension. The precipitate was separated by filtration, washed with water and dried at $100 \text{ }^\circ\text{C}$ under vacuum for 2 h. The obtained solid was treated in a furnace with N_2 flow at $5 \text{ }^\circ\text{C min}^{-1}$ until the desired temperature ($200 \text{ }^\circ\text{C}$ or $350 \text{ }^\circ\text{C}$) and with soak time of 3 h [267].

ECT-1023t TiO₂

The new catalyst was synthesized following a sol-gel procedure. For this, an ethanol-titanium butoxide (99.5%) and (97%) respectively) 50:3.5 ratio molar solution was added drop by drop to a water-ethanol-citric acid (99.5%) 50:60.8:0.36 molar ratio solution. The mixing time was 3 h. After this, the final solution was stirred for 30 min and then allowed to age for 48 h. Then, the catalysts were dried at 373 K, 24 h. After this aging and drying treatment, the effect of separating the aggregates by means of sieving the catalysts with a $63 \text{ }\mu\text{m}$ mesh was tested. Larger aggregates than $63 \text{ }\mu\text{m}$ were separated from the smaller ones by sieving, resulting in a weight ratio of 53–47%, respectively. The larger aggregates were removed and the smaller ones were calcinated, being this catalyst denominated as sieved. Finally, thin films of the catalyst were placed on porcelain capsules to achieve the complete contact of the catalyst with air during calcination. A 302 K/h slope temperature program was used and the final temperature was held for 3 h. Synthesis temperature was 1073 K. The new catalyst has been denominated “ECT” (ethanol, citric, tetrabutoxide) followed by the calcination temperature [268].

5.1.2. Cyanotoxins, Taste and Odor Standards, Chemicals

MC-LR was purchased from Abraxis, USA.

CYN was purchased from GreenWater Laboratories, FL USA.

GSM (98.0%) and MIB (99.8%) were purchased by Wako Pure Chemical Industries Ltd.

Silica tungstate ($\text{SiW}_{12}\text{O}_{40}^{4-}$) was obtained by Sigma Aldrich.

Extra pure oxygen and nitrogen were used for oxygenation and evaporation of the solutions. Water was purified with a Millipore Milli-Q Plus System.

Samples were filtered through Millex PVDF Durapore-GF 13mm 0.22 μm (low protein binding) filters.

5.2. Instrumentation

5.2.1. Analytical Instruments

HPLC

MC-LR degradation was monitored by HPLC, using an HPLC apparatus consisted of a Waters (Milford, MA, USA) Model 600E pump associated with a Waters Model 600 gradient controller, a Rheodyne (Cotati, CA, USA) Model 7725i sample injector equipped with 20 μL sample loop and a Waters Model 486 tunable absorbance detector, set at 238 nm, controlled by the Millennium (Waters) software.

LC-MS/MS

The LC-MS/MS system used was a Thermo Finnigan (San Jose, USA) consisting of a Thermo Surveyor LC pump, a Thermo Surveyor AS auto-sampler and a TSQ Quantum Discovery MAX triple quadrupole mass spectrometer equipped with an electrospray ionization (ESI) interface operating in the positive ionization mode. Xcalibur software 1.4 was used to control the mass spectrometric conditions and for data acquisition. Mass axis calibration was performed by infusion of a polytyrosine-1,3,6 standard solution at 5 $\mu\text{L min}^{-1}$. High-purity nitrogen was used as sheath and auxiliary gas and argon was used as collision gas.

GC-MS

The GC-MS system used through was an Agilent 6890 Series gas chromatograph equipped with an HP-5 MS capillary column (30 m x 0.25 mm x 0.25 μm film thickness), interfaced to an Agilent 5973 mass selective detector. Data acquisition, processing and instrument control were performed by the Agilent MSD Chem-Station software.

TOC

Total Organic Carbon (TOC) was measured on filtered samples using a Shimadzu TOC-5000A. Calibration of the TOC analyser was achieved using potassium hydrogen phthalate standards.

IC

For the monitoring of inorganic ions (NO_2^- , NO_3^- , NH_4^+ and SO_4^{2-}) an Ionic Chromatograph of Metrom which consists of an electrochemical detector 761 Compact IC and Metrosep C2 150 and Anion Dual 2 analytical columns for cations and anions, respectively, was used.

5.2.3. Photolysis Systems

An Oriel 1000W Xe-Hg lamp equipped with a cool water circulating filter to absorb the near-IR radiation and a cut-off filter $\lambda > 320$ nm was used, emitting spotted light of 370 mW cm^{-2} for the illumination of a quartz cell, measured by a by a power meter (Newport, optical meter).

Illumination in UV-A (320-400 nm) was also performed with a laboratory constructed "illumination box" equipped with four F15W/T8 black light tubes (Sylvania GTE, USA). The maximum emission of these tubes is around 365 nm, emitting ~ 1 mW cm^{-2} .

Solar light was provided by an Oriel photolysis apparatus (Photomax) equipped with an Oriel 150 W Xe arc lamp, a cool water circulating liquid filter to absorb the near IR radiation and finally with an Oriel AM1.5 G air mass filter. This filter corrects the output

of a 150 W xenon arc lamp to approximate the solar spectrum when the sun is at a zenith angle of 48.2 °. Light intensity was measured to be 85 mW cm⁻².

Visible light illumination covering the whole visible range (400 – 700 nm) was provided by the same photolysis apparatus (Photomax) equipped with a 435 nm cut-off filter exhibiting a zero transmittance below 410 nm. Light intensity was measured to be 107 mW cm⁻² by a power meter (Newport, optical meter). In all cases a borosilicate glass vessel reactor was sealed and placed inside a water thermostated jacket in order to prevent evaporation and retain the sample temperature constant at 25 °C during illumination.

5.3. Methods

In this section are included the analytical methods developed and applied for the determination of analytes concentration, in order to estimate the degradation rate of the starting compound and for identification of the intermediate products formed. Special techniques like HPLC-UV, SPME-GC/MS, LC-MS/MS and LLE-GC-MS were used. Also for the toxicity measurement the PPIA method was applied.

5.3.1. HPLC-UV for MC-LR determination

On the HPLC elution solvents used were Acetonitrile – Water both containing 0.05% TFA, with gradient elution mode, an injection volume of 20 µl, sample manually injected and with ambient column temperature.

The column selected was Agilent Eclipse XDB C-18, 4.6 x 150mm, Pz 3.5µm at a column flow rate of 1.2 ml/min. MC-LR eluted at 4.72 min. The gradient elution program is shown in Table 5.1.

Table 5.1. Gradient elution program applied with Agilent Eclipse XDB C-18 column.

Time (min)	MeCN (0.05%TFA) %	H ₂ O (0.05%TFA) %	Flow rate (ml/min)
0.00	35	65	1.2
2.00	70	30	1.2
2.10	100	0	1.2
3.00	0	100	1.2
3.10	35	65	1.2
8.00	35	65	1.2

5.3.2. HPLC-UV for CYN determination

The HPLC-UV method for the determination of CYN developed utilized the same HPLC equipment in the case of MC-LR, with the difference that a LiChrospher 100 RP-18 (5 µm) Hibar RT 250-4 column column was used and the UV detector was set at 262 nm. An isocratic elution program was applied, consisted in 90 % of H₂O and 10% MeOH, with 0.05% TFA.

5.3.3. SPME-GC/MS for GSM and MIB determination

The following method aimed in the identification and quantification of MIB and GSM in water. The two compounds are extracted from the headspace of the water sample by Solid Phase Micro-Extraction, SPME [269]. In specific, in a 4 ml vial, 0.75 g NaCl and a magnetic stirrer are added. Total volume of the sample is 2 ml. The temperature of the plate is set at 70 °C and stirring is set at 1000 rpm. The sample is extracted for 30 min.

Table 5.2. GC conditions for GSM and MIB quantification

Injector temperature	250 °C
Injection mode	Splitless – At 2 min split 20 ml/min
Duration of injection	2 min
Column	HP-5 MS, 30m x 0.25 mm i.d. x 0.25 µm film thickness
He flow rate	1 ml/min constant flow
Oven temperature program	50 °C for 1 min, 12 °C/min to 250 °C for 6 min

Table 5.3. The MS conditions are as in the following table:

Tuning mode	Autotune, standard spectra
Acquisition mode	SIM
Solvent delay	5 min
Monitored ions (<i>m/z</i>)	MIB: 95 (basic), 108, 135 (from 5 to 10 min), GSM: 112 (basic), 126 (from 10 min until to the end of the run)

5.3.4. LC-MS/MS for MC-LR Intermediates products

LC-MS/MS for MC-LR intermediates identification was carried out using a Kromasil 100-5C18 (5 μm , 150 mm \times 2.1 mm) reversed-phase LC column. Acetonitrile (A) and high-purity water (B), both containing 0.1 % HCOOH, were the mobile phase solutions and gradient elution was programmed from 15 to 25 % of acetonitrile in 10 min, followed by an increase to 40 % in 10 min and to 80 % in the next 15 min [30]. Flow rate was set at 0.2 ml min⁻¹ and the injection volume was 50 μL , using a full loop injection. MC-LR eluted at 25.9 min.

Detection was carried out in full scan mode (300-1200 *m/z*). Sheath gas was set at 20 arbitrary units (a.u.), auxiliary gas was set at 5 a.u. and spray voltage was 5 kV. Capillary temperature was set at 350 °C and collision pressure was 1.5 mbar. Collision energy and tube lens offset were optimized for MC-LR. For full scan MS/MS spectra, the selected precursor ions were isolated with an isolation width of 1 Da and product ions were formed with normalized collision energy of 30.

5.3.5. LC-MS/MS for CYN Intermediates products

Identification of reaction intermediates of CYN was carried out using LC-MS/MS. Detection was performed in full scan mode (100-520 *m/z*). Chromatographic separation was performed by using a Kromasil 100-5C18 (5 μm , 150 mm \times 2.1 mm) reversed-phase LC column. For full scan MS/MS spectra, the selected precursor ions were isolated with an isolation width of 1 Da and product ions were formed with normalized collision energy of 30.

Liquid chromatography configuration for CYN intermediates identification was performed using as mobile phase A: 97.8% H₂O, 2% acetonitrile and 0.2% acetic acid and for B: 99.8% acetonitrile and 0.2% acetic acid. Gradient elution was programmed as 2 % of B for 10 min, followed by a linear increase to 95% of B to 50 min and then held constant for an additional 10 min. Flow rate was set at 0.2 ml min⁻¹ and the injection volume was 100 µL, using a full loop injection.

5.3.6. LLE-GC-MS for GSM and MIB Intermediates products

Identification of intermediate products during the photocatalytic degradation of either GSM or MIB was performed with employment of a gas chromatography-mass spectrometry (GC-MS) system. A GC temperature gradient program from 50 °C (held for 1 min) to 250 °C (held for 6 min), using a temperature ramp (12 °C min⁻¹) under constant flow (1 mL min⁻¹) was used. Extraction of the intermediate products was achieved using liquid-liquid extraction technique. For the organic phase, dichloromethane was used as a solvent with a volume of 20 ml in triplicate and a volume of 20 ml from the aqueous photolysed solution. Total volume of dichloromethane was then condensed into a final volume of 0.5 ml.

Scanning was monitored at a *m/z* range from 20 to 300 amu. The injection was carried out splitless at 250 °C and the injection volume was 2.0 µl. The electron energy was set at 70 eV, the ion source temperature was maintained at 230 °C and the quadrapole temperature at 150 °C.

5.3.7. Toxicity Measurements

Evaluation of a photocatalytic process should be consisted of data concerning the toxicity of the photocatalytic reaction intermediates and final products. Toxicity results obtained by the application of PPIA and *Microtox* bioluminescence assays. The PPIA assay has a high specificity regarding MCs, as it was developed on the basis of the ability of microcystins (MCs) to inhibit serine and threonine phosphatase enzymes. The extent of inhibition of these enzymes is related to the hepatotoxicity of these compounds and their tumor promotion properties as well. The inhibition reaction by these toxins can be used as measure of toxin concentrations. On the other hand, *Microtox* assay has an

extended use as a screening test for a broad spectrum of toxic substances and can be sensitive in toxicity detection of byproducts and intermediates formed during photocatalysis.

Protein phosphatase inhibition assay (PPIA)

In order to assess the residual toxicity of water samples during the course of the photocatalytic degradation of toxin MC-LR, the protein phosphatase inhibition assay (PPIA) was used. It was developed on the basis of the ability of microcystins (MCs) to inhibit serine and threonine phosphatase enzymes. The extent of inhibition of these enzymes is related to the hepatotoxicity of these compounds and their tumor promotion properties as well. The inhibition reaction by these toxins can be used as a measure of toxin concentrations. The most common assays used are based on colorimetric applications because they are less expensive and more convenient than the others using radioisotopic techniques. The PPIA assay is fast and easy to use, although it needs a lot of work for solution preparation. The PPIA assay provides important toxicological information regarding the bioactivity of MCs, since detection is based on functional activity rather than on recognition of chemical structure.

Protein phosphatase 2A (PP2A) is a serine/threonine phosphatase isolated from human red blood cells. It is isolated as a heterodimer of 60kDa (A) and 36kDa (C) subunits. PPase-2A has the ability to dephosphorylate the α -subunit of phosphorylase kinase. PP2A was supplied in lots of 25 units from Promega Corp., USA. P-nitrophenyl phosphate (Interchim, France) was used as a substrate. Enzyme (PP2A) and substrate solutions were prepared according to known procedure (Heresztyn and Nicholson, 2001). Samples (20 μ l) were combined with PP2A solutions (20 μ l) in microplate wells and incubated at 37°C for 5 min. After addition of 200 μ l of substrate solution, the microplate was incubated at 37°C for 1.5 h and the absorbance of the wells was measured at 410 nm using a Tecan Infinite M200 microplate reader (Tecan Group Ltd., Switzerland).

Storage Buffer: 20mM MOPS (pH 7.5), 150mM NaCl, 1mM MgCl₂, 1mM EGTA, 0.1mM MnCl₂, 1mM DTT, 0.1mg/ml BSA, 60mM 2-mercaptoethanol, 50% glycerol.

Unit Definition: One unit is the amount of PPase-2A required to release 1nmol of phosphate from PNPP in one minute at 30°C under the assay conditions described below.

Concentration: 0.5u/μl.

Identity: The identity of PPase-2A Catalytic Subunit is confirmed by performing an activity assay in the presence and absence of PPase-1 Inhibitor-2 (50nM), a specific inhibitor for type 1 protein phosphatases. In the presence of 50nM PPase-1 Inhibitor-2 the enzyme activity is inhibited by less than 10%.

Toxin concentrations were calculated from calibration curves which were plotted as percentage inhibition of PP2A, expressed as %B /Bo, versus microcystin concentration on a semi-log scale, where B and Bo are the absorbance values of the sample and the blank, respectively. In blanks, microcystin standards were replaced by high-purity water so full color development was obtained.

Calculation of Enzyme Activity:

$$\text{Enzyme Activity (nmol P}_i \text{ / min / } \mu\ell) = \frac{(\text{assay volume}) \times (\text{dilution factor}) \times (\text{sample absorbance}_{410\text{nm}} - \text{control absorbance}_{410\text{nm}})}{(\text{sample volume}) \times (\text{reaction time}) \times (\text{extinction coefficient}) \times (\text{path length})}$$

Where:

Assay volume = 200 μl

Dilution factor = fold dilution of enzyme

Sample volume = 20 μl

Reaction time = 15 minutes

Extinction coefficient of p-nitrophenolate (pH 7.4) = 17.5/cm[nmol/μl]

Path length = 0.4 cm

Microtox utilizes *vibrio fischeri* as the organism for toxicity testing. *Vibrio fischeri* are nonpathogenic, marine, luminescent bacteria which are sensitive to a wide range of toxicants. The organisms are supplied for use in a standard freeze-dried (lyophilized) state, which serves to maintain the sensitivity and stability of the test organisms. This bacterium emits light as a result of normal metabolic processes. A reduction in luminescent ability during exposure to contaminants or pollutants is taken as a measure of toxicity. The more toxic the sample, the less light will be produced by the bacteria.

Each test uses approximately 1 million organisms and each organism is less than 1 mm in diameter, so a very high surface-to-volume ratio is presented. Sensitivity and statistical significance are, therefore, high; the response being an integrated effect of the toxicant on the entire population, which is very large.

Dilutions of the sample substances are then added to vials of bacteria, and measurements are made at certain intervals of time of the light output of these bacteria. The standard time is fifteen minutes. The measurements of the light output are then adjusted with changes in the control, as light outputs change naturally over time.

The effective concentration (EC50) is determined as the concentration of a toxicant that causes a 50% reduction in light.

$$\text{Toxicity Units (TU)} = 100 / \text{IC}_{50} (\text{EC}_{50})$$

Experimental Procedure

Luminescent bacteria are exposed to a range of concentrations of the testing substance (MC-LR). The light emitted from the bacteria (490 nm maximum emission) is measured by a light reader (Model 500 Analyzer) to set up a dose response relationship. IC50, a concentration which inhibits 50% of light output, is then determined. The results are expressed as a percentage of the control. Use of the control sample compensates errors up to 20 %, due to pipetting and to correct samples for the time-dependent drift in light output. Samples and standards prepared are measured in three time intervals 5, 15 and 30 minutes.

The selected Microtox protocol uses a 50% dilution of the sample. Especially, 250 µL of an aqueous solution of 4 % NaCl (Diluent) and 250 µL of sample were used. The final solution has a total salinity of 2 %. Reagent solution is prepared by adding reconstitution solution to the freeze dried bacteria in order to be activated.

After mixing and coming to appropriate temperature (15 °C for sample and 5 °C for reagent), 10 µL of reagent was used in each cuvette. In each experiment four control (250 µl distilled water instead of sample) and one positive (2,4-dichlorophenol, 2,4-DCP) samples were used. Percent toxicity effect is reported for 15 min of reaction.

The control cuvette is used to correct samples for the time-dependent drift in light output.

$$\text{toxic effect} = (I_0 - I_t) / I_0$$

$$G = (I_0 / I_t) - 1$$

Where:

I_0 is the average initial bacterial luminescence (I_0) of the control samples

I_t is luminescence of the sample after time t (15 min)

G is luminescence intensity

The percentage of luminance reduction of the bacteria is calculated as below:

$$\% \text{ Effect}_t = [G_t / (1 + G_t)] \times 100$$

Samples with % effect >20 are considered positive for toxicity.

5.4. Experimental

5.4.1. Degradation Experiments

In a typical experiment for MC-LR or CYN degradation, 5 mL of aqueous of the compound solution (10 mg L^{-1}) containing 200 mg L^{-1} of the TiO_2 photocatalyst were added to a cylindrical pyrex cell, oxygenated for twenty minutes and covered air tightly with a serum cap. Illumination was carried out at $25 \text{ }^\circ\text{C}$ in the photolysis apparatus under constant stirring.

In a typical experiment for GSM/MIB degradation, aqueous solution (20 mL) containing the photocatalyst $\text{SiW}_{12}\text{O}_{40}^{4-}$ ($7 \times 10^{-4} \text{ M}$, 200 mg L^{-1}) or TiO_2 was added to a cylindrical pyrex cell, oxygenated for 20 min, spiked with GSM or MIB solution giving a total concentration of 1 mg L^{-1} and covered air tightly with a serum cap. Photocatalysts loadings were selected according to previous studies for comparison reasons [34, 44]. Illumination was performed at ambient temperature in the photolysis apparatus. The solutions were magnetically stirred throughout the experiment. In experiments with $\cdot\text{OH}$ radical trapping reagents (scavengers) KBr (10^{-2} M) and tertiary butyl alcohol (10^{-2} M) were used.

The initial rate constants were calculated from the trace of the variation of the concentration of substrates divided by their initial concentration with time for the first 30 % of the reaction and are roughly within 20%.

5.4.2. Mineralization Experiments

The mineralization extent of the compounds has been evaluated by employing total organic carbon (TOC) and ionic chromatography (IC) measurements.

N/No of NO_3^- , NH_4^+ , NO_2^- is the ratio between the concentration (M) of each ion as determined at various time intervals during MC-LR photocatalytic degradation divided by the concentration (M) of nitrogen based on MC-LR chemical structure and initial concentration.

5.4.3. Intermediates Elucidation Experiments

For the identification of MC-LR and CYN intermediate products, a solution of 12 mL containing 10 mg L^{-1} of the toxin and 200 mg L^{-1} of TiO_2 was irradiated and samples were taken at certain time intervals during the process.

For intermediates identification experiments in the case of GSM and MIB, a concentration of 20 mg L^{-1} was used. Total volume (20 mL) was extracted in dichloromethane and evaporated to 0.5 mL, using low nitrogen flow at 35°C .

CHAPTER 6

Photocatalytic degradation and Mineralization of MC-LR, CYN, GSM and MIB in water under UV-A, Solar and visible light

6.1. Introduction

A variety of traditional water treatment methods, including coagulation/sedimentation [143], activated carbon adsorption [144] and membrane separation [145], have been attempted for the removal of cyanotoxins, but with limited success. Previous studies have demonstrated that TiO₂ photocatalysis [11-18, 20] can effectively destroy cyanotoxins in aqueous solution and that hydroxyl radical is responsible for a significant fraction of the observed degradation.

In this chapter is reported the photocatalytic degradation and mineralization of MC-LR, CYN, GSM and MIB under UV-A, solar and visible light irradiation in the presence of new nanostructured TiO₂ photocatalysts. Commercial Degussa P25 TiO₂, Kronos and Ref-TiO₂ nanopowders were used for comparison. In addition, the mineralization extent has been evaluated by using TOC and inorganic ions (NO₂⁻, NO₃⁻ and NH₄⁺) determinations.

6.2. Photocatalytic Degradation and Mineralization of MC-LR under UV-A and Solar light

MC-LR degradation has been the object of study to a number of papers some of them using TiO₂ photocatalysis [20, 22, 270]. As far as one can tell from the literature there are only few studies concerning the MC-LR photocatalytic mineralization [15, 20].

In this chapter is reported the photocatalytic degradation of MC-LR using UV-A and solar light irradiation in the presence of new nanostructured TiO₂ photocatalysts.

6.2.1. Photocatalytic Degradation and Mineralization of MC-LR under UV-A irradiation

Illumination of an aqueous solution of MC-LR with $\lambda_{\max}= 365$ nm in the presence of commercial Degussa P25 TiO₂, Kronos vlp-7000, N-TiO₂, NF-TiO₂, GO-TiO₂, ECT-1023t or Ref-TiO₂ nanopowder results in the photodegradation of the substrate (Figure 6.1.), whereas experiments performed in the dark indicated that the contribution of hydrolysis is negligible. These results are in agreement with those reported by others concerning commercial Degussa P25 TiO₂ and Kronos vlp-7000. As can be seen in Figure 6.1., under UV-A irradiation ($\lambda_{\max}= 365$ nm) all photocatalysts were effective in toxin elimination. The higher MC-LR degradation was observed with Degussa P25 TiO₂ with 98% toxin destruction followed by ECT-1023t, N-TiO₂, GO-TiO₂, Kronos vlp-7000 and NF-TiO₂ with 97.5, 96.5, 88.9 and 75.6% toxin destruction, respectively, after 20 minutes of irradiation.

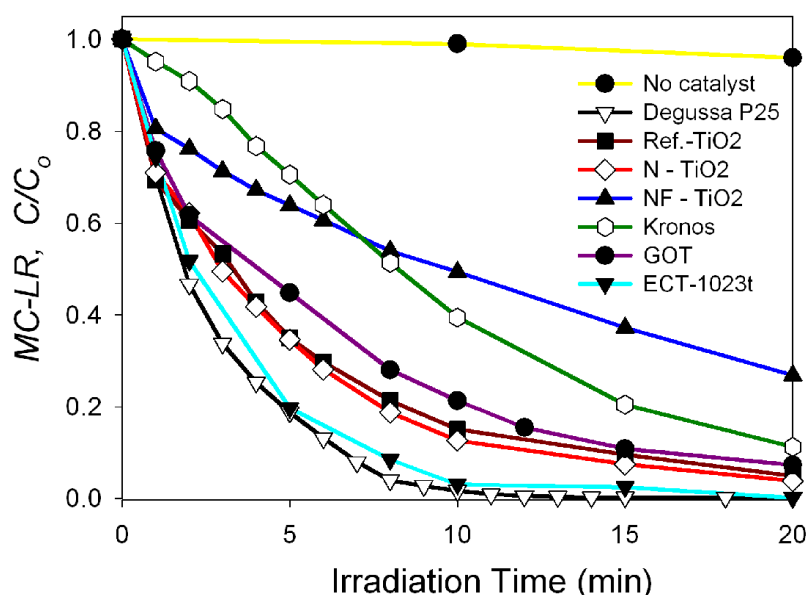


Figure 6.1. Photocatalytic degradation of MC-LR under UV-A irradiation in the presence of different TiO₂ based nanostructured materials.

To the best of my knowledge, the degradation process has been studied only during limited time of irradiation. In this study, prolonged illumination of an aqueous solution of MC-LR in presence of Degussa P25 TiO₂, N-TiO₂ and NF-TiO₂ has been performed. It was found that it leads to the almost total mineralization of the substrate giving as final products CO₂ and inorganic ions (NO₃⁻ and NH₄⁺) (Figure 6.2.). NO₂⁻ that is produced in traces during the process finally is oxidized to NO₃⁻.

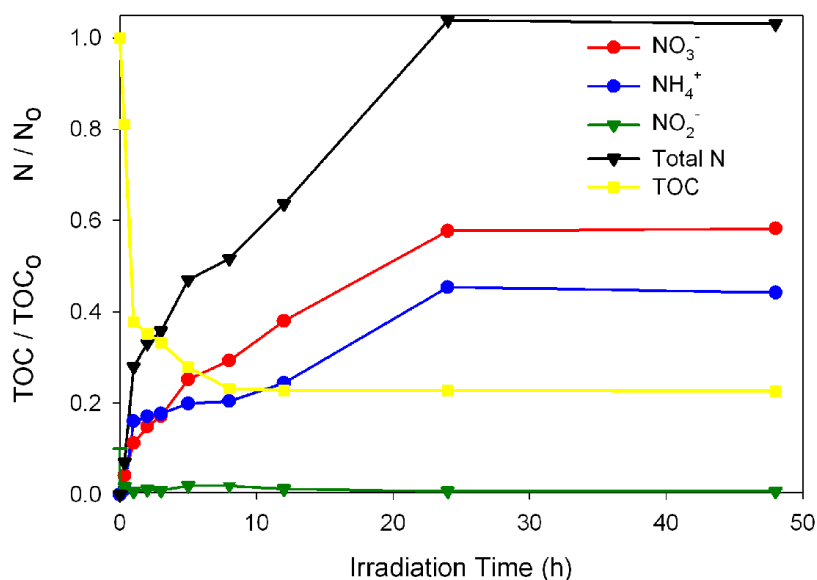


Figure 6.2. Carbon mineralization and time evolution of nitrate, nitrite, ammonium ions and total nitrogen during MC-LR degradation under UV-A irradiation in the presence of Degussa P25 TiO₂ [20].

As can be seen in Figure 6.2., after 8h of irradiation ~80% of organic carbon and ~50% of organic nitrogen have been recovered, while degradation of MC-LR has been completed in less than 20 min (Figure 6.1.). The complete disappearance of the MC-LR in a much shorter time than the evolution of CO₂ and inorganic ions is due to the presence of organic intermediates before the complete mineralization of the substrate. The lack of ~20% on initial TOC value should be assigned to still remaining nitrogen containing compounds, like linear sequences of amino acids as those identified after intense photocatalysis with TiO₂ [19, 230]. Within these peptide derivatives and related structures, there are molecules containing C-N bonds, with or without H extractable atoms.

According to an overview on the fate of organic nitrogen in photocatalysis with TiO₂, in case of structures with extractable H on carbon [271], the proposed mechanism of transformation accounts for an •OH attack on the α-CH bond with an hydrogen extraction. Through further oxidation steps the nitrogen is finally released as ammonium ions. This general model is closely related to that for amino acids, peptides and proteins which has been deeply discussed [272, 273].

Nitrate formation cannot be explained on the basis of the mechanism described above. When no extractable H exists on carbon, •OH radical attack seems to occur on the nitrogen instead of the carbon atom. This is the case of guanidine and its derivatives,

structural units of arginine in MC-LR, where OH attack occur on the amino group with the release of nitrogen mainly as nitrite, suddenly transformed into nitrate ions [274].

After 24h of irradiation, the total nitrogen produced accounts for almost the stoichiometric quantity of the initial organic nitrogen. The remaining organic carbon ~20% can be attributed to small aliphatic hydrocarbon compounds (Figure 6.2.).

The ratio $[\text{NH}_4^+]/[\text{NO}_3^-]$ which is characteristic of the substrate molecular structure was after 5h of irradiation, 3:4. These results are in agreement with those reported for guanidine and methylguanidine derivatives, where the organic nitrogen is mainly released as nitrate ions [271, 274]. The increased yield of nitrate ions can also be attributed to a secondary pathway proposed for amino acids photocatalytic degradation, which could occur through the release of an amino group as hydroxylamine from the parent molecule being then transformed into nitrate ions and acetic acid [273, 275]. The acid can subsequently undergo oxidation via a photo-Kolbe type process (oxidation via electron transfer and decarboxylation) to generate carbon dioxide and formic acid, which also generates carbon dioxide via a similar process [273].

In Figure 6.3. the photocatalytic mineralization of MC-LR under UV-A irradiation in the presence of N-TiO₂ is presented. Based on TOC measurements, almost complete mineralization has been achieved after illumination for 48 h.

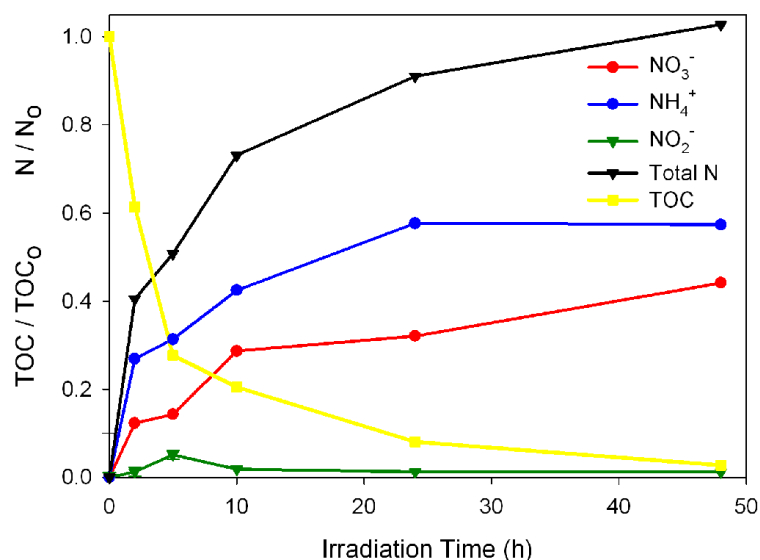


Figure 6.3. Mineralization of MC-LR using N-TiO₂ under UV-A light [20].

In Figure 6.4. photocatalytic mineralization of MC-LR under UV-A irradiation in the presence of NF-TiO₂ is presented. Based on TOC measurements, almost complete mineralization has also been achieved after illumination for 48 h.

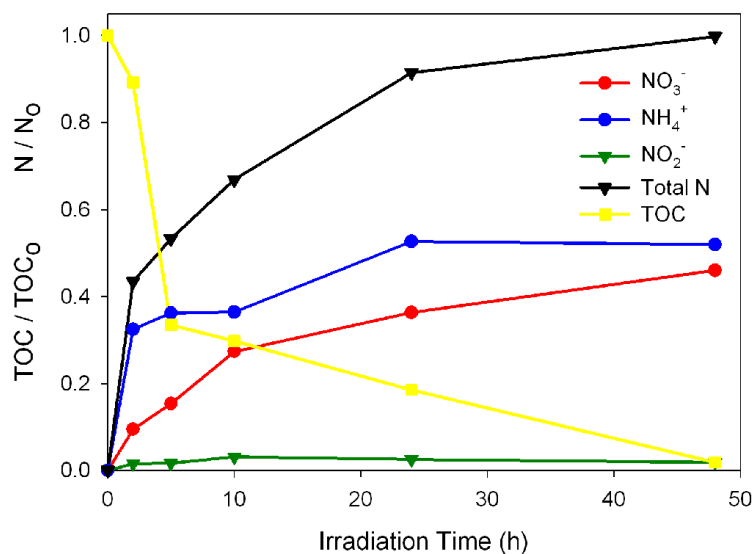


Figure 6.4. Mineralization of MC-LR using NF-TiO₂ under UV-A light.

At the same time period, the total nitrogen produced accounts for the stoichiometric quantity of the initial organic nitrogen. As comes out from the time evolution curves of nitrate and ammonium ions, the characteristic ratio $[\text{NH}_4^+]/[\text{NO}_3^-]$ was changed to 3:2 after 10h of irradiation.

The greater overall yield of NH_4^+ ions than the corresponding amount of NO_3^- was attributed to the release of inorganic nitrogen from N-TiO₂ photocatalyst during the process. From blank experiments which are performed upon stirring and illumination of N- TiO₂ in the absence of MC-LR it was shown that after 2h, nitrogen mainly as NH_4^+ was released corresponding to 25% of the initial organic nitrogen present in MC-LR.

Various model compounds such as aminoacids, sorbic acid, 2-acetamidoacrylic acid have been used to mimic degradation of individual functional groups of MC-LR [159, 273, 274]. These results should be assessed carefully because MC-LR is not simply an assemblage of these small molecules. Finally, although there are many unclear points in understanding mineralization pathways, it is clearly observed the complete mineralization of MC-LR by TiO₂ photocatalysts.

6.2.2. Photocatalytic Degradation and Mineralization of MC-LR under solar light

As it was shown in the previous section, the tested nanostructured TiO₂ catalysts exhibit significant photocatalytic activity for the MC-LR degradation under UV-A light irradiation. TiO₂ photocatalysts for toxin degradation was also used under solar light irradiation. The employed illumination apparatus provides a very close spectral match to solar spectra offering significant advantages such as control of the local environmental parameters, repeated and comparable experimental conditions, unlimited availability of solar radiation etc. Under these experimental conditions, the nanostructured TiO₂ materials exhibited high photocatalytic activity as it is presented in Figure 6.5.

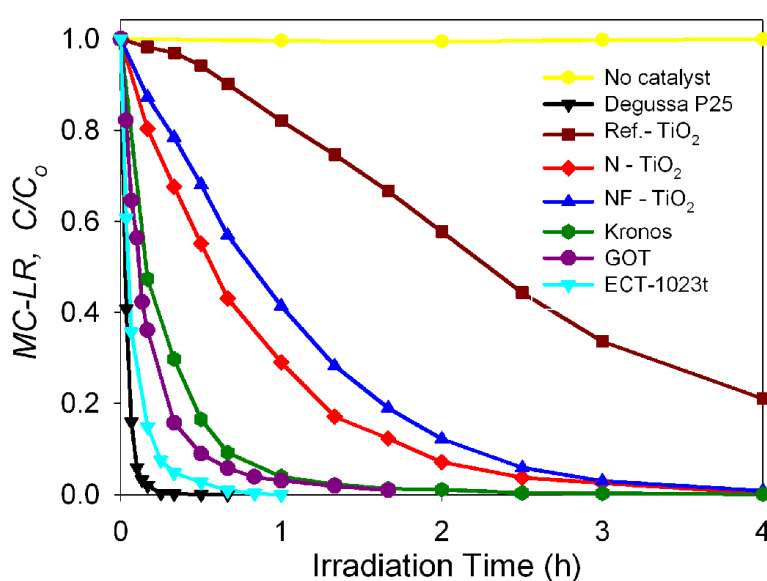


Figure 6.5. Photocatalytic degradation of MC-LR under Solar light irradiation (AM 1.5G), in the presence of TiO₂ based materials. Experimental conditions: MC-LR C₀=10 ppm, catalyst concentration 200 ppm, 25 °C, oxygenated and non buffered solutions.

As can be seen in Figure 6.5., N- and NF- doped TiO₂ nanocatalysts exhibit very close photocatalytic activity with that of commercially available materials such as Degussa P25 TiO₂ and Kronos vlp-7000 for the destruction of MC-LR. GO-TiO₂ and ECT-1023t photocatalysts show even better photocatalytic activity than commercially available Kronos. Under solar light illumination, both photocatalysts (N- and NF- TiO₂) have shown complete elimination of MC-LR after irradiation for 4 h.

These results show that the prepared N-TiO₂, NF-TiO₂, GO-TiO₂ and ECT-1023t nanocatalysts exhibit high photocatalytic activity for the destruction of microcystin MC-LR under UV-A and solar irradiation. Under the employed experimental conditions the tested photocatalysts achieved complete degradation of MC-LR toxin.

The mineralization of MC-LR using N-TiO₂ under solar light is presented in Figure 6.6. Based on TOC measurements, after illumination for 48 h a mineralization extent of 85% have been achieved. The total nitrogen produced after 48 h of illumination accounts for the 80% of the initial organic nitrogen.

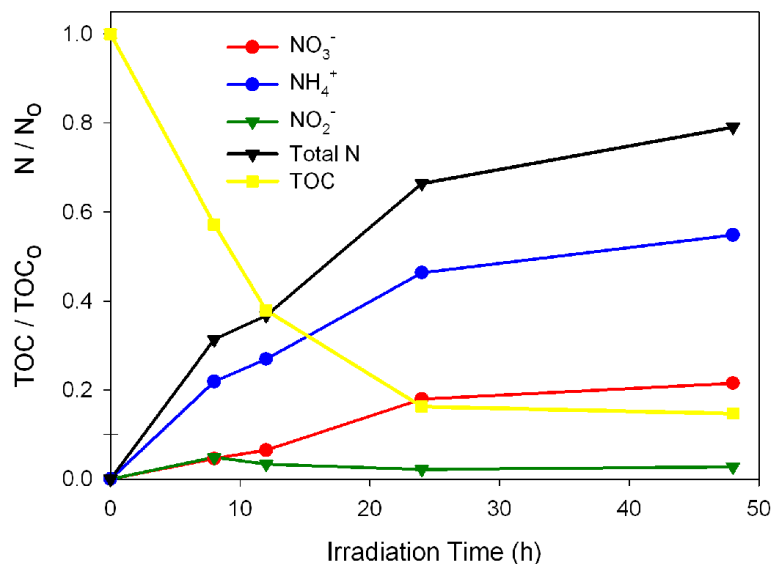


Figure 6.6. Mineralization of MC-LR using N-TiO₂ under solar light [20].

These results shown that the tested N- TiO₂ nanocatalyst exhibits high photocatalytic activity for the destruction of MC-LR under UV-A and solar irradiation. Under the employed experimental conditions the tested photoctalyst achieved complete degradation of MC-LR toxin. The similar behavior of N-TiO₂ with that of Degussa P25 standard material suggests common degradation pathways mainly through the •OH radical generation.

6.3. Photocatalytic Degradation and Mineralization of CYN under UV-A and Solar light

As far as concerning removal and degradation of CYN in drinking water treatment plants a number of studies have been conducted. A variety of oxidants have been studied for the destruction of CYN [155-159], with the majority of those techniques being effective on the process. Although common oxidants have been able to oxidize CYN, AOPs have been proposed as an alternative to chemical oxidation. In a recent study by He *et al.* [276] the destruction of CYN by hydroxyl and sulphate radicals was investigated, using UV activation of hydrogen peroxide, persulfate and peroxymonosulfate. Also, few

studies have demonstrated that TiO₂ photocatalysis can effectively destroy CYN in aqueous solution [21, 22].

6.3.1. Photocatalytic Degradation of CYN under UV-A and solar light

Complete degradation of the cyanotoxin was achieved within 15 and 40 min of irradiation under UV-A light using Degussa P25 and Kronos vlp-7000 respectively (Figure 6.7.), whereas experiments in the absence of photocatalysts showed that direct photolysis was negligible. Under solar light irradiation both photocatalysts appeared to be effective in CYN degradation (Figure 6.8.) with Degussa P25 showing better performance under either UV-A or solar light.

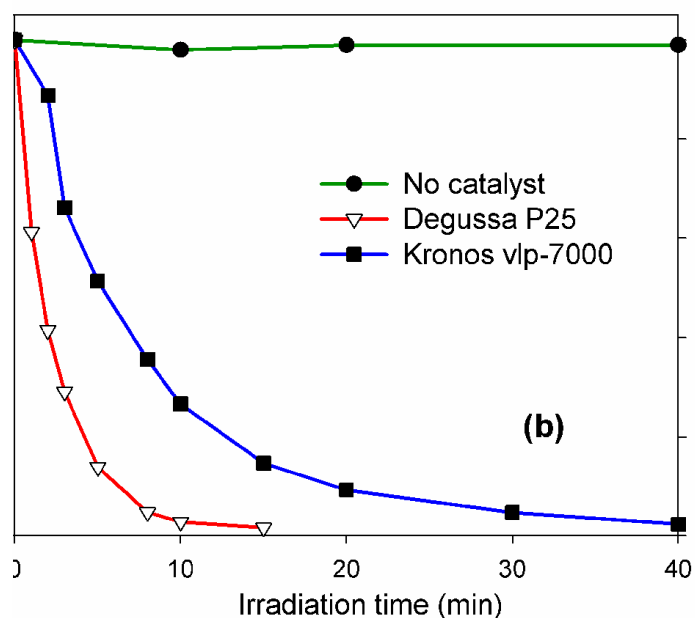


Figure 6.7. Degradation of CYN (10 mg L⁻¹) in the absence and presence of photocatalyst (Degussa P25 or Kronos vlp-700, 200 mg L⁻¹) under UV-A light [277].

Degussa P25 demonstrated an improved performance like in previous studies concerning another cyanotoxin, the heptapeptide microcystin-LR [20]. This is attributed to its mixed-phase, (anatase-rutile). The smaller band gap of rutile extends the photoactivity range into the visible region. The improved performance of Degussa P25 is also attributed to the slower recombination through stabilization of charge separation by electron transfer from rutile to anatase and to the small size of rutile crystallites facilitating this transfer, making catalytic hot spots at the rutile/anatase interface [278].

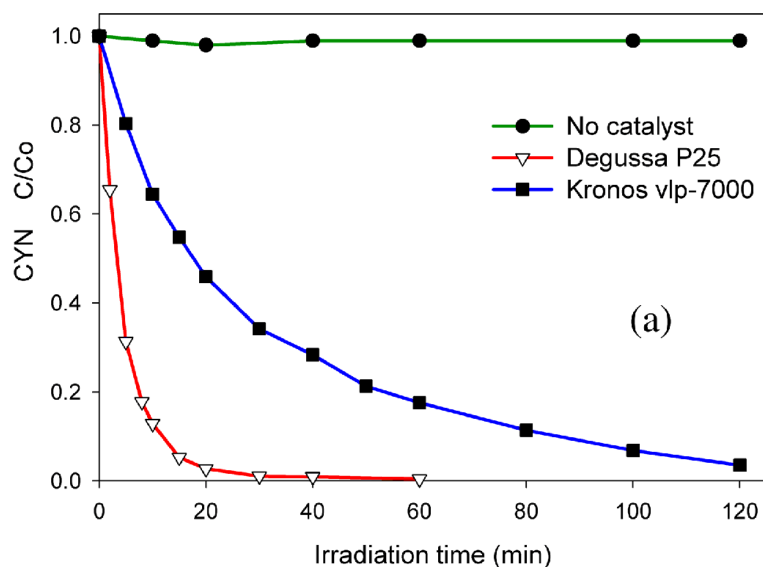


Figure 6.8. Photocatalytic degradation of CYN (10 mg L^{-1}) using TiO_2 photocatalysts (200 mg L^{-1}) under solar light (AM 1.5 G) [277].

In conclusion, employment of TiO_2 photocatalysis appeared to be an effective process for CYN elimination in aqueous solution, coming in agreement with previous studies [21, 22].

6.3.2. Photocatalytic mineralization of CYN under UV-A light

The photocatalytic degradation process of CYN can lead to complete mineralization, i.e. to complete oxidation to carbon dioxide and inorganic ions (NO_2^- , NO_3^- , NH_4^+ and SO_4^{2-}). Monitoring of this mineralization process was carried out by measurements of TOC and inorganic ions, in order to assess if the parent compound and intermediate products could be completely removed from water at the end of a treatment process. There are no reports in the literature regarding the extent of mineralization, since degradation of CYN has been studied only under limited time of irradiation [21, 22, 242].

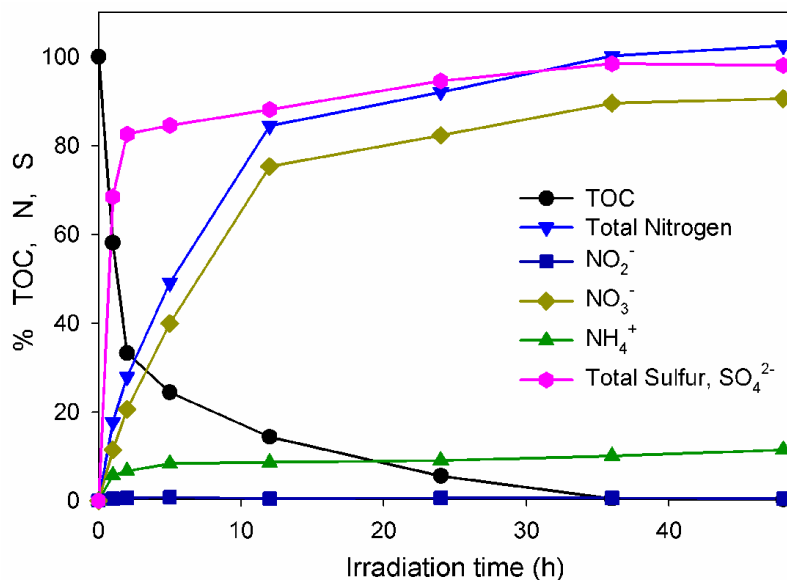


Figure 6.9. Carbon mineralization and time evolution of total nitrogen (NO_2^- , NO_3^- and NH_4^+ ions) and total sulphur (SO_4^{2-} ion) during CYN degradation under UV-A irradiation in the presence of P25 TiO_2 [277].

As shown in Figure 6.9., after 12 h of irradiation ~ 80% of total organic carbon (%TOC), ~80% of total nitrogen (% N) and ~90% of total sulphur (% S), were converted to inorganic forms, while complete degradation of the parent CYN molecules was completed within the first 15 min of irradiation under UV-A using Degussa P25. % N of NO_2^- , NO_3^- , and NH_4^+ ions, is the ratio between the concentration (M) of each ion as determined at various time intervals during CYN photocatalytic degradation divided by the concentration (M) of nitrogen based on CYN chemical structure and initial concentration. Total nitrogen % N represents the sum of % N of NO_2^- , NO_3^- , and NH_4^+ at various time intervals of illumination.

TOC and inorganic ions (NO_2^- , NO_3^- , SO_4^{2-} and NH_4^+) measurements showed that complete mineralization of CYN was achieved under UV-A light in the presence of Degussa P25 photocatalyst after 36h of irradiation. Degradation of CYN proceeds to 100 % recovery of carbon as CO_2 , 100% sulphur as SO_4^{2-} and 100 % nitrogen as NO_3^- and NH_4^+ . The complete disappearance of the parent compound CYN occurs in a shorter time than the evolution of CO_2 and inorganic ions, suggesting the presence of organic intermediates before the complete mineralization of the substrate. As shown in Figure 6.9., there is a particular ratio between NH_4^+ and NO_3^- concentration. According to an overview on the fate of organic nitrogen in TiO_2 photocatalysis, it has been reported to be related essentially to the initial oxidation state of nitrogen in the organic molecule and the structure of the organics [271].

A mechanism proposed for the formation of NH_4^+ applies for structures with extractable H on carbon and accounts for an $\cdot\text{OH}$ attack on the $\alpha\text{-CH}$ bond resulting in hydrogen extraction. Through a further $\cdot\text{OH}$ attack giving an $\cdot\text{OH}$ addition, cleavage on the C-C bond and formation of a carbonyl group and an amine, the nitrogen is finally released as NH_4^+ [279]. This mechanism is closely related to that for amino acids, peptides and proteins which has been deeply discussed [272, 273]. Nitrate formation cannot be explained on the basis of the mechanism described above. In this case probably the $\cdot\text{OH}$ attack seems to occur on the nitrogen instead of the carbon atom, when no extractable hydrogen is available [274].

After 5 h of irradiation, about ~75 % of organic carbon and ~50% of organic nitrogen were mineralized, from which the 10 % is NH_4^+ and the 40 % is NO_3^- with the ratio of $[\text{NH}_4^+]/[\text{NO}_3^-]$ being ~1/5. When complete organic carbon was mineralized after 36 h of irradiation, total organic nitrogen was also mineralized with NH_4^+ being ~11% and with NO_3^- coming up to ~89% of the initial, with a ratio of $[\text{NH}_4^+]/[\text{NO}_3^-]$ at ~1/10. Based on this observation and the mechanisms discussed above, the dominance of NO_3^- could be attributed to preferable attack of $\cdot\text{OH}$ radical on nitrogen rather on $\alpha\text{-CH}$ carbon atoms of CYN.

6.4. Photocatalytic Degradation and Mineralization of GSM and MIB under UV-A and Solar light

In cyanobacteria bloom events when GSM and MIB are released, removal processes are required. Studies have shown that employment of standard water treatments and the use of common oxidants for their removal appeared to be ineffective [160-162]. TiO_2 photocatalysis was proven to be effective in their photocatalytic degradation. Lawton *et al.* [235] reported rapid degradation of both GSM and MIB with more than 99% removal within 60 minutes of illumination in the presence of suspended TiO_2 . Bellu *et al.* [23], using a pellet form of TiO_2 completely removed GSM within 25 minutes of treatment. A preliminary study was also performed by Pemu *et al.* [24] using TiO_2 photocatalysis of GSM in which few intermediate products were identified.

In this chapter is reported the photocatalytic degradation and mineralization of GSM and MIB in water using TiO_2 -based photocatalysts under UV-A and solar light irradiation.

6.4.1. Photocatalytic Degradation of GSM and MIB under UV-A and solar light

Illumination of an aqueous solution of GSM and MIB (1 mgL^{-1} for each compound) under UV-A ($\lambda_{\text{max}}=365 \text{ nm}$) in the presence of 200 mgL^{-1} of several TiO_2 based nanocatalysts (commercial Degussa P25 TiO_2 , Kronos, N- TiO_2 , NF- TiO_2 , GO- TiO_2 , ECT-1023t and Ref- TiO_2 nanopowders) results in photodegradation of substrates (Figures 6.10. and 6.11., for GSM and MIB, respectively). These results are in agreement with those reported by others in a preliminary study concerning commercial Degussa P25 TiO_2 [31]. Under UV-A irradiation all photocatalysts were effective in both compounds elimination as can be seen in Figures 6.10. and 6.11. Degussa P25 TiO_2 showed the higher GSM and MIB degradation, followed by ECT-1023t, Kronos, NF- TiO_2 N- TiO_2 , GO- TiO_2 and Ref- TiO_2 which exhibited similar photocatalytic activity.

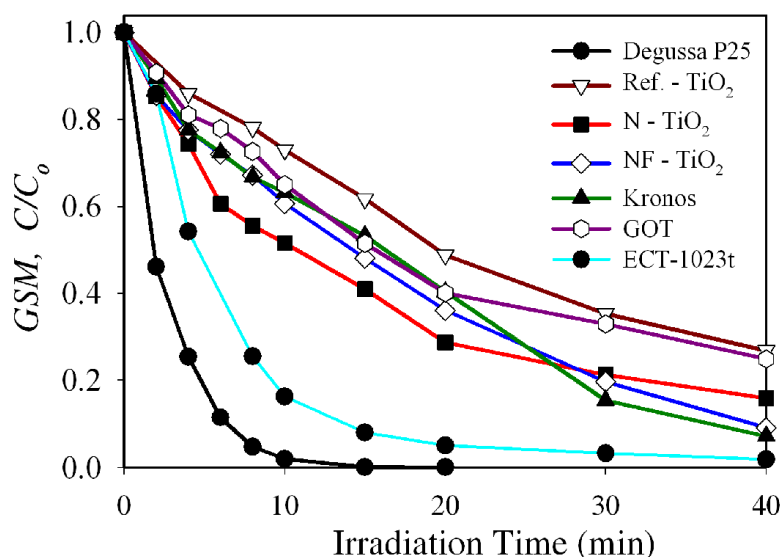


Figure 6.10. Photocatalytic degradation of 1 mgL^{-1} GSM under UV-A ($\lambda_{\text{max}}=365 \text{ nm}$) in the presence of different TiO_2 based nanostructured materials.

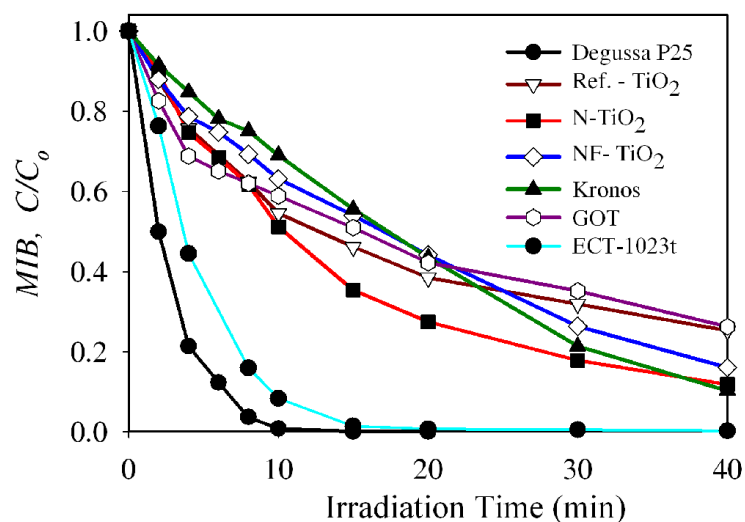


Figure 6.11. Photocatalytic degradation of 1 mgL^{-1} MIB under UV-A ($\lambda_{\text{max}}=365 \text{ nm}$) in the presence of different TiO_2 based nanostructured materials.

All photocatalysts were also active on degradation of GSM and MIB under solar light illumination, as it is depicted in Figures 6.12. and 6.13. Compared to Ref-TiO₂ undoped material, N-TiO₂ and NF-TiO₂ showed better performance. The same was also observed for the commercial Kronos TiO₂ which is a C-doped visible light activated photocatalyst. The better performance of Degussa P25 TiO₂ and ECT-1023t seems to be due to the UV part of the solar light. Similar results have been reported for the photocatalytic behavior of these TiO₂ based nanomaterials towards microcystin-LR (MC-LR) [31]. As a result, visible light activated N-TiO₂ and NF-TiO₂ exhibit improved photocatalytic activity for the destruction of GSM and MIB under UV-A and solar irradiation.

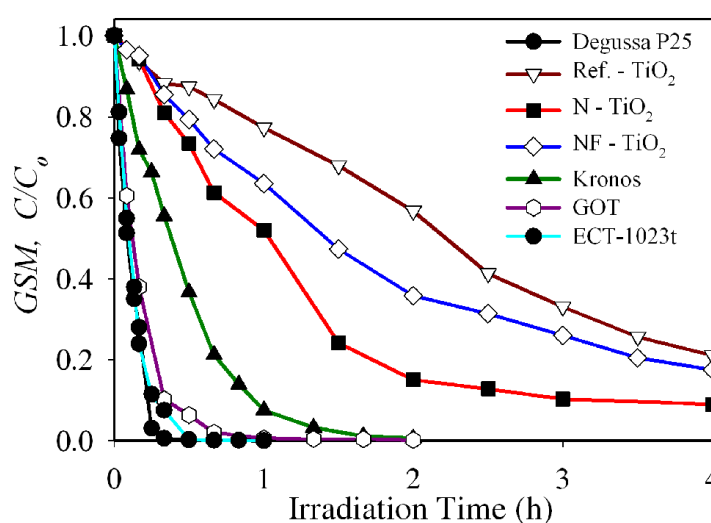


Figure 6.12. Photocatalytic degradation of 1 mgL⁻¹ GSM under solar light (AM 1.5 G) in the presence of different TiO₂ based nanostructured materials.

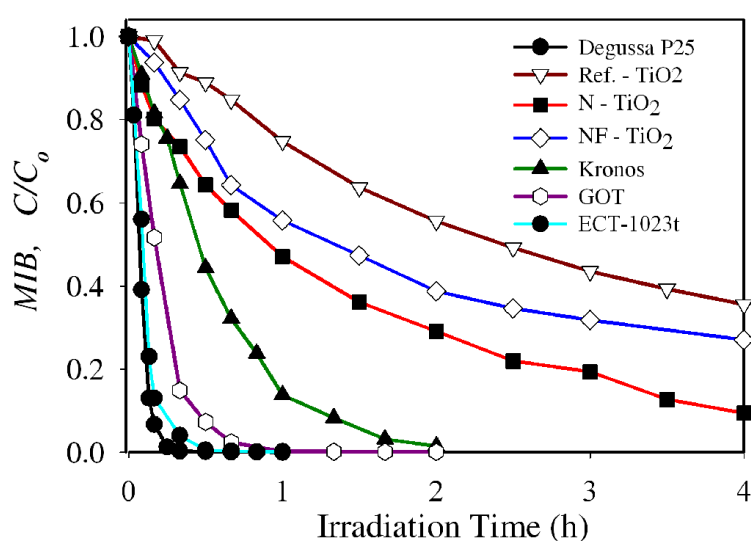


Figure 6.13. Photocatalytic degradation of 1 mgL⁻¹ MIB under solar light (AM 1.5 G) in the presence of different TiO₂ based nanostructured materials.

6.4.2. Photocatalytic Mineralization of MIB and GSM under UV-A and solar light irradiation

Even though degradation of GSM and MIB is complete under both UV-A or solar light in the first 60 minutes of irradiation, is highly important to determine total organic carbon in the solution in order to explain the fate of starting materials under these experimental conditions. Remaining total organic carbon (TOC) in photodegraded solutions is monitored with organic carbon measurements. In order to accomplish appropriate amount of TOC for measurement, the initial concentration of GSM and MIB was set at 10 mg L^{-1} . Under constant stirring in dark conditions in air-tightened vessel, a solution containing 10 mgL^{-1} of GSM and MIB was kept, in order to evaluate forthcoming volatilization. Results suggested that no significant volatilization of the substrates took place.

Prolonged illumination of aqueous solution of MIB or GSM in the presence of TiO_2 catalysts leads to mineralization of the substrate giving as final product CO_2 . Figure 6.14. shows the photocatalytic mineralization of MIB and GSM under UV-A irradiation using Degussa P25 TiO_2 as a photocatalyst while in Figure 6.15. it is presented the photocatalytic mineralization of MIB and GSM under solar light irradiation using GO- TiO_2 photocatalyst.

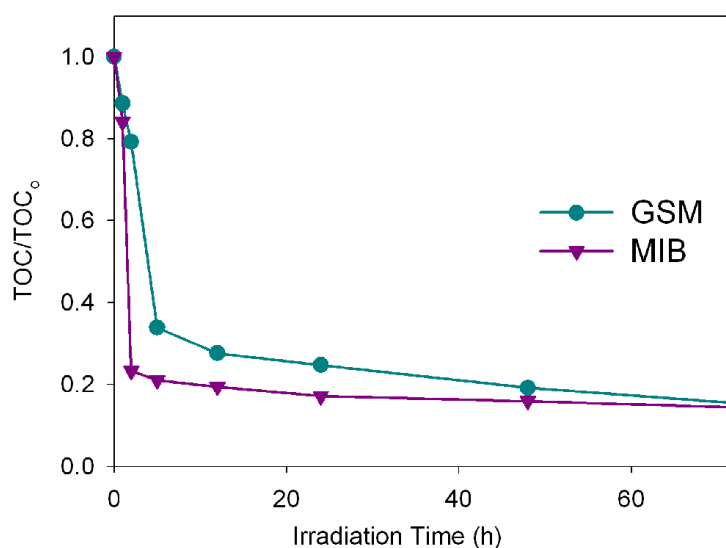


Figure 6.14. Photocatalytic Mineralization of GSM and MIB under UV-A ($\lambda_{\text{max}} = 365 \text{ nm}$) irradiation using Degussa P25 TiO_2 catalyst.

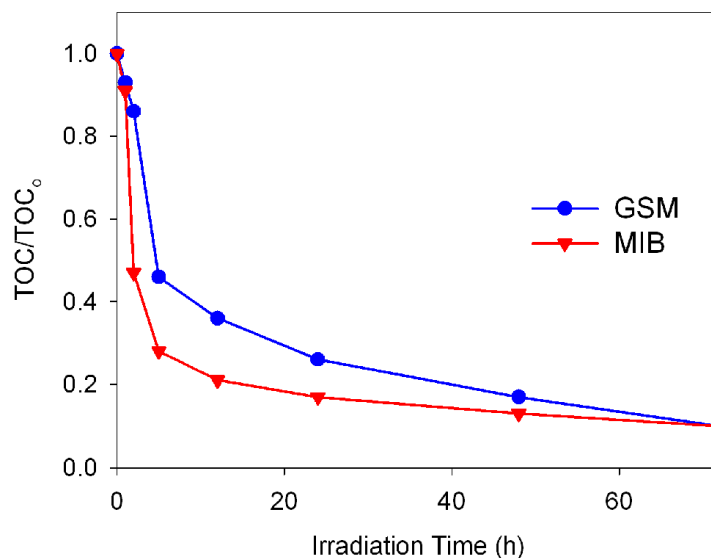


Figure 6.15. Photocatalytic Mineralization of GSM and MIB under solar light (AM 1.5 G) irradiation using GO- TiO₂ catalyst.

Almost complete mineralization for both compounds in both UV-A and solar light was observed. GSM mineralization seems to be a bit slower than MIB.

The shorter time needed for degradation than for mineralization is due to formation of organic intermediates that also react with the photocatalysts. Reduction of TOC is evidenced only after a small induction period indicating also that the mineralization proceeds through several intermediate steps. The incomplete removal of TOC (~80% - 85%) can be assigned to the formation of small partially oxidised molecules that are mineralized slowly.

6.5. Application in real water samples

To explore natural water degradation from cyanobacterial metabolites with TiO₂ photocatalysis process, GO-TiO₂ nanocomposite was used. Experiments with surface water were carried out (in the presence of the natural constituents of water), using solar light irradiation. Surface waters that were collected from two lakes of Greece that also serve as water reservoirs for the population of Athens (Mornos Lake and Marathonas Lake), were used as natural matrices. The basic physicochemical parameters of these waters are shown in Table 6.1.

Table 6.1. Physicochemical parameters of surface water samples (before spiking)

Parameter	Marathonas Lake	Mornos Lake
pH	8.2	8.1
Dissolved Org. Carbon (mg L ⁻¹)	2.5	1.4
Total Alkalinity (mg CaCO ₃ L ⁻¹)	123	132
Conductivity (mS)	386	304
Total Hardness (mg L ⁻¹)	169	145
Turbidity (NTU)	1.7	1.5

Water samples were spiked with known concentrations of MC-LR, MIB and GSM at concentrations of 10 mg L⁻¹, 1 mg L⁻¹ and 1 mg L⁻¹ respectively.

Irradiation of samples was carried out with solar light and GO-TiO₂ (200 mg L⁻¹) was used as the photocatalyst. As shown in Figures 6.16. and 6.17., all pollutants were removed from spiked natural water solutions, similarly to the experiments that were carried out in ultrapure water.

The observed rate constants (k , x10⁻³) for MC-LR, GSM and MIB were 5.3, 3.2 and 5.7 min⁻¹, respectively for Marathonas Lake, and 4.5, 2.3 and 3.7 min⁻¹ for Mornos Lake, respectively. Although these rate constants were generally lower than those of ultrapure water, results showed that GO-TiO₂ remains an effective photocatalyst even in natural waters which contain natural organic matter and other constituents (Table 6.1.) that may compete with the target pollutants for the reactive oxidative species produced by the photocatalytic process. The results are promising for up-scaling of the process for natural water detoxification/decontamination (e.g. fisheries-aquaculture) as well as for drinking water treatment. These results are in accordance with Pelaez *et al.* [280] who studied the effects of water parameters on the degradation of MC-LR using TiO₂ based photocatalysis. In that study they showed that the solution pH is a major factor influencing the degradation rate, with higher pH values resulting in the reduction of the degradation. As far as concerning alkalinity the main responsible species are bicarbonate ion HCO₃⁻, carbonate ion CO₃²⁻ and hydroxide ion OH⁻. Both HCO₃⁻ and CO₃²⁻ can act as scavengers of the radical species produced, also reducing the initial degradation rates [280].

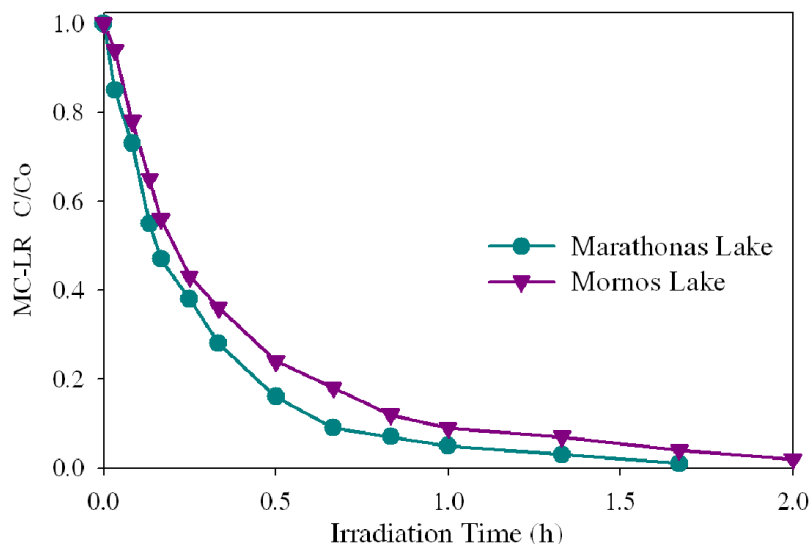


Figure 6.16. Photocatalytic degradation of MC-LR (10 mg L^{-1}) under solar light irradiation, using GO-TiO_2 photocatalyst (200 mg L^{-1}) in real water samples [270].

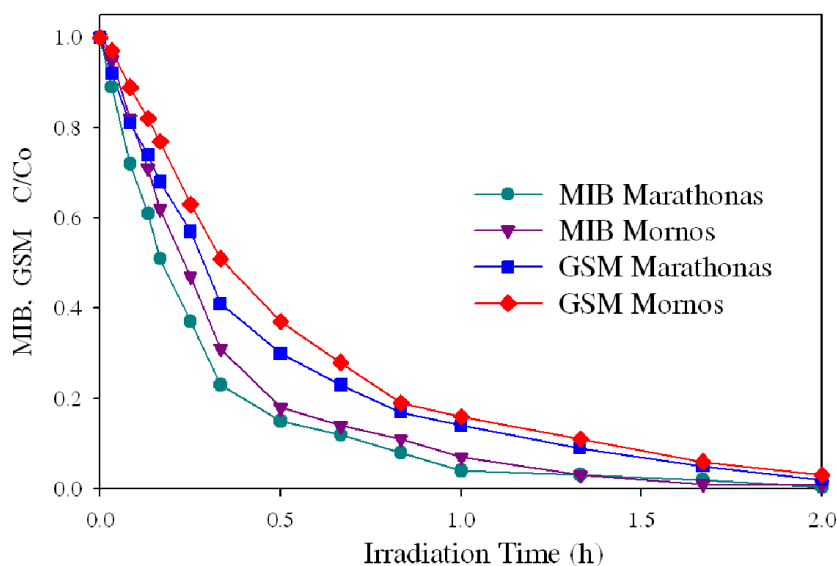


Figure 6.17. Photocatalytic degradation of MIB and GSM (1 mg L^{-1}) under solar light irradiation, using GO-TiO_2 photocatalyst (200 mg L^{-1}) in real water samples [270].

6.6. Photocatalytic Degradation of MC-LR, CYN, GSM and MIB under visible light

Experiments have been performed to test the photocatalytic efficiency of the new TiO_2 nanostructured materials under visible light illumination. As it can be seen in Figure 6.18, when illumination was performed only the visible light activated TiO_2 photocatalysts (Kronos TiO_2 , N- TiO_2 , NF- TiO_2) show remarkable activity in MC-LR degradation, while Degussa P25 and Ref- TiO_2 are completely inactive. Among the tested materials, N- TiO_2 shows the better photocatalytic activity for MC-LR degradation followed by and NF- TiO_2 then Kronos TiO_2 . This behavior of N- TiO_2 is attributed to a

red-shift of the energy band gap to the visible range at about 2.3 eV that justifies visible light photocatalytic activity towards degradation of MC-LR [258]. The photocatalytic activity of NF-TiO₂ is due to the effective doping with nitrogen and fluorine and their synergistic effects towards visible light photoresponse [136]. C-doping in Kronos TiO₂ produces new energy states deep in the TiO₂ band gap (substitution of oxygen by carbon atoms), which are responsible for the visible light absorption [256, 257].

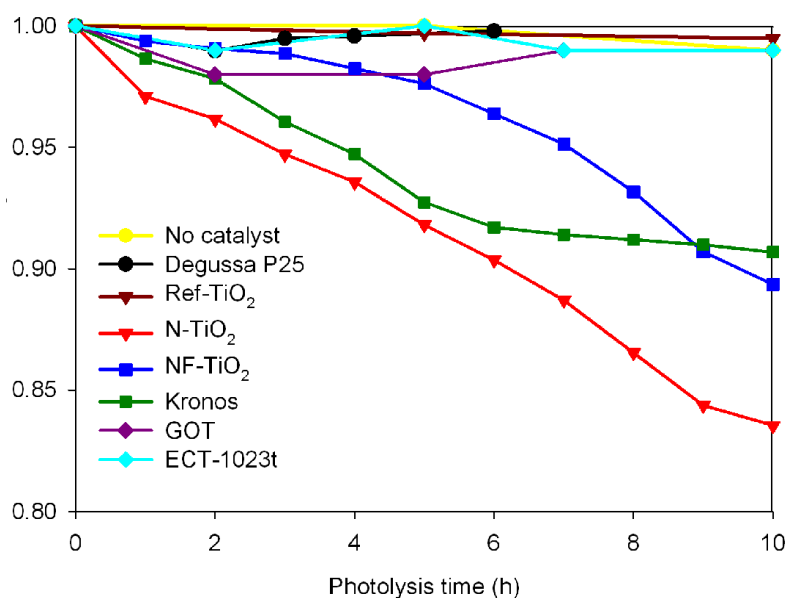


Figure 6.18. Photocatalytic degradation of MC-LR (10 mg L⁻¹) under visible light illumination in the presence of TiO₂ nanomaterials (200 mg L⁻¹).

In the case of CYN illumination under visible light the commercially available materials were tested and only Kronos vlp-7000 showed photocatalytic activity, while Degussa P25 was completely inactive, Figure 6.19. Kronos vlp-7000 is a C-doped visible light activated TiO₂ based material. In conclusion, employment of TiO₂ photocatalysis appeared to be an effective process for CYN elimination in aqueous solution, coming in agreement with previous studies [21, 22].

Experiments were also performed to investigate GSM and MIB degradation under visible light. Catalyst loading was 200 mg L⁻¹ and the concentration of GSM and MIB was set at 1 mg L⁻¹ for each target analyte. Lower concentrations were used (2x10⁻³ mg L⁻¹) but still no degradation was observed for both concentration levels of GSM and MIB. To eliminate the case that the experimental error from the SPME was overlapping the small percentage of destruction, liquid-liquid extraction was applied with dichloromethane as the organic solvent. Based on those results, it can be concluded

that in the cases of GSM and MIB, the mechanism followed in the visible light photocatalysis process could not lead to their degradation.

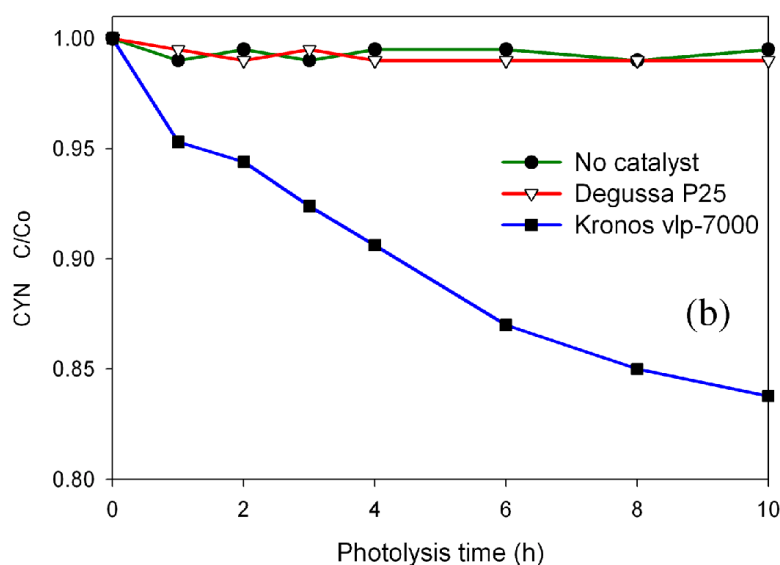


Figure 6.19. Photocatalytic degradation of CYN (10 mg L^{-1}) using TiO_2 photocatalysts (200 mg L^{-1}) under visible [277].

6.7. Conclusions

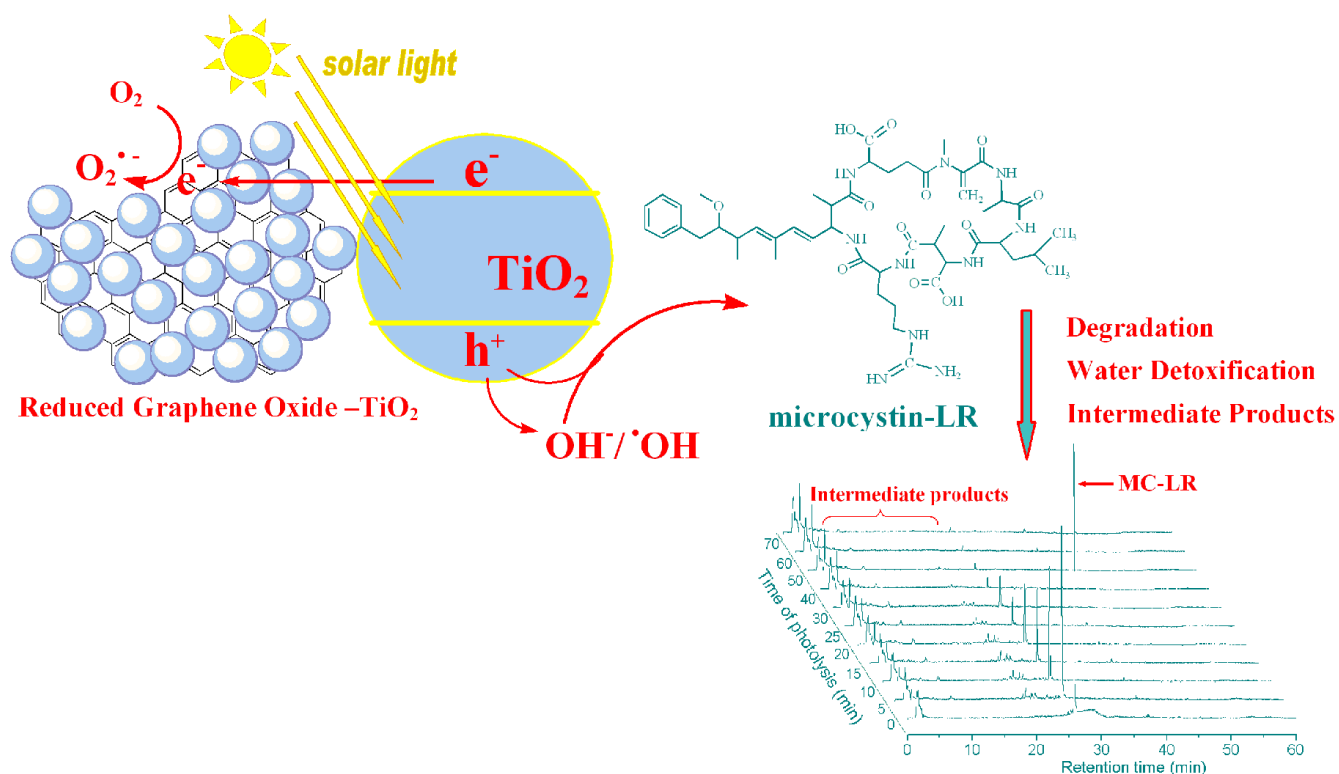
The novel TiO_2 photocatalysts (ECT-1023t, N-, NF- and GO- TiO_2) showed significant photocatalytic activity for the destruction of MC-LR, CYN, GSM and MIB. Under UV-A and solar light illumination all photocatalysts were effective for the complete degradation of the target compounds, exhibiting similar photocatalytic activity with that of the well known Degussa P25 catalyst. Under visible light illumination, the tested N- and NF-doped TiO_2 photocatalysts showed higher photocatalytic activity for MC-LR degradation than that of commercial Kronos TiO_2 , while Degussa P25 and Ref- TiO_2 catalysts were completely inactive. Determination of the mineralization extent of the tested compounds was performed with total organic carbon (TOC) and inorganic ion measurements. It was proved that for MC-LR, mineralization higher than 90% was achieved under UV-A and solar light illumination using N- and NF- doped TiO_2 . CYN mineralization was complete using Degussa P25 under UV-A light. In the case of GSM and MIB the mineralization was higher than 90% utilizing GO- TiO_2 catalyst under solar light. These results confirm the ability of the prepared photocatalysts to effectively degrade and mineralize the target compounds under UV-A and solar light. Taking into account all results it can be concluded that the tested photocatalysts are highly active under UV-A and solar light for the destruction of the tested compounds and can be further applied in lab and pilot-plant scale photoreactors.

CHAPTER 7

Degradation Pathway of MC-LR

7.1. Introduction

The purpose of the chapter was to investigate the reaction mechanism for the photocatalytic degradation of MC-LR in water. Commercially available Degussa P25 photocatalyst was used under UV-A and GO-TiO₂ composite photocatalyst under solar light irradiation. Identification of intermediate products formed was performed using LC-MS/MS. Assessment of the residual toxicity was also carried out during the course of photocatalysis.



Scheme 7.1. Objective of Chapter 7 [270].

7.2. Intermediate products of MC-LR under UV-A and solar light using TiO₂

Even though employing TiO₂ photocatalysis has been proved to be very useful and successive for the degradation of organic pollutants in aquatic environment, the elucidation of degradation pathway and the determination of intermediate products, is also necessary for the verification of detoxification. So far, a number of studies have examined degradation pathways of MC-LR when conventional oxidants or AOPs are applied, including ozonation [25, 26], chlorination [27], ultra-sonication [28], photolysis [29], TiO₂/UV-A [18, 19, 30, 31] and N-TiO₂/UV-A [18]. The fact that analytical standards for MC-LR reaction intermediates are not commercially available complicates the identification of primary intermediates [2, 154]. In this chapter, identification of intermediate products formed during the photocatalytic degradation of MC-LR using GO-TiO₂ under solar light and Degussa P25 under UV-A was carried out using LC-MS/MS. The majority of byproducts detected, were produced within the first 2 min of irradiation. The concentration of most of the byproducts during photocatalysis initially increased followed by a decrease over time, due to their subsequent oxidation. Structural characterization of intermediates produced during photocatalysis of MC-LR was based on the analysis of LC-MS chromatograms and the respective mass spectrum. Although many of the intermediates that were identified were already known,[19, 31, 281] a number of new intermediates were observed (*m/z*: 313.5, 368.5, 389, 411.5, 417, 437, 457, 515.5, 544, 781.5, 980.5 and 1031.5) and possible structures are proposed (Table 7.2.).

The majority of intermediates detected under UV-A and solar light irradiation were the same, since photocatalysis under solar light is mainly due to the UV part of the spectrum. Chromatograms resulted from photocatalytic degradation of MC-LR are presented in Figure 7.1.a. for Degussa P25 under UV-A irradiation (0 - 15 min) and in Figure 7.1.b. for GO-TiO₂ under solar light irradiation (0 – 70 min).

Table 7.1. presents all products that were detected during the photocatalytic degradation of MC-LR under UV-A and solar light irradiation, their retention times (*R_t*), molecular weight (MW), formulas and possible chemical structures.

MC-LR is consisted of seven aminoacids, 3-amino-9-methoxy-2,6,8-trimethyl-10-phenyl-4,6-decadienoic acid (Adda), iso-glutamic acid (Glu), methyl dehydroalanine (Mdha), D-

alanine (Ala), L-leucine (Leu), D-methylaspartic acid (MeAsp) and L-arginine (Arg), and it can be denoted as Cyclo[-Adda-Glu-Mdha-Ala-Leu-MeAsp-Arg-] [282]. One of the most intense peak observed (higher peak area in relative abundance) corresponded to a product at m/z 1029 with a mass spectrum showing a molecular ion $(M + H)^+$. This product is generated by hydroxyl radical attack at either double bond C_4 or C_6 on the conjugated diene structure system, of the Adda chain [Adda(OH)₂], resulting in double hydroxylation of MC-LR.[19, 28-31] In relative abundance chromatogram (Figure 7.2.), multiple peaks for m/z 1029 appeared, suggesting that except C_4 - C_5 and C_6 - C_7 dihydroxy addition, geometrical isomers of dihydroxy-MC-LR could be deduced, which was also suggested by Antoniou *et al.* 2008 [283]. Further oxidation of dihydroxylated MC-LR with cleavage of the dihydroxylated bond at positions C_4 - C_5 or C_6 - C_7 on the Adda chain, results in products with m/z 795 (aldehyde intermediate) and m/z 835 (ketone intermediate), respectively. Further oxidation of product m/z 795 forms m/z 811 intermediate, consistent with a carboxylic acid structure. A new intermediate observed at m/z 1031.5 could be possibly formed from double hydroxylation of the double bonds of Adda [Adda(OH)₂]₂ or one hydroxylation on Adda chain and another one on the Mdha chain [Mdha(OH)₂]. Also, m/z 1029 product could be resulted from double hydroxylation of the double bond on the chain of Mdha [Mdha(OH)₂]. Consecutive oxidation leads to the formation of an aldehyde (m/z 1011.5)[19, 28, 30] and cleavage on the C'-CO bond results to the m/z 1015.5 product [19].

Another multiple peak observed was that at $m/z=1011.5$ (Figure 7.2.). There are different possible pathways for the formation of intermediates with this molecular ion. One possibility is a hydroxyl substitution of the hydrogen at C_7 to form enol-MC-LR [Adda(O)] or on the Mdha [Mdha(O)], which rapidly isomerizes to a more stable tautomer of ketone-MC-LR [281]. Another possibility is a hydroxyl substitution on aromatic hydrogen (o-, p- and to a lesser extent the m- hydroxylated product). A second hydroxylation of the aromatic ring follows, yielding m/z 1027.5 [19, 28, 30] intermediate (explaining multiple peaks), (Figure 7.2.). Demethoxylated-MC-LR on the methoxy group of Adda, through the formation of the formic acid ester results in intermediate at $m/z=1009.5$ (double peak, E-Z isomers) [19], (Figure 7.2.). Another intermediate observed with multiple peaks at $m/z=1045.5$ [28], consists to triple hydroxylation of MC-LR (one on aromatic ring and two on Adda chain or one on aromatic ring and two on side chain of the toxin between Mdha and Ala).

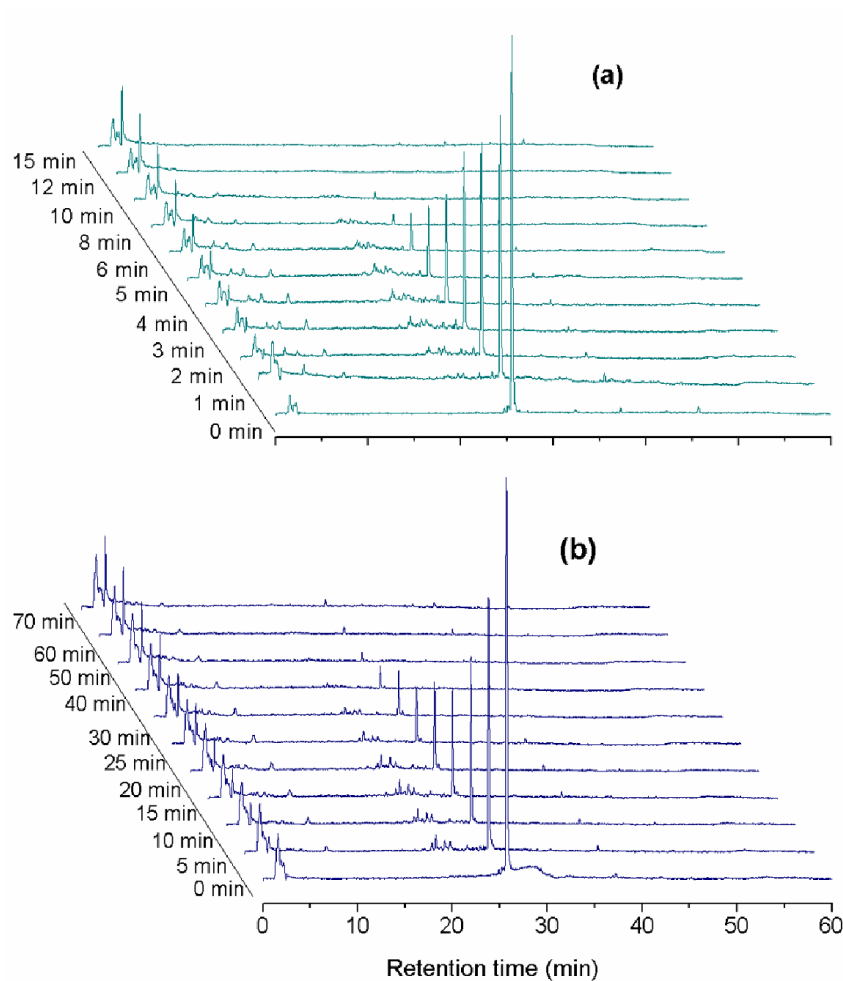


Figure 7.1. Chromatograms resulted from MC-LR photocatalytic degradation using (a) Degussa P25 under UV-A irradiation and (b) GO-TiO₂ under solar light irradiation [270].

The observation of intermediate at m/z 965 ($M+Na^+$) is consistent with linearization of MC-LR, after cleavage ($-C_3O$) on the side chain of the toxin between Mdha and Ala [19]. After production of m/z 965, the generation of product at m/z 999.5 ($M+Na^+$) takes place through dihydroxylation on the Adda subsequent bonds [28, 31]. Further oxidation could result to a ketone with m/z 783.5. A product with m/z 965 could also result from abstraction of the methoxy group from Adda chain [Adda(-Methoxy)]. Upon addition of amino group, a new observed product at m/z 980.5 could be formed.

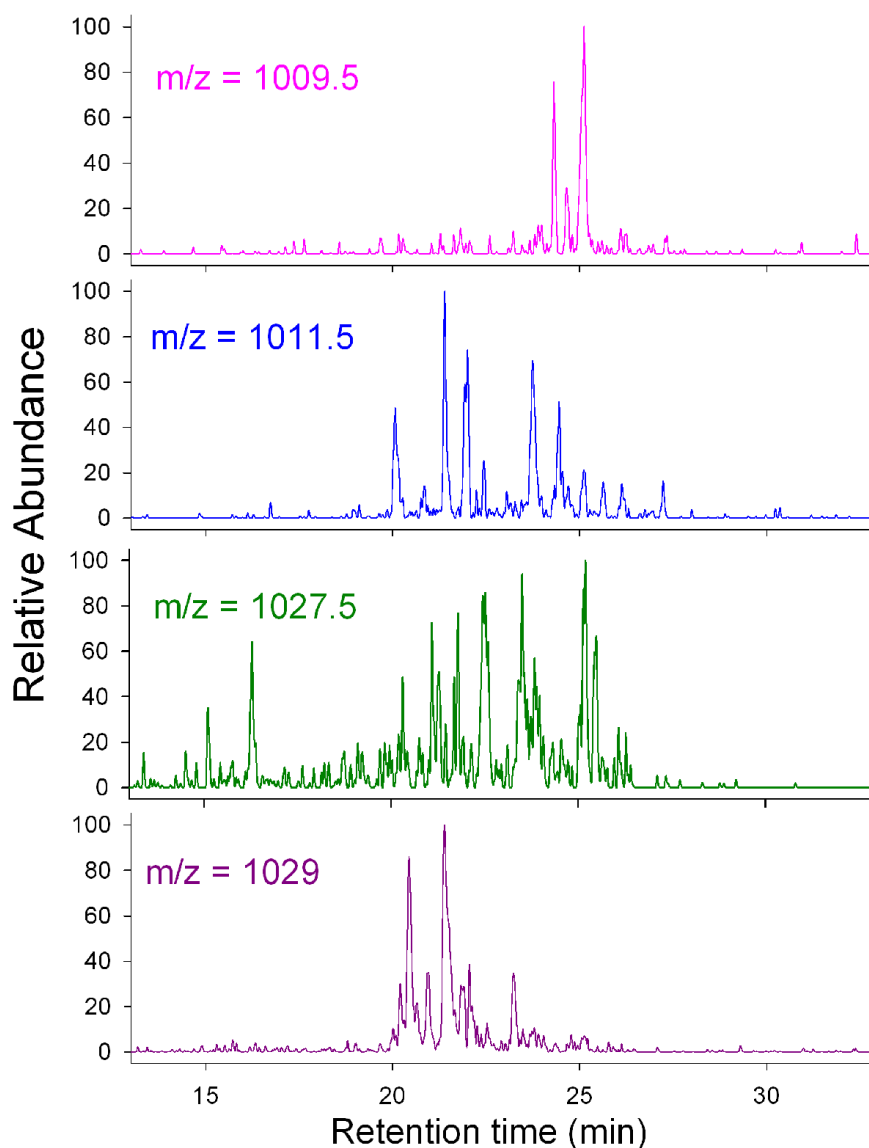


Figure 7.2. LC-MS chromatograms of MC-LR photocatalytic degradation in the presence of Degussa P25 after irradiation with UV-A for 5 min [270].

Products reported in Table 7.1., with $m/z < 781.5$ are observed for the first time and could be oxidation products of those with higher m/z . For example products at m/z 315.5, 368.5 and 411.5, could be formed after oxidation of product at m/z 1045.5.

In Table 7.2. are presented the proposed possible structures of the new intermediates observed (m/z : 313.5, 368.5, 389, 411.5, 417, 437, 457, 515.5, 544, 781.5, 980.5 and 1031.5).

Table 7.1. Products observed from MC-LR degradation using Degussa P25/UV-A and GO-TiO₂/solar light irradiation [270].

No	Peak (m/z)	R _t (min)	MW and Formula	Possible structure	Catalyst
-	995.5	25.9	C ₄₉ H ₇₄ N ₁₀ O ₁₂ , 994.5	MC-LR: Cyclo [-Adda-Glu-Mdha-Ala-Leu-MeAsp-Arg-]	-
1	313.5	38.1- 42.6	C ₁₆ H ₂₄ O ₆ , 312.2	Dihydroxy-7-(hydroxy-phenyl)-6-methoxy-3,5-dimethyl-heptanoic acid	TiO ₂ , GO-TiO ₂
2	368.5	21.2-25.8	C ₂₀ H ₃₃ NO ₅ , 367.2	OH-Adda(H ₂ O) ₂	GO-TiO ₂
3	389.5	5.3- 6.1	C ₁₅ H ₂₈ N ₆ O ₆ , 388.2	H-Arg-NHCH(OH)CH(CH ₃)CO-Glu-H	TiO ₂ , GO-TiO ₂
4	411.5	4.8, 6.4	C ₂₂ H ₃₈ N ₂ O ₅ , 410.3	OH-Adda(H ₂ O) ₂ -NHCH ₂ CH ₃	GO-TiO ₂
5	417	4.7- 6.1	C ₁₇ H ₃₂ N ₆ O ₆ , 416.2 C ₁₈ H ₃₂ N ₄ O ₇ , 416.2	OH-Arg-MeAsp-Leu-H H-MeAsp-Leu-Ala-Mdha(OH)-H	TiO ₂ , GO-TiO ₂
6	437	9.4	C ₁₇ H ₃₀ N ₆ O ₆ Na, 414.2(23)	[H-Arg-NHCH(CHO)CH(CH ₃)CO-Glu-CH ₃] ⁺ Na ⁻	TiO ₂ , GO-TiO ₂
7	457	9.0	C ₂₀ H ₃₆ N ₆ O ₆ , 456.2	H ₃ C-Arg-MeAsp-Leu-COCH ₃	TiO ₂ , GO-TiO ₂
8	515.5	20.3	C ₂₁ H ₃₇ N ₇ O ₈ , 515.3	Arg-MeAsp-Leu-Ala-COOH	TiO ₂
9	544	21.5-23.8	C ₂₃ H ₄₁ N ₇ O ₈ , 543.3	Arg-MeAsp-Leu-Ala-COCHOHCH ₃	TiO ₂ , GO-TiO ₂
10	781.5	6.4	C ₃₄ H ₅₆ N ₁₀ O ₁₁ , 780.4	Cyclo[-NHCH(CH ₃)CH(CH ₃)CO-Glu-Mdha-Ala-Leu-MeAsp-Arg-]	TiO ₂ , GO-TiO ₂
11	783.5	5.1	C ₃₃ H ₅₄ N ₁₀ O ₁₂ , 782.4	Cyclo[-NHCHOHCH(CH ₃)CO-Glu-Mdha-Ala-Leu-MeAsp-Arg-]	TiO ₂ , GO-TiO ₂
12	795	4.8-6.1	C ₃₄ H ₅₄ N ₁₀ O ₁₂ , 794.4	Cyclo[-NHCH(CHO)CH(CH ₃)CO-Glu-Mdha-Ala-Leu-MeAsp-Arg-]	TiO ₂ , GO-TiO ₂
13	811.5	4.8	C ₃₄ H ₅₄ N ₁₀ O ₁₃ , 810.4	Cyclo[-NHCH(COOH)CH(CH ₃)CO-Glu-Mdha-Ala-Leu-MeAsp-Arg-]	TiO ₂
14	835.5	9.1	C ₃₇ H ₅₈ N ₁₀ O ₁₂ , 834.4	Cyclo[-NHCH(CHCHCOCH ₃)CH(CH ₃)CO-Glu-Mdha-Ala-Leu-MeAsp-Arg-]	TiO ₂ , GO-TiO ₂
15	837.5	6.2, 9.0	C ₃₆ H ₅₆ N ₁₀ O ₁₃ , 836.4	Cyclo[-NHCH(CHCHCOOH)CH(CH ₃)CO-Glu-Mdha-Ala-Leu-MeAsp-Arg-]	TiO ₂

Table 7.1. Products observed from MC-LR degradation using Degussa P25/UV-A and GO-TiO₂/solar light irradiation [270].

No	Peak (m/z)	R _t (min)	MW and Formula	Possible structure	Catalyst
16	965	28.7	C ₄₈ H ₇₂ N ₁₀ O ₁₁ , 964.5 C ₄₆ H ₇₄ N ₁₀ O ₁₁ Na, 942.5(23)	Cyclo[-Adda(-Methoxy)-Glu-Mdha-Ala-Leu-MeAsp-Arg-] [H ₃ CNH-Glu-Adda-Arg-MeAsp-Leu- Ala-H] ⁻ Na ⁺	TiO ₂ , GO-TiO ₂
17	980.5	26.0	C ₄₈ H ₇₅ N ₁₁ O ₁₁ , 979.5	Cyclo[-Adda(H ₂ N)(-Methoxy)-Glu-Mdha-Ala-Leu-MeAsp-Arg-]	GO-TiO ₂
18	999.5	26.2	C ₄₈ H ₇₄ N ₁₀ O ₁₃ , 998.5	Cyclo[-Adda-Glu(-Carboxy)-Mdha-Ala-Leu-MeAsp-Arg-]	TiO ₂ , GO-TiO ₂
19	1009.5	24.0-25.2	C ₄₉ H ₇₂ N ₁₀ O ₁₃ , 1008.5	Cyclo[-DmAdda-Glu-Mdha-Ala-Leu-MeAsp-Arg-]	TiO ₂ , GO-TiO ₂
20	1011.5	21.4-25.7	C ₄₉ H ₇₄ N ₁₀ O ₁₃ , 1010.5	(OH)-Cyclo[-Adda-Glu-Mdha-Ala-Leu-MeAsp-Arg-] Cyclo[-Adda(O)-Glu-Mdha-Ala-Leu-MeAsp-Arg-] Cyclo[-Adda-Glu-Mdha(O)-Ala-Leu-MeAsp-Arg-]	TiO ₂ , GO-TiO ₂
21	1015.5	26.0	C ₄₈ H ₇₄ N ₁₀ O ₁₄ , 1014.5	(CO)Ala-Leu-MeAsp-Arg-Adda-Glu(NCOCH ₃)	TiO ₂ , GO-TiO ₂
22	1027.5	22.6-26.4	C ₄₉ H ₇₄ N ₁₀ O ₁₄ , 1026.5	(OH) ₂ -Cyclo[-Adda-Glu-Mdha-Ala-Leu-MeAsp-Arg-]	TiO ₂ , GO-TiO ₂
23	1029	20.3-22.1	C ₄₉ H ₇₆ N ₁₀ O ₁₄ , 1028.6	Cyclo[-Adda(OH) ₂ -Glu-Mdha-Ala-Leu-MeAsp-Arg-] Cyclo[-Adda-Glu-Mdha(OH) ₂ -Ala-Leu-MeAsp-Arg-]	TiO ₂ , GO-TiO ₂
24	1031.5	21.9-22.7	C ₄₉ H ₇₈ N ₁₀ O ₁₄ , 1030.6	Cyclo[-Adda(OH) ₂ -Glu-Mdha-Ala-Leu-MeAsp-Arg-] Cyclo[-Adda(OH) ₂ -Glu-Mdha(OH) ₂ -Ala-Leu-MeAsp-Arg-]	TiO ₂ , GO-TiO ₂
25	1045.5	20-27	C ₄₇ H ₇₇ N ₁₀ O ₁₅ , 1044.6	OH-Cyclo[-Adda(OH) ₂ -Glu-Mdha-Ala-Leu-MeAsp-Arg-] OH-Cyclo[-Adda-Glu-Mdha(OH) ₂ -Ala-Leu-MeAsp-Arg-]	TiO ₂

Table 7.2. Proposed structure and molecular formula of the new intermediates observed from MC-LR degradation using Degussa P25/UV-A and GO-TiO₂/solar light irradiation [270].

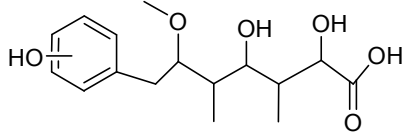
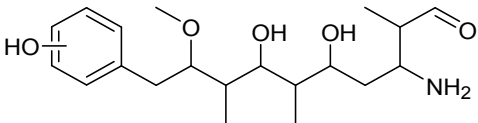
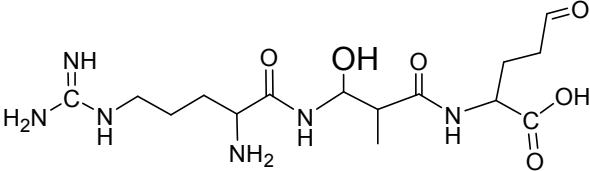
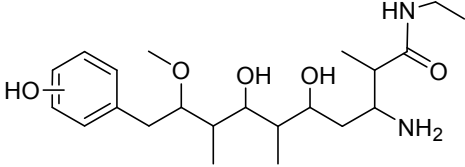
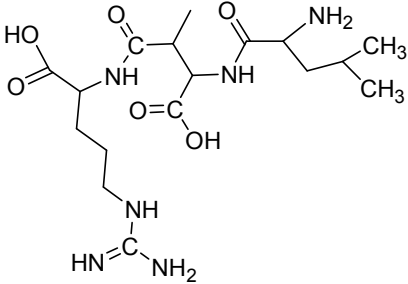
Proposed Structure	Formula, Molecular Weight, <i>m/z</i>
 <p>Dihydroxy-7-(hydroxy-phenyl)-6-methoxy-3,5-dimethyl-heptanoic acid</p>	<p>C₁₆H₂₄O₆ 312.2 mw, <i>m/z</i> 313.5</p>
 <p>OH-Adda(H₂O)₂</p>	<p>C₂₀H₃₃NO₅ 367.2 mw, <i>m/z</i> 368.5</p>
 <p>H-Arg-NHCH(OH)CH(CH₃)CO-Glu-H</p>	<p>C₁₅H₂₈N₆O₆ 388.2 mw, <i>m/z</i> 389.5</p>
 <p>OH-Adda(H₂O)₂-NHCH₂CH₃</p>	<p>C₂₂H₃₈N₂O₅ 410.3 mw, <i>m/z</i> 411.5</p>
 <p>OH-Arg-MeAsp-Leu-H</p>	<p>C₁₇H₃₂N₆O₆ 416.2mw, <i>m/z</i> 417</p>

Table 7.2. Proposed structure and molecular formula of the new intermediates observed from MC-LR degradation using Degussa P25/UV-A and GO-TiO₂/solar light irradiation [270].

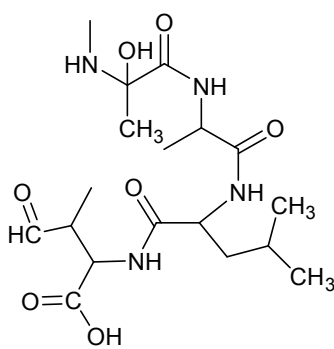
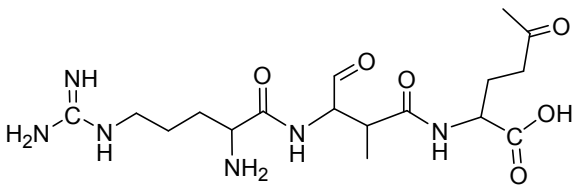
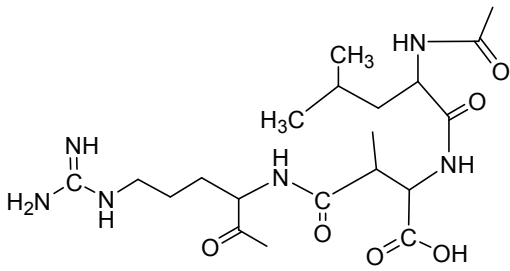
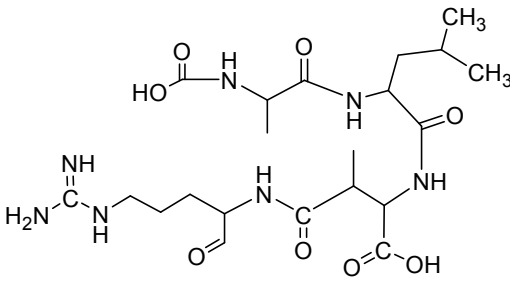
Proposed Structure	Formula, Molecular Weight, <i>m/z</i>
 <p style="text-align: center;">H-MeAsp-Leu-Ala-Mdha(OH)-H</p>	<p style="text-align: center;">C₁₈H₃₂N₄O₇ 416.2mw, <i>m/z</i> 417</p>
 <p style="text-align: center;">H-Arg-NHCH(CHO)CH(CH₃)CO-Glu-CH₃]⁺Na⁺</p>	<p style="text-align: center;">C₁₇H₃₀N₆O₆Na 414.2 (+23) mw, <i>m/z</i> 437</p>
 <p style="text-align: center;">H₃C-Arg-MeAsp-Leu-COCH₃</p>	<p style="text-align: center;">C₂₀H₃₆N₆O₆ 456.2 mw, <i>m/z</i> 457</p>
 <p style="text-align: center;">Arg-MeAsp-Leu-Ala-COOH</p>	<p style="text-align: center;">C₂₁H₃₇N₇O₈ 515.3 mw, <i>m/z</i> 515.5</p>

Table 7.2. Proposed structure and molecular formula of the new intermediates observed from MC-LR degradation using Degussa P25/UV-A and GO-TiO₂/solar light irradiation [270].

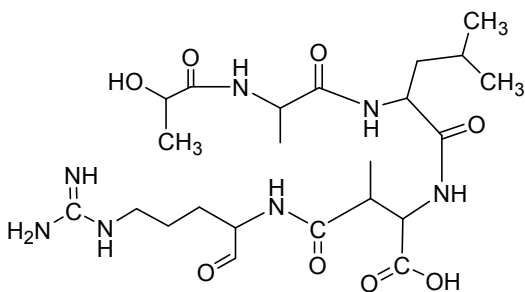
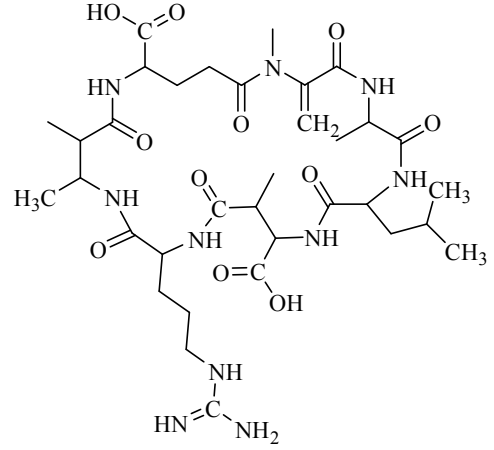
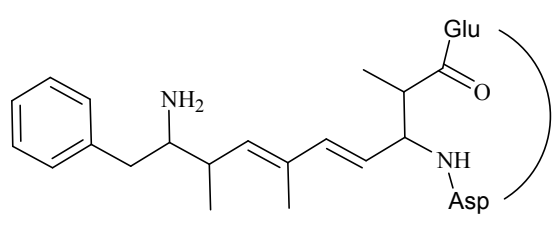
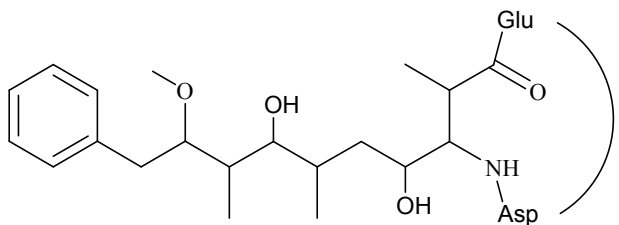
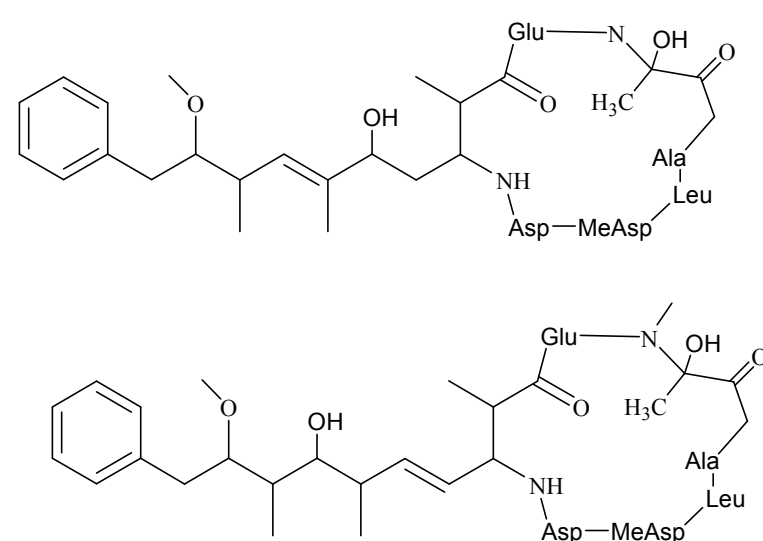
Proposed Structure	Formula, Molecular Weight, <i>m/z</i>
 <p style="text-align: center;">Arg-MeAsp-Leu-Ala-COCHOHCH₃</p>	<p style="text-align: center;">C₂₃H₄₁N₇O₈ 543.3 mw, <i>m/z</i> 544</p>
 <p style="text-align: center;">Cyclo[-NHCH(CH₃)CH(CH₃)CO-Glu-Mdha-Ala-Leu-MeAsp-Arg-]</p>	<p style="text-align: center;">C₃₄H₅₆N₁₀O₁₁ 780.4 mw, <i>m/z</i> 781.5</p>
 <p style="text-align: center;">Cyclo[-Adda(H₂N)(-Methoxy)-Glu-Mdha-Ala-Leu-MeAsp-Arg-]</p>	<p style="text-align: center;">C₄₈H₇₅N₁₁O₁₁ 979.5 mw. <i>m/z</i> 980.5</p>

Table 7.2. Proposed structure and molecular formula of the new intermediates observed from MC-LR degradation using Degussa P25/UV-A and GO-TiO₂/solar light irradiation [270].

Proposed Structure	Formula, Molecular Weight, <i>m/z</i>
 <p data-bbox="319 694 1005 750">Cyclo[-Adda(OH)₂-Glu-Mdha-Ala-Leu-MeAsp-Arg-]</p>	<p data-bbox="1244 436 1420 481">C₄₉H₇₈N₁₀O₁₄</p> <p data-bbox="1212 504 1452 582">1030.6 mw, <i>m/z</i> 1031.5</p>
 <p data-bbox="287 1556 1029 1612">Cyclo[-Adda(OH)₂-Glu-Mdha(OH)₂-Ala-Leu-MeAsp-Arg-]</p>	<p data-bbox="1244 1041 1420 1086">C₄₉H₇₈N₁₀O₁₄</p> <p data-bbox="1212 1108 1452 1187">1030.6 mw, <i>m/z</i> 1031.5</p>

7.3. Toxicity measurements

In order to assess the residual toxicity of water samples during the course of the photocatalytic degradation of toxin MC-LR, protein phosphatase inhibition assay (PPIA) was used. This procedure enables us to follow the residual toxicity of the water sample during the photocatalytic degradation of MC-LR and evaluate the photocatalytic activity of the nanostructured TiO₂ photocatalysts under different experimental conditions.

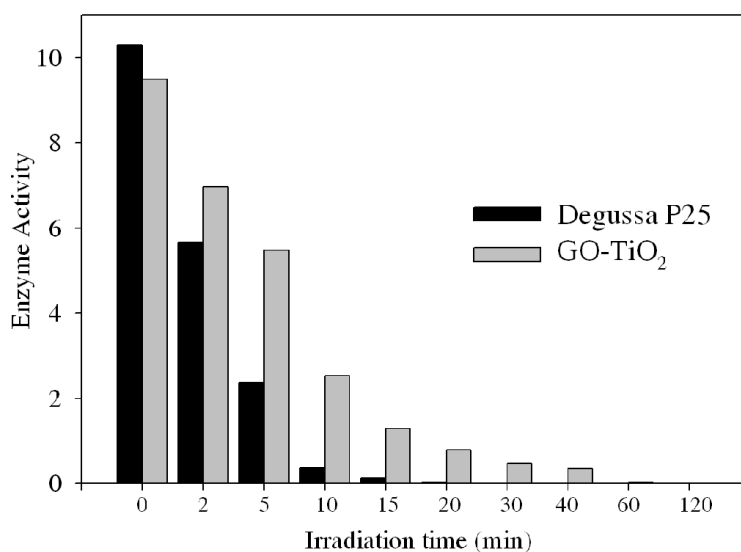


Figure 7.3. Residual toxicity measured during the photocatalytic degradation of MC-LR (10 mg L⁻¹) under UV-A (λ_{\max} =365 nm) irradiation in the presence of Degussa P25 and GO-TiO₂ (200 mg L⁻¹) [270].

PPIA measurements carried out using GO-TiO₂ and Degussa P25 showed that residual toxicity was directly proportional only to the amount of MC-LR that remained intact into solution, Figures 7.3. and 7.4. under UV-A and solar light, respectively. Reduction of MC-LR concentration resulted in reduction of a directly proportional amount of the toxic activity. Moreover, in solutions where MC-LR was completely degraded, no toxic activity was observed, even though those solutions contained oxidation by-products. This implies that MC-LR loses its toxic activity (protein phosphatase inhibition) as soon as the molecule is transformed to oxidized products. This is in agreement with previously reported studies [235] where it was shown that hydroxyl radical attack on the Adda amino acid of MC-LR is the first oxidation step and results in loss of toxic activity. This finding is very important for real applications of the photocatalytic process, since it

denotes that the target of the process could be degradation rather than mineralization, and therefore less energy would be needed for water detoxification.

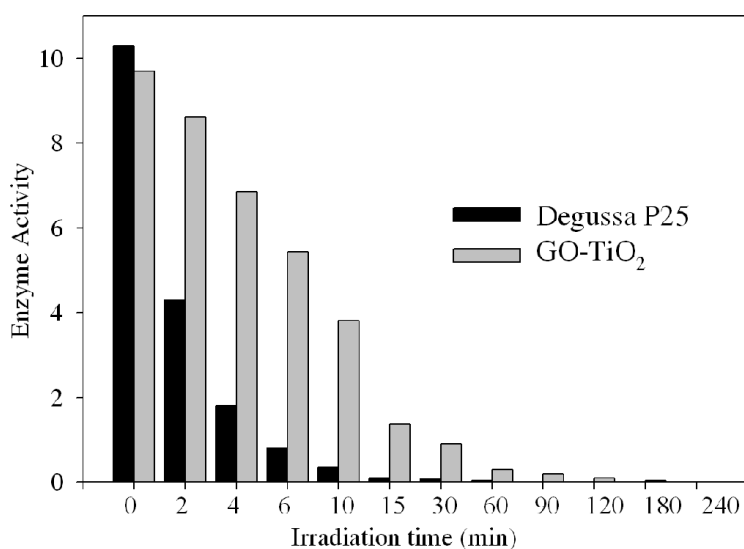


Figure 7.4. Residual toxicity measured during the photocatalytic degradation of MC-LR (10 mg L^{-1}) solar light (AM 1.5 G) irradiation in the presence of Degussa P25 and GO-TiO₂ (200 mg L^{-1}) [270].

In Figures 7.5.–7.8. is presented the toxicity measured (enzyme activity) in the photocatalytic degradation of MC-LR using the novel TiO₂ photocatalysts under UV-A and solar light for longer irradiation times. Taking into account TOC measurements, although complete mineralization was not achieved in all cases, it can be concluded that the remaining organic compounds are not hepatotoxic. This is confirmed by measuring the toxicity for longer irradiation times intervals (up to 48 h of irradiation), were MC-LR is fully degraded and no toxicity is detected in the samples using PPIA method.

As previously reported, the toxicity of MC-LR is associated to Adda aminoacid in MC-LR structure. PPIA is calibrated to give a quantitative value for toxicity as concentration equivalents of MC-LR. The formation and decay of three primary degradation products at $m/z= 1009.5$, 1027.5 , and 1045.5 , associated with Adda transformations, was also monitored during the course of the photocatalytic process.

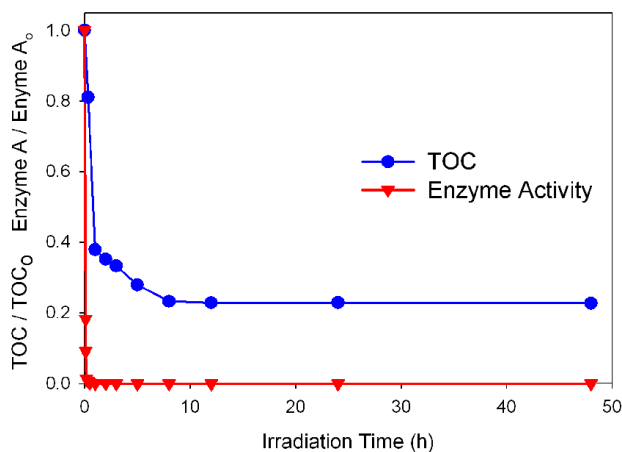


Figure 7.5. Enzyme activity (Toxicity) and mineralization extent (TOC) during MC-LR photocatalytic degradation using Degussa P25 TiO₂, under UV-A.

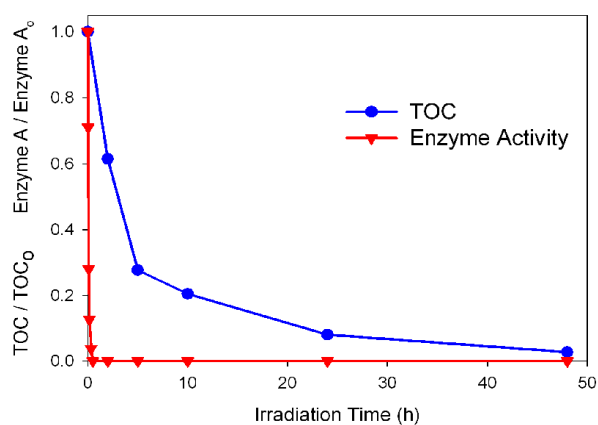


Figure 7.6. Enzyme activity (Toxicity) and mineralization extent (TOC) during MC-LR photocatalytic degradation using N-TiO₂, under UV-A.

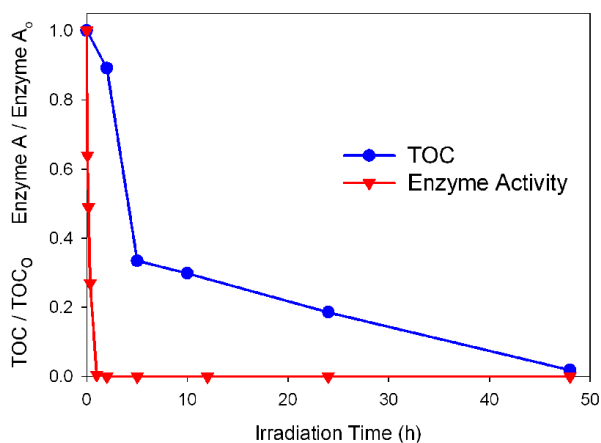


Figure 7.7. Enzyme activity (Toxicity) and mineralization extent (TOC) during MC-LR photocatalytic degradation using NF-TiO₂, under UV-A.

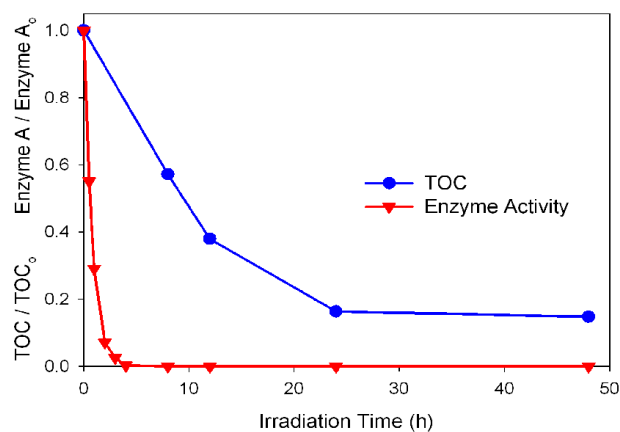


Figure 7.8. Enzyme activity (Toxicity) and mineralization extent (TOC) during MC-LR photocatalytic degradation using N-TiO₂, solar light.

In Figure 7.9., PPIA measurements (in equivalent concentration of MC-LR) and the formation of the primary products during the course of the process are depicted, as they have been identified by LC-MS/MS for the tested TiO₂ photocatalysts. Primary products are presented in arbitrary units, since quantification was not possible due to the lack of commercially available analytical standards. The concurrent formation of oxidation products on the Adda group of MC-LR does not affect the residual toxicity, indicating that it is attributed only to the remaining MC-LR in solution and not to other degradation products. Although a slower degradation process was observed with solar light, the majority of intermediates detected under UV-A and solar light irradiation, were the

same, since photocatalysis under solar light is mainly due to the UV part of the spectrum [270].

This can be seen in Figure 7.10., abundance of products with m/z 781.5 and 1015.5 throughout the photocatalysis experiments using either Degussa P25 under UV-A or GO-TiO₂ under solar light irradiation is presented. Product m/z 781.5 can be resulted by cleavage on the last C on the Adda chain and the Cyclo[-Glu-Mdha-Ala-Leu-MeAsp-Arg-] part of MC-LR, and m/z 1015.5 product can be formed with cleavage on the C'-CO bond of double hydroxylated carbon on the chain of Mdha [Mdha(OH)₂] product (m/z 1029) [270].

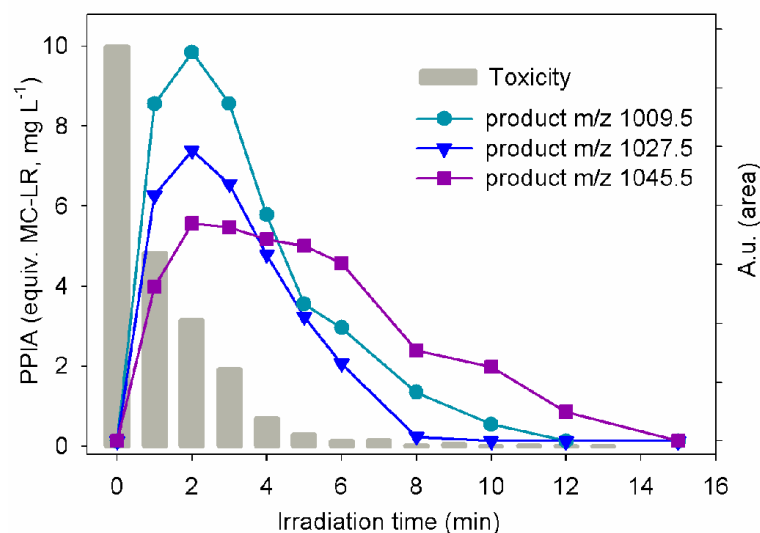


Figure 7.9. PPIA measurements and evolution of products m/z 1009.5, 1027.5 and 1045.5 during photocatalytic degradation of MC-LR (10 mg L^{-1}) using Degussa P25 TiO₂ (200 mg L^{-1}) under UV-A irradiation [284].

These results are important for possible applications of these processes for the detoxification of water from microcystins since they provide evidence that the toxic activity of microcystins is eliminated when the structure of the initial molecule is changed through attack of reactive species, while no toxic byproducts are formed. This also implies that possible applications would be efficient without high requirements of energy consumption since simple alterations in the initial structure (i.e. first steps of degradation) is sufficient for decontamination and complete mineralization of the toxic compound is not required.

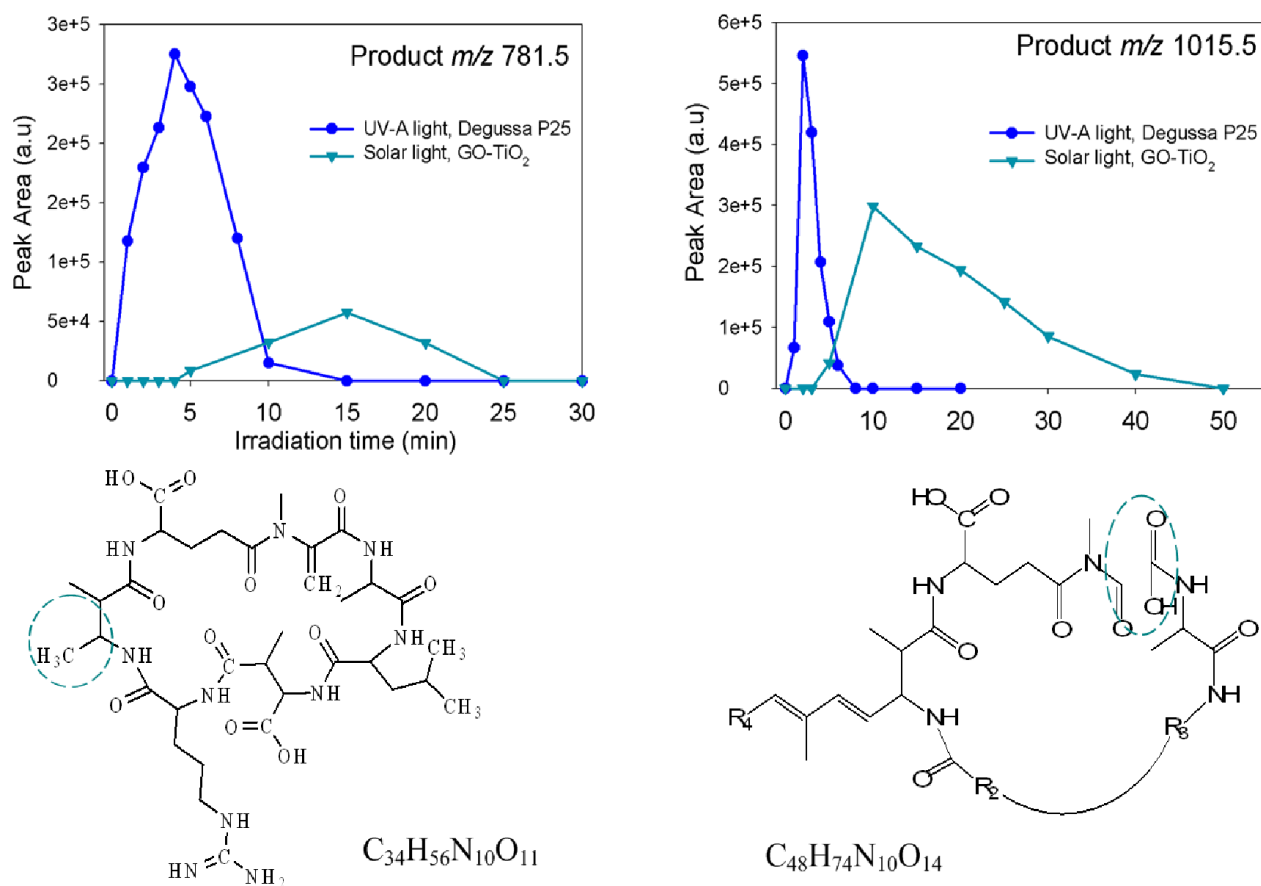


Figure 7.10. Evolution of products m/z 781.5 and 1015.5 during photocatalytic degradation of MC-LR (10 mg L^{-1}) using Degussa P25 TiO_2 (200 mg L^{-1}) under UV-A or GO-TiO_2 (200 mg L^{-1}) under solar light irradiation [284].

7.4. Conclusions

Identification of the intermediate products formed during the photocatalytic degradation of MC-LR by the GO-TiO_2 nanocatalyst under solar light irradiation was carried out. The majority of these products were identical to those observed by Degussa P25 under UV-A, suggesting that photodegradation mechanism takes place via a common active species, hydroxyl radicals ($\cdot\text{OH}$). Assessment of the residual toxicity of MC-LR during the course of degradation under UV-A and solar light irradiation showed that toxicity is proportional only to the remaining MC-LR in the solution; therefore degradation products present no significant protein phosphatase inhibition activity. Results indicate that GO-TiO_2 is an effective photocatalyst for the degradation of MC-LR in water under UV-A and solar irradiation and appears to be a promising material for water treatment applications.

CHAPTER 8

Degradation Pathway of CYN

8.1. Introduction

So far, studies have demonstrated that TiO₂ photocatalysis can effectively destroy CYN in aqueous solution [21, 22]. However, the assessment of CYN disappearance is not sufficient to ensure the absence of residual products since the photocatalytic treatment is a complex procedure leading to the formation of degradation products, which in some cases may be more toxic and stable than the parent compound. To the best of my knowledge only few studies dealt with the transformation products formed during removal of CYN using chlorination [285] and via hydroxyl radical ([•]OH) oxidation [286] and also, in very recent studies by Wang *et al.* [287] using bismuth oxybromide (BiOBr) promoted detoxification of CYN under UV and visible light irradiation, and also by He *et al.* [276] by hydroxyl and sulphate radicals was investigated, using UV activation of hydrogen peroxide, persulfate and peroxymonosulfate. The aim in this chapter is the, identification of intermediate products formed during the photocatalytic process using LC-MS/MS analysis.

8.2. Intermediate products of CYN under UV-A and solar light using TiO₂

In this chapter, identification of intermediate products formed during the photocatalytic degradation of CYN using Degussa P25 under UV-A and Kronos vlp-7000 under solar light irradiation, was carried out using LC-MS/MS. Structural characterization of intermediates produced during photocatalysis of CYN was based on the analysis of LC-MS chromatograms and the respective mass spectra. The majority of byproducts detected, appeared within the first 2-5 minutes of irradiation. The intermediates identified were the same under UV-A and solar light irradiation since photocatalysis under solar light is mainly due to activation of the catalyst by the UV part of the solar spectrum. During photocatalysis the concentration of most of the byproducts initially increased followed by a decrease due to their subsequent oxidation after prolonged time of irradiation.

Some of the intermediates observed here, were previously found by others upon chlorination (m/z 350, 375) [285], radiolysis (m/z 320, 350, 375, 414, 432, 448) [286] and by UV-254 nm/H₂O₂ (m/z 320, 375, 414, 432, 448) [276] of CYN, where m/z corresponds to (M + H)⁺.

A number of new intermediates were also observed with m/z 195, 227, 280, 287, 316, 338, 347, 373, 434 and 450. Isobaric compounds were detected as multiple peaks in the TIC chromatogram (Figures 8.1. and 8.2.) i.e. 227 (4 main peaks), 287 (2 peaks), 320 (2 main peaks), 338 (2 peaks), 350 (2 peaks), 375 (2 peaks), 432 (2 peaks), 434 (2 peaks) and 448 (2 peaks), indicating the formation of stereoisomers or structural isomers. In Scheme 8.1. all intermediate products found are presented with their m/z ratios, formulas and their monoisotopic molecular masses (Mass), formulas and a degradation pathway is proposed.

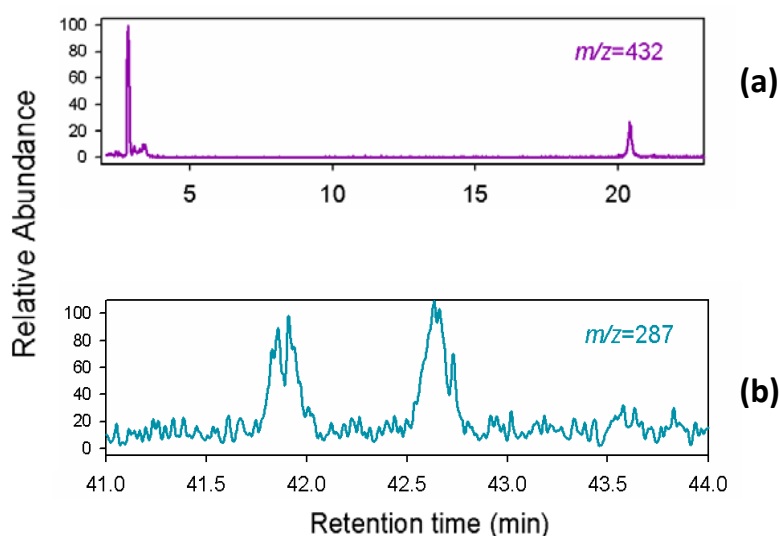


Figure 8.1. Relative abundance chromatograms for products m/z (a) 432 and (b) 287 of CYN photocatalytic degradation in the presence of Degussa P25 after 3 min of irradiation under UV-A light [277].

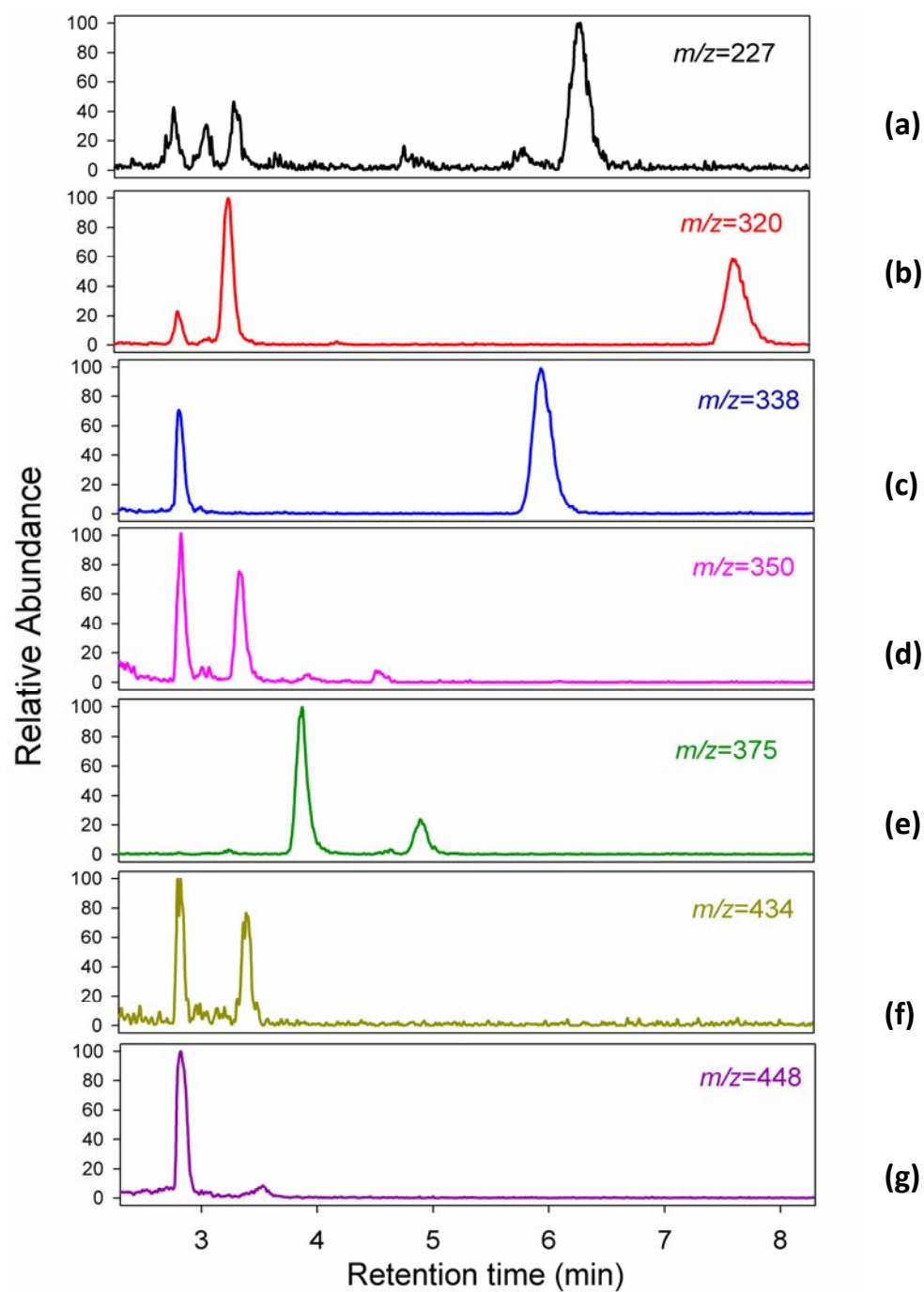
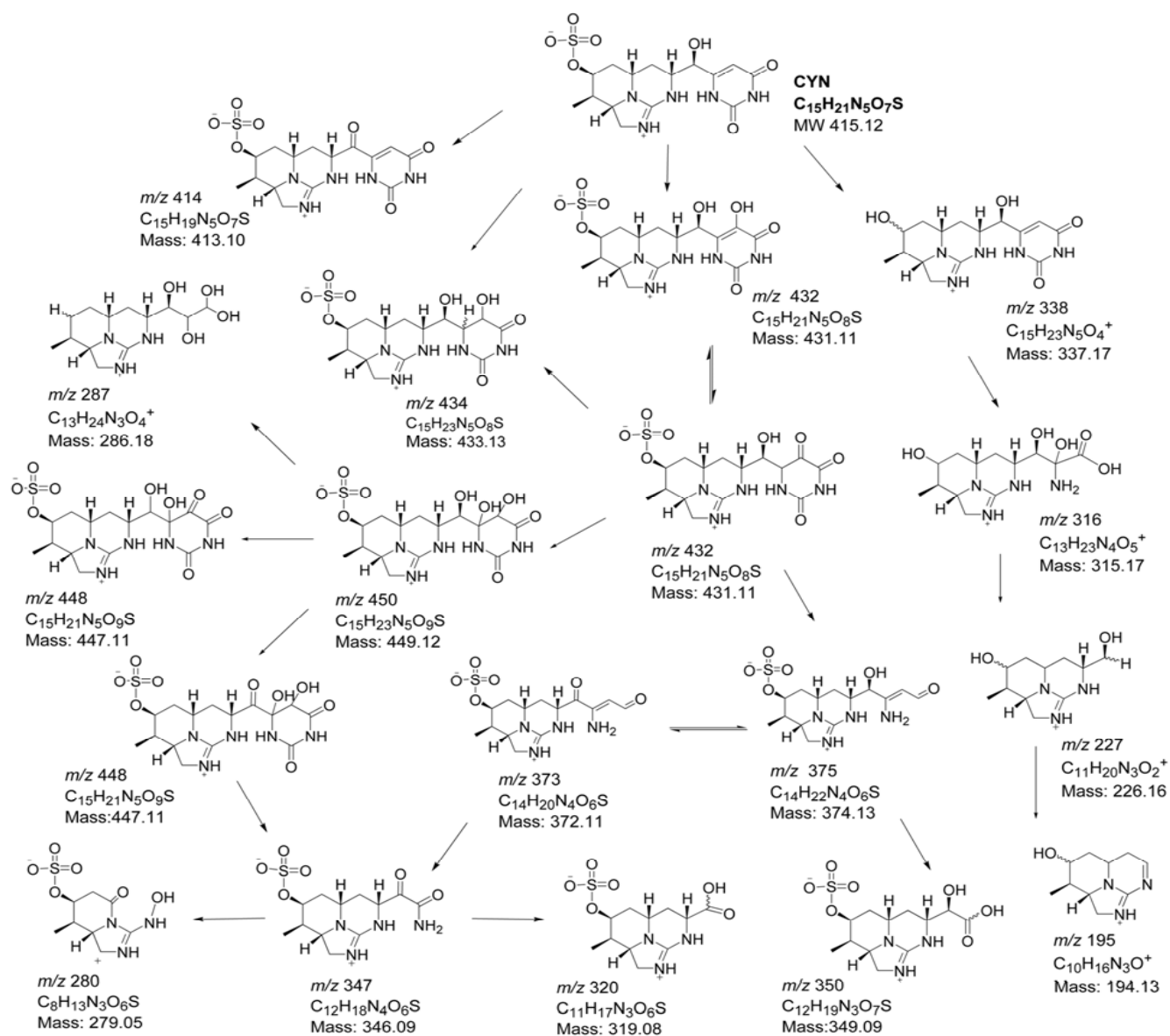


Figure 8.2. Relative abundance chromatograms for products m/z (a) 227, (b) 320, (c) 338, (d) 350, (e) 375, (f) 434 and (g) 448 of CYN photocatalytic degradation in the presence of Degussa P25 after 3 min of irradiation under UV-A light [277].



Scheme 8.1. Observed intermediate products and proposed degradation pathway for CYN under UV-A or solar light irradiation using TiO_2 [277].

Upon irradiation under UV-A, TiO₂ is activated and forms reactive oxygen species (ROS) including mainly hydroxyl radicals ([•]OH), superoxide radical anions (O₂^{•-}), and perhydroxyl radicals (HO₂[•]), as well as conduction band electrons (e⁻) [288]. [•]OH radical reacts through addition, hydrogen abstraction and less often electron abstraction. Hydrogen abstraction occurs when α-hydrogen is available resulting into a carbonyl group. Whereas, electron abstraction by [•]OH requires electron rich substrate and it is relatively slow compared to [•]OH addition.

CYN is an uracil derivative with a tricyclic guanidine and a sulphate group. Upon its photocatalytic degradation with TiO₂, [•]OH radicals primarily react through substitution on the unsaturated carbon bond on the uracil group, resulting in the formation of product *m/z* 432. Alcohol on a double bond can give a ketone tautomer explaining the two peaks appearing on the TIC chromatogram for *m/z* 432 (Figure 8.1.a). From product with *m/z* 432, product with *m/z* 450 is formed with further hydroxylation. Product *m/z* 434 (Figure 8.2.f) can be resulted by [•]OH addition. Further oxidation on the uracil group of product *m/z* 432 can leads to the formation of product *m/z* 375 with ring opening at urea group moiety. Through further oxidations cylindrospermopsic acid (*m/z* 350, multiple peak, Figure 8.2.d) is produced. Also, oxidation of product *m/z* 375 can result in product *m/z* 373 (from which the products *m/z* 347 and by further oxidation the acid like *m/z* 320 are formed) while further [•]OH radical attack on product *m/z* 347 can result in the formation of product with *m/z* 280.

Starting from product *m/z* 450 (dihydroxylated CYN), compounds with *m/z* 287 and *m/z* 448 can be produced. Substitution of the sulphate group and oxidation on the uracil group, can lead to the formation of two stereoisomer products with *m/z* 287. Also oxidation to either of the secondary alcohols on *m/z* 450 product (bridging methane group or on the uracil group) with hydrogen abstraction results in the formation of two carbonyl isomers with *m/z* 448 (Figure 8.2.g). The carbonyl product with *m/z* 414 corresponds to the oxidation of CYN by [•]OH radical attack on the secondary alcohol (bridging methane group). Substitution of the sulphate group with [•]OH radical on CYN, can result in the formation of two stereoisomers with *m/z* 338. Oxidation on the uracil group of *m/z* 338 can produce a compound with *m/z* 316. Further oxidation of the *m/z* 316 product can form product *m/z* 227 which gives multiple peaks in the relative abundance chromatogram (Figure 8.2.a) suggesting geometrical isomers. Oxidation of product *m/z* 227 can explain the appearance of the product with *m/z* 195. Intermediate products with *m/z* below 195 were difficult to be detected by LC-MS/MS because of

overwhelming noise signals. In Figures A4-A8 the MS/MS spectra of some of the intermediates with their fragmentation pattern are given. Overall, it was found that the mechanism of CYN degradation proceeds through hydroxyl attack on different sites of CYN, leading to different oxidized products and finally cleavage structures of CYN.

8.3. Toxicity Experiments concerning CYN

In order to determine half maximal effective concentration (EC50) for CYN, a number of standard solutions (0.0065 – 20 ppm) were used. Results presented in Table 8.1., indicated that even though CYN is a toxic compound, does not affect *Vibrio Fischeri*. For that reason EC50 value could not be given.

Table 8.1. CYN standard solutions (0.0065 - 20 ppm).

Sample (ppm CYN)	Gt	% Effect _t
BLANK	1.16	
2,4-DCP	2.11	67.89
0.0065	0.06	5.50
0.0125	0.14	11.93
0.025	0.08	7.34
0.05	0.10	9.17
0.1	0.08	7.34
0.5	0.06	5.50
1	0.08	7.34
2	0.07	6.42
5	0.06	5.50
10	0.09	8.26
20	-0.04	-3.67

CYN has been shown to be cytotoxic, dermatotoxic, genotoxic, hepatotoxic *in vivo*, developmentally toxic, and may be carcinogenic. There is always the possibility that photocatalytic process leads to the formation of toxic intermediates or byproducts so, in order to investigate that, toxicity measurements were performed for CYN mineralization

under UV-A and solar light, using Degussa P25, Kronos and GO-TiO₂. CYN presented no significant toxicity during the course of Microtox assay. Results are presented in Tables 8.2., 8.3. and 8.4.

Table 8.2. CYN degradation under UV-A using Degussa P25

Irradiation time	Gt	% Effect _t
Blank	1.00	
2,4-DCP	2.39	70.53
0	0.08	7.34
10 min	0.08	7.37
20 min	0.20	16.84
1 h	0.13	11.58
1.5 h	0.14	12.63
3 h	0.20	16.84
5 h	0.14	12.63
8 h	0.16	13.68
12 h	0.07	6.32
24 h	0.14	11.93
48 h	0.23	18.70

Table 8.3. CYN degradation under solar

Irradiation time (h)	Kronos % Effect _t
2,4-DCP	69.53
0	7.32
2	12.63
5	9.42
10	11.40
24	8.04
48	17.35

Table 8.4. CYN degradation under solar light.

Irradiation time (h)	GO-TiO ₂ % Effect _t
2,4-DCP	69.96
0	9.14
2	11.46
5	10.83
10	9.67
24	12.75
48	18.58

As it can be concluded from Tables 8.2., 8.3. and 8.4. no significant toxicity is presented during the photocatalysis process of CYN mineralization under UV-A or solar light irradiation, using the innovative TiO₂ photocatalysts.

8.4. Conclusions

Photocatalytic degradation of CYN leads to the formation of a number of intermediates, several of which identified for the first time in CYN degradation processes. Based on these intermediates, a degradation pathway is proposed for the photocatalytic process. Intermediates detected under both UV-A and solar light were the same suggesting that hydroxyl radical attack is mainly responsible for the degradation mechanism. A novel approach is suggested for the detoxification of water from a new class of toxic organic pollutants of biogenic origin in water using solar light photocatalysis in the presence of TiO_2 . Elucidation of degradation pathway provides a better understanding of the photocatalytic process and is expected to initiate further research regarding the fate of CYN under different water treatment technologies.

CHAPTER 9

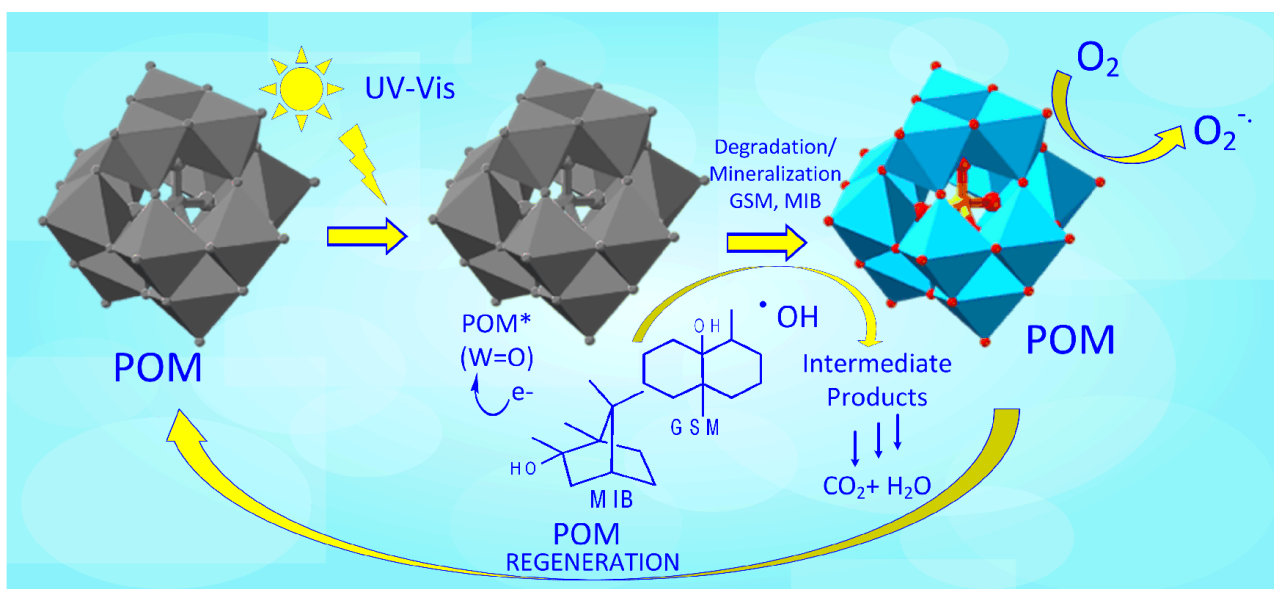
Degradation Pathways of GSM and MIB

9.1. Introduction

The objective of this chapter was the comparison of photodegradation mechanisms followed by a representative POM ($\text{SiW}_{12}\text{O}_{40}^{4-}$) and TiO_2 in the cases of GSM and MIB, via degradation, mineralization and identification of intermediate products, under UV-A irradiation.

Polyoxometalates (POM) have previously been used for degradation of several organic pollutants in water [32-36]. In almost all cases final degradation products were CO_2 , H_2O and inorganic anions. POM are acid condensation products, mainly of molybdenum and tungsten [37-39], that upon excitation with near visible and UV light become powerful oxidizing reagents capable of destroying a great variety of organic compounds in aqueous solutions through a hole-electron ($h^+ + e^-$) mechanism [40-42]. Hydroxyl radicals ($\cdot\text{OH}$) generated by reaction of POM with H_2O seem to play a key role in the process [42]. Oxygen oxidizes (regenerates) the catalyst and through reductive activation may or may not participate further in the process, depending on the substrate [43]. Due to their photocatalytic performance, POM can be recognized as an AOP [33-35]. POM are almost as effective as the widely published TiO_2 [42], presenting similar behaviour with the semi-conducting oxide [42]. $\cdot\text{OH}$ radicals have been used to explain similarities of the two photocatalysts although in some cases the nature of substrate and the mode of investigation seem to play an important role in the process [44].

In this chapter, the photocatalytic degradation and mineralization of GSM and MIB in water was studied and compared using a $\text{SiW}_{12}\text{O}_{40}^{4-}$ and TiO_2 . The comparative study of processes included also the identification of intermediate products formed as well as the effect of hydroxyl radical scavengers. Based on the literature (a) the photocatalytic degradation of both GSM and MIB with POM and (b) the mineralization and the complete degradation pathways in the presence of POM or TiO_2 is reported here for the first time.



Scheme 9.1. Objective of Chapter 9 [245].

9.2. Photocatalytic Degradation of GSM and MIB in the presence of TiO₂ and POM, use of •OH scavengers

9.2.1. Photocatalytic Degradation of GSM and MIB in the presence of TiO₂ and POM

Illumination of aqueous, oxygen saturated solutions of GSM (1 mg L⁻¹) and MIB (1 mg L⁻¹) under UV-A irradiation (λ_{\max} = 365 nm) in the presence of SiW₁₂O₄₀⁴⁻ (7 × 10⁻⁴ M, 200 mg L⁻¹) or commercially available TiO₂ Degussa P25 (200 mg L⁻¹) results in the degradation of both substrates. In Figure 9.1., the disappearance of GSM at various illumination intervals in the presence of (a) SiW₁₂O₄₀⁴⁻ and (b) TiO₂ is presented. Under the experimental conditions used, GSM disappeared after 30 min of illumination in the presence of TiO₂, while in presence of POM required longer time reaching complete degradation at 120 min. Experiments were also performed in the absence of photocatalysts. A destruction of ~15% for GSM in UV-A was observed after 120 min of illumination (Figure 9.1.), indicating photolytic cleavage. Pemu *et al.* [24], in a study using TiO₂ photocatalysis for degradation of GSM, observed remarkable destruction in the absence of photocatalyst, under experimental conditions used. This was attributed to the energy of UV light emitted being of the same order of magnitude with those of bonds in GSM, causing cleavage of C-O and C-C bonds.

The photodegradation of oxygenated aqueous solution of MIB with and without photocatalysts is presented in Figure 9.2., in the presence of (a) $\text{SiW}_{12}\text{O}_{40}^{4-}$ and (b) TiO_2 . When photocatalysis performed in the presence of TiO_2 , MIB was completely removed in the first 25 min. In the case of $\text{SiW}_{12}\text{O}_{40}^{4-}$, the destruction of MIB was complete after 100 min of illumination. Similar to GSM, photodecomposition of MIB also took place in the absence of photocatalysts reaching ~ 20% in 120 min of illumination. Results also showed that degradation of GSM was slightly slower than MIB in the presence of both photocatalysts. This was also observed by Lawton *et al.* using TiO_2 photocatalysis [235].

9.2.2. Photocatalytic Degradation of GSM and MIB in the presence of in the presence of $\cdot\text{OH}$ radicals scavengers

Experiments were also performed in the presence of $\cdot\text{OH}$ radicals scavengers, i.e. KBr and TBA. KBr and TBA are $\cdot\text{OH}$ radical trapping reagents (scavengers) from which Br^- is stronger [289, 290]. Experiments with both photocatalysts (POM, TiO_2), substrates (GSM, MIB) and scavengers were conducted side by side, under exactly the same conditions. Results are presented in Figures 9.1. and 9.2., for GSM and MIB respectively.

In Tables 9.1. and 9.2. the observed rate constants of the photodegradation of the substrates and how these are modified in the presence of $\cdot\text{OH}$ radical scavengers are given. Numbers in parentheses indicate, percentage-wise, the effect of scavengers on the observed rate constants. The observed rate constants of substrates degradation were calculated from the slope of the curve obtained for the first 30% of the substrates destruction upon illumination time.

Figures 9.1.and 9.2. and Tables 9.1. and 9.2., show that both scavengers retard the photodegradation of GSM and MIB, in accordance with their ability to scavenge $\cdot\text{OH}$ radicals.

The second order rate constants ($\text{M}^{-1} \text{s}^{-1}$) of the scavengers used with $\cdot\text{OH}$ radicals are: 1.1×10^{10} for Br^- [289] and 3.1×10^8 for TBA [290]. The retardation of the photodegradation of GSM and MIB, in the presence of scavengers, denotes that $\cdot\text{OH}$ radicals should be the main oxidant for both photocatalysts. It was also appeared that both scavengers have the same influence on both of the substrates. The similarity on

mode of operation of the two photocatalysts on GSM and MIB can be attributed on the similar structure of the substrates. These results come in agreement with previous study on atrazine, fenitrothion, chlorophenols and 2,4-DCP [44], where it was stated that the photooxidizing mode of POM and TiO_2 (i.e. $\cdot\text{OH}$ radicals versus h^+) is circumstantial depending on the nature of the substrate and the mode of investigation.

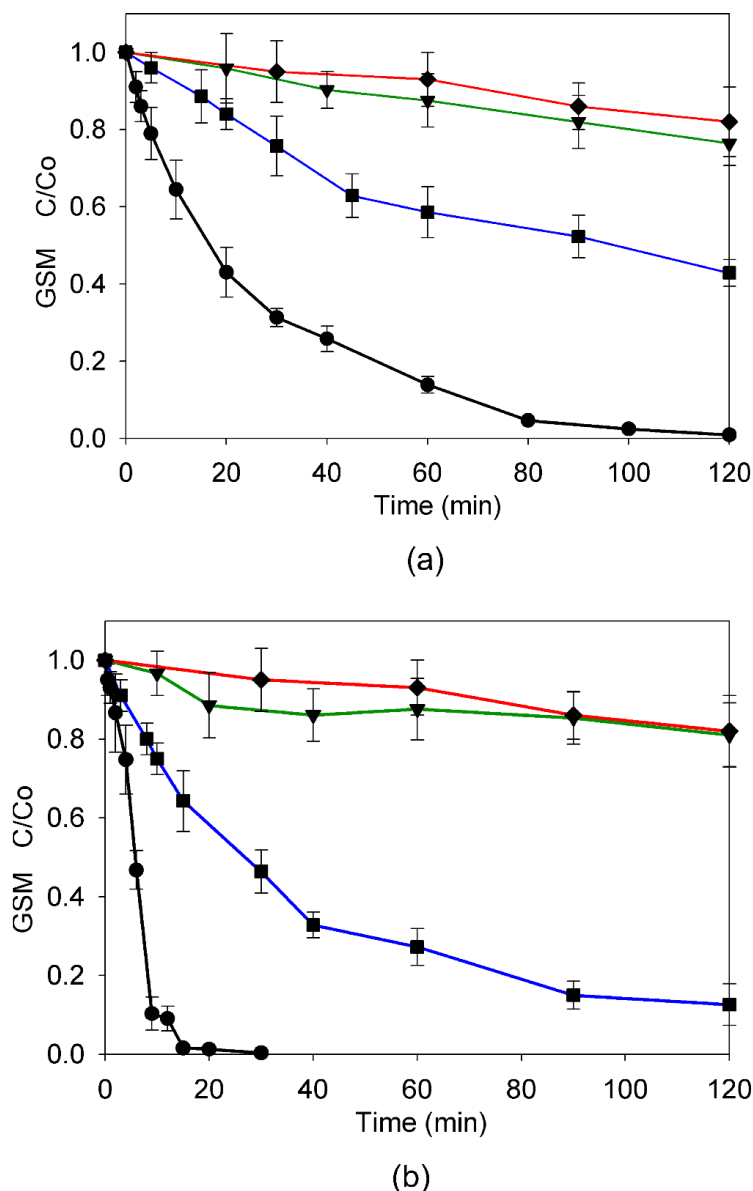
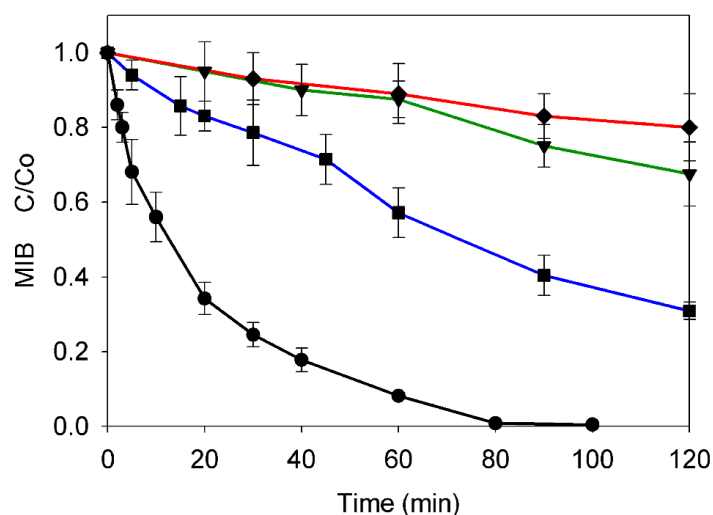
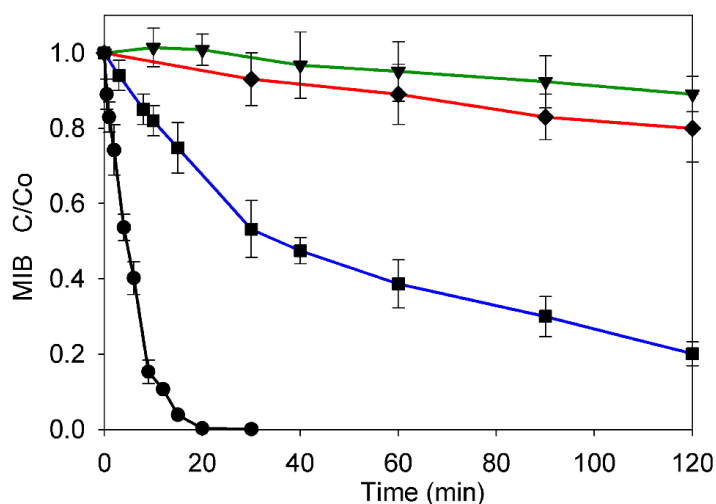


Figure 9.1. Photocatalytic degradation of GSM (1 mg L⁻¹) under UV-A ($\lambda_{\text{max}}= 365$ nm) irradiation with (a) $\text{SiW}_{12}\text{O}_{40}^{4-}$ (7×10^{-4} M, 200 mg L⁻¹) and (b) TiO_2 (200 mg L⁻¹) in the presence and absence of scavengers. Conditions (♦) Photolysis, (●) No scavenger, (▼) KBr and (■) TBA [245].



(a)



(b)

Figure 9.2. Photocatalytic degradation of MIB (1 mg L^{-1}) under UV-A ($\lambda_{\text{max}} = 365 \text{ nm}$) irradiation with (a) $\text{SiW}_{12}\text{O}_{40}^{4-}$ ($7 \times 10^{-4} \text{ M}$, 200 mg L^{-1}) and (b) TiO_2 (200 mg L^{-1}) in the presence and absence of scavengers. Conditions (◆) Photolysis, (●) No scavenger, (▼) KBr and (■) TBA [245].

Table 9.1. Observed rate constants from the initial rates of photodegradation of GSM in the presence of POM or TiO_2 and scavengers, calculated from Figure 9.1 [245].

Scavenger	None	KBr	TBA
Catalyst			
$k \times 10^{-3} \text{ min}^{-1}$; % ($k_{\text{scavenger}} / k_{\text{none}}$)			
No Catalyst	1.5		
POM	34.9 (100)	1.9 (5.6)	8.1 (23.1)
TiO_2	61.3 (100)	3.6 (5.9)	23.6 (38.4)

Table 9.2. Observed rate constants from the initial rates of photodegradation of MIB in the presence of POM or TiO₂ and scavengers, calculated from Figure 9.2 [245].

Scavenger Catalyst	None	KBr	TBA
$k \times 10^{-3} \text{ min}^{-1}; \% (k_{\text{scavenger}}) / (k_{\text{none}})$			
No Catalyst	1.7		
POM	63.9 (100)	2.6 (4.2)	6.1 (9.6)
TiO ₂	123 (100)	1.0 (0.8)	16.9 (15.3)

9.3. Photocatalytic Mineralization of GSM and MIB with of TiO₂ and POM

Based on the literature, degradation process of GSM and MIB has been studied only under limited time of illumination [23, 24, 235]. Even though mineralization of the total organic carbon in the solution might not be necessary for the elimination of the undesirable taste and odor characteristics of GSM and MIB in water, it can provide useful information on the mechanistic aspects of the photocatalytic process of the two materials. Prolonged illumination of aqueous solutions of GSM and MIB leads to the mineralization of substrates giving as final product CO₂, in the presence of both photocatalysts. As can be seen in Figure 9.3., after 5 h of irradiation in the presence of TiO₂ 65% and 80% of organic carbon has been recovered for GSM and MIB, while their degradation has been almost completed in ~30 and 25 min, respectively (Figures 9.1., 9.2.). In the case of SiW₁₂O₄₀⁴⁻ after 5 h of irradiation 50% and 65% mineralization of organic carbon was observed for GSM and MIB, respectively (Figure 9.3.). The shorter time needed for degradation than for mineralization is due to formation of organic intermediates that also react with the photocatalysts. Reduction of TOC is evidenced only after a small induction period indicating also that the mineralization proceeds through several intermediate steps. The incomplete removal of TOC (~80% - 85%) can be assigned to the formation of small partially oxidised molecules that are mineralized slowly.

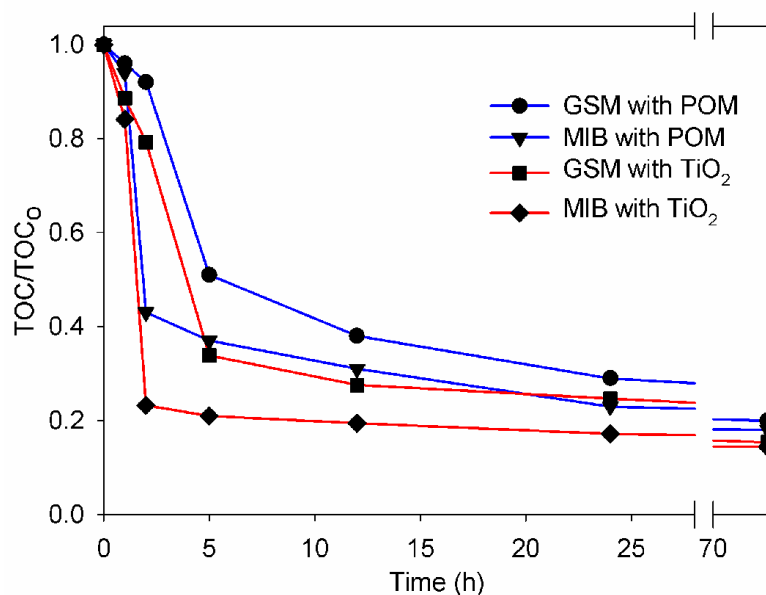


Figure 9.3. Photocatalytic mineralization of GSM (10 mg L⁻¹) and MIB GSM (10 mg L⁻¹) under UV-A ($\lambda_{\text{max}}= 365$ nm) irradiation using SiW₁₂O₄₀⁴⁻ (7x10⁻⁴ M, 200 mg L⁻¹) or TiO₂ (200 mg L⁻¹) catalyst [245].

9.4. Intermediate products of GSM using TiO₂ and POM under UV-A light

In 1999 Saito *et al.* [291] were the first to study GSM's degradation pathway using a microbiological degradation method. In total, three products were identified, two of them were dehydration products of GSM and the third resulted from dehydration followed by enolation. Another study concerning employment of microorganisms, was performed by Eaton [292] using bacteria. Two main intermediates were identified 2- and 7-ketogeosmin. Song *et al.* [227] studied ultrasonically induced degradation of geosmin. Reasoning intermediates produced, dehydration reactions were observed, subsequent dehydrogenations and a ring opening reaction. Another attempt was performed by Bamuza-Pemu and Chirwa [24] using TiO₂. Intermediates identified (3,5-dimethylhex-1-ene, 2,4-dimethylpentan-3-one, 2-methylethylpropanoate and 2-heptanal) showed that GSM undergoes rapid ring opening and subsequent bond cleavage at multiple sites producing acyclic saturated and unsaturated compounds, with those not being of environmental concern.

When illumination of GSM was performed in the presence of POM, the formation of numerous intermediate products took place (Scheme 9.2.). In Table 9.3. all identified intermediates with matching greater than 80 % are presented with their chromatographic retention time (t_R) and their spectral characteristics (M^+ and m/z of major ions). Identification of the species detected was performed on the basis of

comparison with Wiley mass spectra library, literature data and EI fragmentation patterns. The majority of the identified intermediates were cyclic ketones which upon ring opening lead to formation of linear saturated and unsaturated products (Scheme 9.2.). The formation of all intermediates is followed by their decay during the photocatalytic process, coming finally to total photodecomposition to CO₂.

Identification of intermediates was also carried out upon photocatalysis in the presence of TiO₂. As it can be noticed from the chromatograms of the extracted photolysed solutions (Figure 9.4) at various illumination intervals, the chromatographic patterns were mostly the same between POM and TiO₂, supporting the fact that the majority of intermediates reported in Table 9.3 are present during the photocatalytic degradation using either of the two photocatalysts.

Product IV (8,8a-Dimethyl-decahydro-naphthalen-1-ol) and product VI (8,8a-Dimethyl-decahydro-naphthalen-1-ol), due to their high abundance could be considered as the main intermediates produced during the photocatalytic degradation of GSM under UV-A irradiation in the presence of POM or TiO₂. In Figure 9.5, the formation and decay of products IV and VI during the photocatalytic procedure is presented, with a peak on their concentrations at ~2h of irradiation. A possible mechanism followed for the formation of product IV could be α -hydrogen abstraction from the tertiary carbon of GSM, β -scission abstraction, followed by hydroxylation from \cdot OH radical attack and finally ketone formation (Figure 9.6) [293]. The second main intermediate product VI could be formed by dehydration of GSM and \cdot OH addition followed π -bond rearrangement (rgm), (Figure 9.7) [293].

The presence of majority of oxygenated degradation products suggests that the mechanism involved in most identified intermediates is indeed \cdot OH oxidation, driven by electrophilic substitution reactions. Subsequent bond cleavage at multiple sites produces mainly cyclic ketones that upon further bond cleavage form open chain saturated and unsaturated compounds, i.e. alkenes, aldehydes and acids.

A few studies concerning the identification of degradation products of GSM under various processes have been reported in the literature. In 1999 Saito *et al.* [291] were the first to study a microbiological degradation pathway for GSM. In total, three products were identified; two of them were dehydration products of GSM and the third resulted from dehydration followed by enolation. Another study employing bacteria was performed by Eaton [292]. Two main intermediates were identified, i.e. 2- and 7-

ketogeosmin. Song *et al.* [227] studied the ultrasonically induced degradation of GSM. Dehydrations, subsequent dehydrogenations and a ring opening reaction were observed due to pyrolytic bond scissions taking place.

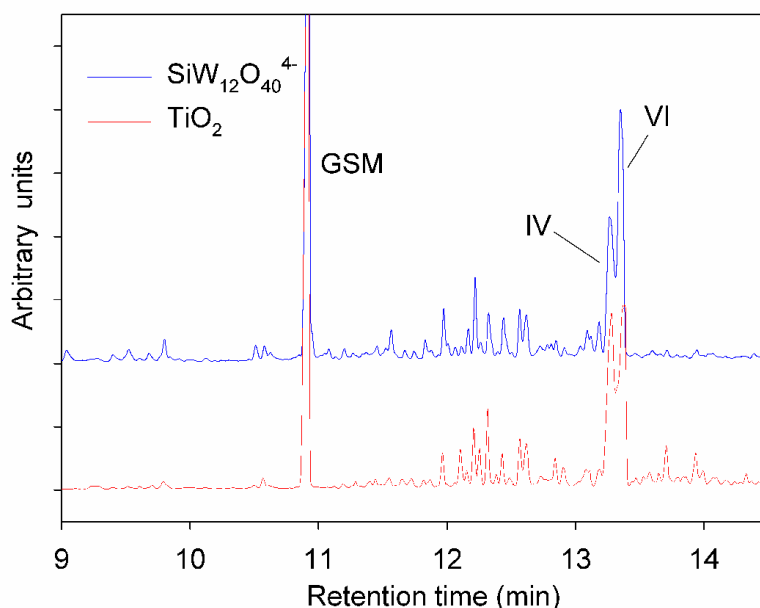


Figure 9.4. Chromatograms extracted during photocatalytic degradation of GSM [245].

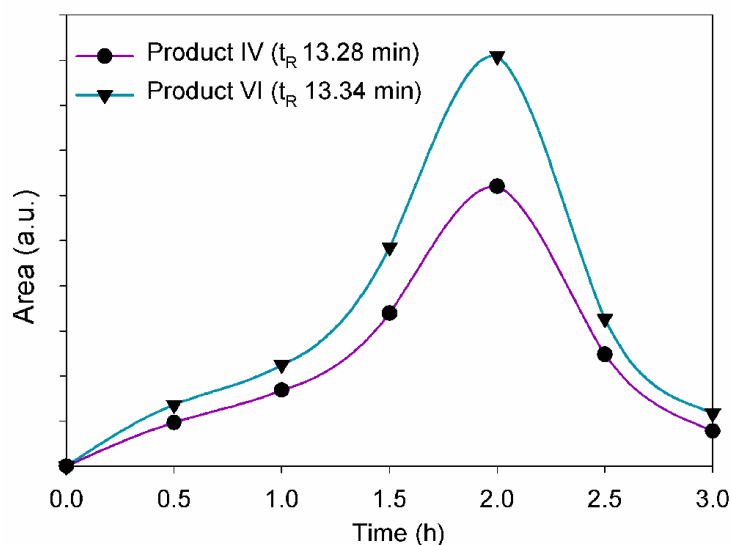


Figure 9.5. Evolution and decay of main intermediate products (product IV: 8a-Hydroxy-4a-methyl-octahydro-naphthalen-2-one and product VI: 8,8a-Dimethyl-decahydro-naphthalen-1-ol), upon photocatalytic degradation of GSM (20 mg L^{-1}), using $\text{SiW}_{12}\text{O}_{40}^{4-}$ ($7 \times 10^{-4} \text{ M}$, 200 mg L^{-1}) under UV-A irradiation [245].

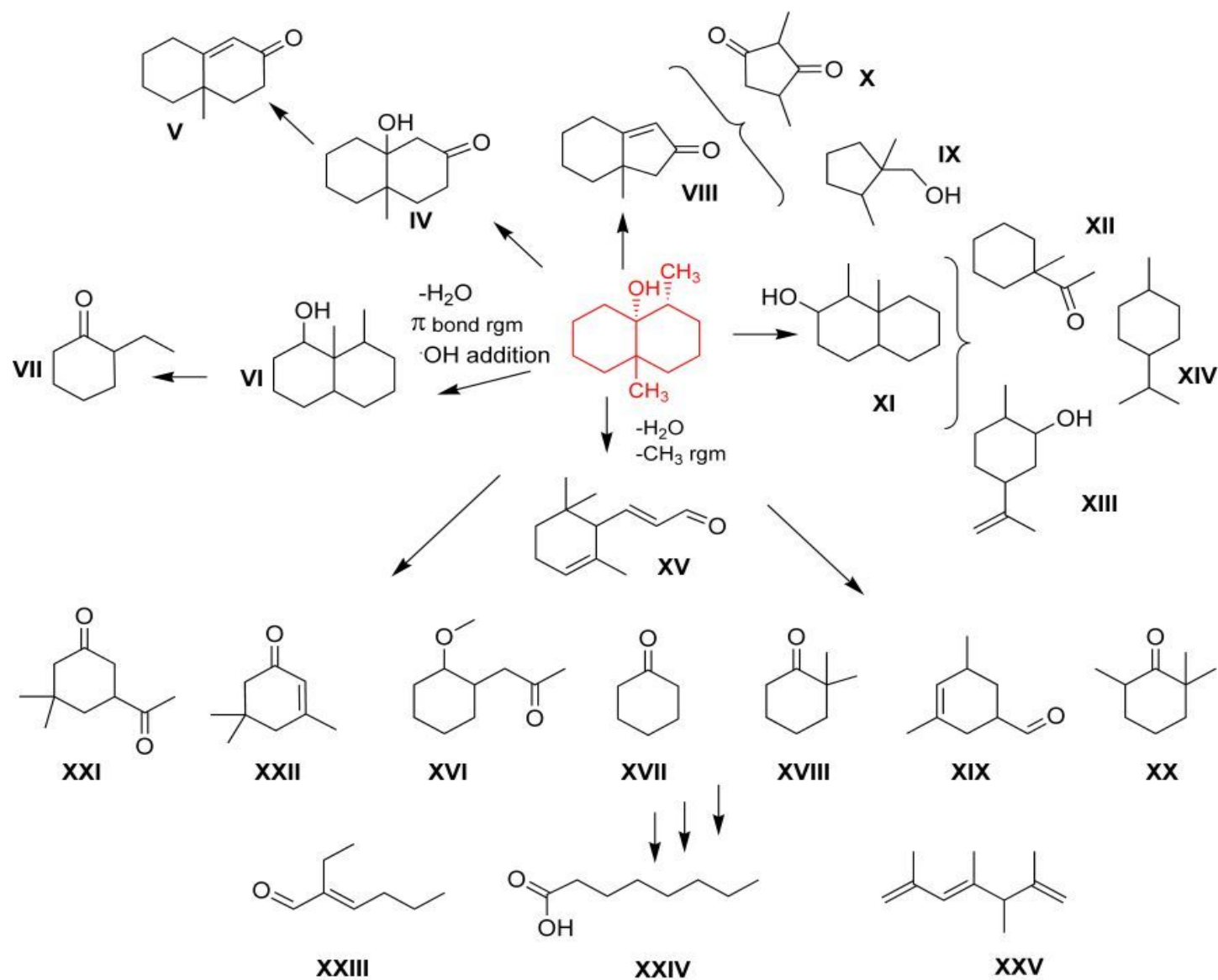
Prior to this work, Pemu *et al.* [294] studied GSM degradation using photocatalysis with TiO_2 . Only a small number of intermediates were identified (3,5-dimethylhex-1-ene, 2,4-

dimethylpentan-3-one, 2-methylethylpropanoate and 2-heptanal) showing that GSM undergoes rapid ring opening producing aliphatic saturated and unsaturated compounds, including some alkanones and esters.

The intermediates detected in this study were similar in the presence of $\text{SiW}_{12}\text{O}_{40}^{4-}$ and TiO_2 (Scheme 9.2.). This is in good agreement with previous studies where it has been demonstrated that the photocatalytic performance of POM and TiO_2 is similar in terms of the overall mechanism of photodecomposition of organic compounds, the intermediate species involved and the final photodegradation products (i.e., CO_2 , H_2O and inorganic anions) [42]. This also tends to suggest, despite the recent arguments that exist [44], that the photodegradation mechanism in the case of GSM, by both catalysts ought to take place mainly via a common reagent, i.e. $\cdot\text{OH}$ radicals.

Table 9.3. Intermediates identified during the photocatalytic degradation of GSM with their retention time (t_R) and their spectral characteristics (M^+ , m/z), in Scheme 9.2 [245].

Name	Symbol	t_R (min)	M^+	m/z	SiW ₁₂ O ₄₀ ⁴⁻	TiO ₂
GEOSMIN		10.89	182	112, 43, 55		
8a-Hydroxy-4a-methyl-octahydro-naphthalen-2-one	IV	13.28	182	112, 55, 97, 82	√	√
4a-Methyl-4,4a,5,6,7,8-hexahydro-3H-naphthalen-2-one	V	12.44	178	121, 136, 93	√	√
8,8a-Dimethyl-decahydro-naphthalen-1-ol	VI	13.34	182	112, 43, 55, 97, 126	√	√
2-Ethyl-cyclohexanone	VII	12.11	126	98, 55, 126	√	√
7a-Methyl-1,4,5,6,7,7a-hexahydro-inden-2-one	VIII	12.61	150	150, 135, 79, 93		√
2,4-Dimethyl-cyclopentane-1,3-dione	IX	7.48	126	126, 56, 111, 43	√	√
(1,2-Dimethyl-cyclopentyl)-methanol	X	11.83	128	97, 55		√
1,8a-Dimethyl-decahydro-naphthalen-2-ol	XI	12.86	182	112, 55, 41	√	√
1-(1-Methyl-cyclohexyl)-ethanone	XII	11.41	140	55, 97	√	√
5-Isopropenyl-2-methyl-cyclohexanol	XIII	12.44	154	136, 107, 121, 79	√	√
1-Isopropyl-4-methyl-cyclohexane	XIV	11.82	140	97, 55, 140, 41	√	√
3-(2,6,6-Trimethyl-cyclohex-2-enyl)-propenal	XV	12.86	182	112, 55, 41	√	√
1-(2-Methoxy-cyclohexyl)-propan-2-one	XVI	12.55	170	112, 43, 94	√	√
Cyclohexanone	XVII	5.27	112	68, 84, 112	√	
2,2-Dimethyl-cyclohexanone	XVIII	12.20	126	126	√	
3,5-Dimethyl-cyclohex-3-enecarbaldehyde	XIX	11.37	138	107, 95, 67	√	
2,2,6-Trimethyl-cyclohexanone	XX	6.37	140	82, 56, 69, 140	√	
5-Acetyl-3,3-dimethyl-cyclohexanone	XXI	7.73	152	68, 96, 152		√
3,5,5-Trimethyl-cyclohex-2-enone	XXII	7.48	138	82, 138, 39, 54		√
2-Ethyl-hex-2-enal	XXIII	11.96	126	55, 97, 126	√	√
Octanoic acid	XXIV	7.98	144	60, 73, 41, 101		√
2,4,5,6-Tetramethyl-hepta-1,3,6-triene	XXV	11.26	136	93, 79, 121, 108	√	√



Scheme 9.2. Intermediates formed during photocatalytic degradation of GSM by $\text{SiW}_{12}\text{O}_{40}^{4-}$ or TiO_2 [245]

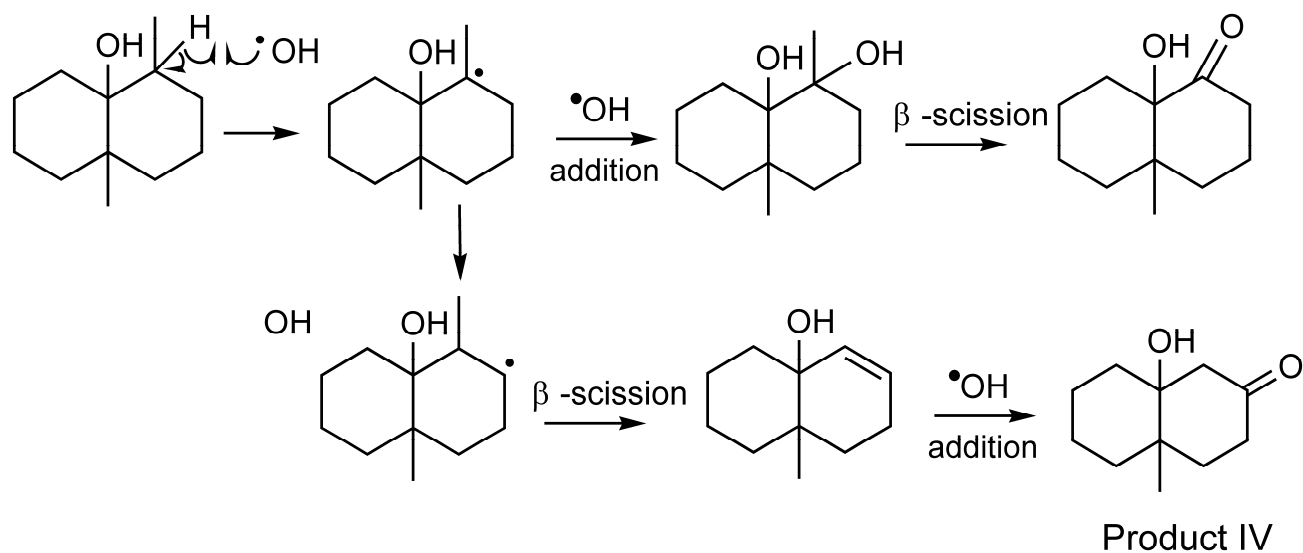


Figure 9.6. Proposed mechanism followed for the formation of product IV (8,8a-Dimethyl-decahydro-naphthalen-1-ol) during the photocatalytic degradation of GSM with $\text{SiW}_{12}\text{O}_{40}^{4-}$ or TiO_2 catalyst [245].

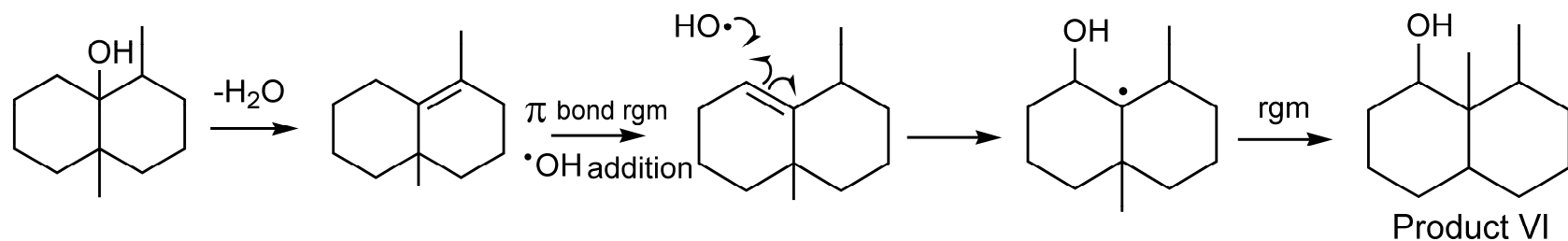


Figure 9.7. Proposed mechanism followed for the product VI (8,8a-Dimethyl-decahydro-naphthalen-1-ol) during the photocatalytic degradation of GSM with $\text{SiW}_{12}\text{O}_{40}^{4-}$ or TiO_2 catalyst [245].

9.5. Intermediate products of MIB using TiO₂ and POM under UV-A light

As far as concerning MIB's degradation products, in 1992 Sumimoto [295] was the first to study the degradation pathway of MIB, using biodegradation by gravel sand filtration. Tanaka *et al.* [296] followed biodegrading MIB using two different types of bacteria, identified some of the products formed which were dehydration products and camphor. In a later study Eaton and Sandusky [297] studied the biotransformations of MIB by three strains of camphor-degrading bacteria. These three strains of bacteria together appeared to produce metabolites resulting from hydroxylation all secondary carbons available on the six-member ring of MIB. Song *et al.* [227] studied the ultrasonically induced degradation of MIB and defined the degradation pathway. For pyrolytic transformations taking place in this study, simple bond scissions lead to free radicals. Degradation products of MIB indicated the formation of two directly dehydrated products; also under those conditions MIB being susceptible to C-C dissociation and subsequent skeletal rearrangement, products observed were due to C-C hemolytic-bond scissions leading to ring opening pathways. Qi *et al.* [294] and later Li *et al.* [298] both applied ozonation processes in order to investigate degradation of MIB and proposing a pathway of MIB's ozonation. The majority of products identified in those two studies were identical, proposing that *d*-camphor was likely to be the primary degradation product and further degraded into other byproducts, observing some of these aldehyde byproducts causing off-flavors in drinking water. Qi *et al.* [294] they also investigated the effect of hydroxyl radical using scavengers on the ozonation of MIB, with results suggesting that hydroxyl radicals presence was the predominant oxidant.

In this study, during photolysis of MIB in the absence of catalyst, a few peaks were detected in the chromatogram of the photolysed solution indicating photolytic cleavage. One of them was identified as 1,2,7,7-Tetramethyl-bicyclo[2.2.1]hept-2-ene (I) (Scheme 9.3.), that is possibly formed by dehydration of MIB. Its retention time (t_R) and spectral characteristics are given in Table 9.4.

A detailed study of the photodegradation of MIB (Scheme 9.3.) with SiW₁₂O₄₀⁴⁻ revealed the formation and decay of several products prior to the final decomposition to CO₂. Many chromatographic peaks appeared in the photolyzed solution in the presence of SiW₁₂O₄₀⁴⁻ which were not present without photocatalyst. The intermediates identified together with their retention times (t_R) and spectral characteristics are given in Table 9.4. They are compiled as follows: alcohol- (III), ketone- (II) and diketone- (IV, V, VI) derivatives of MIB, oxygen containing cyclic compounds (VII, VIII, IX, X, XI) and open

chain aliphatic compounds (XII, XIII). Similar photocatalytic experiments were also performed in the presence of TiO_2 . The intermediates detected were identical with those found in the presence of $\text{SiW}_{12}\text{O}_{40}^{4-}$ (Table 9.4., Figure 9.8.). In Scheme 9.3. a possible photodegradation mechanism for MIB, which applies to both POM and TiO_2 , which provides a reasonable explanation for the similar intermediates formed in both processes.

Product III (1,6,7,7-Tetramethyl-bicyclo[2.2.1]hept-5-en-2-ol) is formed with hydroxylation of product I suggesting the presence of $\cdot\text{OH}$ radicals. Product II (*d*-camphor) is proposed to be the primary intermediate produced during photocatalysis of MIB formed with a β -scission reaction mechanism on the methyl group of MIB that generates a ketone. Products IV, V and VI are possibly formed by hydrogen elimination followed by $\cdot\text{OH}$ addition and oxidation of secondary alcohol, leading to the formation of ketone, starting from product II. As far as concerning the other identified saturated and unsaturated oxygen containing cyclic intermediates, mechanisms involved are hydroxyl radical oxidation of compounds, driven by electrophilic substitution. The majority of those are five-membered rings revealing ring opening on MIB molecule. Linear aliphatic compounds were identified during the later stages of photo-oxidation similar to previous studies of Hiskia *et al.* [299].

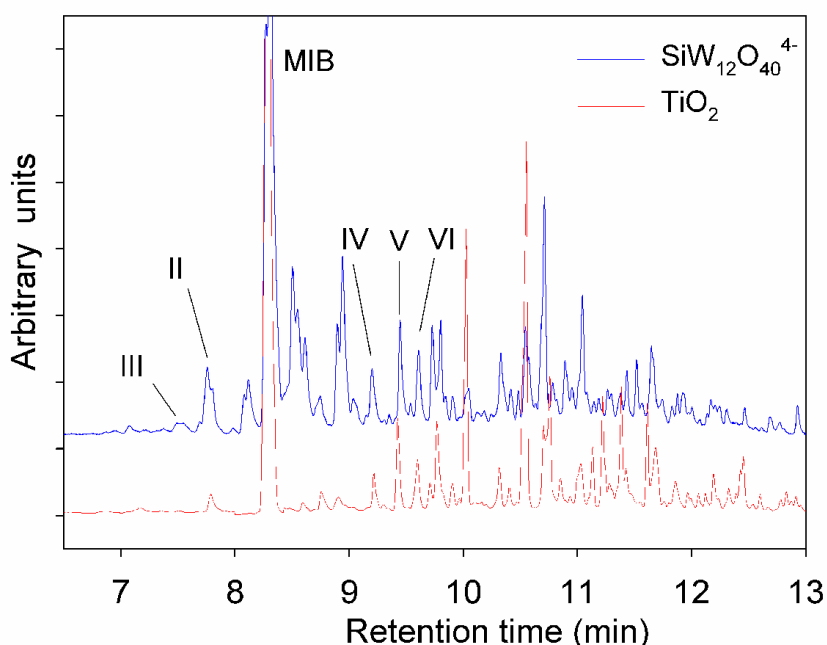
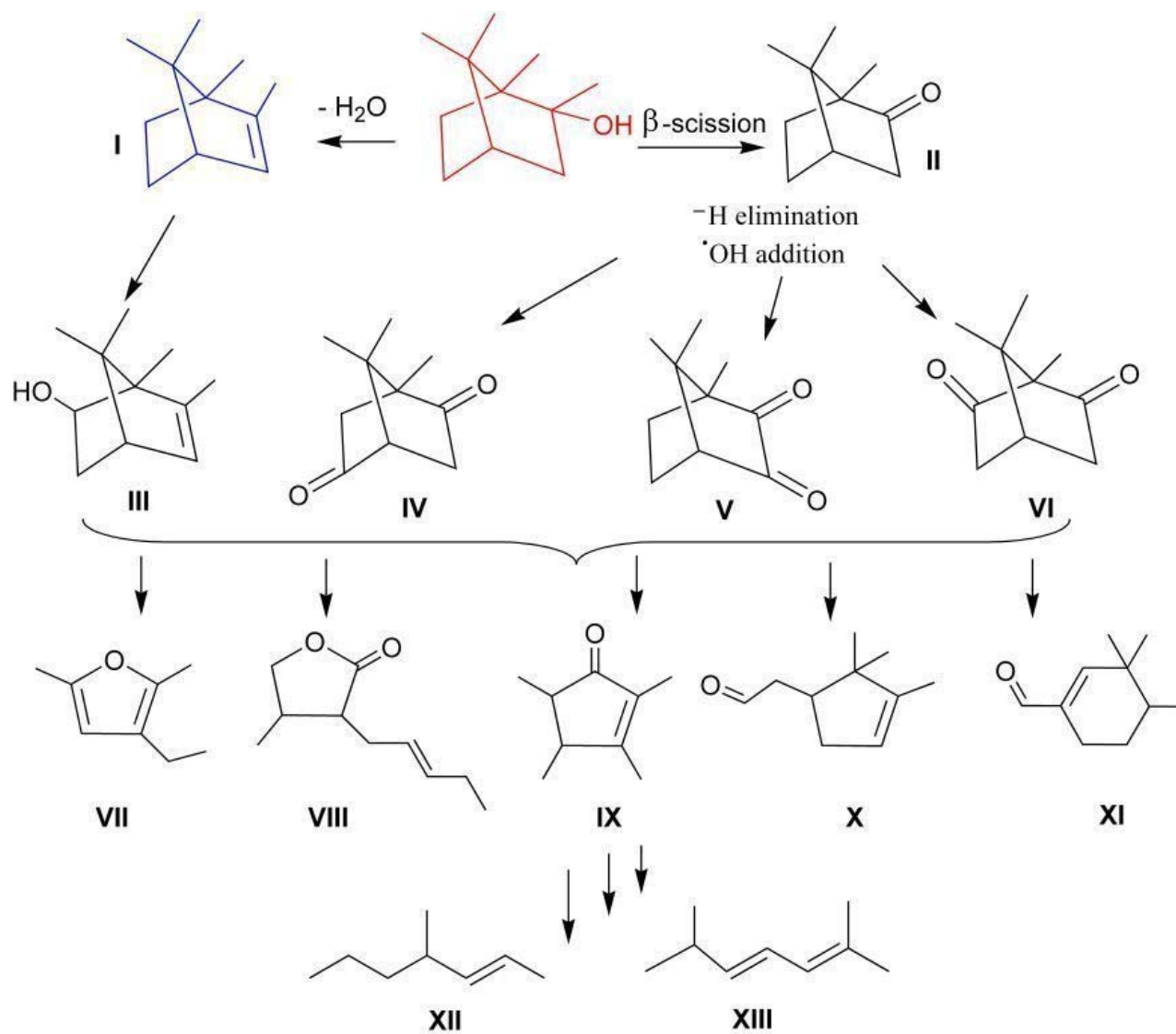


Figure 9.8. Chromatograms extracted during photocatalytic degradation of MIB [245].

Table 9.4. Intermediates identified during photolysis and the photocatalytic degradation of MIB with their spectral characteristics (M^+ , m/z), in Scheme 9.3 [245].

Name	Symbol	t_R (min)	M^+	m/z	SiW ₁₂ O ₄₀ ⁴⁻	TiO ₂
2-methylisoborneol		8.28	168	95, 108		
1,2,7,7-Tetramethyl-bicyclo[2.2.1]hept-2-ene	I	6.08	150	107, 79, 93, 135		
1,7,7-Trimethyl-bicyclo[2.2.1]heptan-2-one (d-camphor)	II	7.80	152	95, 81, 41, 55, 108	√	√
1,6,7,7-Tetramethyl-bicyclo[2.2.1]hept-5-en-2-ol	III	7.48	166	108, 93	√	
1,7,7-Trimethyl-bicyclo[2.2.1]heptane-2,5-dione	IV	9.21	166	166, 69, 109, 83, 123	√	√
1,7,7-Trimethyl-bicyclo[2.2.1]heptane-2,3-dione	V	9.64	166	95, 83, 69, 55	√	√
1,7,7-Trimethyl-bicyclo[2.2.1]heptane-2,6-dione	VI	9.73	166	166, 41, 67, 97, 83	√	√
3-Ethyl-2,5-dimethyl-furan	VII	10.85	124	109, 124	√	√
4-Methyl-3-pent-2-enyl-dihydro-furan-2-one	VIII	10.74	168	99, 43	√	√
2,3,4,5-Tetramethyl-cyclopent-2-enone	IX	8.77	138	123, 95, 138, 67	√	√
(2,2,3-Trimethyl-cyclopent-3-enyl)-acetaldehyde	X	11.34	152	108, 93, 67	√	√
3,3,4-Trimethyl-cyclohex-1-enecarbaldehyde	XI	9.03	152	95, 81, 123, 67	√	
2,6-Dimethyl-hepta-2,4-diene	XII	10.81	124	109, 124	√	√
4-Methyl-hept-2-ene	XIII	8.09	112	69, 41, 55, 112	√	√



Scheme 9.3. Intermediates formed during photolysis and photocatalytic degradation of MIB by $SiW_{12}O_{40}^{4-}$ or TiO_2 [245].

Qi *et al.* [294] and later Li *et al.* [300] applying ozonation processes investigated the degradation of MIB and proposed a degradation pathway. The majority of the intermediates identified in those two studies were identical. According to these studies, *d*-camphor was likely to be the primary degradation product that it is further degraded into other byproducts, including aldehydes. Qi *et al.* [294] also investigated the effect of $\cdot\text{OH}$ using scavengers on the ozonation of MIB, with results suggesting that the presence of $\cdot\text{OH}$ was the predominant oxidant. The full agreement of these results with those of ozonation of MIB [294, 300] is a further evidence that the main oxidant is $\cdot\text{OH}$ in all cases, i.e. photocatalysis with $\text{SiW}_{12}\text{O}_{40}^{4-}$ or TiO_2 and ozonation.

9.6. Toxicity Experiments concerning MIB and GSM

In order to determine EC50 for MIB and GSM, a number of standard solutions (0.125 – 1 ppm) were used. MIB and GSM are generally known as non toxic compounds, which is indicated also in Table 9.5. For that reason no EC50 value could be given.

Table 9.5. Odors standard solutions (0.125 - 1 ppm).

Sample (ppm)	Gt	% Effect _t
BLANK	1.04	
2,4-DCP	3.29	76.71
MIB (0.125)	0.12	10.96
MIB (0.25)	0.11	9.59
MIB (0.5)	0.09	8.22
MIB (1)	0.06	5.48
GSM (0.125)	0.14	12.33
GSM (0.25)	0.09	8.22
GSM (0.5)	0.04	4.11
GSM (1)	0.12	10.96

Even though MIB and GSM are non toxic compounds, there is a possibility photocatalytic process lead to the formation of toxic intermediates. In order to investigate that, toxicity measurements using Microtox assay were performed for MIB and GSM mineralization under UV-A and solar light, using Degussa P25 and $\text{SiW}_{12}\text{O}_{40}^{4-}$. Results are presented in Tables 9.6 and 9.7 and as it can be concluded from them, no significant toxicity is presented during the photocatalysis process.

Table 9.6. Odors degradation under UV-A using Degussa P25

Irradiation time (h)	MIB % Effect _t	GSM % Effect _t
2,4-DCP	77.05	77.05
0	7.32	4.87
2	4.92	14.75
5	1.64	8.20
12	14.75	9.84
24	11.48	12.95
48	13.11	13.11
72	10.45	12.89

Table 9.7. Odors degradation under UV-A using SiW₁₂O₄₀⁴⁻

Irradiation time (h)	MIB % Effect _t	GSM % Effect _t
2,4-DCP	72.79	72.79
0	6.33	8.50
2	7.47	3.25
5	12.51	11.53
12	13.74	8.86
24	9.21	5.46
48	5.95	13.24
72	11.69	16.16

9.7. Photocatalytic degradation mechanisms of GSM/MIB in the presence of SiW₁₂O₄₀⁴⁻ and TiO₂: A comparison study

An objective of this study was the comparison of photodegradation mechanisms followed by POM and TiO₂ in the cases of GSM and MIB, via degradation, mineralization and identification of intermediate products, under UV-A irradiation.

Several examples, from both photocatalysts, have been reported to demonstrate that their performance is similar in terms of the overall mechanism of photodecomposition of organic compounds, the intermediate species involved and the final photodegradation products (i.e., CO₂, H₂O and inorganic anions) [51]. However, parallel experiments under similar conditions, using various substrates (atrazine, fenitrothion, 4-chlorophenol and 2,4-dichlorophenoxyacetic acid) and [•]OH radical scavengers, have shown that the photooxidizing mode of POM and TiO₂, i.e., [•]OH radicals and/or holes (h⁺), depends on the nature of substrate and the mode of investigation [54, 68]. Atrazine showed that both POM and TiO₂ mainly operate through [•]OH radicals and with a lower extent with h⁺, whereas fenitrothion suggested the almost exclusive operation of both photocatalysts via [•]OH radicals. On the other hand, differences between the two photocatalysts have been proposed with 4-chlorophenol and 2,4-dichlorophenoxyacetic acid, with POM operating via [•]OH radicals and TiO₂ mainly via h⁺. Overall, the action of [•]OH radicals relative to h⁺ appears to be more pronounced with POM than TiO₂ [54]. An example against the above mechanism for POM has been reported for the degradation

of dichlorobenzene in the presence of $\cdot\text{OH}$ radicals scavengers suggesting that POM act via h^+ rather than $\cdot\text{OH}$ mediated oxidations [69]. As a conclusion, whether an $\cdot\text{OH}$ or h^+ mediated mechanism is followed depends on various parameters (e.g., the kind of substrates, the substrate-photocatalyst interaction) and should be considered on a case by case basis [68].

In accordance with the results given in this study on degradation and mineralization (TOC measurements and identification of formed intermediates) of GSM and MIB, it has been concluded that the same photodegradation mechanism is followed when POM and TiO_2 are used as photocatalysts. The similarities of the intermediates identified (presence of the same oxidized derivatives) and results from experiments with $\cdot\text{OH}$ radical scavengers, as well tend to suggest that $\cdot\text{OH}$ is the common oxidant, as has been also mentioned for other organic compounds[43].

9.8. Conclusions

Removal of taste and odor compounds GSM and MIB from water was achieved using photocatalysis with POM and TiO_2 . Both photocatalysts found to be effective in degradation of target analytes. Experiments were also performed in the presence of $\cdot\text{OH}$ radicals scavengers showing retardation of the photodegradation of GSM and MIB, which indicates that $\cdot\text{OH}$ radicals should be the main oxidant for both photocatalysts. The photocatalytic degradation of GSM and MIB in the presence of both photocatalysts leads to the formation of a plethora of intermediates prior to mineralization. In the case of GSM the majority of the identified intermediates were cyclic ketones which upon ring opening lead to formation of linear saturated and unsaturated products. For MIB degradation identified intermediates are consisted by alcohol-, ketone- and diketone-derivatives of MIB, oxygen containing cyclic compounds and open chain aliphatic compounds. A complete degradation pathway is proposed for target compounds during their photocatalytic degradation with common intermediates identified, using either POM or TiO_2 with $\cdot\text{OH}$ radical attack to be mainly responsible for the mechanism. These results suggest that photocatalysis using either POM or TiO_2 demonstrates significant potential for the complete removal of taste and odor compounds that taint water.

CHAPTER 10

Photocatalytic degradation of MC-LR, CYN, GSM and MIB in water using TiO₂ under visible light. Unveiling new degradation Pathways

10.1. Introduction

The degradation pathway followed for the degradation of MC-LR was studied by several [270] in the UV light and yet by only few studied so far in the visible range of the solar light [301, 302]. As far as concerning the CYN, GSM and MIB their degradation pathway is studied only under UV light irradiation [2].

In this chapter is reported the mechanism followed for the photocatalytic degradation of MC-LR, and CYN, under visible light. In the case of MC-LR, PPIA measurements showed that toxicity is only proportional to the toxin concentration and no toxic intermediates are formed during the process.

10.2. Photocatalytic Degradation of MC-LR, CYN, GSM and MIB under visible light

All four target compounds were studied for degradation under visible light using Kronos vlp-7000 as the photocatalyst. Degussa P25 TiO₂ was also used as a reference material, whereas no degradation was observed in any of the compounds. For MC-LR (10 ppm) and CYN (10 ppm) a destruction of 10% and 14% was observed, as shown in Figure 10.1. For GSM (1 ppm) and MIB (1 ppm) no degradation was observed. To eliminate the case that the experimental error from the SPME was overlapping the small percentage of destruction, liquid-liquid extraction was applied with dichloromethane as the organic solvent. Also, utilization of a different visible light active photocatalyst (nitrogen doped) and using lower analytes concentration, yet no degradation was

observed. Based on those results, it can be concluded that in the cases of GSM and MIB, the mechanism followed in the visible light photocatalysis process could not lead to their degradation.

Degradation experiments for MC-LR and CYN were repeated in the presence of superoxide dismutase enzyme. In the case of the enzyme whereas the superoxide anion was conjugated, degradation was almost eliminated, proving that is the main specie responsible for degradation. Having that in mind the absence of degradation in the case of GSM and MIB can be explained on the fact that either of those compounds have a double bond, on which superoxide anion can be attached and modify their structure.

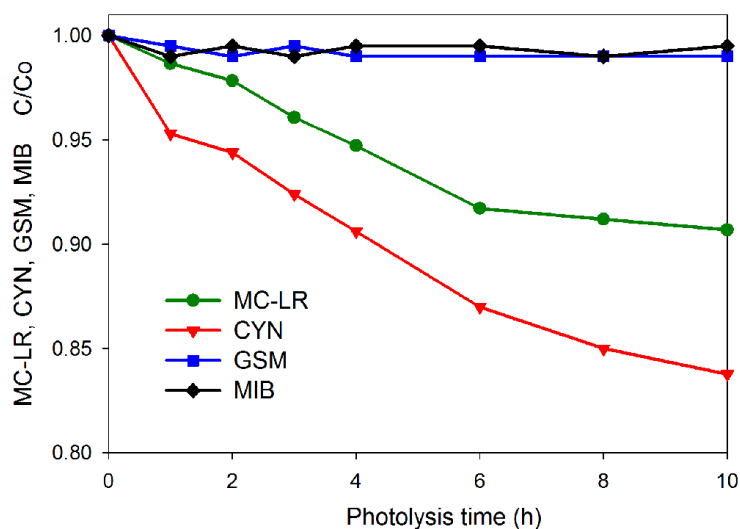


Figure 10.1. Photocatalytic degradation of target analytes using Kronos TiO_2 under visible light.

10.3. Intermediate products of MC-LR under visible light using TiO_2

In photocatalysis, light of energy greater than the band gap of the semiconductor excites an electron from the valence band to the conduction band with oxidation of adsorbed H_2O by photogenerated holes and reduction of an electron acceptor (dissolved oxygen) by photoexcited electrons, leading to the production of a hydroxyl ($\text{HO}\cdot$) and superoxide radical anion ($\text{O}_2\cdot^-$), respectively [303]. $\text{O}_2\cdot^-$ may further react with H^+ to generate hydroperoxyl radical ($\cdot\text{OOH}$) and further electrochemical reduction yields H_2O_2 and then $\text{HO}\cdot$. When $\text{O}_2\cdot^-$ reacts with a double bond, C-C bonds cleave through the formation of a dioxetane giving two carbonyl groups. When $\cdot\text{OOH}$ or H_2O_2

reacts with a double bond, dihydroxylation follows. The objective of this study was to define the contribution of those ROS in the process of photodegradation under visible light.

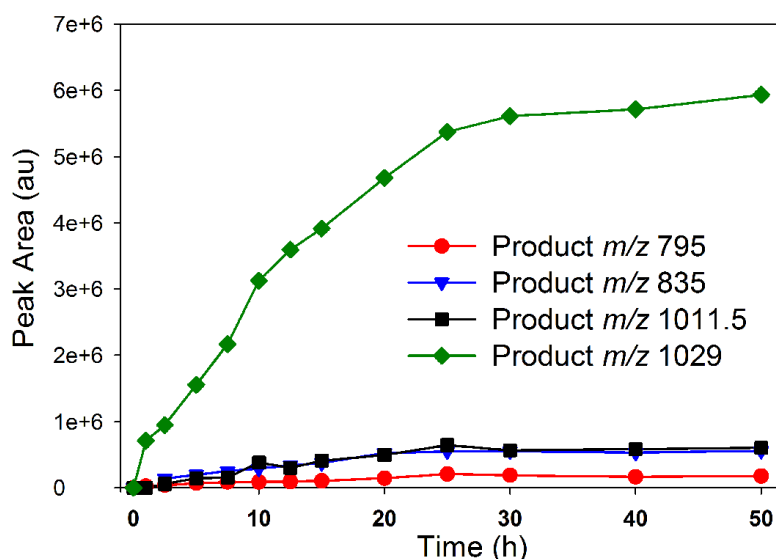


Figure 10.2. Evolution of products during the photocatalytic degradation of MC-LR under visible light.

In the case of MC-LR under visible light degradation, the products with the more intense peak areas were found to be 795, *m/z* 835, *m/z* 1011.5 and *m/z* 1029. Product with *m/z* 1029 is a dihydroxylation product [2, 270] and has the highest peak area of all (formed through reaction with $\cdot\text{OOH}$ and H_2O_2 , or from two $\text{HO}\cdot$ additions required). Production of *m/z* 1011.5 intermediate (monohydroxylation, from $\text{HO}\cdot$ attack) is evidenced after an induction period. Also products with *m/z* 795 and *m/z* 835 could be formed after superoxide anion addition followed on either of the double bonds of Adda amino acid, followed by cleavage and formation of carbonyl compounds.

10.3.1. Toxicity assessment

Reduction of MC-LR concentration resulted in the directly proportional reduction amount of the toxic activity, implying that MC-LR loses its toxic activity (protein phosphatase inhibition) as soon as the molecule is transformed to and no toxic products are formed.

10.4. Intermediate products of CYN under visible light using TiO₂

In the case of CYN degradation, the main products formed are *m/z* 347, 350, 414, 432, *m/z* 448 and *m/z* 450. Product of *m/z* 448 has the highest peak area and thus is the main intermediate. It can be formed when O₂^{•-} reacts on CYN's double bond giving two carbonyl groups. Product *m/z* 448 is formed with double hydroxylation of the double bond (through reaction with •OOH and H₂O₂, or -less possible- after two HO• additions) [2, 277]. Product of *m/z* 432 (monohydroxylation, from HO• attack) appeared after an induction period.

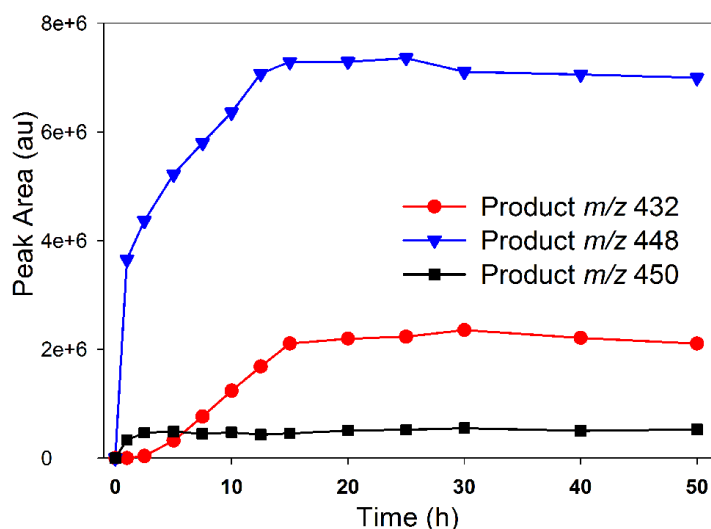


Figure 10.3. Evolution of products during the photocatalytic degradation of CYN under visible light.

10.5. Conclusions

Under visible light photocatalysis, degradation of MC-LR and CYN was achieved, whereas elimination of GSM and MIB was negligible. Based on the identified intermediate products, during the degradation of both MC-LR and CYN, it was revealed that superoxide anion radical is the main specie during photocatalysis under visible light. In cases like GSM and MIB that compounds don't carry a double bond, the degradation process under visible light is inefficient due to inactivity of the main specie (superoxide anion radical) with the analyte. Modification on the structure of an organic compound under visible light photocatalysis that can further lead to its destruction can benefit from having double bonds which superoxide anion radical can react with.

Chapter 11

Parameters influencing TiO₂ photocatalysis towards degradation of MC-LR, CYN, GSM and MIB in water

11.1. Introduction

Evaluation of the photocatalytic activity of TiO₂ based photocatalysts is highly depended on a number of parameters that govern the kinetics of photodegradation and mineralization. Parameters that were taken under consideration in this chapter for the photocatalytic degradation of cyanobacterial toxin MC-LR, CYN and water taste and odor compounds GSM and MIB, were the light intensity, dissolved oxygen, catalyst loading, initial concentration of the substrate, adsorption, pH and light wavelength. All those parameters can affect in a different way the photocatalytic activity of a catalyst, and the evaluation should be performed under investigation of those [284].

11.2. Light Intensity

To access the effect of light intensity in the photocatalytic degradation process of MC-LR, the same experiment was performed, under two different irradiation apparatus (Figure 11.1.). In the experimental procedure 10 mg L⁻¹ of MC-LR were irradiated in the presence of 200 mg L⁻¹ Degussa P25 TiO₂ using at first an Oriel Photomax 150 W Xe lamp with a cut-off filter at $\lambda > 320$ nm with light intensity of 121 mW cm⁻² and then under UV-A black light (320-400 nm), emitting ~1 mW cm⁻². Results showed that even though the light intensity with the Photomax 150 W Xe lamp was ~120 times higher that the one used under black light irradiation, the photodegradation efficiency was similar, indicating that the photocatalytic rate of MC-LR is not dependant on the intensity of the light source used.

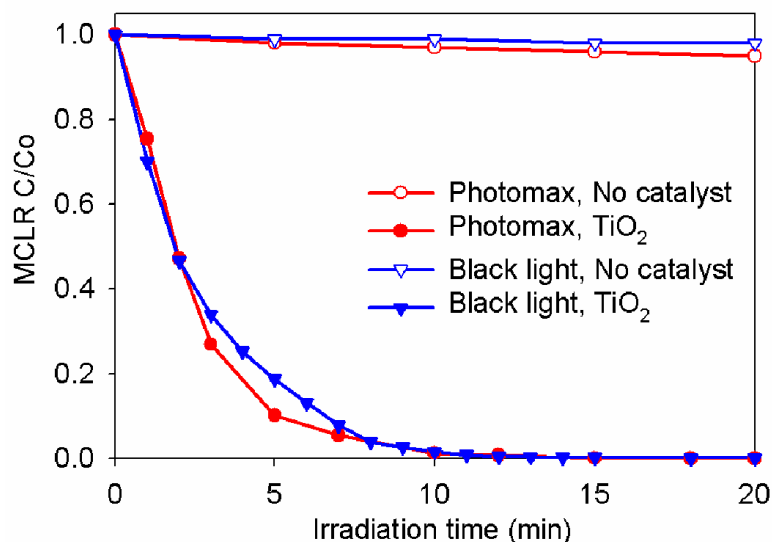


Figure 11.1. Photocatalytic degradation of MC-LR (10 mg L^{-1}) using of Degussa P25 TiO_2 (200 mg L^{-1}) under light sources with different intensity (150 W Xe lamp and Black light) [284].

Light intensity is one of the parameters affecting the photocatalytic process. In 2000 Fujishima *et al.* [304], indicated that reaction rates of TiO_2 photocatalysis are not highly dependent on light intensity, whereas the surface reactions can be induced by a few photons of low energy (i.e. $1 \mu\text{W cm}^{-2}$). For not modified TiO_2 based materials, photons required for reaction are for wavelengths shorter than 400 nm. Many studies have shown that the degradation of many organic substrates followed linear proportionality correlation to the incident radiant flux [305-307]. Radiant flux (Φ), is the optical power or rate of flow of radiant energy and intensity (E), is the flux per unit area striking a surface. Above certain threshold value the linear of the reaction rate on radiant flux (Φ) changes to square root dependency ($\Phi^{0.5}$). This shift is supposed to be due to the amount of holes (h^+) available during the electron-hole pair formation (e^-+h^+). In TiO_2 photocatalysis, the photogenerated holes are much less than the conduction band available electrons. For this reason the photogenerated holes are the rate limiting component [241]. In this case at high intensities the dependency of radiant flux changes to zero (Φ^0). This can be explained by the saturation of the catalyst's surface, limiting the mass transfer for adsorption and desorption and thus, under these conditions degradation rates are not affected by increasing the light intensity.

This could be the case in these experiments, in which the $\sim 1 \text{ mW cm}^{-2}$ of the UV-A black light apparatus used, already cover the light intensity needed, thus when using the Oriel Photomax 150 W Xe lamp with ~ 120 times higher light intensity, the reaction rates were almost the same. In conclusion, better evaluation of the photocatalysts can be

performed using light intensities above saturation effect. In this case experimental errors and under evaluation of the photocatalysts can be avoided and inter-laboratory comparisons could be possible.

11.3. Presence of oxygen

To explore the effect of dissolved oxygen in the photocatalytic degradation process, 10 mg L⁻¹ of MC-LR were irradiated using 1000 mg L⁻¹ Degussa P25 TiO₂ using an Oriel 1000 W Xe-Hg lamp with a cut-off filter at $\lambda > 320$ nm, in the presence of oxygen (1.2x10⁻³ M of O₂), air (2.5x10⁻³ M of O₂) and nitrogen (deaerated, ~0 M of O₂) conditions (T = 22 °C) [308]. The photocatalytic degradation of MC-LR was higher when the solution was oxygen saturated, followed by degradation under air and finally nitrogen atmosphere, (Figure 11.2.).

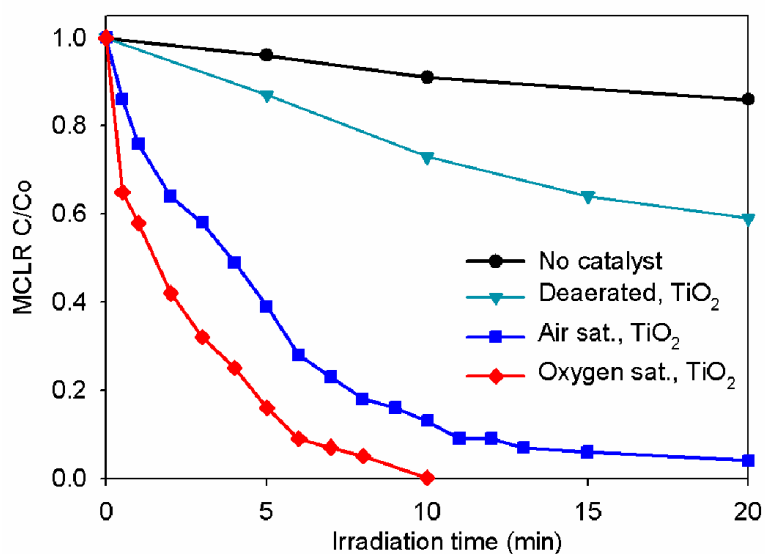


Figure 11.2. Photocatalytic degradation of MC-LR (10 mg L⁻¹) under UV-A ($\lambda \geq 320$ nm) irradiation in the presence of Degussa P25 TiO₂ (1000 mg L⁻¹) with different oxygen concentrations in the solution (deaerated, air saturated and oxygen saturated) [284].

Initial degradation rates were calculated as 0.3, 2.4, and 5.2 $\mu\text{M min}^{-1}$, in deaerated, air saturated and oxygen saturated solutions, respectively. This implies that the photocatalytic degradation of MC-LR is relatively more efficient as the concentration of dissolved oxygen in the solution increases. The difference between air and oxygen is not very drastic as it is under deaerated conditions. Dissolved oxygen plays an important role in TiO₂ photocatalysis of MC-LR as an electron scavenger, trapping

excited conduction band electrons from recombination [309]. Oxygen may also be involved in the formation of superoxide anion radical and other reactive oxygen species (ROS), stabilization of radical intermediates, mineralization and direct photocatalytic reactions [241].

11.4. Catalyst loading

Figure 11.3. illustrates the influence of catalyst concentration on the MC-LR degradation in oxygenated solutions. Experiments have been performed in presence of Degussa P25 TiO₂ under UV-A irradiation ($\lambda_{\max}=365$ nm), at five different concentrations, i.e. 50, 100, 200, 500 and 1000 mg L⁻¹.

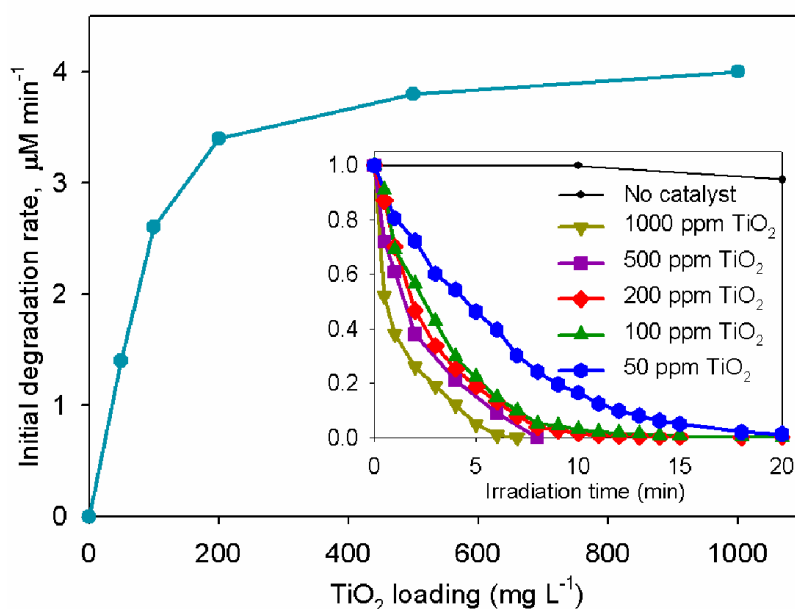


Figure 11.3. Dependence of initial rate of MC-LR degradation towards TiO₂ loading. UV-A irradiation ($\lambda_{\max}=365$ nm) in the presence of Degussa P25 TiO₂; MC-LR 10 mg L⁻¹ [284].

It can be seen that increase of the catalyst initial concentration from 50 to 100 and finally to 200 mg L⁻¹ results in increase of the MC-LR degradation rate from 1.4 to 2.6 and 3.4 M min⁻¹, respectively. Further increase of the catalyst initial concentration to 500 and 1000 mg L⁻¹ had only a slight influence on MC-LR degradation from 3.8 to 4.0 M min⁻¹, respectively. Overall, a linear dependency holds until the ~200 mg L⁻¹ catalysts loading when the reaction rate starts to decrease and becomes independent of TiO₂ concentration. So, the concentration of 200 mg L⁻¹ being below the saturation level of

TiO₂ has been used as initial concentration for all tested photocatalytic materials in order to compare their photocatalytic effectiveness towards toxin destruction.

11.5. Initial concentration of substrate

In the photocatalytic degradation of organic pollutants in the presence of TiO₂, it has been traditionally reported that the initial rate of disappearance of the pollutant fits a Langmuir–Hinshelwood (L–H) kinetic scheme [241]. According to the L–H model, at low concentrations of organic substrate, the initial photoreaction is first order with respect to substrate, moving progressively (flat area) to zero order. Due to the high cost of MC-LR analytical standards, experiments for the construction of Figure 11.4. have been performed up to 12 mg L⁻¹ for MC-LR. At this point, the limit where the relationship between initial reaction and initial concentration remains constant seems to be reached. The concentration that has been selected for use as initial concentration for MC-LR for all tested materials in order to compare their photocatalytic effectiveness towards toxin destruction was 10 mg L⁻¹, being in the linear part of Figure 11.4. Similar results were given in the case of CYN.

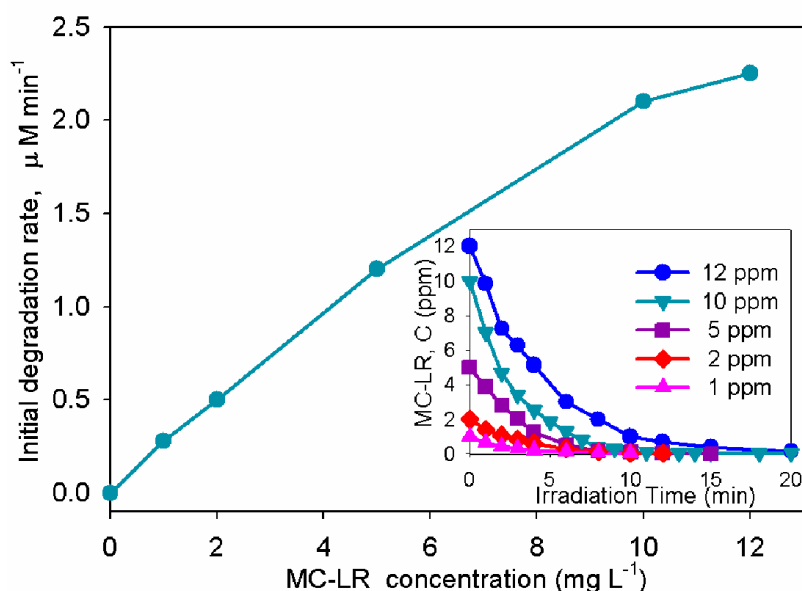


Figure 11.4. Variation of the initial rate of the MC-LR degradation as a function of increased initial concentration; Inset: Photocatalytic degradation of MC-LR (1, 2, 5, 10, 12 mg L^{-1}) under UV-A ($\lambda_{\text{max}}=365$ nm) irradiation in the presence of Degussa P25 TiO₂ (200 mg L^{-1}) [284].

Similar experiments have been performed with GSM and MIB giving similar results, whereas for GSM are presented in Figure 11.5. For analytical purpose the initial concentration of GSM was set to 2×10^{-3} , 0.2 and 1 mg L^{-1} . The concentration that has been selected for use as initial concentration for both GSM and MIB for all tested materials in order to compare their photocatalytic effectiveness towards these compounds was 1 mg L^{-1} , being in the linear part of Figure 11.5.

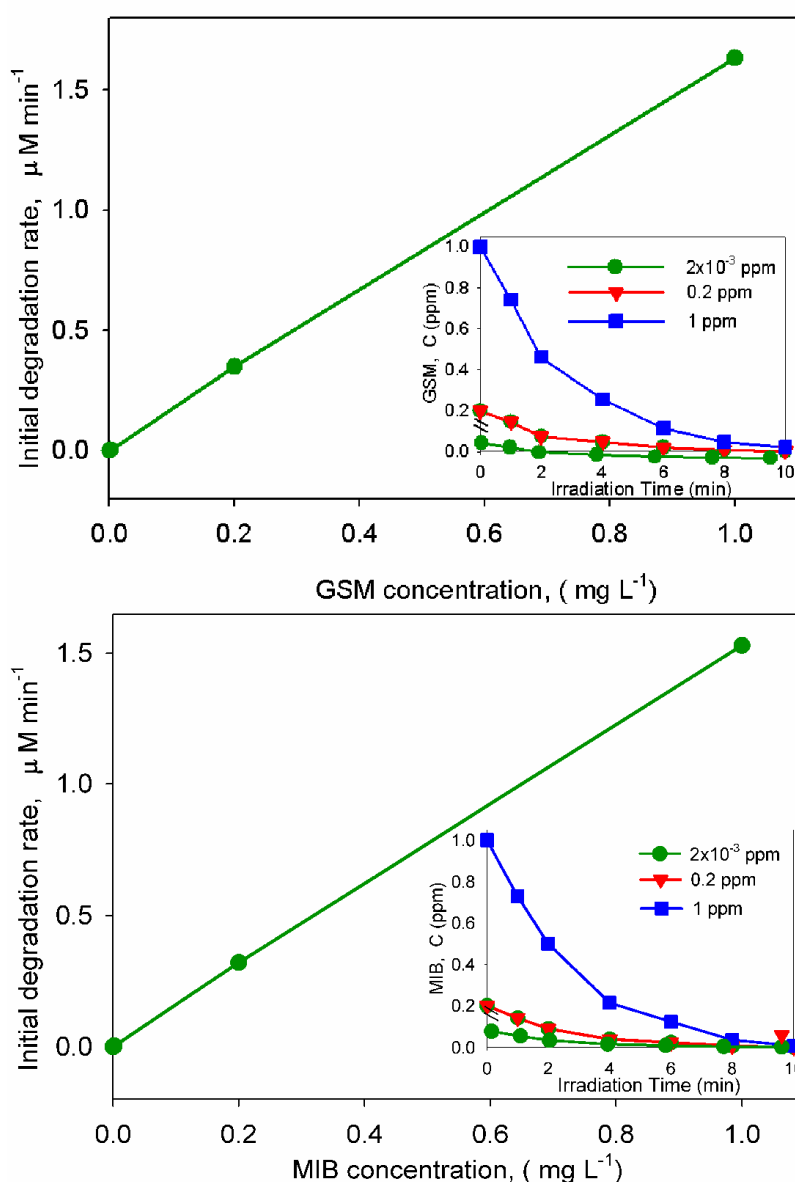


Figure 11.5. Variation of the initial rate of the GSM and MIB degradation as a function of increased initial concentration; Inset: Photocatalytic degradation of (a) GSM and (b) MIB (2×10^{-3} , 0.2 and 1 mg L^{-1}) under UV-A ($\lambda_{\text{max}} = 365 \text{ nm}$) irradiation in the presence of Degussa P25 TiO_2 (200 mg L^{-1}) [284].

11.6. Adsorption on catalysts surface

Another important parameter on the evaluation of the photocatalytic activity of new materials towards certain substrates is the dark adsorption of these substrate on the photocatalyst surface. The amount adsorbed should be determined and photocatalytic experiments should be performed when equilibrium has been reached. Initial pH has to be well defined because pH value can affect dark adsorption of substrate by photocatalyst under investigation.

Adsorption of MC-LR on photocatalysts' surface (Degussa P25 TiO₂, Kronos TiO₂, Ref-TiO₂, N-TiO₂, NF-TiO₂, ECT-10213t and GO-TiO₂) was investigated for 10 mgL⁻¹ initial concentration of MC-LR and 200 mgL⁻¹ of catalyst loading at pH 5.7 (Figure 11.6.). As can be seen in Figure 11.6., under the experimental conditions used all photocatalysts have presented toxin adsorption. The higher MC-LR adsorption (20%) was observed with GO-TiO₂ followed by Kronos TiO₂, ECT-10213t, N-TiO₂, NF-TiO₂, Ref-TiO₂ and Degussa P25 TiO₂ with 11, 8, 8, 8, 8 and 6% toxin adsorption, respectively. The higher adsorption of MC-LR on GO-TiO₂ can be attributed to the remarkable enhanced adsorption capability of the catalyst for pollutant molecules [310].

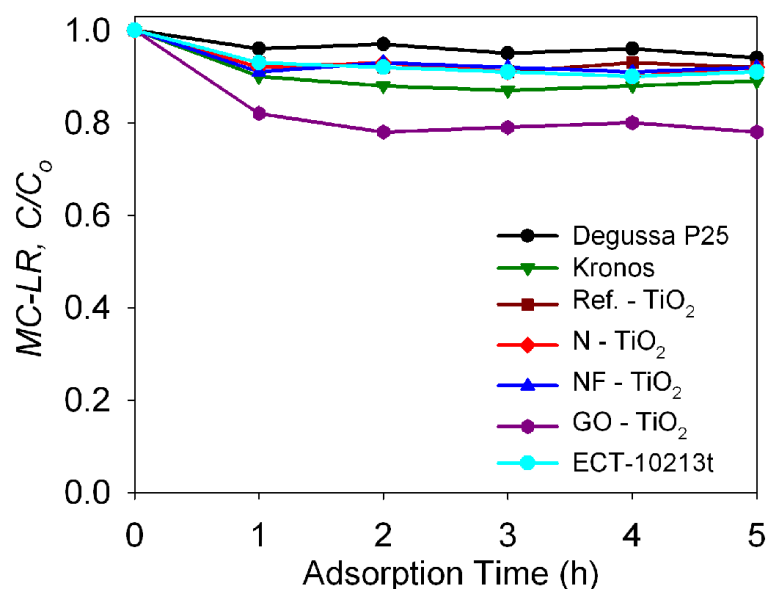


Figure 11.6. Adsorption% of MC-LR on Degussa P25 TiO₂, Kronos TiO₂, Ref-TiO₂, N-TiO₂, NF-TiO₂, ECT-10213t and GO-TiO₂; 10 mgL⁻¹ initial concentration of MC-LR and 200 mgL⁻¹ of catalyst loading at pH 5.7 [284].

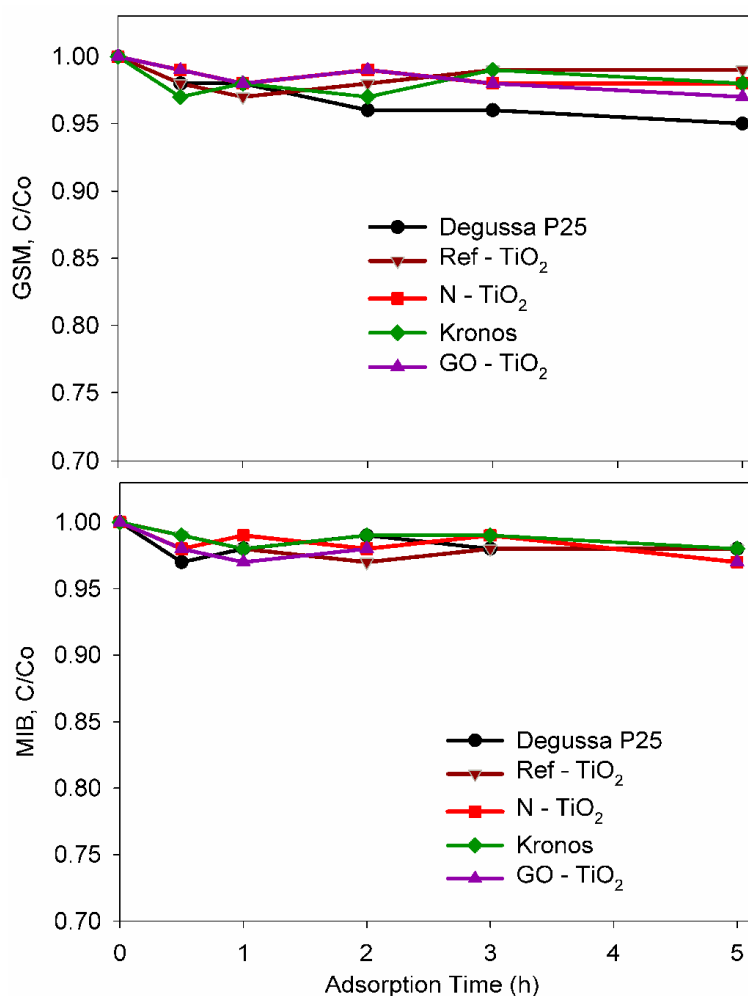


Figure 11.7. Adsorption% of (a) GSM and (b) MIB on Degussa P25 TiO_2 , Kronos TiO_2 , Ref- TiO_2 , N- TiO_2 , NF- TiO_2 , ECT-10213t and GO- TiO_2 ; 10 mgL^{-1} initial concentration of MC-LR and 200 mgL^{-1} of catalyst loading at pH 5.7 [284].

The adsorption of GSM and MIB was also investigated for all photocatalysts using 1 mgL^{-1} initial concentration of GSM and MIB under the same experimental conditions. Results obtained suggested that both GSM and MIB had negligible adsorption on the catalysts' surfaces, Figure 11.7.

Adsorption experiments were carried out in order to evaluate the extent to which CYN is adsorbed on the surface of the photocatalysts. Under the experimental conditions used, about 15% and 30% of adsorption of CYN was observed for Kronos vlp-7000 and Degussa P25 respectively, after ~2 hours of stirring in the dark (Figure 11.8.).

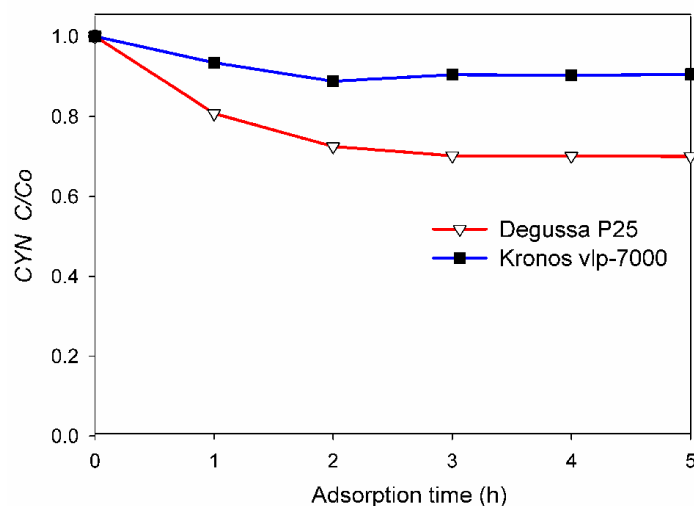


Figure 11.8. Adsorption in dark of CYN (10 mg L^{-1}) under UV-A using Degussa P25 and Kronos vlp-7000 photocatalysts (200 mg L^{-1}) [284].

CYN is a very hydrophilic compound that carries both positively and negatively charged groups at neutral pH [311], with an estimated pK_a to be around 8.8 [159]. Therefore at pH lower than 8.8 (as in the experimental conditions used, pH 5.7), the majority of CYN molecules have both positively and negatively charged groups. The pH of zero point charge (pH_{zpc}) of TiO_2 is 6.25 [231]; below this pH the surface is positively charged. CYN can be adsorbed on TiO_2 surface via electrostatic interactions between the positively charged surface of catalysts and the negatively charged group (SO_4^{2-}) of CYN. In another study [242], where polymorphic TiO_2 was used, the CYN's negative group also reach the positively charged photocatalyst's surface at pH lower than its pH_{zpc} . On the contrary, no significant adsorption was observed reported with NF- TiO_2 photocatalytic films at pH 3, since CYN at this pH is positively charged as is the photocatalyst's surface [22].

11.7. Initial Solution pH

To explore the effect of pH on the photocatalytic degradation of MC-LR (10 mg L^{-1}) and GSM/MIB (1 mg L^{-1}), experiments were performed using 200 mg L^{-1} of Degussa P25 under UV-A irradiation ($\lambda_{\text{max}} = 365 \text{ nm}$) at different pH values. Figure 11.9. shows the photocatalytic degradation of MC-LR for three pH values (3, 5.7 and 7). The degradation of MC-LR is pH depended with initial degradation rates of 3.8, 2.7 and 2.4 $\mu\text{M min}^{-1}$ for pH 3, 5.7 and 7, respectively.

MC-LR is structured by a D-methylaspartic acid and a D-glutamic acid, having free carboxylic groups. The pKa for both aminoacids is around 3.0. MC-LR, also contains an L-arginine unit having a basic amino group with pKa=12.48. With increasing pH ($3 < \text{pH} < 12$), MC-LR loses two protons from the carboxylic groups, making the overall charge -1 . At extremely basic pH (>12), MC-LR loses the proton from the protonated basic group and the overall charge is -2 [240].

Solution pH also influences the surface charge, band edge position, and the particle size of TiO_2 . Surface charge is governed by the ionisation reaction of the surface-adsorbed HO- groups. Depending on the solution pH, these surface groups can either remove or add protons, resulting in negatively or positively charged surface, respectively. The pH value being around $\text{pH} \approx 6.4$ for Degussa P25, at which TiO_2 surface carries no charge, is defined as the zero point charge (pH_{zpc}). When $\text{pH} < \text{pH}_{\text{zpc}}$ the surface charge of the catalysts becomes positively charged and presents electrostatic attractions towards negatively charged species [241].

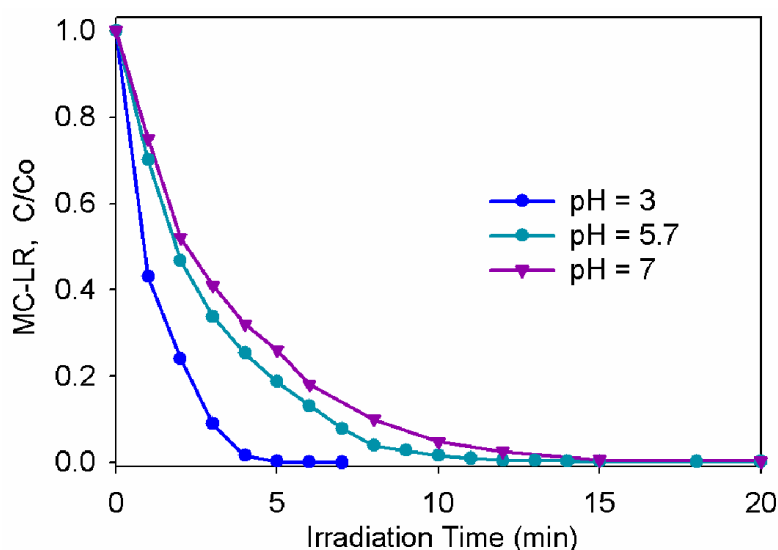


Figure 11.9. Photocatalytic degradation of MC-LR (10 mg L^{-1}) under UV-A irradiation ($\lambda_{\text{max}}=365 \text{ nm}$) in the presence of Degussa P25 TiO_2 (200 mg L^{-1}) at pH 3, 5.7 and 7 [284].

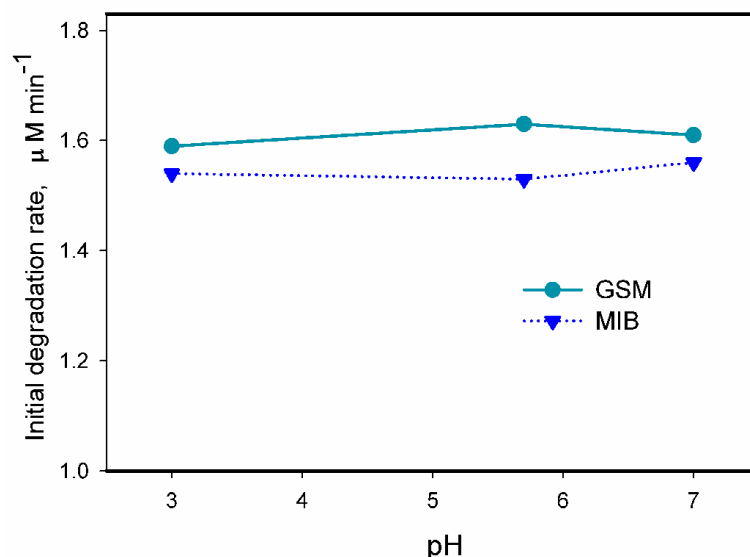


Figure 11.10. Initial rates of photocatalytic degradation of GSM and MIB (1 mg L^{-1}) under UV-A irradiation ($\lambda_{\text{max}} = 365 \text{ nm}$) in the presence of Degussa P25 TiO_2 (200 mg L^{-1}) at pH 3, 5.7 and 7 [284].

Based on all that, the higher initial degradation rate for MC-LR at pH 3, can be explained due to positively charged surface of the catalyst and the negatively charged molecules of MC-LR being electrostatically attracted. At higher pH values (5.7 and 7) the photocatalytic degradation is no strongly dependant upon pH.

Based on the same argument it can be explained why degradation for CYN, GSM and MIB was not pH dependent. Cyindrospermopsin is very hydrophilic and carries both a positive and a negative charge at neutral pH. GSM and MIB being very low ionizable bicyclic tertiary alcohols ($\text{pK}_a > 15$), present weak intermolecular attraction forces with the photocatalysts. This is in agreement with these results concerning the zero adsorption observed for these compounds on catalysts surface.

11.8. Irradiation Wavelength

In order to evaluate the photocatalytic efficiency of the new TiO_2 nanostructured materials, degradation was investigated under UV-A, solar and visible light. In the case of visible light cut-off filters were used. Visible light illumination covering the whole visible range (400 – 700 nm) was provided using a 435 nm cut-off filter exhibiting a zero transmittance below 410 nm. When a 420 nm cut-off filter was used instant of the 435 nm cut-off one, a transmittance of 3.25% was observed below 400 nm giving rise to not reliable results, due to the exposure of photocatalysts under UV-A irradiation Figure

11.11.c. As it can be seen in Figure 11.11.a, when illumination was performed using the 420 nm cut-off filter, all catalysts showed photocatalytic activity with Degussa P25 being the better and even some photolysis of MC-LR was present.

When illumination of MC-LR was performed using the 435 nm cut-off (wavelengths greater than 410 nm), only the visible light activated TiO₂ photocatalysts (Kronos TiO₂, N-TiO₂) show remarkable activity in MC-LR degradation, while Degussa P25 and Ref-TiO₂ are completely inactive, Figure 11.11.b. Inactivity of Degussa P25 has been confirmed, as it absorbs light with $\lambda < 410$ nm due to rutile phase (30% of Degussa P25 TiO₂, $E_{bg} = 3.0$ eV) [278]. For that reason, the cut-off filter used for the evaluation of a catalyst under visible light illumination should exhibit zero transmittance at wavelengths lower than 410 nm.

Among the tested materials, N-TiO₂ shows the better photocatalytic activity for MC-LR degradation followed by Kronos TiO₂. This behavior of N-TiO₂ is attributed to a red-shift of the energy band gap to the visible range at about 2.3 eV that justifies visible light photocatalytic activity towards degradation of MC-LR [258]. C-doping in Kronos TiO₂ produces new energy states deep in the TiO₂ band gap (substitution of oxygen by carbon atoms), which are responsible for the visible light absorption [256, 257]. Inactivity of Degussa P25 has been confirmed, as it absorbs light with $\lambda < 410$ nm due to rutile phase (30% of Degussa P25 TiO₂, $E_{bg} = 3.0$ eV) [278]. For that reason, the cut-off filter used for the evaluation of a catalyst under visible light illumination should exhibit zero transmittance at wavelengths lower than 410 nm.

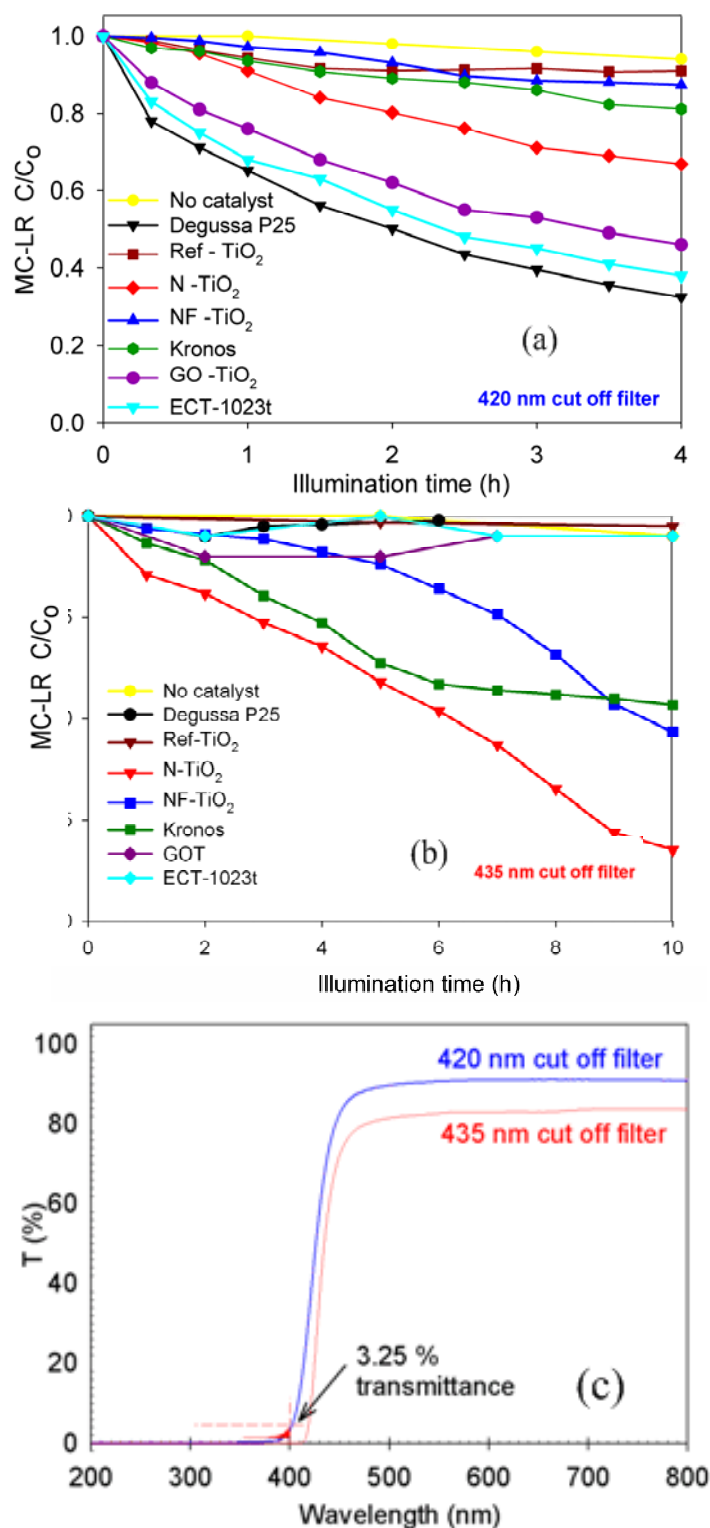


Figure 11.11. Photocatalytic degradation of MC-LR (10 mg L^{-1}) under using a cut-off filter at (a) 420 nm and at (b) 435 nm in the presence of TiO₂ nanomaterials (200 mg L^{-1}). (c) The transmittance spectrum of the 420 nm and 435 nm cut-off filters [284].

11.9. Conclusions

TiO₂ based photocatalysis can be effective for water purification from new classes of emerging pollutants such as cyanobacterial toxins and metabolites. Standardized procedures for testing photocatalytic materials for water purification are needed to support marketing and applications. Evaluation of the photocatalytic performance is a complicated process, influenced by many different parameters (e.g. light intensity, presence of oxygen, catalyst loading, initial concentration of substrate, adsorption, pH, different irradiation wavelength, mineralization, intermediate products and toxicity). Reproducible evaluation results (intra and inter-laboratory) require a careful selection of all parameters.

The light intensity used is selected to be above of a threshold value, for avoiding under-estimation of photocatalytic activity of the catalysts. Oxygenation, catalyst loading and initial concentration of substrate, also play an essential role in the process. Parameters such as adsorption and pH of the solution can differ on their effect based on the catalysts and the substrates structural characteristics. A photocatalyst should be evaluated under conditions similar to those that is intended to be applied, i.e. under UV-A, solar or visible light. Investigation of the degradation pathway as well as the mineralization extent and toxicity assessment is important in order to evaluate whether a catalyst is appropriate for application.

Overall, results for the degradation of MC-LR under different irradiation (UV-A, solar and visible light) can provide us information whether a catalyst is better than other for specific experimental conditions i.e. Degussa P25 TiO₂ was the best photocatalyst under UV-A irradiation but it was completely inactive under visible light. On the other hand doped TiO₂ materials being more active under solar light in comparison with undoped one (Ref-TiO₂) present remarkable activity under visible light. In addition, GO-TiO₂ being generally similar to other home prepared materials in UV-A seems to be more promising for use under solar light. For that reason a catalyst should be evaluated under conditions similar to those that is intended to be applied.

Chapter 12

Recommendations

12.1. Recommendations

This dissertation examined the photocatalytic performance of new synthesized materials concerning the degradation and mineralization of cyanobacteria metabolites such as cyanotoxins (MC-LR and CYN) and water taste and odor compounds (GSM and MIB). TiO₂ based photocatalysts (Degussa P25, Kronos vlp-7000, Ref-TiO₂, N-TiO₂, NF-TiO₂, GO-TiO₂ and ECT-1023t) were tested for their photocatalytic ability towards degradation and mineralization of the analytes from aqueous solutions using UV-A, solar and visible light. Parameters like light intensity, presence of oxygen, catalyst loading, initial concentration of substrate, adsorption, pH, different irradiation wavelength, were investigated for their influence in the process. In addition, photocatalytic degradation of GSM and MIB using a polyoxometalate photocatalyst, H₄SiW₁₂O₄₀, was studied and compared with photodegradation by TiO₂.

Also, mineralization and the identification of intermediate products and their toxicity under different experimental conditions were studied. Emphasis was given to the mechanistic understanding of the process by identification of intermediate and final products formed during photocatalysis process and a complete degradation pathway is proposed for MC-LR, CYN, GSM and MIB. Assessment of the residual toxicity during the course of treatment showed that detoxification of the solutions was achieved.

From a scientific point of view, a novel approach is suggested for the destruction of a new class of toxic organic pollutants of biogenic origin in water using solar light photocatalysis in the presence of TiO₂ and elucidation of degradation pathway provides a better understanding of the photocatalytic process and is expected to initiate further research regarding the fate of analytes under different water treatment technologies. The interdisciplinary nature of this research enables the continuation of this work in diverse conditions. Below are listed a few recommendations:

- **Other cyanotoxins**

Microcystins and especially MC-LR have been the main focus of several studies listed in the literature. However, there are several other groups with many toxins that are known to harm the ecosystem and necessitate appropriate treatment. Among them are other microcystins (-LA, -LW, etc), nodularins, anatoxins, saxitoxins or BMAA.

- **Competitive kinetics**

One strain of cyanobacteria can produce up to twelve different cyanotoxins [312], so is important to study the photocatalytic degradation of toxins among different derivatives of the same group or different groups, to investigate potential competitive kinetics among them.

- **Mechanism elucidation in real water**

In this study real water was only used for the degradation of the cyanobacterial metabolites and the intermediates identification was performed in distilled water. A really good application of the process could be the elucidation of the photocatalysis mechanism in real water samples, in which several components of natural waters can affect the intermediate products formation, along with toxicity measurements.

- **Use of Polyoxometalate on Cyanotoxins**

Photocatalysis with polyoxometalates was only performed with GSM and MIB. Those catalysts could be employed for the degradation of several cyanotoxins and compare the photocatalysis mechanism with TiO_2 , using radical scavengers.

- **Hybrid nanostructured TiO_2 -POM**

Hybrid nanostructured TiO_2 -POM materials prepared by the sol-gel technique [313], or by adsorption (wetness impregnation) of POMs on the surface of TiO_2 [314] show increased activity in organic pollutants photodegradation due

to their synergistic action [315] and could be used for the degradation of cyanobacterial metabolites compounds. Recent experimental data show that the presence of POMs decreases the recombination rate between electron-holes in TiO_2 and significantly increases the efficiency of the photocatalytic process. Furthermore, the formation of reduced POM (POM^-), which is generated by a one-electron reduction reaction with a conduction band electron in TiO_2 , subsequently absorbs visible light to form the excited-state POM (POM^*), which synergistically catalyzes the reduction of organic pollutants during TiO_2 photocatalytic [315, 316]. Appropriate selection of POM and experimental conditions (ratio of POM/ TiO_2 , nanoparticle size, pH, etc.) can result in the development of new, innovative TiO_2 -POM nanostructured materials with enhanced photocatalytic properties in both ultraviolet and solar light.

ABBREVIATIONS

ADDA	3-amino-9-methoxy-2,6,8-trimethyl-10-phenyldeca-4,6-dienoic acid
Ala	Alanine
AOPs	Advanced Oxidation Processes
Arg	Arginine
CYN	cylindrospermopsin
GC-MS	Gas chromatography–mass spectrometry
Glu	Glutamic Acid
GSM	geosmin
HPLC	High-performance liquid chromatography
LC-MS/MS	Liquid chromatography-tandem mass spectrometry
Leu	Leucine
MCs	microcystins
Mdha	Methyl dehydroalanine
MeAsp	Methyl Aspartic Acid
MC-LR	microcystin-LR
MIB	2-methylisoborneol
PPIA	Protein Phosphatase Inhibition assay
POM	polyoxometalates
ROS	Reactive Oxygen Species
SPME	Solid Phase Micro-Extraction
TIC	Total Ion Chromatogram
TiO ₂	Titanium Dioxide
TOC	Total Organic Carbon
UV-A	(300 < λ < 400 nm)

Appendix I

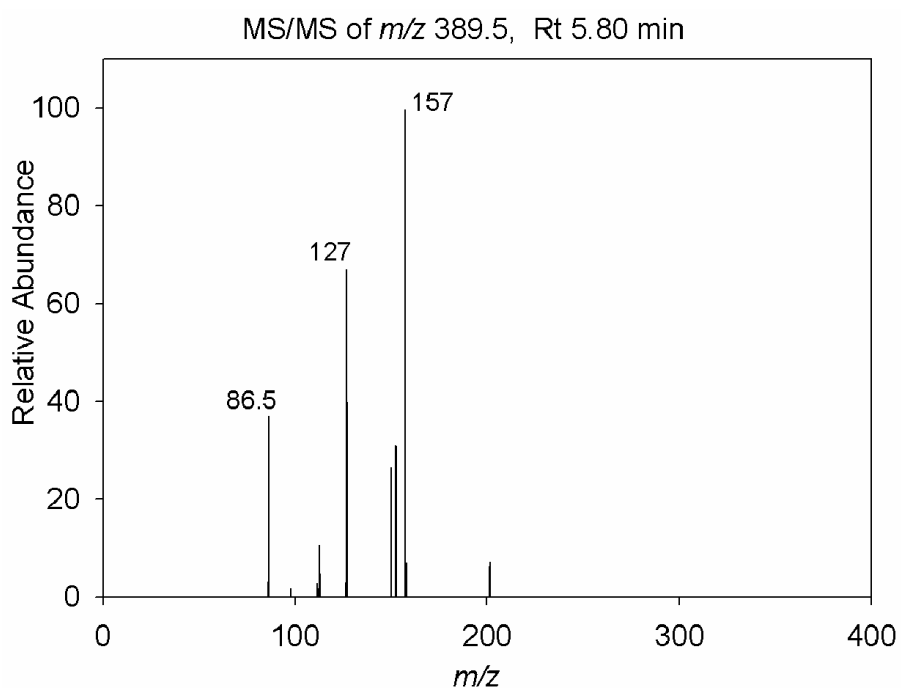


Figure A1. MS/MS spectrum of the intermediate with m/z 389.5 at R_t 5.80 min, for MC-LR degradation under UV-A light using Degussa P25.

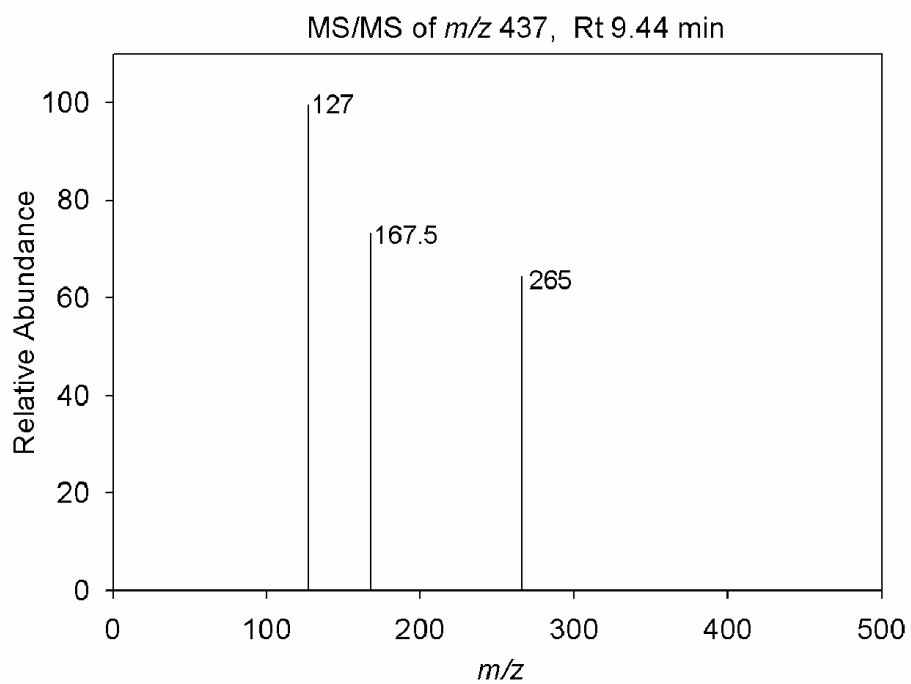


Figure A2. MS/MS spectrum of the intermediate with m/z 437 at R_t 9.44 min, for MC-LR degradation under UV-A light using Degussa P25.

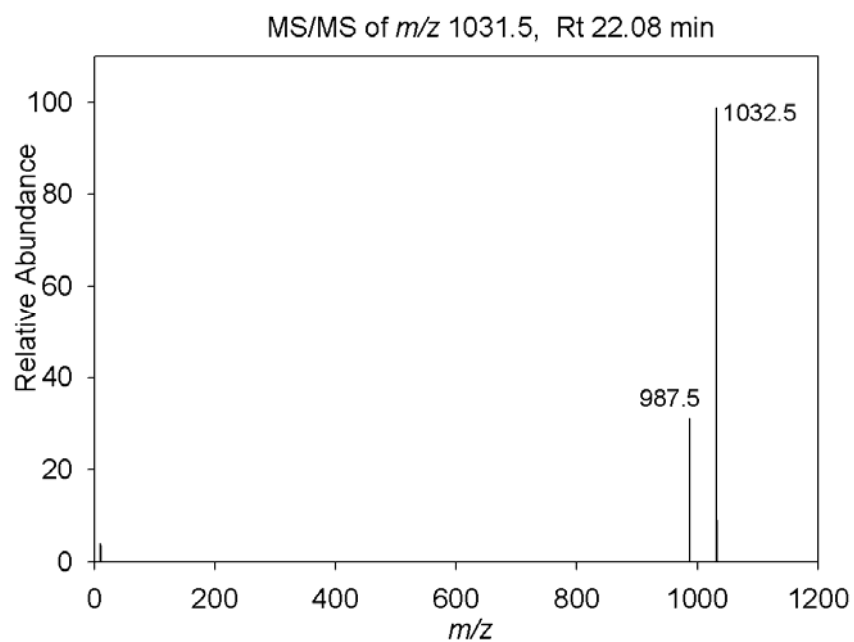


Figure A3. MS/MS spectrum of the intermediate with m/z 1031.5 at R_t 22.08 min, for MC-LR degradation under UV-A light using Degussa P25.

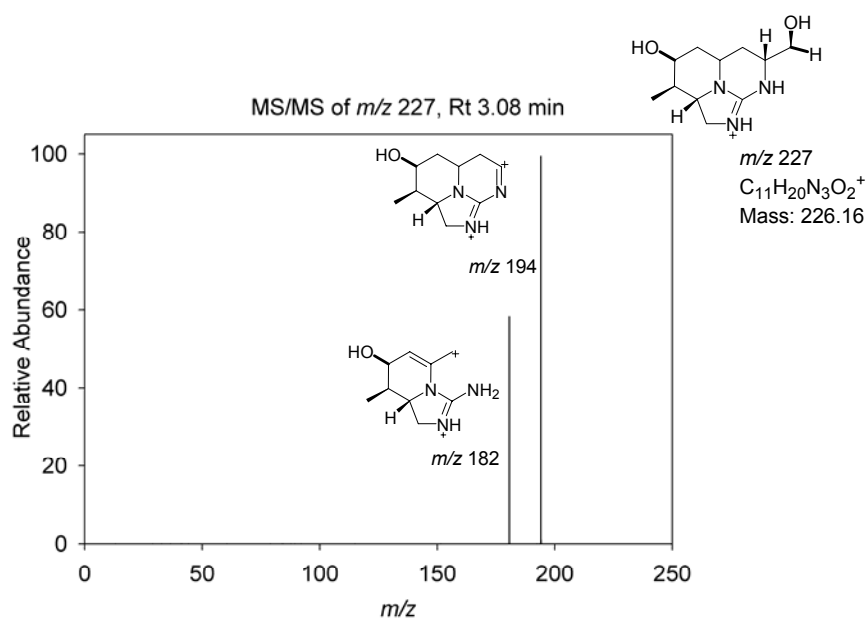


Figure A4. MS/MS spectrum of the intermediate with m/z 227 at R_t 3.08 min, for CYN degradation under UV-A light using Degussa P25.

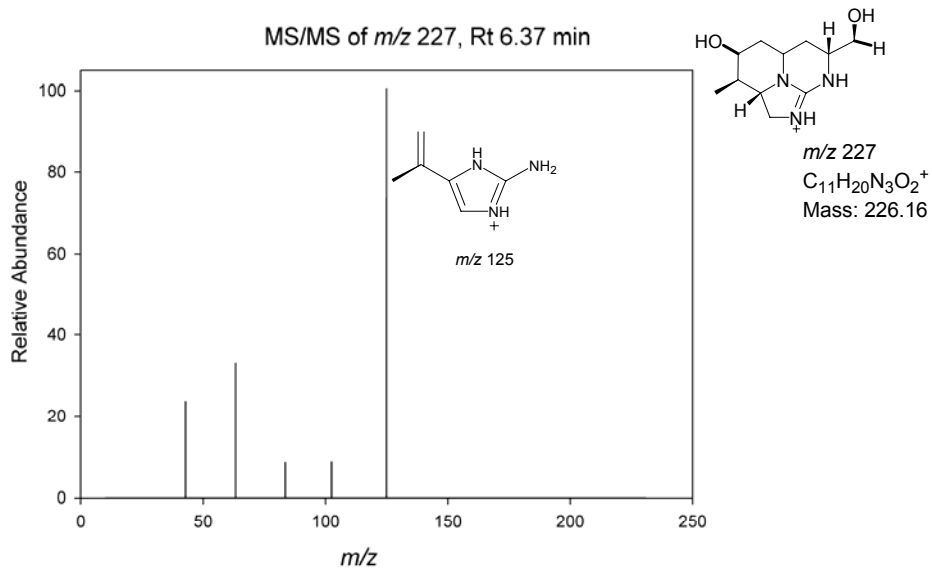


Figure A5. MS/MS spectrum of the intermediate with m/z 227 at R_t 6.37 min, for CYN degradation under UV-A light using Degussa P25.

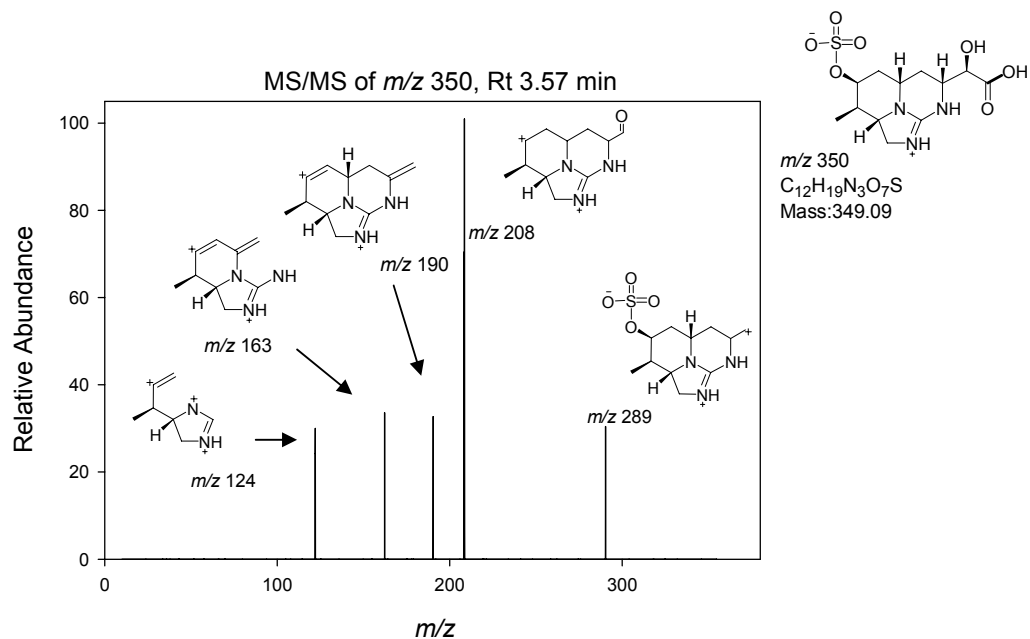


Figure A6. MS/MS spectrum of the intermediate with m/z 350 at R_t 3.57 min, for CYN degradation under UV-A light using Degussa P25.

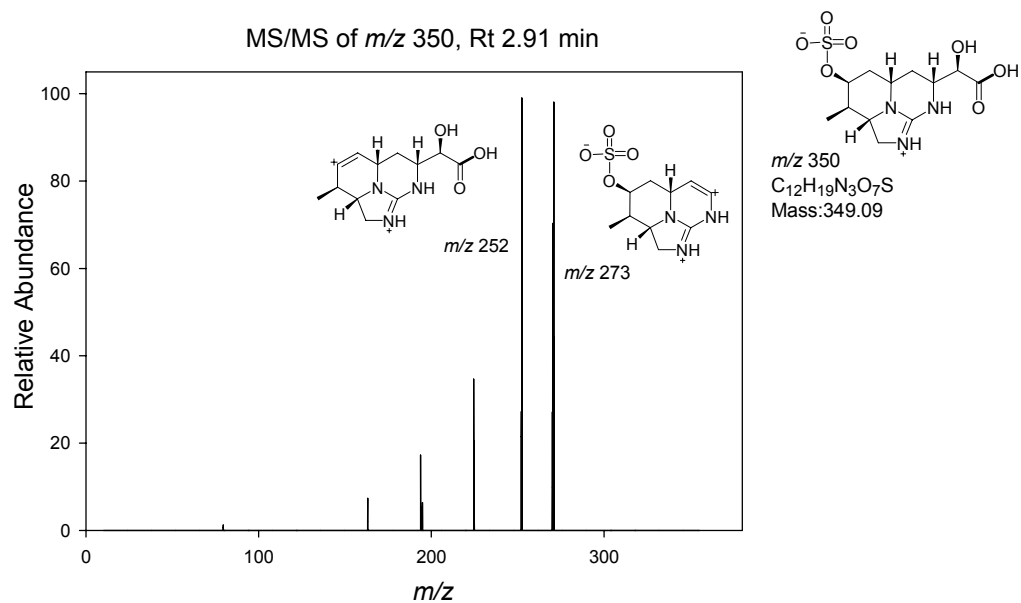


Figure A7. MS/MS spectrum of the intermediate with m/z 350 at R_t 2.91 min, for CYN degradation under UV-A light using Degussa P25.

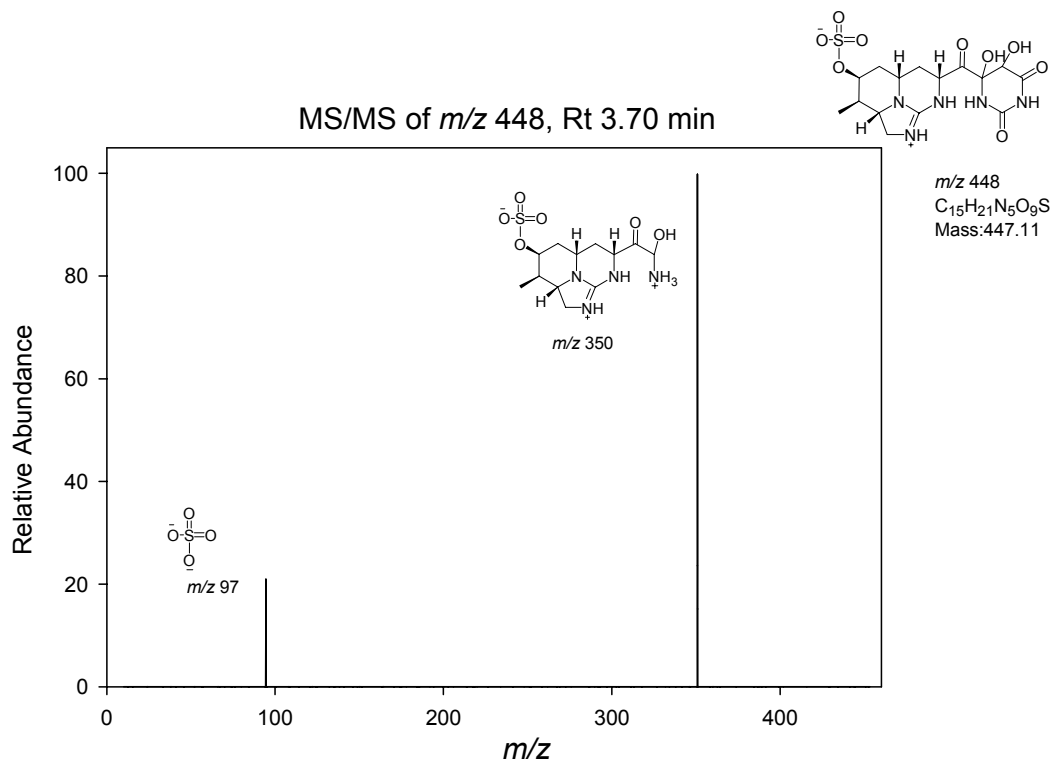


Figure A8. MS/MS spectrum of the intermediate with m/z 448 at R_t 3.70 min, for CYN degradation under UV-A light using Degussa P25.

References

1. J. Metcalf and G. Codd, *Cyanotoxins*, in *Ecology of Cyanobacteria II*, B.A. Whitton, Editor 2012, Springer Netherlands. p. 651-675.
2. A. Hiskia, T. M. Triantis, M. G. Antoniou, A. A. De La Cruz, K. O'Shea, W. Song, T. Fotiou, T. Kaloudis, X. He, J. Andersen, and D. D. Dionysiou, *Transformation Products of Hazardous Cyanobacterial Metabolites in Water*, in *Transformation Products of Emerging Contaminants in the Environment: Analysis, Processes, Occurrence, Effects and Risks*, L. Nollet and D. Lambropoulou, Editors. 2013, Wiley. p. 687-720.
3. C. MacKintosh, K.A. Beattie, S. Klumpp, P. Cohen, and G.A. Codd, *Cyanobacterial microcystin-LR is a potent and specific inhibitor of protein phosphatases 1 and 2A from both mammals and higher plants*. FEBS Letters, 1990. **264**(2): p. 187-192.
4. I.R. Falconer, *Cyanobacterial toxins of drinking water supplies* 2005, Boca Raton, Florida, USA: CRC Press.
5. S. Kinnear, *Cylindrospermopsin: a decade of progress on bioaccumulation research*. Mar Drugs, 2010. **8**(3): p. 542-64.
6. G.A. Burlingame, R.M. Dann, and G.L. Brock, *A case study of geosmin in Philadelphia's water*. American Water Works Association, 1986. **78**(3): p. 56-61.
7. G.A. Codd, L.F. Morrison, and J.S. Metcalf, *Cyanobacterial toxins: risk management for health protection*. Toxicol Appl Pharmacol, 2005. **203**(3): p. 264-72.
8. I.H. Suffet, A. Corado, D. Chou, M.J. McGuire, and S. Butterworth, *AWWA: Taste and odor survey*. American Water Works Association, 1996. **88**(4): p. 168-180.
9. D.M.C. Rashash, A.M. Dietrich, and R.C. Hoehn, *FPA of selected odorous compounds*. American Water Works Association, 1997. **89**(4): p. 131-141.
10. M.J. McGuire, *Off-flavor as the consumer's measure of drinking water safety*. Water Science and Technology, 1995. **31**(11): p. 1-8.
11. P.K.J. Robertson, L.A. Lawton, and B.J.P.A. Cornish, *The Involvement of Phycocyanin Pigment in the Photodecomposition of the Cyanobacterial Toxin, Microcystin-LR*. Journal of Porphyrins and Phthalocyanines, 1999. **3**(6-7): p. 544-551.
12. P.K.J. Robertson, L.A. Lawton, B. Munch, and B.J.P. Cornish, *The Destruction of Cyanobacterial Toxins by Titanium Dioxide Photocatalysis*. Journal of Advanced Oxidation Technologies, 1999. **4**: p. 20-26.
13. P.K.J. Robertson, L.A. Lawton, B. Munch, and J. Rouzade, *Destruction of cyanobacterial toxins by semiconductor photocatalysis*. Chemical Communications, 1997(4): p. 393-394.
14. A.J. Feitz, T.D. Waite, G.J. Jones, B.H. Boyden, and P.T. Orr, *Photocatalytic degradation of the blue green algal toxin microcystin-LR in a natural organic-aqueous matrix*. Environmental Science and Technology, 1999. **33**(2): p. 243-249.
15. L.A. Lawton, P.K.J. Robertson, B.J.P.A. Cornish, and M. Jaspars, *Detoxification of microcystins (cyanobacterial hepatotoxins) using TiO₂ photocatalytic oxidation*. Environmental Science and Technology, 1999. **33**(5): p. 771-775.

16. A.J. Feitz and T.D. Waite, *Kinetic modeling of TiO₂-Catalyzed photodegradation of trace levels of Microcystin-LR*. Environmental Science and Technology, 2003. **37**(3): p. 561-568.
17. X. Feng, F. Rong, D. Fu, C. Yuan, and Y. Hu, *Photocatalytic degradation of trace-level of Microcystin-LR by nano-film of titanium dioxide*. Chinese Science Bulletin, 2006. **51**(10): p. 1191-1198.
18. H. Choi, M.G. Antoniou, M. Pelaez, A.A. De La Cruz, J.A. Shoemaker, and D.D. Dionysiou, *Mesoporous nitrogen-doped TiO₂ for the photocatalytic destruction of the cyanobacterial toxin microcystin-LR under visible light irradiation*. Environmental Science & Technology, 2007. **41**(21): p. 7530-7535.
19. M.G. Antoniou, J.A. Shoemaker, A.A. de la Cruz, and D.D. Dionysiou, *LC/MS/MS structure elucidation of reaction intermediates formed during the TiO₂ photocatalysis of microcystin-LR*. Toxicon, 2008. **51**(6): p. 1103-1118.
20. T.M. Triantis, T. Fotiou, T. Kaloudis, A.G. Kontos, P. Falaras, D.D. Dionysiou, M. Pelaez, and A. Hiskia, *Photocatalytic degradation and mineralization of microcystin-LR under UV-A, solar and visible light using nanostructured nitrogen doped TiO₂*. J Hazard Mater, 2012. **211-212**: p. 196-202.
21. P.J. Senogles, J.A. Scott, G. Shaw, and H. Stratton, *Photocatalytic Degradation of the Cyanotoxin Cylindrospermopsin, using Titanium Dioxide and UV Irradiation*. Water Res, 2001. **35**(5): p. 1245-1255.
22. M. Pelaez, P. Falaras, A.G. Kontos, A.A. de la Cruz, K. O'Shea, P.S.M. Dunlop, J.A. Byrne, and D.D. Dionysiou, *A comparative study on the removal of cylindrospermopsin and microcystins from water with NF-TiO₂-P25 composite films with visible and UV-vis light photocatalytic activity*. Applied Catalysis B: Environmental, 2012. **121-122**: p. 30-39.
23. E. Bellu, L.A. Lawton, and P.K.J. Robertson, *Photocatalytic Destruction of Geosmin Using Novel Pelleted Titanium Dioxide*. Journal of Advanced Oxidation Technologies, 2008. **11**(2): p. 384-388.
24. E.E. Bamuza-Pemu and E.M.N. Chirwa, *Photocatalytic Degradation of Geosmin: Intermediates and Degradation Pathway Analysis*. Chemical Engineering Transactions, 2011. **24**: p. 91.
25. H.F. Miao, F. Qin, G.J. Tao, W.Y. Tao, and W.Q. Ruan, *Detoxification and degradation of microcystin-LR and -RR by ozonation*. Chemosphere, 2010. **79**(4): p. 355-361.
26. F.A. Al Momani and N. Jarrah, *Treatment and kinetic study of cyanobacterial toxin by ozone*. Journal of Environmental Science and Health - Part A Toxic/Hazardous Substances and Environmental Engineering, 2010. **45**(6): p. 719-731.
27. T.P.J. Kull, P.H. Backlund, K.M. Karlsson, and J.A.O. Meriluoto, *Oxidation of the cyanobacterial hepatotoxin microcystin-LR by chlorine dioxide: Reaction kinetics, characterization, and toxicity of reaction products*. Environmental Science and Technology, 2004. **38**(22): p. 6025-6031.
28. W. Song, A.A. de la Cruz, K. Rein, and K.E. O'Shea, *Ultrasonically induced degradation of microcystin-LR and -RR: Identification of products, effect of pH, formation and destruction of peroxides*. Environmental Science & Technology, 2006. **40**(12): p. 3941-3946.

29. K. Tsuji, S. Naito, F. Kondo, N. Ishikawa, M.F. Watanabe, M. Suzuki, and K.I. Harada, *Stability of microcystins from cyanobacteria: effect of light on decomposition and isomerization*. Environmental Science & Technology, 1994. **28**(1): p. 173-177.
30. M.G. Antoniou, A.A. De La Cruz, and D.D. Dionysiou, *Intermediates and reaction pathways from the degradation of microcystin-LR with sulfate radicals*. Environmental Science and Technology, 2010. **44**(19): p. 7238-7244.
31. I. Liu, L.A. Lawton, and P.K.J. Robertson, *Mechanistic studies of the photocatalytic oxidation of microcystin-LR: An investigation of byproducts of the decomposition process*. Environmental Science and Technology, 2003. **37**(14): p. 3214-3219.
32. S. Antonaraki, T.M. Triantis, E. Papaconstantinou, and A. Hiskia, *Photocatalytic degradation of lindane by polyoxometalates: Intermediates and mechanistic aspects*. Catalysis Today, 2010. **151**(1-2): p. 119-124.
33. E. Androulaki, A. Hiskia, D. Dimotikali, C. Minero, P. Calza, E. Pelizzetti, and E. Papaconstantinou, *Light induced elimination of mono- and polychlorinated phenols from aqueous solutions by PW12O40³⁻. The case of 2,4,6-trichlorophenol*. Environmental Science and Technology, 2000. **34**(10): p. 2024-2028.
34. P. Kormali, D. Dimotikali, D. Tsipi, A. Hiskia, and E. Papaconstantinou, *Photolytic and photocatalytic decomposition of fenitrothion by PW₁₂O₄₀³⁻ and TiO₂: A comparative study*. Applied Catalysis B: Environmental, 2004. **48**(3): p. 175-183.
35. A. Hiskia, M. Ecke, A. Troupis, A. Kokorakis, H. Hennig, and E. Papaconstantinou, *Sonolytic, photolytic, and photocatalytic decomposition of atrazine in the presence of polyoxometalates*. Environmental Science and Technology, 2001. **35**(11): p. 2358-2364.
36. R.R. Ozer and J.L. Ferry, *Photocatalytic Oxidation of Aqueous 1,2-Dichlorobenzene by Polyoxometalates Supported on the NaY Zeolite*. The Journal of Physical Chemistry B, 2002. **106**(16): p. 4336-4342.
37. M.T. Pope, *Heteropoly and isopoly oxometalates* 1983, Berlin: Springer-Verlag.
38. M.T. Pope and A. Müller, *Polyoxometalate Chemistry: An Old Field with New Dimensions in Several Disciplines*. Angewandte Chemie International, 1991. **30**(1): p. 34-48.
39. V.W. Day and W.G. Klemperer, *Metal oxide chemistry in solution: the early transition metal polyoxoanions*. Science, 1985. **228**: p. 533.
40. E. Papaconstantinou, *Photochemistry of polyoxometalates of molybdenum and tungsten and/or vanadium*. Chemical Society Reviews, 1989. **18**: p. 1-31.
41. A. Mylonas and E. Papaconstantinou, *Photocatalytic degradation of chlorophenols to CO₂ and HCl with polyoxotungstates in aqueous solution*. Journal of Molecular Catalysis, 1994. **92**(3): p. 261-267.
42. A. Hiskia, A. Mylonas, and E. Papaconstantinou, *Comparison of the photoredox properties of polyoxometalates and semiconducting particles*. Chemical Society Reviews, 2001. **30**(1): p. 62-69.
43. A. Hiskia and E. Papaconstantinou, *Photocatalytic oxidation of organic compounds by polyoxometalates of molybdenum and tungsten. Catalyst regeneration by dioxygen*. Inorganic Chemistry, 1992. **31**(2): p. 163-167.

44. P. Kormali, T. Triantis, D. Dimotikali, A. Hiskia, and E. Papaconstantinou, *On the photooxidative behavior of TiO₂ and PW₁₂O₄₀³⁻: OH radicals versus holes*. Applied Catalysis B: Environmental, 2006. **68**(3-4): p. 139-146.
45. H.a. Long, *Toxic cyanobacteria (blue green algae): an emerging concern*. In: *Envirologix*, editor. *Natural Water Toxins*. 2008. *Envirologix*, in *Natural Water Toxins* 1999: Portland.
46. K. Sivonen and G.J. Jones, *Cyanobacterial toxins*, in *Toxic Cyanobacteria in Water: A Guide to Public Health Significance, Monitoring and Management*, I. Chorus and J. Bartram, Editors. 1999, E&FN Spon /Chapman & Hall: London. p. 41-111.
47. G.A. Codd, S.G. Bell, K. Kunimitsu, J.W. Clive, K.A. Beattie, and S.J. Metcalf, *Cyanobacterial toxins, exposure routes and human health*. European Journal of Phycology, 1999. **34**: p. 405-415.
48. W.W. Carmichael, J.T. Eschedor, G.M. Patterson, and R.E. Moore, *Toxicity and partial structure of a hepatotoxic peptide produced by the cyanobacterium Nodularia spumigena Mertens emend. L575 from New Zealand*. Appl. Environ. Microbiol., 1988. **54**(9): p. 2257-2263.
49. R. Jayaraj and P.V. Lakshmana Rao, *Protein phosphorylation profile and adduct formation in liver and kidney of microcystin-LR-treated mice*. Toxicol, 2006. **48**(3): p. 272-277.
50. P.F. Solter, G.K. Wollenberg, X. Huang, F.S. Chu, and M.T. Runnegar, *Prolonged sublethal exposure to the protein phosphatase inhibitor microcystin-LR results in multiple dose-dependent hepatotoxic effects*. Toxicol Sci, 1998. **44**(1): p. 87-96.
51. L. Zhou, D. Yu, H. Yu, K. Chen, G. Shen, Y. Shen, Y. Ruan, and X. Ding, *Drinking water types, microcystins and colorectal cancer*. Chinese journal of preventive medicine, 2000. **34**(4): p. 224-226.
52. Z. Svircev, S. Krstic, M. Miladinov-Mikov, V. Baltic, and M. Vidovic, *Freshwater cyanobacterial blooms and primary liver cancer epidemiological studies in Serbia*. J Environ Sci Health C Environ Carcinog Ecotoxicol Rev, 2009. **27**(1): p. 36-55.
53. J.S. Metcalf, R. Richer, P.A. Cox, and G.A. Codd, *Cyanotoxins in desert environments may present a risk to human health*. Sci Total Environ, 2012. **422**: p. 118-23.
54. Sivonen K and J. G, *Cyanobacterial toxins*, in *Toxic cyanobacteria in water: a guide to their public health consequences. Monitoring and management.*, E.F. Spon, Editor 1999: London. p. 55–124.
55. J. Rapala, K.A. Berg, C. Lyra, R.M. Niemi, W. Manz, S. Suomalainen, L. Paulin, and K. Lahti, *Paucibacter toxinivorans gen. nov., sp. nov., a bacterium that degrades cyclic cyanobacterial hepatotoxins microcystins and nodularin*. Int J Syst Evol Microbiol, 2005. **55**(4): p. 1563-1568.
56. R.E. Guzman and P.F. Solter, *Characterization of sublethal microcystin-LR exposure in mice*. Vet Pathol, 2002. **39**(1): p. 17-26.
57. Y. Xing, Y. Xu, Y. Chen, P.D. Jeffrey, Y. Chao, Z. Lin, Z. Li, S. Strack, J.B. Stock, and Y. Shi, *Structure of protein phosphatase 2A core enzyme bound to tumor-inducing toxins*. Cell, 2006. **127**(2): p. 341-53.
58. T. Krishnamurthy, W.W. Carmichael, and E.W. Sarver, *Toxic peptides from freshwater cyanobacteria (blue-green algae). I. Isolation, purification and*

- characterization of peptides from Microcystis aeruginosa and Anabaena flos-aquae*. Toxicon, 1986. **24**(9): p. 865-73.
59. M.F. Watanabe, S. Oishi, K. Harda, K. Matsuura, H. Kawai, and M. Suzuki, *Toxins contained in Microcystis species of cyanobacteria (blue-green algae)*. Toxicon, 1988. **26**(11): p. 1017-25.
60. Q. Wang, P. Xie, J. Chen, and G. Liang, *Distribution of microcystins in various organs (heart, liver, intestine, gonad, brain, kidney and lung) of Wistar rat via intravenous injection*. Toxicon, 2008. **52**(6): p. 721-727.
61. Y. Zhao, P. Xie, and X. Zhang, *Oxidative stress response after prolonged exposure of domestic rabbit to a lower dosage of extracted microcystins*. Environmental Toxicology and Pharmacology, 2009. **27**(2): p. 195-199.
62. R. Nishiwaki-Matsushima, T. Ohta, S. Nishiwaki, M. Suganuma, K. Kohyama, T. Ishikawa, W.W. Carmichael, and H. Fujiki, *Liver tumor promotion by the cyanobacterial cyclic peptide toxin microcystin-LR*. J Cancer Res Clin Oncol, 1992. **118**(6): p. 420-4.
63. S.Z. Yu, *Primary prevention of hepatocellular carcinoma*. J Gastroenterol Hepatol, 1995. **10**(6): p. 674-82.
64. T. Ohta, E. Sueoka, N. Iida, A. Komori, M. Suganuma, R. Nishiwaki, M. Tatematsu, S.J. Kim, W.W. Carmichael, and H. Fujiki, *Nodularin, a potent inhibitor of protein phosphatases 1 and 2A, is a new environmental carcinogen in male F344 rat liver*. Cancer Res, 1994. **54**(24): p. 6402-6.
65. J.G. Sivonen K, *Cyanobacterial toxins*. In: Chorus I, Bartram J (eds) *Toxic cyanobacteria in water: a guide to their public health consequences. Monitoring and management*. E & FN Spon, London, pp 55–124 1999.
66. S.U. Dow CS, *Cyanotoxins*. In: Whitton BA, Potts M (eds) *The ecology of cyanobacteria: their diversity in time and space*. Kluwer Academic Publishers, Dordrecht, pp 613–632, 229 pp. 2000.
67. G. Codd, J. Lindsay, F. Young, L. Morrison, and J. Metcalf, *Harmful Cyanobacteria*, in *Harmful Cyanobacteria*, J. Huisman, H.P. Matthijs, and P. Visser, Editors. 2005, Springer Netherlands. p. 1-23.
68. R. Aráoz, J. Molgó, and N. Tandeau de Marsac, *Neurotoxic cyanobacterial toxins*. Toxicon, 2010. **56**(5): p. 813-828.
69. W. Carmichael, D. Biggs, and P. Gorham, *Toxicology and pharmacological action of anabaena flos-aquae toxin*. Science, 1975. **187**(4176): p. 542-544.
70. W.W. Carmichael, D.F. Biggs, and M.A. Peterson, *Pharmacology of Anatoxin-a, produced by the freshwater cyanophyte Anabaena flos-aquae NRC-44-1*. Toxicon, 1979. **17**(3): p. 229-236.
71. E.H. Rogers, E.S. Hunter, V.C. Moser, P.M. Phillips, J. Herkovits, L. Munoz, L.L. Hall, and N. Chernoff, *Potential developmental toxicity of anatoxin-a, a cyanobacterial toxin*. J Appl Toxicol, 2005. **25**(6): p. 527-34.
72. O.M. Skulberg, R. Skulberg, W.W. Carmichael, R.A. Andersen, S. Matsunaga, and R.E. Moore, *Investigations of a neurotoxic oscillatorialean strain (Cyanophyceae) and its toxin. Isolation and characterization of homoanatoxin-a*. Environmental Toxicology and Chemistry, 1992. **11**(3): p. 321-329.

73. C.W. W., M.N. A., and H.E. G., *Natural Toxins from Cyanobacteria (Blue-Green Algae)*, in *Marine Toxins: Origin, Structure, and Molecular Pharmacology*, S. Hall and G. Strichartz, Editors. 1990, American Chemical Society: Washington. p. 87-106.
74. N.A. Mahmood and W.W. Carmichael, *The pharmacology of anatoxin-a(s), a neurotoxin produced by the freshwater cyanobacterium Anabaena flos-aquae NRC 525-17*. *Toxicon*, 1986. **24**(5): p. 425-434.
75. N.A. Mahmood and W.W. Carmichael, *Paralytic shellfish poisons produced by the freshwater cyanobacterium Aphanizomenon flos-aquae NH-5*. *Toxicon*, 1986. **24**(2): p. 175-186.
76. S. Matsunaga, R.E. Moore, W.P. Niemczura, and W.W. Carmichael, *Anatoxin-a(s), a potent anticholinesterase from Anabaena flos-aquae*. *Journal of the American Chemical Society*, 1989. **111**(20): p. 8021-8023.
77. W.W. Carmichael, S.M. Azevedo, J.S. An, R.J. Molica, E.M. Jochimsen, S. Lau, K.L. Rinehart, G.R. Shaw, and G.K. Eaglesham, *Human fatalities from cyanobacteria: chemical and biological evidence for cyanotoxins*. *Environ Health Perspect*, 2001. **109**(7): p. 663-8.
78. L.E. Llewellyn, *Saxitoxin, a toxic marine natural product that targets a multitude of receptors*. *Natural Product Reports*, 2006. **23**(2): p. 200-222.
79. V.M. Bricelj, L. Connell, K. Konoki, S.P. MacQuarrie, T. Scheuer, W.A. Catterall, and V.L. Trainer, *Sodium channel mutation leading to saxitoxin resistance in clams increases risk of PSP*. *Nature*, 2005. **434**(7034): p. 763-767.
80. L. Llewellyn, *Sodium Channel Inhibiting Marine Toxins*, in *Marine Toxins as Research Tools*, N. Fusetani and W. Kem, Editors. 2009, Springer Berlin Heidelberg. p. 67-97.
81. J.S. Metcalf, J.A.O. Meriluoto, and G.A. Codd, *Legal and security requirements for the air transportation of cyanotoxins and toxigenic cyanobacterial cells for legitimate research and analytical purposes*. *Toxicology Letters*, 2006. **163**(2): p. 85-90.
82. J.S. Metcalf, M. Reilly, F.M. Young, and G.A. Codd, *Localization of Microcystin synthetase genes in colonies of the cyanobacterium Microcystis using fluorescence in situ hybridization1*. *Journal of Phycology*, 2009. **45**(6): p. 1400-1404.
83. R.K. Chiswell, G.R. Shaw, G. Eaglesham, M.J. Smith, R.L. Norris, A.A. Seawright, and M.R. Moore, *Stability of cylindrospermopsin, the toxin from the cyanobacterium, Cylindrospermopsis raciborskii: Effect of pH, temperature, and sunlight on decomposition*. *Environmental Toxicology*, 1999. **14**(1): p. 155-161.
84. G.R. Shaw, A.A. Seawright, M.R. Moore, and P.K. Lam, *Cylindrospermopsin, a cyanobacterial alkaloid: evaluation of its toxicologic activity*. *Ther Drug Monit*, 2000. **22**(1): p. 89-92.
85. R. Mazmouz, F. Chapuis-Hugon, V. Pichon, A. Mejean, and O. Ploux, *The last step of the biosynthesis of the cyanotoxins cylindrospermopsin and 7-epicylindrospermopsin is catalysed by CyrI, a 2-Oxoglutarate-dependent iron oxygenase*. *Chembiochem*, 2011. **12**(6): p. 858-862.
86. I. Ohtani, R.E. Moore, and M.T.C. Runnegar, *Cylindrospermopsin: a potent hepatotoxin from the blue-green alga Cylindrospermopsis raciborskii*. *Journal of the American Chemical Society*, 1992. **114**(20): p. 7941-7942.

87. P.R. Hawkins, M.T. Runnegar, A.R. Jackson, and I.R. Falconer, *Severe hepatotoxicity caused by the tropical cyanobacterium (blue-green alga) *Cylindrospermopsis raciborskii* (Woloszynska) Seenaya and Subba Raju isolated from a domestic water supply reservoir*. *Appl Environ Microbiol.*, 1985. **50**(5): p. 1292-1295.
88. R. Banker, B. Teltsch, A. Sukenik, and S. Carmeli, *7-Epicylindrospermopsin, a toxic minor metabolite of the cyanobacterium *Aphanizomenon ovalisporum* from lake Kinneret, Israel*. *J Nat Prod*, 2000. **63**(3): p. 387-389.
89. J. Briand, S. Jacquet, C.H. Bernard, and J. Humbert, *Health hazards for terrestrial vertebrates from toxic cyanobacteria in surface water ecosystems*. *Vet. Res.*, 2003. **34**(4): p. 361-377.
90. R.E. Looper, M.T. Runnegar, and R.M. Williams, *Synthesis of the putative structure of 7-deoxycylindrospermopsin: C7 oxygenation is not required for the inhibition of protein synthesis*. *Angew Chem Int Ed Engl*, 2005. **44**(25): p. 3879-3881.
91. C. Neumann, P. Bain, and G. Shaw, *Studies of the comparative in vitro toxicology of the cyanobacterial metabolite deoxycylindrospermopsin*. *J Toxicol Environ Health A*, 2007. **70**(19): p. 1679-1686.
92. R. Banker, S. Carmeli, M. Werman, B. Teltsch, R. Porat, and A. Sukenik, *Uracil Moiety is Required for Toxicity of the Cyanobacterial Hepatotoxin *Cylindrospermopsis**. *Journal of Toxicology and Environmental Health, Part A*, 2001. **62**(4): p. 281-288.
93. I.R. Falconer and A.R. Humpage, *Health risk assessment of cyanobacterial (blue-green algal) toxins in drinking water*. *Int J Environ Res Public Health*, 2005. **2**(1): p. 43-50.
94. A.A. De la Cruz, A. Hiskia, T. Kaloudis, N. Chernoff, D. Hill, G.M. Antoniou, X. He, K. Loftin, K. O'Shea, C. Zhao, M. Pelaez, C. Han, J.T. Lynch, and D.D. Dionysiou, *A review on cylindrospermopsin: The global occurrence, detection, toxicity and degradation of a potent cyanotoxin*. *Environ. Sci.: Processes Impacts*, 2013. **15**: p. 1979-2003.
95. P. J., **Cylindrospermopsis raciborskii* (Woloszynska) Seenayya et Subba Raju, an expanding highly adaptive cyanobacterium: worldwide distribution and review of its ecology*. *Arch Hydrobiol.*, 1997. **4**(107): p. 563-593.
96. K. H.J., **Cylindrospermopsis raciborskii* (Nostocales, Cyanobacteria): A brief historic overview and recent discovery in the assiniboine river (Canada)*. *Fottea*, 2009. **9**: p. 45-47.
97. D. Chonudomkul, W. Yongmanitchai, G. Theeragool, M. Kawachi, F. Kasai, K. Kaya, and M.M. Watanabe, *Morphology, genetic diversity, temperature tolerance and toxicity of *Cylindrospermopsis raciborskii* (Nostocales, Cyanobacteria) strains from Thailand and Japan*. *FEMS Microbiol Ecol*, 2004. **48**(3): p. 345-55.
98. B.A. Neilan, M.L. Saker, J. Fastner, A. Torokne, and B.P. Burns, *Phylogeography of the invasive cyanobacterium *Cylindrospermopsis raciborskii**. *Mol Ecol*, 2003. **12**(1): p. 133-40.
99. C. Wiedner, J. Rucker, R. Bruggemann, and B. Nixdorf, *Climate change affects timing and size of populations of an invasive cyanobacterium in temperate regions*. *Oecologia*, 2007. **152**(3): p. 473-84.

100. A. Vega and E.A. Bell, *α -Amino- β -methylaminopropionic acid, a new amino acid from seeds of *Cycas circinalis**. *Phytochemistry*, 1967. **6**(5): p. 759-762.
101. P.A. Cox, S.A. Banack, and S.J. Murch, *Biomagnification of cyanobacterial neurotoxins and neurodegenerative disease among the Chamorro people of Guam*. *Proceedings of the National Academy of Sciences*, 2003. **100**(23): p. 13380-13383.
102. E.A. Bell, *The discovery of BMAA, and examples of biomagnification and protein incorporation involving other non-protein amino acids*. *Amyotrophic Lateral Sclerosis*, 2009. **10**: p. 21-25.
103. V.T. Karamyan and R.C. Speth, *Animal models of BMAA neurotoxicity: a critical review*. *Life Sci*, 2008. **82**(5-6): p. 233-246.
104. J.H. Cardellina, F.J. Marner, and R.E. Moore, *Seaweed dermatitis: structure of lyngbyatoxin A*. *Science*, 1979. **204**(4389): p. 193-195.
105. A. Capper, I.R. Tibbetts, J.M. O'Neil, and G.R. Shaw, *The Fate of Lyngbya majuscula Toxins in Three Potential Consumers*. *Journal of Chemical Ecology*, 2005. **31**(7): p. 1595-1606.
106. J.S. Mynderse, R.E. Moore, M. Kashiwagi, and T.R. Norton, *Antileukemia activity in the Oscillatoriaceae: isolation of Debromoaplysiatoxin from Lyngbya*. *Science*, 1977. **196**(4289): p. 538-40.
107. H. Fujiki, M. Suganuma, M. Nakayasu, H. Hoshino, R.E. Moore, and T. Sugimura, *The third class of new tumor promoters, polyacetates (debromoaplysiatoxin and aplysiatoxin), can differentiate biological actions relevant to tumor promoters*. *Gann*, 1982. **73**(3): p. 495-497.
108. M.E. van Apeldoorn, H.P. van Egmond, G.J.A. Speijers, and G.J.I. Bakker, *Toxins of cyanobacteria*. *Molecular Nutrition & Food Research*, 2007. **51**(1): p. 7-60.
109. J.L. Smith, G.L. Boyer, and P.V. Zimba, *A review of cyanobacterial odorous and bioactive metabolites: Impacts and management alternatives in aquaculture*. *Aquaculture*, 2008. **280**(1-4): p. 5-20.
110. E. Ito and H. Nagai, *Morphological observations of diarrhea in mice caused by aplysiatoxin, the causative agent of the red alga *Gracilaria coronopifolia* poisoning in Hawaii*. *Toxicon*, 1998. **36**(12): p. 1913-1920.
111. Drews G and W. J. *Function, structure and composition of cell walls and external layers*. In: Carr NG, Whitton BA (eds) *The biology of cyanobacteria*. Blackwell Scientific Publications Ltd., Oxford. 1982.
112. I. Stewart, P.J. Schluter, and G.R. Shaw, *Cyanobacterial lipopolysaccharides and human health - a review*. *Environ Health*, 2006. **5**(7).
113. G. Keleti and J.L. Sykora, *Production and properties of cyanobacterial endotoxins*. *Appl Environ Microbiol*, 1982. **43**(1): p. 104-109.
114. C. Erridge, E. Bennett-Guerrero, and I.R. Poxton, *Structure and function of lipopolysaccharides*. *Microbes and Infection*, 2002. **4**(8): p. 837-851.
115. S. Raziuddin, H.W. Siegelman, and T.G. Tornabene, *Lipopolysaccharides of the cyanobacterium *Microcystis aeruginosa**. *European Journal of Biochemistry*, 1983. **137**(1-2): p. 333-336.
116. C. Martin, G. Codd, H. Siegelman, and J. Weckesser, *Lipopolysaccharides and polysaccharides of the cell envelope of toxic *Microcystis aeruginosa* strains*. *Archives of Microbiology*, 1989. **152**(1): p. 90-94.

117. Z. Spacil, J. Eriksson, S. Jonasson, U. Rasmussen, L.L. Ilag, and B. Bergman, *Analytical protocol for identification of BMAA and DAB in biological samples*. *Analyst*, 2010. **135**(1): p. 127-132.
118. S. Banack, H. Johnson, R. Cheng, and P. Cox, *Production of the Neurotoxin BMAA by a Marine Cyanobacterium*. *Marine Drugs*, 2007. **5**(4): p. 180-196.
119. P. Omür-Ozbek, J. Little, and A.M. Dietrich, *Ability of humans to smell geosmin, 2-MIB and nonadienal in indoor air when using contaminated drinking water*. *Water Sci Technol.*, 2007. **55**(5): p. 249-56.
120. Z.G. Papp, É. Kerepeczki, F. Pekár, and D. Gál, *Natural origins of off-flavours in fish related to feeding habits*. 2007. **55**: p. 301-309.
121. W.L. Steven and C.G. Casey, *Analysis of 2-Methylisoborneol and Geosmin in Catfish by Microwave Distillation-Solid-Phase Microextraction*. *Journal of Agricultural and Food Chemistry*, 1999. **47**: p. 164-169.
122. G. Lu, J.K. Fellman, C.G. Edwards, D.S. Mattinson, and J. Navazio, *Quantitative Determination of Geosmin in Red Beets (Beta vulgaris L.) Using Headspace Solid-Phase Microextraction*. *Journal of Agricultural and Food Chemistry*, 2003. **51**: p. 1021-1025.
123. H.H. Jelen, M. Majcher, R. Zawirska-Wojtasiak, M. Wiewiorowska, and E. Wasowicz, *Determination of Geosmin, 2-Methylisoborneol, and a Musty-Earthy Odor in Wheat Grain by SPME-GC-MS, Profiling Volatiles, and Sensory Analysis*. *Journal of Agricultural and Food Chemistry*, 2003. **51**: p. 7079-7085.
124. S. Boutou and P. Chatonnet, *Rapid headspace solid-phase microextraction/gas chromatographic/mass spectrometric assay for the quantitative determination of some of the main odorants causing off-flavours in wine*. *J Chromatogr A*, 2007. **1141**(1): p. 1-9.
125. P.E. Persson, *Muddy odour: a problem associated with extreme eutrophication*. *Hydrologia*, 1982. **86**: p. 161-164.
126. A. Matsumoto and Y. Tsuchiya, *Earthy-musty odor-producing cyanophytes isolated from five water areas in Tokyo*. *Wat. Sci. Tech.*, 1988. **20**(8-9): p. 179-183.
127. M. Yagi, U. Matsuo, K. Ashitani, T. Kita, and T. Nakamura, *Odor Problems in Lake Biwa*. *Water Science & Technology*, 1983. **15**(6-7): p. 311-321.
128. C. Klausen, M.H. Nicolaisen, B.W. Strobel, F. Warnecke, J.L. Nielsen, and N.O. Jorgensen, *Abundance of actinobacteria and production of geosmin and 2-methylisoborneol in Danish streams and fish ponds*. *FEMS Microbiol Ecol*, 2005. **52**(2): p. 265-78.
129. T. Negoro, M. Ando, and N. Ichikawa, *Blue-Green Algae in Lake Biwa Which Produce Earthy-Musty Odors*. *Water Science & Technology*, 1988. **20**(8-9): p. 117-123.
130. F. Juttner and S.B. Watson, *Biochemical and ecological control of geosmin and 2-methylisoborneol in source waters*. *Appl Environ Microbiol*, 2007. **73**(14): p. 4395-406.
131. W.F. Young, H. Horth, R. Crane, T. Ogden, and M. Arnott, *Taste and odour threshold concentrations of potential potable water contaminants*. *Water Research*, 1996. **30**(2): p. 331-340.

132. S. Giglio, C.P. Saint, and P.T. Monis, *Expression of the Geosmin synthase gene in the cyanobacterium anabaena circinalis AWQC3181*. Journal of Phycology, 2011. **47**(6): p. 1338-1343.
133. M. Koksai, W.K.W. Chou, D.E. Cane, and D.W. Christianson, *Structure of 2-methylisoborneol synthase from Streptomyces coelicolor and implications for the cyclization of a noncanonical C-methylated monoterpene substrate*. Biochemistry, 2012. **51**: p. 3011-3020.
134. C.P. Dionigi, T.E. Lawlor, J.E. McFarland, and P.B. Johnsen, *Evaluation of geosmin and 2-methylisoborneol on the histidine dependence of TA98 and TA100 Salmonella typhimurium tester strains*. Water Research, 1993. **27**(11): p. 1615-1618.
135. J.L. Graham, K.A. Loftin, M.T. Meyer, and A.C. Ziegler, *Cyanotoxin Mixtures and Taste-and-Odor Compounds in Cyanobacterial Blooms from the Midwestern United States*. Environmental Science & Technology, 2010. **44**(19): p. 7361-7368.
136. M. Pelaez, P. Falaras, V. Likodimos, A.G. Kontos, A.A. de la Cruz, K. O'Shea, and D.D. Dionysiou, *Synthesis, structural characterization and evaluation of sol-gel-based NF-TiO₂ films with visible light-photoactivation for the removal of microcystin-LR*. Applied Catalysis B: Environmental, 2010. **99**(3-4): p. 378-387.
137. W.W. Carmichael, *Cyanobacteria secondary metabolites-the cyanotoxins*. Journal of Applied Microbiology, 1992. **72**(6): p. 445-459.
138. P.V. Rao, N. Gupta, A.S. Bhaskar, and R. Jayaraj, *Toxins and bioactive compounds from cyanobacteria and their implications on human health*. J Environ Biol, 2002. **23**(3): p. 215-24.
139. W.W. Carmichael, *Health Effects of Toxin-Producing Cyanobacteria: "The CyanoHABs"*. Human and Ecological Risk Assessment, 2001. **7**(5): p. 1393-1407.
140. I.R. Falconer, *Is there a Human Health Hazard from Microcystins in the Drinking Water Supply?* Acta hydrochimica et hydrobiologica, 2005. **33**(1): p. 64-71.
141. G. Codd, S. Bell, K. Kaya, C. Ward, K. Beattie, and J. Metcalf, *Cyanobacterial toxins, exposure routes and human health*. European Journal of Phycology, 1999. **34**(4): p. 405-415.
142. J. McElhiney, L.A. Lawton, and C. Leifert, *Investigations into the inhibitory effects of microcystins on plant growth, and the toxicity of plant tissues following exposure*. Toxicol, 2001. **39**(9): p. 1411-1420.
143. A.M. Keijola, K. Himberg, A.L. Esala, K. Sivonen, and L. Hiisvirta, *Removal of cyanobacterial toxins in water treatment processes: Laboratory and pilot-scale experiments*. Toxicity Assessment, 1988. **3**(5): p. 643-656.
144. I.R. Falconer, M.T.C. Runnegar, T. Buckley, L. Huyn, and P. Bradshaw, *Using activated carbon to remove toxicity from drinking water containing cyanobacterial blooms*. Journal of the American Water Works Association, 1989. **81**(2): p. 102-106.
145. J. Lee and H.W. Walker, *Effect of process variables and natural organic matter on removal of microcystin-LR by PAC - UF*. Environmental Science and Technology, 2006. **40**(23): p. 7336-7342.
146. M. Campinas and M.J. Rosa, *Removal of microcystins by PAC/UF*. Separation and Purification Technology, 2010. **71**(1): p. 114-120.

147. L. Ho, P. Lambling, H. Bustamante, P. Duker, and G. Newcombe, *Application of powdered activated carbon for the adsorption of cylindrospermopsin and microcystin toxins from drinking water supplies*. *Water Res*, 2011. **45**(9): p. 2954-64.
148. M.R. Teixeira and M.J. Rosa, *Microcystins removal by nanofiltration membranes*. *Separation and Purification Technology*, 2005. **46**(3): p. 192-201.
149. M. Campinas and M.J. Rosa, *Evaluation of cyanobacterial cells removal and lysis by ultrafiltration*. *Separation and Purification Technology*, 2010. **70**(3): p. 345-353.
150. M.B. Dixon, C. Falconet, L. Ho, C.W.K. Chow, B.K. O'Neill, and G. Newcombe, *Removal of cyanobacterial metabolites by nanofiltration from two treated waters*. *J Hazard Mater*, 2011. **188**(1-3): p. 288-295.
151. M.R. Teixeira and M.J. Rosa, *Comparing dissolved air flotation and conventional sedimentation to remove cyanobacterial cells of *Microcystis aeruginosa*: Part I: The key operating conditions*. *Separation and Purification Technology*, 2006. **52**(1): p. 84-94.
152. M. Ma, R. Liu, H. Liu, J. Qu, and W. Jefferson, *Effects and mechanisms of pre-chlorination on *Microcystis aeruginosa* removal by alum coagulation: Significance of the released intracellular organic matter*. *Separation and Purification Technology*, 2012. **86**: p. 19-25.
153. L. A. Lawton and P. K. J. Robertson, *Physico-chemical treatment methods for the removal of microcystins (cyanobacterial hepatotoxins) from potable waters*. *Chemical Society Reviews*, 1999. **28**(4): p. 217-224.
154. V.K. Sharma, T.M. Triantis, M.G. Antoniou, X. He, M. Pelaez, C. Han, W. Song, K.E. O'Shea, A.A. De la Cruz, T. Kaloudis, A. Hiskia, and D.D. Dionysiou, *Destruction of microcystins by conventional and advanced oxidation processes: A review*. *Separation and Purification Technology*, 2012. **91**: p. 3-17.
155. X. Cheng, H. Shi, C.D. Adams, T. Timmons, and Y. Ma, *Effects of oxidative and physical treatments on inactivation of *Cylindrospermopsis raciborskii* and removal of cylindrospermopsin*. *Water Sci Technol*, 2009. **60**(3): p. 689-97.
156. U. von Gunten, *Ozonation of drinking water: Part I. Oxidation kinetics and product formation*. *Water Research*, 2003. **37**(7): p. 1443-1467.
157. E. Rodriguez, A. Sordo, J.S. Metcalf, and J.L. Acero, *Kinetics of the oxidation of cylindrospermopsin and anatoxin-a with chlorine, monochloramine and permanganate*. *Water Research*, 2007. **41**(9): p. 2048-2056.
158. E. Rodriguez, G.D. Onstad, T.P. Kull, J.S. Metcalf, J.L. Acero, and U. von Gunten, *Oxidative elimination of cyanotoxins: comparison of ozone, chlorine, chlorine dioxide and permanganate*. *Water Res*, 2007. **41**(15): p. 3381-93.
159. G.D. Onstad, S. Strauch, J. Meriluoto, G.A. Codd, and U. von Gunten, *Selective Oxidation of Key Functional Groups in Cyanotoxins during Drinking Water Ozonation*. *Environ Sci Technol*, 2007. **41**(12): p. 4397-4404.
160. D. Bruce, P. Westerhoff, and A. Brawley-Chesworth, *Removal of 2-methylisoborneol and geosmin in surface water treatment plants in Arizona*. *Journal of Water Supply: Research and Technology - AQUA*, 2002. **51**(4): p. 183-197.
161. S. Lalezary, M. Pirbazari, and M.J. McGuire, *Oxidation of five earthy-musty taste and odor compounds*. *American Water Works Association*, 1986. **78**(3): p. 62-69.

162. W.H. Glaze, W. Chauncey, R.C. Edward, J.J. Zarnoch, E.M. Aieta, C.H. Tate, and M.J. McGuire, *Evaluating oxidants for the removal of model taste and odor compounds from a municipal water supply*. American Water Works Association, 1990. **82**(5): p. 79–84.
163. S. Lalezary, M. Pirbazari, M.J. McGuire, and S.W. Krasner, *Air stripping of taste and odor compounds from water*. Journal of American Water Works Association, 1984. **76**(3): p. 83–87.
164. E.M. Rodriguez, J.L. Acero, L. Spoofo, and J. Meriluoto, *Oxidation of MC-LR and -RR with chlorine and potassium permanganate: Toxicity of the reaction products*. Water Research, 2008. **42**(6-7): p. 1744-1752.
165. S. Merel, M. Clement, and O. Thomas, *State of the art on cyanotoxins in water and their behaviour towards chlorine*. Toxicon, 2010. **55**(4): p. 677-691.
166. J.L. Acero, E. Rodriguez, M.E. Majado, A. Sordo, and J. Meriluoto, *Oxidation of microcystin-LR with chlorine and permanganate during drinking water treatment*. Journal of Water Supply: Research and Technology - AQUA, 2008. **57**(6): p. 371-380.
167. R.I. Daly, L. Ho, and J.D. Brookes, *Effect of chlorination on Microcystis aeruginosa cell integrity and subsequent microcystin release and degradation*. Environmental Science and Technology, 2007. **41**(12): p. 4447-4453.
168. L.E. Fraga, M.A. Anderson, M.L. Beatriz, F.M. Paschoal, L.P. Romao, and M.V. Zanoni, *Evaluation of the photoelectrocatalytic method for oxidizing chloride and simultaneous removal of microcystin toxins in surface waters*. Electrochimica Acta, 2009. **54**(7): p. 2069-2076.
169. T.L. Huang, J.W. Zhao, and B.B. Chai, *Mechanism studies on chlorine and potassium permanganate degradation of microcystin-LR in water using high-performance liquid chromatography tandem mass spectrometry*. Water Science and Technology, 2008. **58**: p. 1079-1084.
170. S. Merel, B. LeBot, M. Clement, R. Seux, and O. Thomas, *Ms identification of microcystin-LR chlorination by-products*. Chemosphere, 2009. **74**(6): p. 832-839.
171. E. Rodriguez, G.D. Onstad, T.P.J. Kull, J.S. Metcalf, J.L. Acero, and U. von Gunten, *Oxidative elimination of cyanotoxins: Comparison of ozone, chlorine, chlorine dioxide and permanganate*. Water Research, 2007. **41**(15): p. 3381-3393.
172. P.J. Senogles-Derham, A. Seawright, G. Shaw, W. Wickramasingh, and M. Shahin, *Toxicological aspects of treatment to remove cyanobacterial toxins from drinking water determined using the heterozygous P53 transgenic mouse model*. Toxicon, 2003. **41**(8): p. 979-988.
173. H.X. Shi, J.H. Qu, A.M. Wang, and J.T. Ge, *Degradation of microcystins in aqueous solution with in situ electrogenerated active chlorine*. Chemosphere, 2005. **60**(3): p. 326-333.
174. J.L. Acero, E. Rodriguez, and J. Meriluoto, *Kinetics of reactions between chlorine and the cyanobacterial toxins microcystins*. Water Research, 2005. **39**(8): p. 1628-1638.
175. L. Ho, G. Onstad, U.V. Gunten, S. Rinck-Pfeiffer, K. Craig, and G. Newcombe, *Differences in the chlorine reactivity of four microcystin analogues*. Water Research, 2006. **40**(6): p. 1200-1209.

176. L. Ho, S. Rinck-Pfeiffer, K. Craig, and G. Newcombe, *Chlorination of four microcystin variants*. *Water*, 2006. **33**(1): p. 65-69.
177. T.P.J. Kull, O.T. Sjøvall, M.K. Tammenkoski, P.H. Backlund, and J.A.O. Meriluoto, *Oxidation of the cyanobacterial hepatotoxin microcystin-LR by chlorine dioxide: Influence of natural organic matter*. *Environmental Science and Technology*, 2006. **40**(5): p. 1504-1510.
178. K. Tsuji, T. Watanuki, F. Kondo, M.F. Watanabe, H. Nakazawa, M. Suzuki, H. Uchida, and K.I. Harada, *Stability of microcystins from cyanobacteria-IV. Effect of chlorination on decomposition*. *Toxicon*, 1997. **35**(7): p. 1033-1041.
179. B.C. Nicholson, J. Rositano, and M.D. Burch, *Destruction of cyanobacterial peptide hepatotoxins by chlorine and chloramine*. *Water Research*, 1994. **28**(6): p. 1297-1303.
180. G. Newcombe and B. Nicholson, *Water treatment options for dissolved cyanotoxins*. *Journal of Water Supply: Research and Technology - AQUA*, 2004. **53**(4): p. 227-239.
181. S. Merel, M. Clément, A. Mouro, V. Fessard, and O. Thomas, *Characterization of cylindrospermopsin chlorination*. *Science of The Total Environment*, 2010. **408**(16): p. 3433-3442.
182. J. Tuerk, B. Sayder, A. Boergers, H. Vitz, T.K. Kiffmeyer, and S. Kabasci, *Efficiency, costs and benefits of AOPs for removal of pharmaceuticals from the water cycle*. *Water Science and Technology*, 2010. **61**: p. 985-993.
183. J. Rositano, B.C. Nicholson, and P. Pieronne, *Destruction of cyanobacterial toxins by ozone*. *Ozone: Science and Engineering*, 1998. **20**(3): p. 223-238.
184. J. Rositano, G. Newcombe, B. Nicholson, and P. Sztajnbock, *Ozonation of nom and algal toxins in four treated waters*. *Water Research*, 2001. **35**(1): p. 23-32.
185. S. Brooke, G. Newcombe, B. Nicholson, and G. Klass, *Decrease in toxicity of microcystins LA and LR in drinking water by ozonation*. *Toxicon*, 2006. **48**(8): p. 1054-1059.
186. H. Miao and W. Tao, *The mechanisms of ozonation on cyanobacteria and its toxins removal*. *Separation and Purification Technology*, 2009. **66**(1): p. 187-193.
187. A.R. Shawwa and D.W. Smith, *Kinetics of microcystin-LR oxidation by ozone*. *Ozone: Science and Engineering*, 2001. **23**(2): p. 161-170.
188. K. Himberg, A.M. Keijola, L. Hiisvirta, H. Pyysalo, and K. Sivonen, *The effect of water treatment processes on the removal of hepatotoxins from Microcystis and Oscillatoria cyanobacteria: A laboratory study*. *Water Research*, 1989. **23**(8): p. 979-984.
189. K. Ikehata, N. Jodeiri Naghashkar, and M. Gamal El-Din, *Degradation of aqueous pharmaceuticals by ozonation and advanced oxidation processes: A review*. *Ozone: Science and Engineering*, 2006. **28**(6): p. 353-414.
190. J.P. Duguet, A. Bruchet, and J. Mallevalle, *New advances in oxidation processes: the use of the ozone/hydrogen peroxide combination for micropollutant removal in drinking water*. *J. Water Supply*, 1989. **7**: p. 115-123.
191. K. Terashima, *Reduction of musty odor substances in drinking water - A pilot plant study*. *Water Science and Technology*, 1988. **20**(8-9): p. 275-281.

192. S.W. Jung, K.H. Baek, and M.J. Yu, *Treatment of taste and odor material by oxidation and adsorption*. Water Sci Technol, 2004. **49**(9): p. 289-95.
193. L. Ho, G. Newcombe, and J.P. Croue, *Influence of the character of NOM on the ozonation of MIB and geosmin*. Water Res, 2002. **36**: p. 511 - 518.
194. C. Liang, D. Wang, J. Chen, L. Zhu, and M. Yang, *Kinetics Analysis on the Ozonation of MIB and Geosmin*. Ozone: Science & Engineering, 2007. **29**(3): p. 185-189.
195. C. Collivignarelli and S. Sorlini, *AOPs with ozone and UV radiation in drinking water: contaminants removal and effects on disinfection byproducts formation*. Water Science and Technology, 2004. **49**(4): p. 51-56.
196. J.C. Crittenden, R.R. Trussell, D.W. Hand, K.J. Howe, and G. Tchobanoglous, *Water Treatment - Principles and Design (2nd Edition)* 2005, Hoboken, New Jersey: John Wiley & Sons. 555-559.
197. J. Rositano and A. Urban Water Research Association of, *The destruction of cyanobacterial peptide toxins by oxidants used in water treatment* 1996: Urban Water Research Association of Australia.
198. J. Ding, H. Shi, T. Timmons, and C. Adams, *Release and removal of microcystins from microcystis during oxidative-, physical-, and UV-based disinfection*. Journal of Environmental Engineering, 2010. **136**(1): p. 2-11.
199. E. Rodriguez, M.E. Majado, J. Meriluoto, and J.L. Acero, *Oxidation of microcystins by permanganate: Reaction kinetics and implications for water treatment*. Water Research, 2007. **41**(1): p. 102-110.
200. X. Chen, B. Xiao, J. Liu, T. Fang, and X. Xu, *Kinetics of the oxidation of MCRR by potassium permanganate*. Toxicon, 2005. **45**(7): p. 911-917.
201. J. Blanco and S. Malato Rodriguez, *Solar detoxification* 2003: UNESCO Pub.
202. J.A. He, Y.Z. Hu, and L.J. Jiang, *Photodynamic action of phycobiliproteins: In situ generation of reactive oxygen species*. Biochimica Et Biophysica Acta-Bioenergetics, 1997. **1320**(2): p. 165-174.
203. K. Tsuji, T. Watanuki, F. Kondo, M.F. Watanabe, S. Suzuki, H. Nakazawa, M. Suzuki, H. Uchida, and K.I. Harada, *Stability of microcystins from cyanobacteria. II. Effect of UV light on decomposition and isomerization*. Toxicon, 1995. **33**(12): p. 1619-1631.
204. L. Wormer, M. Huerta-Fontela, S. Cires, D. Carrasco, and A. Quesada, *Natural Photodegradation of the Cyanobacterial Toxins Microcystin and Cylindrospermopsin*. Environ. Sci. Technol., 2010. **44**: p. 3002-3007.
205. K. Kutschera, H. Bornick, and E. Worch, *Photoinitiated oxidation of geosmin and 2-methylisoborneol by irradiation with 254 nm and 185 nm UV light*. Wat. Res. Vol., 2009. **43**(8): p. 2224-32.
206. W.H. Glaze, Y. Lay, and J.-W. Kang, *Advanced Oxidation Processes. A Kinetic Model for the Oxidation of 1,2-Dibromo-3-chloropropane in Water by the Combination of Hydrogen Peroxide and UV Radiation*. Industrial & Engineering Chemistry Research, 1995. **34**(7): p. 2314-2323.
207. A. Lopez, A. Bozzi, G. Mascolo, and J. Kiwi, *Kinetic investigation on UV and UV/H₂O₂ degradations of pharmaceutical intermediates in aqueous solution*. Journal of Photochemistry and Photobiology A: Chemistry, 2003. **156**(1-3): p. 121-126.

208. H.Y. Shu, M.C. Chang, and H.J. Fan, *Decolorization of azo dye acid black 1 by the UV/H₂O₂ process and optimization of operating parameters*. J Hazard Mater, 2004. **113**(1-3): p. 201-208.
209. M. Muruganandham and M. Swaminathan, *Photochemical oxidation of reactive azo dye with UV-H₂O₂ process*. Dyes and Pigments, 2004. **62**(3): p. 269-275.
210. S. Antonaraki, E. Androulaki, D. Dimotikali, A. Hiskia, and E. Papaconstantinou, *Photolytic degradation of all chlorophenols with polyoxometallates and H₂O₂*. Journal of Photochemistry and Photobiology A: Chemistry, 2002. **148**(1-3): p. 191-197.
211. O. Legrini, E. Oliveros, and A.M. Braun, *Photochemical Processes for Water-Treatment*. Chemical Reviews, 1993. **93**(2): p. 671-698.
212. F.S. Dainton and J. Rowbottom, *The primary radical yield in water a comparison of the photolysis and radiolysis of solutions of hydrogen peroxide*. Transactions of the Faraday Society, 1953. **49**: p. 1160-1173.
213. Y.S. Shen, Y. Ku, and K.C. Lee, *Decomposition of chlorophenols in aqueous solution by UV/H₂O₂ process*. Toxicological and Environmental Chemistry, 1996. **54**(1-4): p. 51-67.
214. B.J.P.A. Cornish, L.A. Lawton, and P.K.J. Robertson, *Hydrogen peroxide enhanced photocatalytic oxidation of microcystin-LR using titanium dioxide*. Applied Catalysis B: Environmental, 2000. **25**(1): p. 59-67.
215. R.P. Qiao, Y.M. Ma, X.H. Qi, N. Li, X.C. Jin, Q.S. Wang, and Y.Y. Zhuang, *Degradation of microcystin-RR by combination of UV/H₂O₂ technique*. Chinese Chemical Letters, 2005. **16**(9): p. 1271-1274.
216. L. Li, N.Y. Gao, Y. Deng, J.J. Yao, K.J. Zhang, H.J. Li, D.D. Yin, H.S. Ou, and J.W. Guo, *Experimental and model comparisons of H₂O₂ assisted UV photodegradation of Microcystin-LR in simulated drinking water*. Journal of Zhejiang University: Science A, 2009. **10**(11): p. 1660-1669.
217. R.P. Qiao, N. Li, X.H. Qi, Q.S. Wang, and Y.Y. Zhuang, *Degradation of microcystin-RR by UV radiation in the presence of hydrogen peroxide*. Toxicon, 2005. **45**(6): p. 745-752.
218. M. Sorensen and F.H. Frimmel, *Photochemical degradation of hydrophilic xenobiotics in the UV/H₂O₂ process: Influence of nitrate on the degradation rate of EDTA, 2-amino-1-naphthalenesulfonate, diphenyl-4-sulfonate and 4,4'-diaminostilbene-2,2'-disulfonate*. Water Research, 1997. **31**(11): p. 2885-2891.
219. C.H. Liao and M.D. Gurol, *Chemical oxidation by photolytic decomposition of hydrogen peroxide*. Environmental Science and Technology, 1995. **29**(12): p. 3007-3014.
220. E.J. Rosenfeldt, B. Melcher, and K.G. Linden, *UV and UV/H₂O₂ treatment of methylisoborneol (MIB) and geosmin in water*. Journal of Water Supply: Research and Technology - AQUA, 2005. **54**(7): p. 423-434.
221. D. Romain, B. Kuslikis, and M. Carlson. *Advanced oxidation of geosmin using UV, hydrogen peroxide and aluminum-based coagulant in Water Quality Technology Conference, American Water Works Association*. 2003. Quebec City, Canada
222. A. Royce and M. Stefan. *Application of UV in drinking water treatment for simultaneous disinfection and removal of taste and odor compounds*. in *Water*

Quality Technology Conference, American Water Works Association. 2005. Quebec City, Canada

223. A. Peter and U. Von Gunten, *Oxidation Kinetics of Selected Taste and Odor Compounds During Ozonation of Drinking Water*. Environmental Science & Technology, 2007. **41**(2): p. 626–631.
224. G. Park, M. Yu, J.Y. Koo, W.H. Joe, and H. Kim, *Oxidation of geosmin and MIB in water using O₃/H₂O₂: Kinetic evaluation*. Water Science and Technology: Water Supply, 2006. **6**: p. 63-69.
225. K.S. Suslick, *Sonochemistry*. Science, 1990. **247**(4949): p. 1439-1445.
226. W. Song, T. Teshiba, K. Rein, and K.E. O'Shea, *Ultrasonically induced degradation and detoxification of microcystin-LR (Cyanobacterial Toxin)*. Environmental Science and Technology, 2005. **39**(16): p. 6300-6305.
227. W. Song and K.E. O'Shea, *Ultrasonically induced degradation of 2-methylisoborneol and geosmin*. Water Research, 2007. **41**(12): p. 2672-2678.
228. M. Antoniou, A. De la Cruz, and D. Dionysiou, *Cyanotoxins: New Generation of Water Contaminants*. Journal of Environmental Engineering, 2005. **131**(9): p. 1239-1243.
229. P.K.J. Robertson, J.M.C. Robertson, and D.W. Bahnemann, *Removal of microorganisms and their chemical metabolites from water using semiconductor photocatalysis*. J Hazard Mater, 2012. **211–212**: p. 161-171.
230. A.A. de la Cruz, M.G. Antoniou, A. Hiskia, M. Pelaez, W. Song, K.E. O'Shea, X. He, and D.D. Dionysiou, *Can we effectively degrade microcystins? - implications on human health*. Anti-Cancer Agents in Medicinal Chemistry, 2011. **11**(1): p. 19-37.
231. M.R. Hoffmann, S.T. Martin, W. Choi, and D.W. Bahnemann, *Environmental applications of semiconductor photocatalysis*. Chemical Reviews, 1995. **95**(1): p. 69-96.
232. I. Liu, L.A. Lawton, B. Cornish, and P.K.J. Robertson, *Mechanistic and toxicity studies of the photocatalytic oxidation of microcystin-LR*. Journal of Photochemistry and Photobiology A: Chemistry, 2002. **148**(1–3): p. 349-354.
233. M.G. Antoniou, P.A. Nicolaou, J.A. Shoemaker, A.A. de la Cruz, and D.D. Dionysiou, *Impact of the morphological properties of thin TiO₂ photocatalytic films on the detoxification of water contaminated with the cyanotoxin, microcystin-LR*. Applied Catalysis B: Environmental, 2009. **91**(1-2): p. 165-173.
234. L.A. Lawton, P.K.J. Robertson, B.J.P. Cornish, and M. Jaspars, *Detoxification of microcystins (cyanobacterial hepatotoxins) using TiO₂ photocatalytic oxidation*. Environmental Science and Technology, 1999. **33**(5): p. 771–775.
235. L. Lawton, P.K.J. Robertson, and D. Bruce, *The destruction of 2-methylisoborneol and geosmin using titanium dioxide photocatalysis*. Applied Catalysis B: Environmental, 2003. **44**(1): p. 9–13.
236. E.E. Bamuza Pemu and E.M. Chirwa, *Photocatalytic Degradation of Geosmin: Intermediates and Degradation Pathway Analysis*. Chemical Engineering Transactions, 2011. **24**: p. 91.
237. G.S. Shephard, S. Stockenstrom, D. De Villiers, W.J. Engelbrecht, E.W. Sydenham, and G.F.S. Wessels, *Photocatalytic degradation of cyanobacterial microcystin toxins in water*. Toxicon, 1998. **36**(12): p. 1895-1901.

238. G.S. Shephard, S. Stockenstrom, D. De Villiers, W.J. Engelbrecht, and G.F.S. Wessels, *Degradation of microcystin toxins in a falling film photocatalytic reactor with immobilized titanium dioxide catalyst*. Water Research, 2002. **36**(1): p. 140-146.
239. L.A. Lawton, P.K.J. Robertson, B.J.P.A. Cornish, I.L. Marr, and M. Jaspars, *Processes influencing surface interaction and photocatalytic destruction of microcystins on titanium dioxide photocatalysts*. Journal of Catalysis, 2003. **213**(1): p. 109-113.
240. P.G.-J. de Maagd, A.J. Hendriks, W. Seinen, and D.T.H.M. Sijm, *pH-Dependent hydrophobicity of the cyanobacteria toxin microcystin-LR*. Water Research, 1999. **33**(3): p. 677-680.
241. S. Malato, P. Fernández-Ibáñez, M.I. Maldonado, J. Blanco, and W. Gernjak, *Decontamination and disinfection of water by solar photocatalysis: Recent overview and trends*. Catalysis Today, 2009. **147**(1): p. 1-59.
242. G. Zhang, M.N. Nadagouda, K. O'Shea, S.M. El-Sheikh, A.A. Ismail, V. Likodimos, P. Falaras, and D.D. Dionysiou, *Degradation of cylindrospermopsin by using polymorphic titanium dioxide under UV-Vis irradiation*. Catalysis Today, 2014. **224**: p. 49-55.
243. P.K.J. Robertson, D.W. Bahnemann, L.A. Lawton, and E. Bellu, *A study of the kinetic solvent isotope effect on the destruction of microcystin-LR and geosmin using TiO₂ photocatalysis*. Applied Catalysis B: Environmental, 2011. **108-109**(0): p. 1-5.
244. S.-J. Yoon, Y.H. Lee, W.-J. Cho, I.-O. Koh, and M. Yoon, *Synthesis of TiO₂-entrapped EFAL-removed Y-zeolites: Novel photocatalyst for decomposition of 2-methylisoborneol*. Catalysis Communications, 2007. **8**(11): p. 1851-1856.
245. T. Fotiou, T.M. Triantis, T. Kaloudis, E. Papaconstantinou, and A. Hiskia, *Photocatalytic Degradation of Taste and Odour Compounds in the presence of Polyoxometalates: Degradation pathway and comparison with TiO₂*. Photochem. & Photobiol. A Chemistry, 2014. **286**: p. 1-9.
246. P.V. Kamat, *Photochemistry on nonreactive and reactive (semiconductor) surfaces*. Chemical Reviews, 1993. **93**(1): p. 267-300.
247. N.T. Nolan, M.K. Seery, and S.C. Pillai, *Spectroscopic investigation of the anatase-to-rutile transformation of sol-gel-synthesized TiO₂ photocatalysts*. Journal of Physical Chemistry C, 2009. **113**(36): p. 16151-16157.
248. A. Wisitsoraat, A. Tuantranont, E. Comini, G. Sberveglieri, and W. Wlodarski, *Characterization of n-type and p-type semiconductor gas sensors based on NiOx doped TiO₂ thin films*. Thin Solid Films, 2009. **517**(8): p. 2775-2780.
249. M. Pelaez, N.T. Nolan, S.C. Pillai, M.K. Seery, P. Falaras, A.G. Kontos, P.S.M. Dunlop, J.W.J. Hamilton, J.A. Byrne, K. O'Shea, M.H. Entezari, and D.D. Dionysiou, *A review on the visible light active titanium dioxide photocatalysts for environmental applications*. Applied Catalysis B: Environmental, 2012. **125**: p. 331-349.
250. T. Tachikawa, M. Fujitsuka, and T. Majima, *Mechanistic insight into the TiO₂ photocatalytic reactions: Design of new photocatalysts*. Journal of Physical Chemistry C, 2007. **111**(14): p. 5259-5275.
251. A.J. Hoffman, E.R. Carraway, and M.R. Hoffmann, *Photocatalytic production of H₂O₂ and organic peroxides on quantum-sized semiconductor colloids*. Environmental Science and Technology, 1994. **28**(5): p. 776-785.

252. W. Choi, A. Termin, and M.R. Hoffmann, *The role of metal ion dopants in quantum-sized TiO₂: Correlation between photoreactivity and charge carrier recombination dynamics*. Journal of Physical Chemistry, 1994. **98**(51): p. 13669-13679.
253. R. Asahi, T. Morikawa, T. Ohwaki, K. Aoki, and Y. Taga, *Visible-light photocatalysis in nitrogen-doped titanium oxides*. Science, 2001. **293**(5528): p. 269-271.
254. D. Mitoraj and H. Kisch, *The nature of nitrogen-modified titanium dioxide photocatalysts active in visible light*. Angewandte Chemie - International Edition, 2008. **47**(51): p. 9975-9978.
255. Y. Yang, H. Zhong, and C. Tian, *Photocatalytic mechanisms of modified titania under visible light*. Research on Chemical Intermediates, 2011. **37**(1): p. 91-102.
256. S. Goldstein, D. Behar, and J. Rabani, *Mechanism of visible light photocatalytic oxidation of methanol in aerated aqueous suspensions of carbon-doped TiO₂*. Journal of Physical Chemistry C, 2008. **112**(39): p. 15134-15139.
257. S. Goldstein, D. Behar, and J. Rabani, *Nature of the oxidizing species formed upon uV photolysis of c-TiO₂ aqueous suspensions*. Journal of Physical Chemistry C, 2009. **113**(28): p. 12489-12494.
258. A.I. Kontos, A.G. Kontos, Y.S. Raptis, and P. Falaras, *Nitrogen modified nanostructured titania: Electronic, structural and visible-light photocatalytic properties*. Physica Status Solidi - Rapid Research Letters, 2008. **2**(2): p. 83-85.
259. G. Williams, B. Seger, and P.V. Kamat, *TiO₂-Graphene Nanocomposites. UV-Assisted Photocatalytic Reduction of Graphene Oxide*. ACS Nano, 2008. **2**(7): p. 1487-1491.
260. W.W. Carmichael, *The toxins of cyanobacteria*. Sci. Am., 1994. **270**(1): p. 78-86.
261. R. Sivakumar, J. Thomas, and M. Yoon, *Polyoxometalate-based molecular/nano composites: Advances in environmental remediation by photocatalysis and biomimetic approaches to solar energy conversion*. Journal of Photochemistry and Photobiology C: Photochemistry Reviews, 2012. **13**(4): p. 277-298.
262. E. Papaconstantinou and A. Hiskia, *Photochemistry and Photocatalysis by Polyoxometalates*, in *Polyoxometalate Molecular Science*, J. Borrás-Almenar, et al., Editors. 2003, Springer Netherlands. p. 381-416.
263. A. Mylonas, E. Papaconstantinou, and V. Roussis, *Photocatalytic degradation of phenol and p-cresol by polyoxotungstates. mechanistic implications*. Polyhedron, 1996. **15**(19): p. 3211-3217.
264. P. Kormali, A. Troupis, T. Triantis, A. Hiskia, and E. Papaconstantinou, *Photocatalysis by polyoxometallates and TiO₂: A comparative study*. Catalysis Today, 2007. **124**(3-4): p. 149-155.
265. S. Kim, H. Park, and W. Choi, *Comparative Study of Homogeneous and Heterogeneous Photocatalytic Redox Reactions: PW(12)O(40)(3-) vs TiO(2)*. J Phys Chem B, 2004. **108**(20): p. 6402-11.
266. R.R. Ozer and J.L. Ferry, *Kinetic Probes of the Mechanism of Polyoxometalate-Mediated Photocatalytic Oxidation of Chlorinated Organics*. The Journal of Physical Chemistry B, 2000. **104**(40): p. 9444-9448.

267. L.M. Pastrana-Martínez, S. Morales-Torres, V. Likodimos, J.L. Figueiredo, J.L. Faria, P. Falaras, and A.M.T. Silva, *Advanced nanostructured photocatalysts based on reduced graphene oxide–TiO₂ composites for degradation of diphenhydramine pharmaceutical and methyl orange dye*. Applied Catalysis B: Environmental, 2012. **123–124**: p. 241-256.
268. J. Araña, J.M. Doña-Rodríguez, D. Portillo-Carrizo, C. Fernández-Rodríguez, J. Pérez-Peña, O. González Díaz, J.A. Navío, and M. Macías, *Photocatalytic degradation of phenolic compounds with new TiO₂ catalysts*. Applied Catalysis B: Environmental, 2010. **100**(1–2): p. 346-354.
269. K. Saito, K. Okamura, and H. Kataoka, *Determination of musty odorants, 2-methylisoborneol and geosmin, in environmental water by headspace solid-phase microextraction and gas chromatography--mass spectrometry*. J Chromatogr A, 2008. **1186**(1-2): p. 434-7.
270. T. Fotiou, T.M. Triantis, T. Kaloudis, L.M. Pastrana-Martínez, V. Likodimos, P. Falaras, A.M.T. Silva, and A. Hiskia, *Photocatalytic Degradation of Microcystin-LR and Off-Odor Compounds in Water under UV-A and Solar Light with a Nanostructured Photocatalyst Based on Reduced Graphene Oxide–TiO₂ Composite. Identification of Intermediate Products*. Industrial & Engineering Chemistry Research, 2013. **52**(39): p. 13991-14000.
271. P. Calza, E. Pelizzetti, and C. Minero, *The fate of organic nitrogen in photocatalysis: An overview*. Journal of Applied Electrochemistry, 2005. **35**(7-8): p. 665-673.
272. W.M. Garrison, *Reaction mechanisms in the radiolysis of peptides, polypeptides, and proteins*. Chemical Reviews, 1987. **87**(2): p. 381-398.
273. H. Hidaka, S. Horikoshi, K. Ajisaka, J. Zhao, and N. Serpone, *Fate of amino acids upon exposure to aqueous titania irradiated with UV-A and UV-B radiation: Photocatalyzed formation of NH₃, NO₃⁻, and CO₂*. Journal of Photochemistry and Photobiology A: Chemistry, 1997. **108**(2-3): p. 197-205.
274. P. Calza, C. Medana, C. Baiocchi, and E. Pelizzetti, *Photo-induced transformation of methylguanidine derivatives on titanium dioxide*. Applied Catalysis B: Environmental, 2006. **63**(1-2): p. 124-130.
275. K. Nohara, H. Hidaka, E. Pelizzetti, and N. Serpone, *Processes of formation of NH₃⁺ and NO₃⁻ ions during the photocatalyzed oxidation of N-containing compounds at the titania/water interface*. Journal of Photochemistry and Photobiology A: Chemistry, 1997. **102**(2-3): p. 265-272.
276. X. He, A.A. de la Cruz, and D.D. Dionysiou, *Destruction of cyanobacterial toxin cylindrospermopsin by hydroxyl radicals and sulfate radicals using UV-254nm activation of hydrogen peroxide, persulfate and peroxymonosulfate*. Journal of Photochemistry and Photobiology A: Chemistry, 2013. **251**: p. 160-166.
277. T. Fotiou, T. Triantis, T. Kaloudis, and A. Hiskia, *Photocatalytic degradation of Cylindrospermopsin under UV-A, solar and visible light using TiO₂. Mineralization and intermediate products*. Chemosphere, 2014(in press).
278. D.C. Hurum, A.G. Agrios, K.A. Gray, T. Rajh, and M.C. Thurnauer, *Explaining the Enhanced Photocatalytic Activity of Degussa P25 Mixed-Phase TiO₂ Using EPR*. The Journal of Physical Chemistry B, 2003. **107**(19): p. 4545-4549.

279. M. Klare, J. Scheen, K. Vogelsang, H. Jacobs, and J.A.C. Broekaert, *Degradation of short-chain alkyl- and alkanolamines by TiO₂- and Pt/TiO₂-assisted photocatalysis*. Chemosphere, 2000. **41**(3): p. 353-362.
280. M. Pelaez, A.A. de la Cruz, K. O'Shea, P. Falaras, and D.D. Dionysiou, *Effects of water parameters on the degradation of microcystin-LR under visible light-activated TiO₂ photocatalyst*. Water Research, 2011. **45**(12): p. 3787-3796.
281. M.G. Antoniou, J.A. Shoemaker, A.A. De La Cruz, and D.D. Dionysiou, *Unveiling new degradation intermediates/pathways from the photocatalytic degradation of microcystin-LR*. Environmental Science and Technology, 2008. **42**(23): p. 8877-8883.
282. D.P. Botes, P.L. Wessels, H. Kruger, M.T.C. Runnegar, S. Santikarn, R.J. Smith, J.C.J. Barna, and D.H. Williams, *Structural studies on cyanoginosins-LR, -YR, -YA, and -YM, peptide toxins from Microcystis aeruginosa*. Journal of the Chemical Society, Perkin Transactions 1, 1985: p. 2747-2748.
283. M. G. Antoniou, H. Choi, A. A. De La Cruz, J. A. Shoemaker, and D. D. Dionysiou. *Intermediates of cyanobacterial toxins with hydroxyl-radical based advanced oxidation technologies (HR-AOTs)*. in *Annual Conference Exposition (ACE) of American Water Works Association (AWWA)*. 2008. Atlanta, GA.
284. T. Fotiou, T.M. Triantis, T. Kaloudis, and A. Hiskia, *Evaluation of the photocatalytic activity of TiO₂ based catalysts for the degradation and mineralization of cyanobacterial toxins and water off-odor compounds under UV-A, solar and visible light*. Chemical Engineering Journal, 2014(in press).
285. S. Merel, M. Clement, A. Mourot, V. Fessard, and O. Thomas, *Characterization of cylindrospermopsin chlorination*. Sci Total Environ, 2010. **408**(16): p. 3433-42.
286. W. Song, S. Yan, W.J. Cooper, D.D. Dionysiou, and K.E. O'Shea, *Hydroxyl radical oxidation of cylindrospermopsin (cyanobacterial toxin) and its role in the photochemical transformation*. Environ Sci Technol, 2012. **46**(22): p. 12608-15.
287. S. Wang, W. Ma, Y. Fang, M. Jia, and Y. Huang, *Bismuth oxybromide promoted detoxification of cylindrospermopsin under UV and visible light illumination*. Applied Catalysis B: Environmental, 2014. **150–151**: p. 380-388.
288. P. Pichat, *A brief overview of photocatalytic mechanisms and pathways in water*. Water Sci Technol, 2007. **55**(12): p. 167-173.
289. D. Zehavi and J. Rabani, *Pulse Radiolysis of Aqueous Ferro-Ferricyanide System .1. Reactions of OH, HO₂, and O₂⁻ Radicals*. Journal of Physical Chemistry, 1970. **76**: p. 3703-3709.
290. M. Anbar and P. Neta, *A compilation of specific bimolecular rate constants for the reactions of hydrated electrons, hydrogen atoms and hydroxyl radicals with inorganic and organic compounds in aqueous solution*. The International Journal Of Applied Radiation And Isotopes, 1967. **18**(7): p. 493-523.
291. A. Saito, T. Tokuyama, A. Tanaka, T. Oritani, and K. Fuchigami, *Microbiological Degradation of (-)-Geosmin*. Wat. Res. Vol., 1999. **33**(13): p. 3033-3036.
292. R.W. Eaton and P. Sandusky, *Biotransformations of (+/-)-geosmin by terpene-degrading bacteria*. Biodegradation, 2010. **21**(1): p. 71-9.
293. M.A. Henderson, *A surface science perspective on photocatalysis*. Surf. Sci. Rep., 2011. **66**(6–7): p. 185-297.

294. F. Qi, B. Xu, Z. Chen, J. Ma, D. Sun, and L. Zhang, *Efficiency and products investigations on the ozonation of 2-methylisoborneol in drinking water*. *Water Environ Res*, 2009. **81**(12): p. 2411–2419.
295. H. Sumimoto, *Biodegradation of 2-methylisoborneol by gravel sand filtration*. *Wat. Sci. Tech.*, 1992. **25**(2): p. 191-198.
296. A. Tanaka, T. Oritani, F. Uehara, A. Saiot, H. Kishita, Y. Niizeki, H. Yokota, and K. Fuchigami, *Biodegradation of a musty Odour component, 2-methylisoborneol*. *Wat. Res.*, 1996. **30**(3): p. 759-761.
297. R.W. Eaton and P. Sandusky, *Biotransformations of 2-methylisoborneol by camphor-degrading bacteria*. *Appl Environ Microbiol*, 2009. **75**(3): p. 583-8.
298. Xueyan Li, Yong Huang, and D. Wang. *Efficiency and Mechanism of Degradation of 2-Methylisoborneol(2-MIB) by O₃/H₂O₂ in Water*. in *4th International Conference on Bioinformatics and Biomedical Engineering (iCBBE)*. 2010.
299. A. Hiskia, E. Androulaki, A. Mylonas, S. Boyatzis, D. Dimoticali, C. Minero, E. Pelizzetti, and E. Papaconstantinou, *Photocatalytic Mineralization of Chlorinated Organic Pollutants in Water By Polyoxometallates. Determination of Intermediates and Final Degradation Products*. *Research on Chemical Intermediates*, 2000. **26**(3): p. 235-251.
300. X. Li, Y. Huang, and D. Wang. *Efficiency and Mechanism of Degradation of 2-Methylisoborneol(2-MIB) by O₃/H₂O₂ in Water*. in *4th iCBBE*. 2010.
301. H. Choi, M. G. Antoniou, M. Pelaez, A. A. de La Cruz, J. A. Shoemaker, and D. D. Dionysiou, *Mesoporous nitrogen-doped TiO₂ for the photocatalytic destruction of the cyanobacterial toxin microcystin-LR under visible light irradiation*. *Environmental Science & Technology*, 2007. **41**(21): p. 7530.
302. J. Andersen, C. Han, K. O'Shea, and D.D. Dionysiou, *Revealing the degradation intermediates and pathways of visible light-induced NF-TiO₂ photocatalysis of microcystin-LR*. *Applied Catalysis B: Environmental*, 2014. **154–155**(0): p. 259-266.
303. M. Pelaez, N. T. Nolan, S. C. Pillai, M. K. Seery, P. Falaras, A. G. Kontos, P.S. M.Dunlop, J. W. J. Hamilton, J. A. Byrne, K. O'Shea, M. H. Entezari, and D. D. Dionysiou, *A review on the visible light active titanium dioxide photocatalysts for environmental applications*. *Applied Catalysis B: Environmental*, 2012. **125**: p. 331.
304. A. Fujishima, T.N. Rao, and D.A. Tryk, *Titanium dioxide photocatalysis*. *J. Photochem. Photobiol. C: Photochem. Rev.*, 2000. **1**: p. 1-21.
305. G.C. Glatzmaier, R.G. Nix, and M.S. Mehos, *Solar destruction of hazardous chemicals*. *Journal of Environmental Science and Health - Part A Environmental Science and Engineering*, 1990. **25**(5): p. 571-581.
306. G.C. Glatzmaier, T.A. Milne, C. Tyner, and J. Sprung, *Innovative solar technologies for treatment of concentrated organic wastes*. *Solar Energy Materials*, 1991. **24**(1-4): p. 672-673.
307. K.A. Magrini and J.D. Webb. *Photocatalytic decomposition of aqueous organic compounds as a function of solar irradiation intensity*. 1990.
308. R.C. Weast and C.R. Company, *Handbook of Chemistry and Physics: A Ready-reference Book of Chemical and Physical Data*. *Advances in Photochemistry*, ed. J.N. Pitts. Vol. 10. 1969-1970: Chemical Rubber Company.

309. M.N. Chong, B. Jin, C.W.K. Chow, and C. Saint, *Recent developments in photocatalytic water treatment technology: A review*. Water Research, 2010. **44**(10): p. 2997-3027.
310. Q. Xiang, J. Yu, and M. Jaroniec, *Graphene-based semiconductor photocatalysts*. Chemical Society Reviews, 2012. **41**(2): p. 782-796.
311. J. Meriluoto and L. Spoof, *Cyanotoxins: sampling, sample processing and toxin uptake*, in *Cyanobacterial Harmful Algal Blooms: State of the Science and Research Needs*, H.K. Hudnell, Editor 2008, Springer New York. p. 483-499.
312. C.W. Diehnelt, N.R. Dugan, S.M. Peterman, and W.L. Budde, *Identification of microcystin toxins from a strain of Microcystis aeruginosa by liquid chromatography introduction into a hybrid linear ion trap-Fourier transform ion cyclotron resonance mass spectrometer*. Anal Chem, 2006. **78**(2): p. 501-12.
313. H. Jin, Q. Wu, and W. Pang, *Photocatalytic degradation of textile dye X-3B using polyoxometalate-TiO₂ hybrid materials*. J Hazard Mater, 2007. **141**(1): p. 123-127.
314. G. Marci, E. García-López, L. Palmisano, D. Carriazo, C. Martín, and V. Rives, *Preparation, characterization and photocatalytic activity of TiO₂ impregnated with the heteropolyacid H₃PW₁₂O₄₀: Photo-assisted degradation of 2-propanol in gas-solid regime*. Applied Catalysis B: Environmental, 2009. **90**(3-4): p. 497-506.
315. T. Tachikawa, M. Fujitsuka, and T. Majima, *Mechanistic Insight into the TiO₂ Photocatalytic Reactions: Design of New Photocatalysts*. Journal of Physical Chemistry C, 2007. **111**(14): p. 5259-5275.
316. T. Tachikawa, S. Tojo, M. Fujitsuka, and T. Majima, *One-electron redox processes during polyoxometalate-mediated photocatalytic reactions of TiO₂ studied by two-color two-laser flash photolysis*. Chemistry, 2006. **12**(11): p. 3124-31.